

**SKB**

---

**TECHNICAL**

---

**REPORT**

---

**93-26**

**Dipole tracer experiment in a low-angle fracture zone at Finnsjön  
- results and interpretation.  
The Fracture Zone Project - Phase 3**

Peter Andersson, Rune Nordqvist, Tony Persson,  
Carl-Olof Eriksson, Erik Gustafsson, Thomas Ittner

Geosigma AB, Uppsala, Sweden

November 1993

---

**SVENSK KÄRNBRÄNSLEHANTERING AB**

*SWEDISH NUCLEAR FUEL AND WASTE MANAGEMENT CO*

BOX 5864 S-102 40 STOCKHOLM

TEL 08-665 28 00 TELEX 13108 SKB S

TELEFAX 08-661 57 19

DIPOLE TRACER EXPERIMENT IN A LOW-ANGLE FRACTURE ZONE  
AT FINNSJÖN - RESULTS AND INTERPRETATION.  
THE FRACTURE ZONE PROJECT - PHASE 3

Peter Andersson, Rune Nordqvist, Tony Persson,  
Carl-Olof Eriksson, Erik Gustafsson, Thomas Ittner

Geosigma AB, Uppsala, Sweden

November 1993

This report concerns a study which was conducted for SKB. The conclusions and viewpoints presented in the report are those of the author(s) and do not necessarily coincide with those of the client.

Information on SKB technical reports from 1977-1978 (TR 121), 1979 (TR 79-28), 1980 (TR 80-26), 1981 (TR 81-17), 1982 (TR 82-28), 1983 (TR 83-77), 1984 (TR 85-01), 1985 (TR 85-20), 1986 (TR 86-31), 1987 (TR 87-33), 1988 (TR 88-32), 1989 (TR 89-40), 1990 (TR 90-46), 1991 (TR 91-64) and 1992 (TR 92-46) is available through SKB.

**GEOSIGMA**

MARK BERG VATTEN

Client: **SKB**

Grp: 93 069

1993-11-05

**DIPOLE TRACER EXPERIMENT IN A LOW-  
ANGLE FRACTURE ZONE AT FINNSJÖN -  
RESULTS AND INTERPRETATION**

**THE FRACTURE ZONE PROJECT - PHASE 3**

Peter Andersson  
Rune Nordqvist  
Tony Persson  
Carl-Olof Eriksson  
Erik Gustafsson  
Thomas Ittner

GEOSIGMA AB  
Uppsala

November 1993

## ABSTRACT (ENGLISH)

This report describes a large scale tracer experiment performed in a dipole flow geometry in the upper highly transmissive part of a low angle fracture zone, called Zone 2, at the Finnsjön study site. The experiment was performed as a part of Phase 3 of the Fracture Zone Project aiming to characterize a major fracture zone. The purpose of the experiment was to determine transport parameters for Zone 2 and to test the applicability of the experimental method for characterization of major fracture zones. The dipole experiment involved a total of 15 tracer injections including 14 short-lived radionuclides and 5 inactive tracers. Both sorbing and non-sorbing tracers were injected and some of them several times.

Tracer breakthrough was monitored both in the pumping hole at a distance of 168 m and in two observation holes inside the flow field at distances 157 and 223 m, respectively.

The evaluation of the results included both 1-D modelling of individual flow paths as well as 2-D modelling of the entire flow system. Inverse modelling technique was applied for both models including regression statistics. The statistics were used to assess the uniqueness and goodness of the model fits. The 1-D modelling was used to study effects of multiple flow paths and to determine transport parameters such as mean travel times and dispersivity. The purpose of the 2-D modelling was to study effects of the magnitude and direction of the natural gradient, anisotropy, and leakage. Comparison with previous predictions was also made with the 2-D model.

The report also contains a comparison of all three tracer experiments performed in the upper part of Zone 2.

## ABSTRACT (SWEDISH)

Denna rapport beskriver ett storskaligt spår försök utfört i dipolgeometri i den övre högtransmissiva delen av den flacka sprickzonen, Zon 2, i Finnsjöns försöksområde. Försöket utgjorde en del av Fas 3 i Sprickzonsprojektet som syftade till att karakterisera en större sprickzon. Syftet med experimentet var att bestämma transportparametrar för Zon 2 och att testa den experimentella metodens applicerbarhet för karakterisering av större sprickzoner.

Dipolförsöket omfattade totalt 15 spårämnesinjiceringar inkluderande 14 kortlivade radionuklider och 5 inaktiva spårämnen. Både sorberande och icke-sorberande spårämnen användes, några av dem flera gånger.

Spårämnesgenombrott registrerades både i pumphålet på ett avstånd av 168 m och i två observationshål inne i flödesfältet på avstånden 157 och 223 m från injiceringshålet.

Utvärderingen av resultaten inkluderade både 1D-modellering av individuella flödesvägar och 2D-modellering av hela flödessystemet. Invers modelleringsteknik med regressionsstatistik användes för båda modellerna. Regressionsstatistiken användes för att bedöma hur bra och unika modellpassningarna kunde sägas vara. 1D-modelleringen användes för att studera effekter av multipla flödesvägar och för att ta fram transportparametrar såsom medeltransporttider och dispersivitet. Syftet med 2D-modelleringen var att studera effekter av storlek och riktning på den naturliga gradienten, anisotropi samt läckage. Jämförelser med prediktioner gjordes också med 2D-modellen.

Rapporten innehåller också en kvantitativ jämförelse av alla tre spår försök genomförda i den övre delen av Zon 2.

**TABLE OF CONTENTS**

	page
<b>SUMMARY</b>	iii
<b>1 INTRODUCTION</b>	<b>1</b>
1.1 BACKGROUND	1
1.2 OBJECTIVES	2
1.3 FINNSJÖN SITE	2
<b>2 EXPERIMENTAL SETUP</b>	<b>4</b>
2.1 INSTRUMENTATION AND PROCEDURES	4
2.2 DATA COLLECTED	8
2.2.1 Tracer Breakthrough Data	8
2.2.2 Supporting Data	9
<b>3 MODELLING APPROACH</b>	<b>10</b>
3.1 MODELLING PERFORMED	10
3.2 MODELLING PURPOSE	11
3.2.1 General Purpose	11
3.2.2 Purpose of Dipole Evaluation	11
3.3 CONCEPTUAL MODEL	12
3.4 MATHEMATICAL/NUMERICAL MODEL	12
3.4.1 2-D Flow and Transport Model	12
3.4.2 1-D Transport Model	14
3.4.3 Parameter Estimation Methods	15
3.4.4 Parameter Considerations for the 1-D Inverse Analysis	16
3.4.5 Parameter Considerations for the 2-D Inverse Analysis	17
<b>4 RESULTS AND INTERPRETATION</b>	<b>19</b>
4.1 GENERAL	19
4.2 RESULTS OF 1-D MODELLING	21
4.2.1 Transport between BFI01 and KFI11	21
4.2.2 Transport between BFI01 and KFI06	25
4.2.3 Transport between KFI11 and BFI02	26
4.3 ANALYSIS AND RESULTS OF 2-D MODELLING	28
4.3.1 Flow Domain and Boundary Conditions	28
4.3.2 Modelled Cases	29
4.4 COMPARISON WITH OTHER TRACER TESTS IN ZONE 2	42
<b>5 DISCUSSION AND CONCLUSIONS</b>	<b>46</b>
5.1 EXPERIMENTAL SETUP	46
5.2 FLOW AND TRANSPORT WITHIN ZONE 2	47
<b>6 REFERENCES</b>	<b>49</b>

APPENDIX A: 1-D INVERSE MODELLING OF  
TRACER BREAKTHROUGH

APPENDIX B: DIPOLE EXPERIMENTS IN A LOW-ANGLE  
FRACTURE ZONE AT THE FINNSJÖN SITE,  
CENTRAL SWEDEN. Experimental design  
and preliminary results.

## **SUMMARY**

The characterization of Zone 2 in Phase 1 and 2 of the Fracture Zone Project constitutes the basis for a previously performed radially converging tracer experiment and the dipole tracer experiment in Phase 3 of the study. This report describes the evaluation and interpretation of the dipole experiment.

The objectives of the dipole tracer experiment were primarily to determine parameters essential for the understanding of radionuclide transport in major fracture zones and to utilize the results for calibration and verification of radionuclide transport models. Secondly, the applicability of the experimental method in a large scale and in a highly conductive rock, was tested. The test geometry also enables the results to be directly compared to the results obtained from the radially converging experiment and the preliminary tracer test performed during the interference test.

The dipole tracer experiment was performed in the upper part of the major low angle fracture zone, Zone 2, in which most of the investigations of the Fracture Zone Project have been performed. A recirculating flow system created by pumping in borehole BFI02 and reinjection of the pumped water in borehole BFI01. The distance between the boreholes was 168 meters. Two other boreholes, KFI06 and KFI11, were used as observation boreholes inside the flow field and borehole KFI11 was also used for some of the tracer injections.

A total of 15 tracer injections were performed including 14 radionuclides and 5 inactive tracers. Both sorbing as well as conservative tracers were injected and some of them also several times. In addition to the tracer breakthrough data, the following supporting data were collected:

- pumping rate in BFI02
- hydraulic heads in 19 borehole intervals within 9 boreholes
- electrical conductivity and temperature of the pumped water
- redox potential of the pumped water

The analysis of the dipole tracer experiment includes two major parts;

1. 2-dimensional flow and transport analysis (SUTRA).
2. 1-dimensional analysis of tracer breakthrough in observation boreholes.

The main purpose of the evaluation of the dipole tracer experiment described in this report was to perform inverse modeling on breakthrough curves in order to quantify certain parameters related to the flow and transport properties of the zone and the used tracers.

One-dimensional inverse modeling was made in order to evaluate and compare transport parameters for the breakthrough data in those observation

holes where the transport can be assumed to be one-dimensional. This analysis focused mainly on comparison of the behavior of different tracers and some of their sorption properties.

Two-dimensional inverse modeling was made as an integrated evaluation of flow and transport properties of the zone. This analysis emphasized the differences of breakthrough data in different boreholes, rather than comparing different tracers. The main question here was to what extent temporal as well as spatial experimental data could be explained by a single, relatively idealized, model of flow and transport.

Another specific purpose of the two-dimensional modelling of the dipole experiment was also to make a direct comparison with earlier predictions and experimental data.

The main feature of the dipole experiment is the fast transport to borehole KFI11. The data suggests that a preferential flow direction exists. The modelling performed has showed that it is possible to explain the observed breakthrough without assumptions of spatial heterogeneity, that needs to be described statistically.

In summary the modelling showed that:

- The variation in residence times and dispersivities is small for the non-sorbing tracers ( $^{82}\text{Br}^-$ ,  $^{186}\text{ReO}_4^-$ ,  $^{131}\text{I}^-$ ,  $^{169}\text{Yb-EDTA}$  while  $^{58}\text{Co-EDTA}$ ).  $^{140}\text{La-DOTA}$ ,  $^{177}\text{Lu-DOTA}$  and Rhodamine WT are markedly delayed.  $^{51}\text{Cr-EDTA}$ ,  $^{111}\text{In-EDTA}$ , and In-EDTA (stable) also show minor delays. Some of the tracers, e.g.  $^{24}\text{Na}^+$  and  $^{160}\text{Tb-EDTA}$ , are not delayed but shows lower peak values and less recovery than others.
- Tracer transport between BFI01 and BFI02 was relatively well predicted. However, significant deviations from the predictions were found when observation holes KFI06 and KFI11 were included in the analysis.
- A change of the gradient direction does not contribute to an improved model.
- Including an anisotropy factor ( $K_{\text{max}}/K_{\text{min}}$ ) of about 8 directed approximately along the strike of the zone, gives a remarkably good agreement between data and model.
- The model estimated anisotropy direction agrees well with the geological character of Zone 2 where the configuration of fracture sets gives intersection lineations, "channels", in an approximately NW-SE direction, i.e. parallel to the strike direction of the zone.
- Flow during the dipole experiment is dominated by advection. The only other mechanism needed to explain breakthrough curves is dispersion. Matrix diffusion or other effects like transient solute storage is likely to have negligible effects.

- Including leakage from the lower parts of Zone 2, as indicated by independent information such as head and electrical conductivity data, gives slightly better fits than by assuming tracer losses.

The dipole experiment also involved injection of  $^{99m}\text{TcO}_4^-$  (pertechnetate). No breakthrough could be registered which only can be explained by an in-situ reduction of mobile pertechnetate to immobile tetravalent Tc(IV). Hence, natural geochemical conditions at depth in granitic rock act as a barrier against technetium dissolution and migration. This has earlier only been indicated by laboratory experiments where it is difficult to simulate reducing conditions.

Comparison of tracer breakthrough data and derived transport parameters from all three tracer experiments performed in the upper part of the zone indicates a velocity dependent dispersivity with the lowest values for the highest flow rates. The comparison also indicates that different preferential flow paths between the boreholes are activated depending on the inferred boundary conditions for flow. Hence, channelling in the form of fixed channels where flow occurs independently of flow geometry does not seem to exist.

# 1 **INTRODUCTION**

## 1.1 **BACKGROUND**

In crystalline rock the flow of groundwater through the intact rock matrix is very low. The rate at which radionuclides in groundwater can migrate through the rock is chiefly dependent upon the fracture system. Hence, fractures and fracture zones represent the primary flow paths along which radionuclides may migrate from a nuclear waste repository to the biosphere.

Lacking a deeper knowledge about the properties and the influence of these major fracture zones on radionuclide transport in crystalline bedrock, the distance between the repository and a major fracture zone was decided not to be shorter than 100 meters in the KBS 3 safety analysis. Thus, it is of great importance to increase the knowledge about the transport conditions in major fracture zones in order to obtain a better basis for determining the distance required from a repository to a major fracture zone. If the distance can be reduced or must be increased this will directly influence the rock volume usable for excavation of the repository. The following may be considered to be main questions:

- How are radionuclides transported in major fracture zones ?
- How do the major fracture zones interact with the surrounding rock regarding radionuclide transport ?

In order to answer the above stated questions, detailed investigations have been carried out in a major fracture zone at the Finnsjön study site /Ahlbom et al., 1986, 1988, 1989/, /Ahlbom & Smellie (editors), 1989/, /Andersson, 1993/. The study was focused on the geologic/tectonic and hydrogeologic character of the extensive low-angle fracture zone, Zone 2, which was encountered at depths ranging from 100 to 250 meters. Results from hydrochemical investigations in the area /Ahlbom et al., 1986/, /Smellie et al., 1987/, /Smellie & Wikberg, 1989/ show that Zone 2 represents a structural boundary between non-saline and saline groundwater. The salinity increases distinctly in the upper part of the zone and remains nearly constant further below.

The characterization of Zone 2 in Phase 1 and 2 of the Fracture Zone Project constitutes the basis for a previously performed radially converging tracer experiment /Gustafsson et al., 1990/, Gustafsson & Nordqvist, 1993/ and the dipole tracer experiment in Phase 3 of the study /Andersson et al., 1990/. An extensive amount of background information regarding the hydrogeological and hydrochemical properties have been gathered during the first two phases of the project. Phase 3 also includes three large-scale interference tests performed in the same radial geometry as the radially converging tracer experiment /Andersson et al., 1989/. The first two phases of the project are

summarized in Ahlbom & Smellie (editors) (1989) and the entire project in Andersson (1993).

## 1.2 OBJECTIVES

The objectives of the dipole tracer experiment were primarily to determine parameters essential for the understanding of radionuclide transport in major fracture zones and to utilize the results for calibration and verification of radionuclide transport models. Secondly, the applicability of the experimental method in a large scale and in a highly conductive rock, was tested. The test geometry also enables the results to be directly compared to the results obtained from the radially converging experiment /Gustafsson & Nordqvist, 1993/ and the preliminary tracer test performed during the interference test /Andersson et al., 1989/. Finally, the use of radiotracers with short half lives (6 hours to 71 days) in a closed recirculating system was tested.

## 1.3 THE FINNSJÖN SITE

The Finnsjön study site is located in northern Uppland, central Sweden. The site has a flat topography with differences in altitude of less than 15 m. Although outcrops are common, the area is covered to 85 % by quaternary sediments, mainly moraine. The site was originally investigated during 1977–1982 as a part of the site investigation programme for a repository for spent nuclear fuel /Olkiewicz et al., 1979/, /Carlsson et al., 1980/, /Carlsson & Gidlund, 1983/, among others. The investigations performed within the Fracture Zone Project, e.g. the dipole tracer experiment, were mainly located to the Brändan area (Figure 1–1). A more thorough description of the geology, geohydrology and hydrochemistry of the site is given in Appendix B and in Ahlbom et al. (1992).

The dipole tracer experiment was performed in the upper part of the major low angle fracture zone, Zone 2 (Figure 1–2), in which most of the investigations of the Fracture Zone Project have been performed.

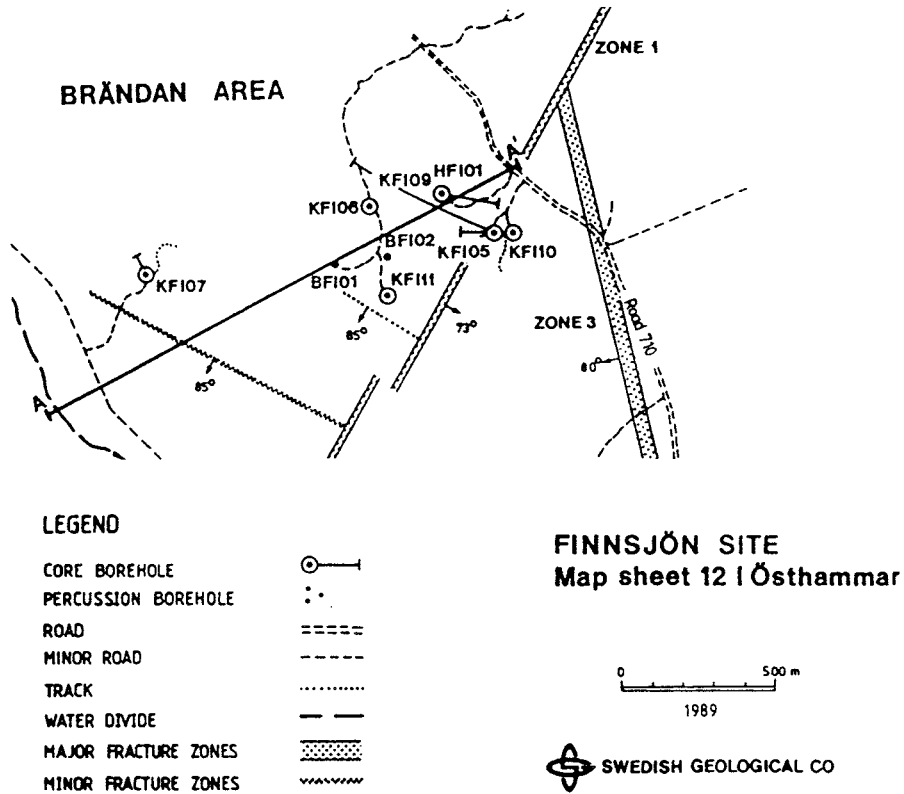


Figure 1-1. Map of the Brändan area, Finnsjön site, showing fracture zones and borehole locations. The location of profile A-A' in Figure 1-2 is also marked.

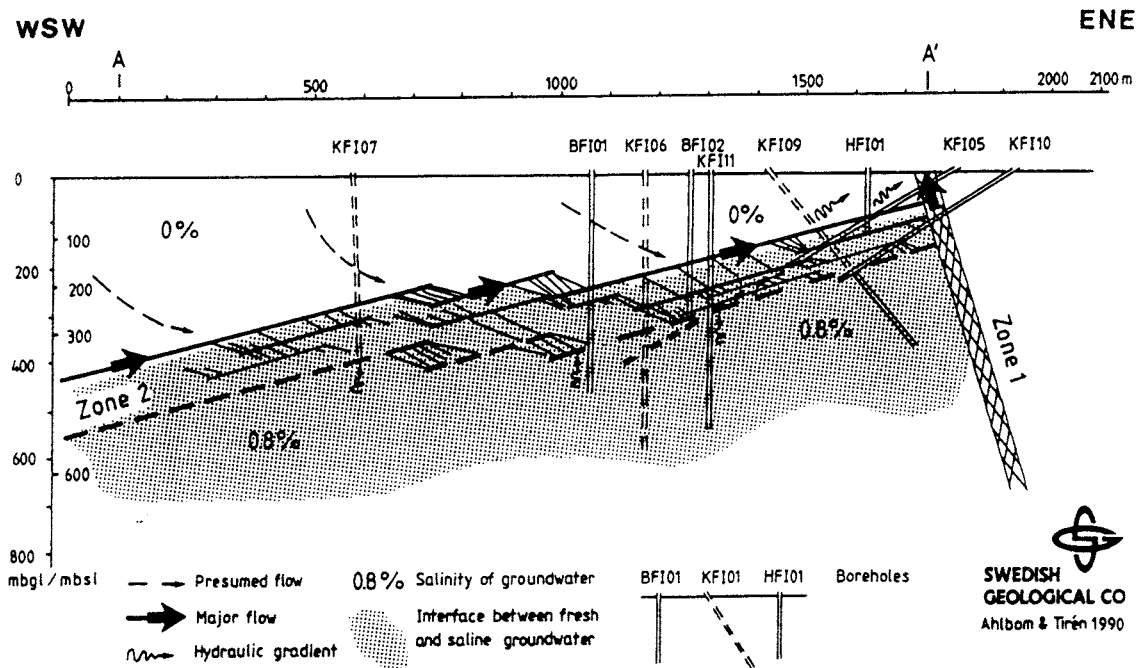


Figure 1-2. Structural profile (A-A' in Figure 1-1) through the Brändan area showing the location of Zone 2. The boreholes are projected into the profile.

## EXPERIMENTAL SETUP

### 2.1 INSTRUMENTATION AND PROCEDURES

The dipole tracer experiment was performed in a recirculating flow system created by pumping in borehole BFI02 and reinjection of the pumped water in borehole BFI01, see Figure 2-1. The distance between the boreholes was 168 meters. Only the upper, highly transmissive part of Zone 2 was used for the test. Two other boreholes, KFI06 and KFI11, were used as observation boreholes inside the flow field and borehole KFI11 was also used for some of the tracer injections. The data concerning borehole geometry, borehole intervals, hydraulic transmissivities, volumes of the pipe system, etc., are given in Appendix B, Section 3.

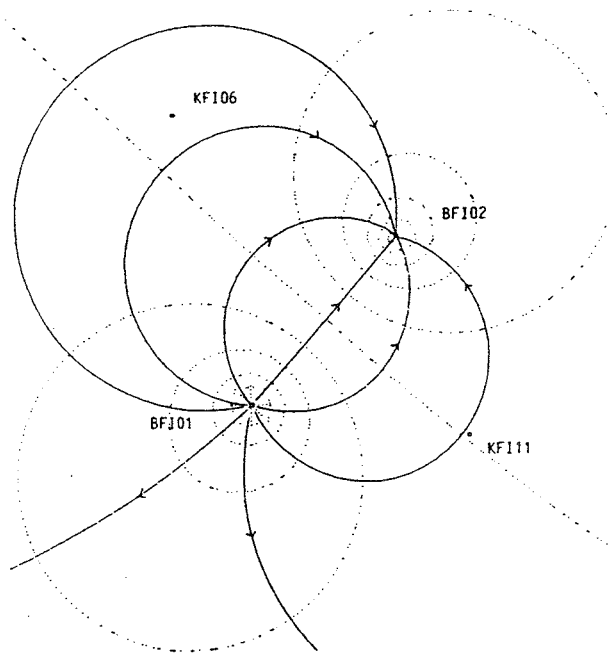


Figure 2-1. Idealized flow model of the dipole tracer experiment.

The choice of a recirculating system was made mainly for two reasons:

- the high transmissivity in combination with a large distance demands high flow rates and it is thereby difficult to supply the injection borehole with enough water.
- the use of radionuclides, where a closed system is preferable as far as licensing and safety is concerned.

A total of 15 tracer injections were performed including 14 radionuclides and 5 inactive tracers, see Table 2-1. Both sorbing as well as conservative tracers were injected and some of them also several times. All data concerning the tracers and tracer injections are presented in Appendix B, Section 3.2. All events during the experiment are listed in Table 2-2.

Table 2-1. Tracer injection schedule. Injections 1-10 involves radionuclides and injections A-E non-radioactive substances.

Injection	Tracer	Radiotracer half-life	Chemical form
1	$^{82}\text{Br}$	1.47 d	$\text{Br(I)}^-$
2	$^{99m}\text{Tc}$	6.01 h	$\text{Tc(VII)O}_4^-$
	$^{186}\text{Re}$	3.78 d	$\text{Re(VII)O}_4^-$
3	$^{131}\text{I}$	8.04 d	$\text{I(I)}^-$
4	$^{99m}\text{Tc}$	6.01 h	$\text{Tc(VII)O}_4^-$
5	$^{58}\text{Co}$	70.92 d	$\text{Co(II)}^+$
	$^{86}\text{Rb}$	18.66 d	$\text{Rb(I)}^+$
6	$^{24}\text{Na}$	14.66 h	$\text{Na(I)}^+$
	$^{82}\text{Br}$	1.47 d	$\text{Br(I)}^-$
	$^{99m}\text{Tc}$	6.01 d	$\text{Tc(VII)O}_4^-$
	$^{131}\text{I}$	8.04 d	$\text{I(I)}^-$
	$^{186}\text{Re}$	3.78 d	$\text{Re(VII)O}_4^-$
	$^{201}\text{Tl}$	3.05 d	$\text{Tl(I)}^+$
7	$^{51}\text{Cr}$	27.70 d	$\text{Cr(III)-EDTA}^-$
	$^{111}\text{In}$	2.81 d	$\text{In(III)-EDTA}^-$
	$^{140}\text{La}$	1.68 d	$\text{La(III)-DOTA}^-$
	$^{160}\text{Tb}$	72.1 d	$\text{Tb(III)-EDTA}^-$
	$^{169}\text{Yb}$	32.0 d	$\text{Yb(III)-EDTA}^-$
	$^{177}\text{Lu}$	6.71 d	$\text{Lu(III)-DOTA}^-$
8	$^{58}\text{Co}$	70.92 d	$\text{Co(III)-EDTA}^-$
9*	$^{131}\text{I}$	8.04 d	$\text{I(I)}^-$
10*	$^{131}\text{I}$	8.04 d	$\text{I(I)}^-$
A	Rhodamine WT	-	Organic dye
B	Blue Dextran 2000	-	Macro molecule
C	In	-	$\text{In(III)-EDTA}^-$
D	Gd	-	$\text{Gd(III)-DTPA}^-$
	Tm	-	$\text{Tm(III)-EDTA}^-$
E	Rhodamine WT	-	Organic dye

\* Injection in borehole KFI11.

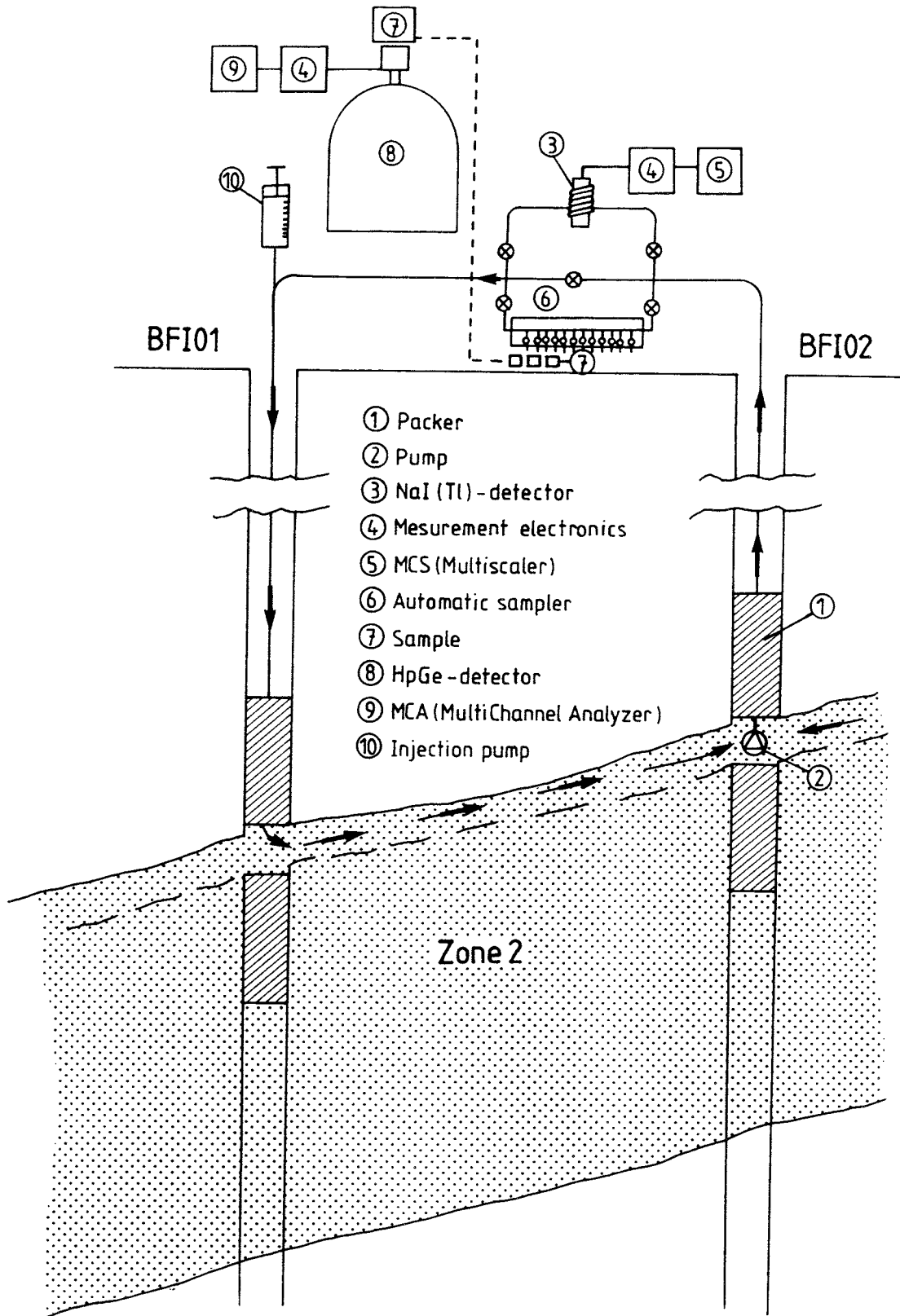


Figure 2-2. Experimental design of the dipole experiment.

Sampling of tracers was made both at the pumping well (BFI02) and in the two observation wells (KFI06 and KFI11). In addition, a gamma detector (NaI) was connected on-line for continuous measurement, c.f. Appendix B, Section 3.3. The injection and sampling setup is shown in Figure 2-2.

Table 2-2. Log of events during the dipole tracer experiment.

Date	Elapsed time (hours)	Event
890403	-217	Stop pumping for the radially converging exp.
890412	0	Start pumping in BFI02, 2 l/s
890425	307	Injection A
890504	524	Injection 1
890505	558	Injection 2
890507	605	Injection 3
890512	703	Injection 4
890513	750	Injection 5
890516	821	Injection 6
890520	918	Injection 7
890524	1014	Injection 8
890526	1054	Injection B
890528	1103	Injection 9
890529	1124	Injection 10
890530	1151	Injection C
890531	1176	Injection D
890605	1294	Injection E
890613	1486	Stop pumping in BFI02

## 2.2 DATA COLLECTED

### 2.2.1 Tracer Breakthrough Data

Tracer breakthrough data was obtained by sampling and subsequent analysis of tracer concentration. In the pumping borehole (BFI02) and in observation borehole KFI11 the sampling was made frequently, 0.5–4 hours between sampling occasions, with the highest sampling frequency at the peak of the breakthrough curves. Borehole KFI06 was sampled manually once a day. Samples were also taken two–three times a week in the lower levels of Zone 2 in both observation holes.

The detectability of the short-lived radionuclides is dependent on the length of the counting period for the gamma radiation and the amount of injected activity. The injected activity together with the counting periods and the decay energies of the different radionuclides determines the detection limits. The detection limits have been calculated for all radionuclide breakthrough curves. An example is given in Figure 2–3 for  $^{82}\text{Br}^-$ . The dashed line on the graph representing the detection limit is based on the mean measurement time, which for BFI02 and KFI11 is 40 minutes. For KFI06 the dashed line represents an overnight measurement (9 hours). The actual position of the dashed detection limit is therefore a result of practical considerations and a reasonable low detection limit. Details regarding the calculation of detection limits and uncertainties are given in Byegård et al. (in prep.)

All breakthrough curves are given as relative concentration,  $C/C_0$ , versus elapsed time after injection, see Appendix B. The data has not been corrected for background concentrations as these are negligible in all breakthrough data except for  $^{131}\text{I}^-$  (Inj. 6) and Rhodamine WT (Inj. E). All data has been corrected for radioactive decay.

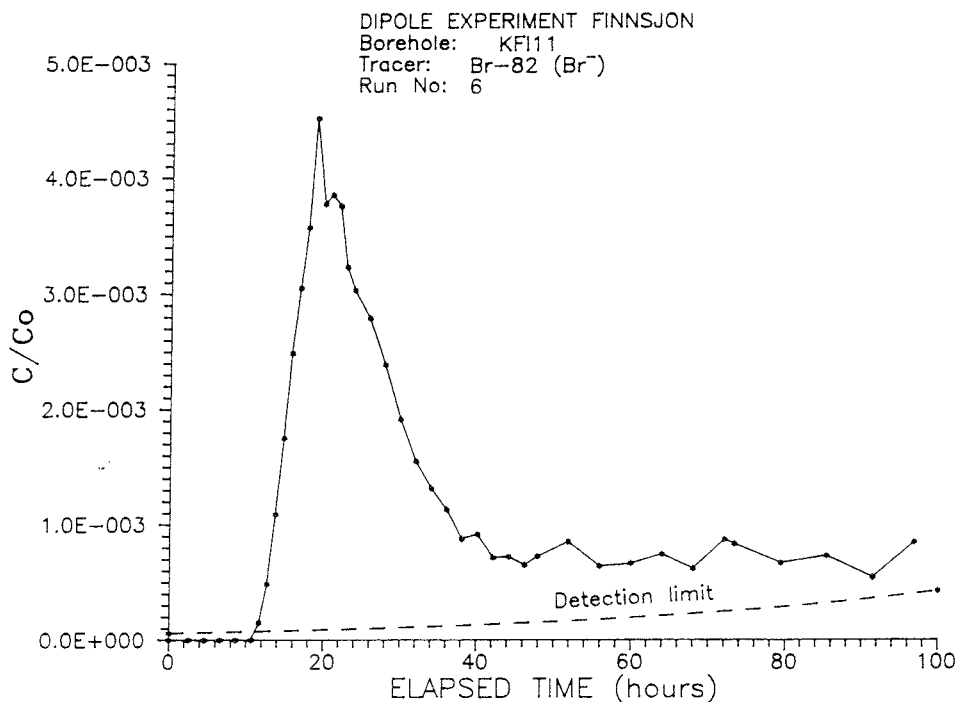


Figure 2–3. Breakthrough curve for  $^{82}\text{Br}^-$  in borehole KFI11. Detection limit is given by dashed line.

## 2.2.2 Supporting Data

In addition to the tracer breakthrough data, the following supporting data were collected:

- pumping rate in BFI02
- hydraulic heads in 19 borehole intervals within 9 boreholes
- electrical conductivity and temperature of the pumped water
- redox potential of the pumped water

All data from the supporting measurements were collected manually, mostly once or twice a day. Borehole intervals for the hydraulic head measurements are given in Table 3-7, Appendix B. Figure 2-4 shows an example of the head monitoring in the upper part of Zone 2 during the dipole tracer experiment.

Additional data for transport calculations such as porosity and diffusivity measurements of rock samples are presented in Gidlund et al. (1990).

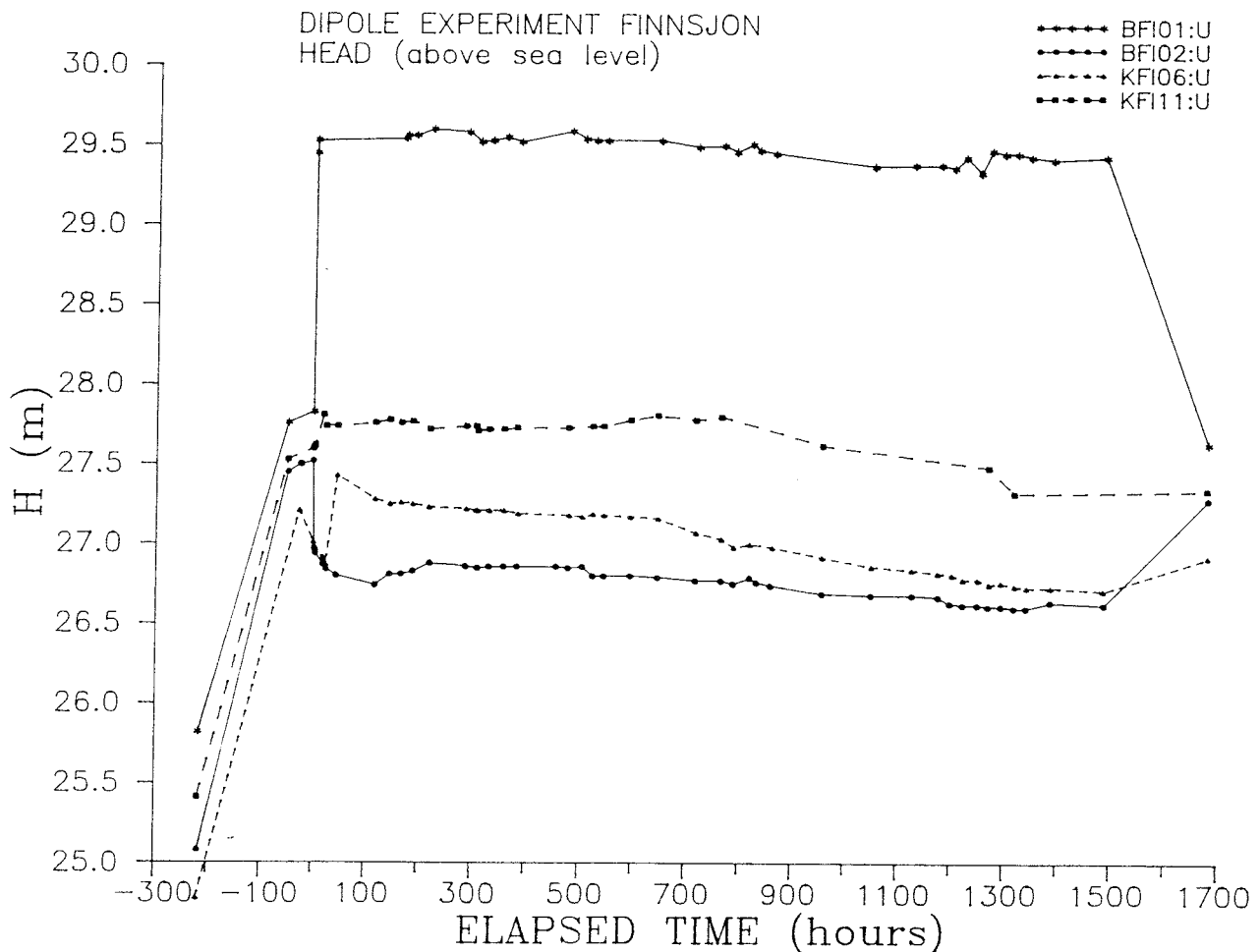


Figure 2-4. Hydraulic head in the upper part of Zone 2 during the dipole experiment. Elapsed time relative start of pumping (c.f. Table 2-2).

**MODELLING APPROACH****3.1 MODELLING PERFORMED**

The flow and transport modelling of the dipole tracer experiment was carried out as a part of a sequence of field experiments and modelling steps: the hydraulic interference tests, the radially converging tracer experiment and the dipole tracer experiment. Figure 3–1 illustrates the general sequence of field experiments and related modelling.

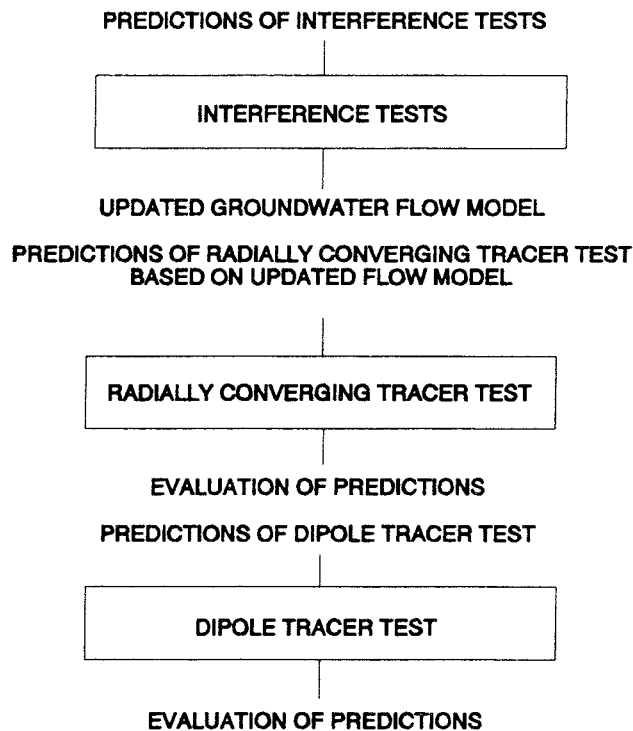


Figure 3–1. General sequence of field experiments and related modelling.

The different modelling steps are published in a number of reports. The interference test modelling is described by Nordqvist & Andersson (1988), Andersson et al. (1989), and Ahlbom & Smellie (1989). Predictions and evaluation of the radially converging experiment is given by Gustafsson et al. (1990) and Gustafsson & Nordqvist (1993). The dipole tracer test predictions are reported by Nordqvist (1989), and a preliminary evaluation of the dipole predictions is given by Andersson et al. (1990) (also in Appendix B). A summary of the modelling steps are presented by Andersson (1993).

The analysis of the dipole tracer experiment includes two major parts;

1. 2-dimensional flow and transport analysis.
2. 1-dimensional analysis of tracer breakthrough in observation boreholes.

## 3.2 MODELLING PURPOSE

### 3.2.1 General Purpose

The general purpose for all the modelling indicated in Figure 3-1 was to predict each field experiment based on all available information and compare the results with the actual outcome of the experiment. As each experiment was completed, new information could be added to the model in order to improve the predictive ability for a prediction of the following experiment. It was emphasized during the this whole sequence that groundwater flow conditions should be predicted as well as solute transport.

In addition to the general modelling purpose described above, model simulations were also performed in order to assist in the design of all the different experiments.

### 3.2.2 Purpose of the Dipole Evaluation

The main purpose of the evaluation of the dipole tracer experiment in this report was to perform inverse modeling on breakthrough curves in order to quantify certain parameters related to the flow and transport properties of the zone and the used tracers.

One-dimensional inverse modeling was made in order to evaluate and compare transport parameters for the breakthrough data in those observation holes where the transport can be assumed to be one-dimensional. This analysis focused mainly on comparison of the behavior of different tracers and some of their sorption properties.

Two-dimensional inverse modeling was made as an integrated evaluation of flow and transport properties of the zone. This analysis emphasized the differences of breakthrough data in different boreholes, rather than comparing different tracers. The main question here was to what extent temporal as well as spatial experimental data could be explained by a single, relatively idealized, model of flow and transport.

Another specific purpose of the two-dimensional modelling of the dipole experiment was also to make a direct comparison with earlier predictions and experimental data. This essentially amounts to a quantification of the deviation of the experimental results from those of an ideal dipole flow field.

### 3.3 CONCEPTUAL MODEL

The low angle fracture zone, Zone 2, is in 2-D generally modelled as a porous medium, where flow and transport can be described using averaged properties of the medium. Figure 3-2 shows a conceptual model of the entire thickness of the fracture zone. The total thickness of the zone is about 100 meters. It consists of highly fractured sub-zones, of which the dominating ones are located at the upper and lower limitations of the zone. Vertical connections between the subzones exist, as indicated in Figure 3-2. However, the variability of media properties is much larger in the vertical direction than in the horizontal, and with the lower hydraulic connectivity in the vertical direction.

The flow and transport modelling for the dipole experiment was performed for the upper, 0.5 m thick, highly conductive part of the fracture zone.

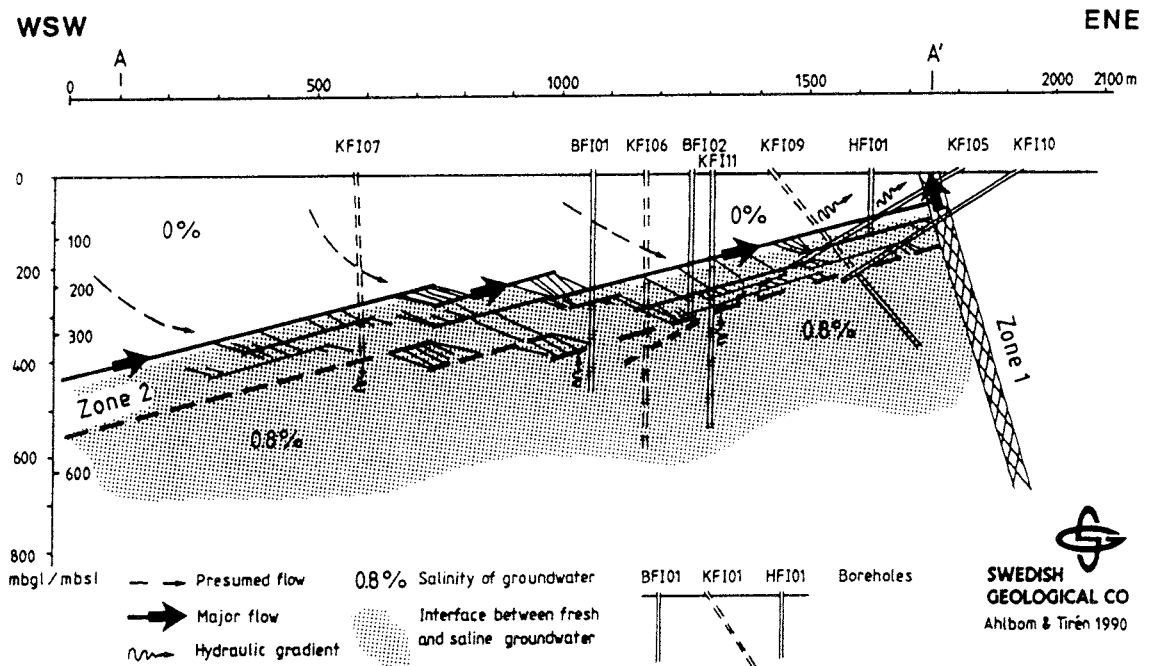


Figure 3-2. Conceptual model of Zone 2.

### 3.4 MATHEMATICAL/NUMERICAL MODEL

#### 3.4.1 2-D Flow and Transport Model

For the analysis in this report, the groundwater flow is generally considered to take place in an anisotropic, inhomogeneous, equivalent porous medium, and is in two dimensions governed by the equation /Freeze & Cherry, 1979/:

$$\frac{\partial}{\partial x} \left( T_x \frac{\partial h}{\partial x} \right) + \frac{\partial}{\partial y} \left( T_y \frac{\partial h}{\partial y} \right) + K' \frac{h' - h}{B'} - Q = 0 \quad (3-1)$$

where  $h(x,y)$  is the hydraulic head (m),  $T_x(x,y)$ ,  $T_y(x,y)$  is the transmissivity

(m<sup>2</sup>/s) in the x, y principal directions, K'(x,y) and B'(x,y) are the hydraulic conductivity (m/s) and thickness (m) of a semi-permeable (leaky) layer, h'(x,y) is the hydraulic head (m) on the distant side of the semi-permeable layer, Q(x,y) is fluid sources or sinks (volume fluid/(volume aquifer x time)).

Equation (3-1) is based on Darcy's law and a continuity equation. Steady state flow, constant density of fluid and saturated flow is assumed. It also allows for simulation of vertical leakage by the possibility to include a semi-permeable layer with a fixed steady-state head on the distant side of the layer.

The water velocity,  $v(x,y)$ , is related to the transmissivity by:

$$v = \frac{T}{pB} = \frac{K}{p} \frac{\partial h}{\partial l} \quad (3-2)$$

where B(x,y) is the thickness of the fracture zone (m), K(x,y) is the hydraulic conductivity, p(x,y) is the flow porosity (dimensionless), and dh/dl represents the hydraulic gradient in the direction of flow, obtained by solving equation (3-1).

The 2-D transport simulations were all performed for a single solute. The transport mechanisms considered in the simulations are:

- advection, governed by the general flow field
- hydrodynamic dispersion, originating from variations in the average velocity field

The governing equation for the solute transport model in two dimensions applied in this work may in a simple form be written as:

$$\frac{\partial}{\partial S_L} (D_L \frac{\partial C}{\partial S_L}) + \frac{\partial}{\partial S_T} (D_T \frac{\partial C}{\partial S_T}) - \frac{\partial}{\partial S_L} (v_L C) = \frac{\partial C}{\partial t} \quad (3-3)$$

where C(x,y) is the solute concentration (e.g. mass/m<sup>3</sup>), S<sub>L</sub> and S<sub>T</sub> are coordinates along and perpendicular to the flow direction, respectively, D<sub>L</sub> and D<sub>T</sub> are the longitudinal and transverse dispersion coefficients, respectively (m<sup>2</sup>/s).

The dispersion coefficients, D<sub>L</sub> and D<sub>T</sub>, are in this analysis assumed to be linearly proportional to the velocity:

$$D_L = a_L v \quad (3-4)$$

$$D_T = a_T v \quad (3-5)$$

where a<sub>L</sub>(x,y) and a<sub>T</sub>(x,y) are the longitudinal and transverse dispersivities (m).

The dispersivities,  $a_L$  and  $a_T$ , may be considered as fundamental transport properties, but only when applied to a particular field situation. The magnitude of the dispersion is largely dependent on the scale of transport and the configuration of the tracer experiment. Thus, the dispersivity values are considered to be some lumped measure of the variability in velocity that is not explicitly explained by the structural features included in the conceptual model.

The transport equations in two dimensions were solved numerically by a two-dimensional finite element code, SUTRA /Voss, 1990/. When solving the flow equations with SUTRA, the required boundary conditions are either specified hydraulic head or constant flow. In cases where flow crosses a boundary, solute concentration of fluid entering the flow domain has to be specified.

Initial conditions are given as hydraulic head and solute concentration over the region. When solving the equations for steady-state flow, initial head distribution is arbitrary. Calculations involving transient solute transport require specification of initial concentrations across the computational domain.

### 3.4.2 **1-D Transport Model**

The governing equation for advective-dispersive one-dimensional transport is analogous to equation (3-3), and may be written as:

$$D \frac{\partial^2 C}{\partial x^2} - v \frac{\partial C}{\partial t} = R \frac{\partial C}{\partial t} \quad (3-6)$$

where  $D$  is the dispersion coefficient ( $m^2/s$ ),  $v$  is the average linear velocity ( $m/s$ ),  $R$  is the retardation coefficient,  $C(x,t)$  is solute concentration, and  $x$  is the distance from the injection point ( $m$ ).

The retardation factor,  $R$ , may also be defined as the ratio between the average velocity for a non-sorbing tracer and a sorbing one:

$$R = \frac{v}{v_R} \quad (3-7)$$

where  $v_R$  is the average velocity of a sorbing tracer. The use of  $R$  in this manner implies the assumption that of reversible, equilibrium sorption with a linear sorption isotherm.

A variety of boundary conditions may be considered when solving equation (3-6). In this study, the following initial boundary conditions were generally applied:

$$C(x,t) = 0 \quad \text{at } t=0 \quad (3-8)$$

$$-D \frac{\partial C}{\partial x} + vC = v f(t) \quad (3-9)$$

where the input concentration takes the form:

$$f(t) = C_0 \quad 0 < t \leq t_0 \quad (3-10)$$

$$f(t) = 0 \quad t > t_0 \quad (3-11)$$

where  $C_0$  represents the injection concentration during the injection period  $t_0$ . The one-dimensional models were solved using analytical solutions as given by Van Genuchten & Alves (1982). Variable injection schemes were simulated by superposition of the solutions.

### 3.4.3 Parameter Estimation Methods

For all inverse modelling in this analysis, non-linear least squares regression was used. The technique that was used for regression is sometimes referred to as the Marquardt method /Marquardt, 1963/ and is in this report formulated as, in an iterative form /Cooley (1985)/:

$$\mathbf{B}_{r+1} = \mathbf{B}_r + p_{r+1}(\mathbf{X}_r^T \mathbf{W} \mathbf{X}_r + u_{r+1})^{-1} \mathbf{X}_r^T \mathbf{W} (\mathbf{C}_r^o - \mathbf{C}_r^m) \quad (3-12)$$

where

- $\mathbf{B}_r$  = vector of parameter estimates
- $\mathbf{X}$  = vector of parameter sensitivities
- $\mathbf{W}$  = reliability weight matrix
- $\mathbf{C}_{ro}$  = vector of observed concentrations
- $\mathbf{C}_r^m$  = vector of model concentrations
- $p$  = damping parameter ( $\leq 1$ )
- $u$  = Marquardt parameter

Equation (3-12) gives the updated parameter estimate at the (r+1)th iteration. The parameter sensitivity vector is obtained by taking partial derivatives of the dependent variable with respect to each parameter. Thus, for an element in the  $\mathbf{X}$  matrix:

$$X_{ij} = \partial C_j^m / \partial B_i \quad (3-13)$$

Thus, each element of the  $\mathbf{X}$  matrix represents the derivative of the modelled concentration at location (or time)  $j$ , to parameter  $i$ . The parameter sensitivities are generally obtained by taking analytical derivatives of the solutions to the one-dimensional models, and discrete derivatives for the numerical solution to the two-dimensional model.

The reliability weight matrix,  $\mathbf{W}$ , may be used to represent the spatial and temporal error structure of the observed data. Alternatively, it may also be

used by the investigator to emphasize/de-emphasize certain components of the data. If the observations are assumed to be random (no correlation between observations) and have a common variance,  $\mathbf{W}$  reduces to an identity matrix, and that is what is assumed in this analysis.

Standard errors of the parameters and linear correlation between parameters were obtained from the variance-covariance matrix,  $s^2(\mathbf{X}^T\mathbf{W}\mathbf{X})^{-1}$ , where  $s^2$  is the error variance. Details of the methods for statistical analysis procedures of regression results are also given by Cooley (1979).

#### 3.4.4 Parameter Considerations for the 1-D Inverse Analysis

The inverse simulation (model fitting) for non-sorbing tracers was generally made for three parameters: dispersion coefficient,  $D$ , mean velocity,  $v$ , and a proportionality factor,  $f$ . The  $f$ -parameter is basically the product of injection concentration, dilution in the sampling section, and a weight representing the contribution from each main flow path (if more than one). The fitted parameters are generally transformed and given in this report as residence time,  $t_0$ , dispersivity,  $D/v$ , and Peclet number. The uniqueness of the parameter estimates was assessed by analyzing the following regression statistics of each inverse run: the correlation coefficient (simulated vs observed data), standard error of the estimated parameters, and the correlation between the parameters /Gustafsson & Nordqvist, 1993/. The classification was made on a scale from 1 to 3 where 1 represents a poor model, 2 represents an acceptable model, and 3 a good model.

For sorbing solutes, the retardation factor,  $R$ , was also estimated. As is apparent from equation (3-7),  $R$  can not be estimated from a single breakthrough curve. The usual method to estimate  $R$  is to estimate  $v$  and  $v_R$  separately, and then compute the ratio. However, in this analysis, two or more breakthrough curves from tracers with varying sorption capacities, are used simultaneously. This approach has the advantage that it utilizes the fact that all curves should have the same value for the dispersion coefficient, as well as for the  $f$ -parameter (after correction for the injection mass of each tracer) and the average water velocity. This approach may in many cases significantly decrease the estimation errors of the evaluated parameters.

The sensitivity matrix,  $\mathbf{X}$ , requires in this case modification to accommodate estimation of multiple data sets simultaneously. For a simple case of using two breakthrough curves, of which one is from a conservative tracer, the sensitivity matrix becomes:

$$\mathbf{X} = \begin{bmatrix} \frac{\partial C_1}{\partial v} & \frac{\partial C_1}{\partial D} & 0 \\ \frac{\partial C_2}{\partial v} & \frac{\partial C_2}{\partial D} & 0 \\ \cdot & \cdot & \cdot \\ \frac{\partial C_m}{\partial v} & \frac{\partial C_m}{\partial D} & 0 \\ \frac{\partial C_{m+1}}{\partial v} & \frac{\partial C_{m+1}}{\partial D} & \frac{\partial C_{m+1}}{\partial R} \\ \cdot & \cdot & \cdot \\ \frac{\partial C_{m+n}}{\partial v} & \frac{\partial C_{m+n}}{\partial D} & \frac{\partial C_{m+n}}{\partial R} \end{bmatrix} \quad (3-14)$$

For this simplified case, m data points for the non-sorbing tracer, and n data points for the sorbing tracer is used. The sensitivity matrix illustrates the way that all data points from both breakthrough curves have some information value for estimation of the average water velocity, v, and the dispersion coefficient, D.

### 3.4.5

#### **Parameter Considerations for the 2-D Inverse Analysis**

The difference compared to the 1-D inverse analysis is basically that both flow parameters and transport parameters are involved in this case. In the 2-D analysis, an attempt is made to find a model that will explain the experimental results both in space and time simultaneously. Thus, the breakthrough curves in all three observation boreholes should be explained by a single flow and transport model. The parameters considered in this case are:

- magnitude and direction of the natural gradient
- hydraulic conductivities
- flow porosity
- longitudinal dispersivity
- leakage coefficient
- proportionality factor analogous to the 1-D analysis

In practice, the influence of the magnitude of the natural gradient was investigated by estimating the value of the prescribed head on one or more segments of the boundaries. Boundary conditions may be considered as a system parameter, just as the hydraulic conductivity, etc.

The hydraulic conductivity was estimated only in the case of anisotropic conditions. What effectively is estimated in this case is the ratio  $K_{\max}/K_{\min}$  (or one of  $K_{\min}$  and  $K_{\max}$  only) and the direction of  $K_{\max}$ .

The flow porosity in this type of model is basically a scale factor for the velocity in any point in the system. In an isotropic system, the porosity is linearly related to the hydraulic conductivity, and only one of them (or the ratio) can be estimated. In an anisotropic system, porosity may be used as a scaling factor for both  $K_{\max}$  and  $K_{\min}$ , and thereby effectively enabling estimation of the ratio  $K_{\max}/K_{\min}$ . If the porosity is held fixed in an isotropic system, it is implied that either  $K_{\max}$  or  $K_{\min}$  is considered known. It should be noted that this choice of approach is rather subjective. One may, of course, estimate all parameters at once, and obtain individual values of  $K_{\max}$ ,  $K_{\min}$ , and the angle of  $K_{\max}$ . However, it is felt that there in general is beneficial to reduce the number of parameters describing a system, and that estimation of individual values rather than the ratio will not give any additional information about the system.

For calculations involving leakage only the ratio  $K'/B'$ , called the leakage coefficient, was used as an estimation parameter.

It should be pointed out that only concentration data are used for the inverse analysis. In principle, one should also include the measured steady-state head data in the sampled borehole sections in the analysis. However, in this case simulated and measured heads (head differences between boreholes) are only checked in a qualitative manner.

The sensitivity matrix,  $\mathbf{X}$ , requires also here some modification for multiple observation data sets, although in a somewhat more straight-forward manner than for the 1-D analysis with sorbing tracers. In this case, the sensitivities for each data set (borehole) are simply stacked on top of each other in the sensitivity matrix. In contrast to the 1-D analysis with multiple tracers, all elements in the sensitivity matrix have non-zero entries. For a simplified case assuming flow porosity and longitudinal dispersivity as the only parameters, and observation data from two boreholes, the matrix becomes:

$$\mathbf{X} = \begin{bmatrix} \frac{\partial C_1}{\partial p} & \frac{\partial C_1}{\partial a_L} \\ \frac{\partial C_2}{\partial p} & \frac{\partial C_2}{\partial a_L} \\ \cdot & \cdot \\ \frac{\partial C_m}{\partial p} & \frac{\partial C_m}{\partial a_L} \\ \frac{\partial C_{m+1}}{\partial p} & \frac{\partial C_{m+1}}{\partial a_L} \\ \cdot & \cdot \\ \frac{\partial C_{m+n}}{\partial p} & \frac{\partial C_{m+n}}{\partial a_L} \end{bmatrix} \quad (3-15)$$

The regression analysis in this case uses  $m$  observation data points from one borehole, and  $n$  data points from the other.

## **RESULTS AND INTERPRETATION**

### 4.1

#### **GENERAL**

The breakthrough curves of the 19 different tracers injected show very different shapes and irregularities, some of them are easy to explain while others are more difficult to understand. Tracers were detected in both the withdrawal borehole BFI02 and in the two observation boreholes, KFI06 and KFI11. Comments on the breakthrough curves are given for each borehole and each injection in Appendix B, Section 4. Appendix B also contains a classification of the tracers based on the breakthrough data.

In general, the hydraulic conditions have been stable during the experiment as shown by the graphs of the groundwater levels and hydraulic heads, see Appendix B, although there are some indications of leakage from the lower parts of Zone 2. Hence, differences in breakthrough curves of different tracer injections are not likely to be a result of transient hydraulic conditions.

During the experiment, a very fast and distinct transport was generally found between the injection borehole BFI01 and observation borehole KFI11, see Figure 4-1. Such fast breakthrough would not be expected from the geometry of the experiment as the distance between BFI01 and KFI11 is almost the same as the distance between BFI01 and BFI02. However, based on the results from the radially converging tracer experiment /Gustafsson et al., 1990/, /Gustafsson & Nordqvist, 1993/, where tracers were injected in the same intervals in BFI01 and KFI11, it was not surprising to find good hydraulic connections in the direction of KFI11.

Since no pumping, except for the small sample volumes, was made in KFI11 and KFI06 during the dipole experiment, these breakthrough curves may be seen as mainly 1-D single flow paths in the flow field between BFI01 and BFI02, see Figures 4-1 and 4-2. The very fast transport to KFI11 indicates that the main flow is diverted towards KFI11 instead of directly between BFI01 and BFI02. The curves also show a second peak at about 60 hours as a result of the re-circulation of tracer. Further peaks may not be distinguished as the dilution and dispersion levels out the concentration. Notable is also the relatively slow transport to borehole KFI06 with mean travel times of 5-600 hours, see Figure 4-2.

The tracer breakthrough in the pumping hole BFI02 represents a sum of all flow paths in the dipole field. This can be seen in the breakthrough curves which are much more diluted, delayed and dispersed compared to KFI11, see Figure 4-1.

The strongly sorbing tracers injected in injections no. 4 and 5 were not observed in any of the boreholes. Hence,  $^{99m}\text{TcO}_4^-$ ,  $^{58}\text{Co}^{2+}$ ,  $^{86}\text{Rb}^+$ , and  $^{201}\text{Tl}^+$  were either completely sorbed or delayed so much that detection was impossible. Sorption of  $^{99m}\text{TcO}_4^-$  is further discussed in Section 5.1.

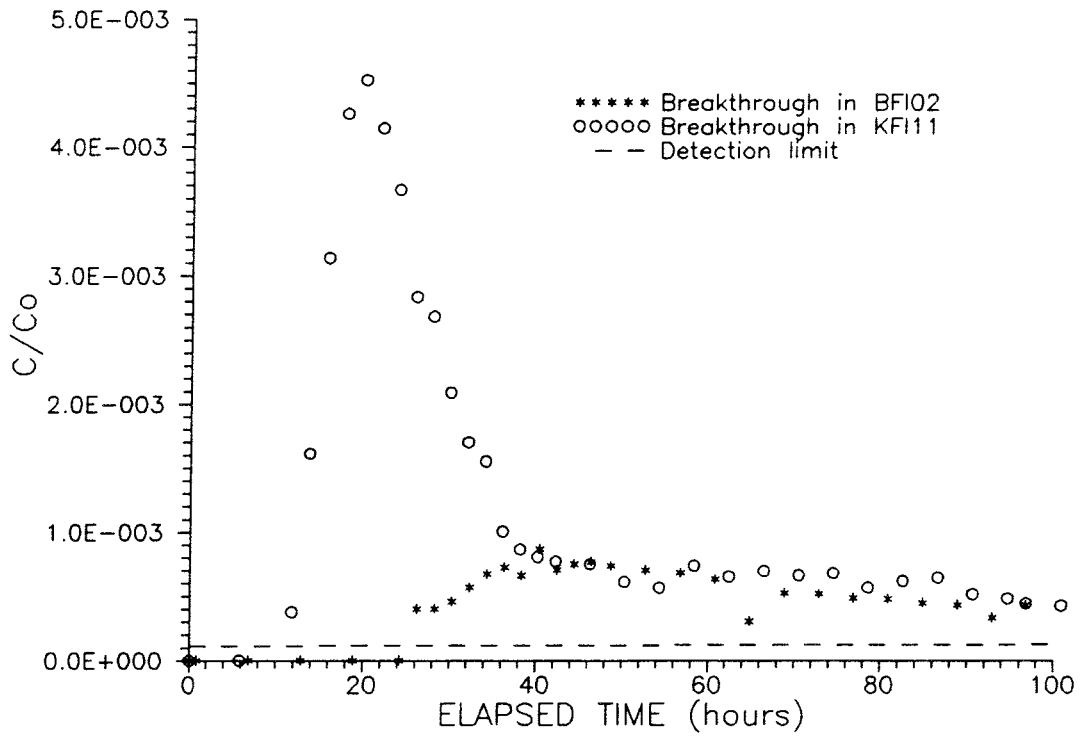


Figure 4-1. Breakthrough of  $^{169}\text{Yb-EDTA}$  (run no. 7) in observation borehole KFI11 and pumping hole BFI02.

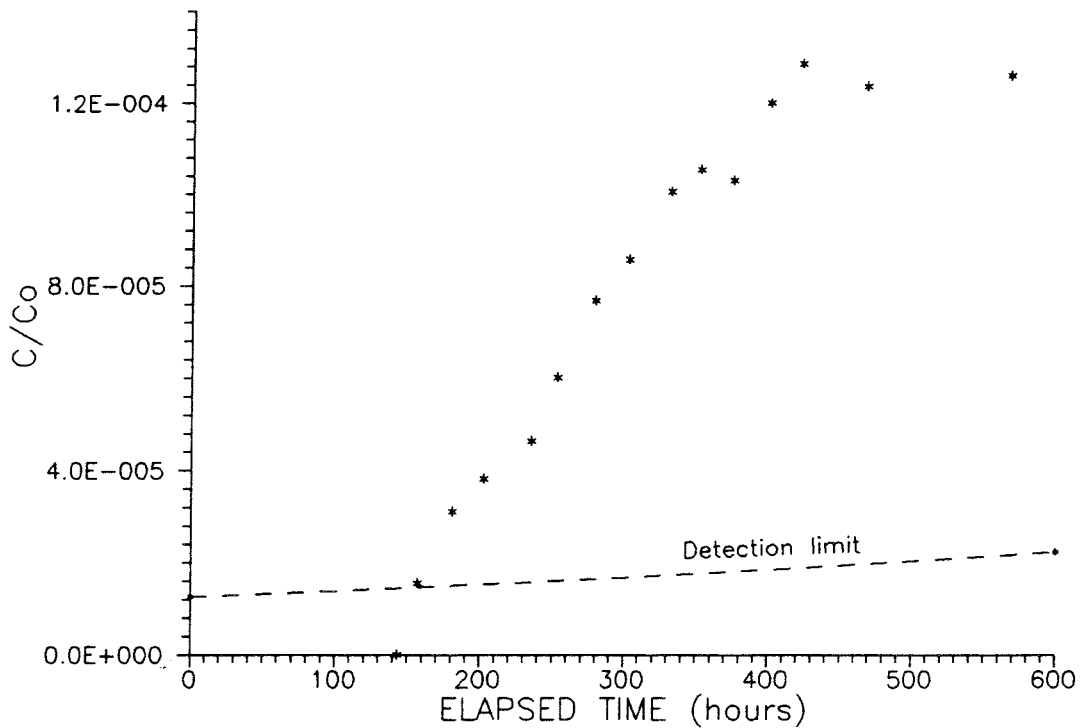


Figure 4-2. Breakthrough of  $^{169}\text{Yb-EDTA}$  (run no. 7) in observation borehole KFI06.

## 4.2 RESULTS OF 1-D MODELLING

The 1-D analysis was performed for three different transport routes:

- from BFI01 to KFI11
- from BFI01 to KFI06
- from KFI11 to BFI02

In general, tracer injection was modelled by a summation of solutions obtained by applying step-input concentrations of finite time duration as upper boundary condition (see eq. 3-10 to 3-11). The actual initial injection period (4 minutes), decaying tracer concentration in the injection section after the initial period, and effects of re-circulation of the breakthrough in BFI02, was modelled in this way.

For each injected tracer, inverse modelling was carried out on the breakthrough curve as if the tracer was a single solute. In the case of  $^{131}\text{I}^-$ , for which more than one injection was done, the entire time series was evaluated as well as each injection separately.

In addition, sorbing tracers were evaluated along with simultaneously injected non-conservative tracers, according to the procedure described in Section 3.4.4.

The one-dimensional modelling was performed with special emphasis on the uniqueness of the estimated model parameters, as described in Section 3.4.1. All inverse modelling results presented in Appendix A together with the regression statistics.

### 4.2.1 Transport between BFI01 and KFI11

The modelling of the transport between BFI01 and KFI11 included 20 model simulations, summarized in Table 4-1 below. The results show that the transport between BFI01 and KFI11 can be well described by a single flow path model. The regression statistics display high correlation coefficients, small standard errors and low correlation between the fitting parameters ( $v$ ,  $D$ , and  $f$ ) for most of the model simulations, c.f Appendix A. Consequently, all model runs of the breakthrough in KFI11, except one, are judged as acceptable or good.

Table 4-1 and Figure 4-3 also shows that the variation in residence times and dispersivities is small for the non-sorbing tracers ( $^{82}\text{Br}^-$ ,  $^{186}\text{ReO}_4^-$ ,  $^{131}\text{I}^-$ ,  $^{169}\text{Yb}^-$ -EDTA, and  $^{58}\text{Co}$ -EDTA).  $^{140}\text{La}$ -DOTA,  $^{177}\text{Lu}$ -DOTA and Rhodamine WT are weakly sorbing and are markedly delayed, see Figure 4-4.  $^{51}\text{Cr}$ -EDTA,  $^{111}\text{In}$ -EDTA, and In-EDTA (stable) also shows minor delays. Some of the tracers, e.g.  $^{24}\text{Na}^+$  and  $^{160}\text{Tb}$ -EDTA, are not delayed but shows lower peak values and less recovery than others, see Figure 4-3. This is further discussed in Appendix B.

Table 4-1. One-dimensional model simulations of the transport between BFI01 and KFI11 during the dipole tracer test.

Transport path	Tracer	Run	$t_0$ (h)	D/v (m)	f	Class*	
BFI01-KFI11	$^{82}\text{Br}^-$	1	22.8	13.5	1.07	2	
		6	23.2	8.4	0.99	3	
	$^{186}\text{ReO}_4^-$	2	24.1	8.9	0.83	2	
		6	22.8	8.6	0.87	3	
	$^{131}\text{I}^-$	3	22.9	7.7	1.15	3	
		6	22.5	7.1	0.75	3	
		3+6	22.8	7.8	1.01	3	
	$^{24}\text{Na}^+$	6	22.5	6.3	0.50	2	
	$^{140}\text{La}$ -DOTA	7	33.1	19.7	0.93	2	
	$^{177}\text{Lu}$ -DOTA	7	44.0	29.3	0.91	2	
	$^{51}\text{Cr}$ -EDTA	7	24.6	11.4	0.86	3	
	$^{111}\text{In}$ -EDTA	7	24.7	11.6	1.02	2	
	$^{160}\text{Tb}$ -EDTA	7	22.2	10.8	0.44	2	
	$^{169}\text{Yb}$ -EDTA	7	22.8	8.8	1.11	3	
	$^{58}\text{Co}$ -EDTA	8	22.9	8.3	0.62	3	
	Rhodamine WT	A		30.6	23.4	1.26	1
		E		40.6	23.6	0.93	2
	In-EDTA	C		27.4	16.6	0.25	2
	Gd-DTPA	D		22.7	8.4	0.38	3
	Tm-EDTA	D		23.4	11.2	0.42	3
<b>Mean value (standard deviation)**</b>			<b>22.8 (0.21)</b>	<b>8.1 (0.59)</b>			

\* Classification of model: 1=poor, 2=acceptable, 3=good

\*\* Based only on non-sorbing tracers (Br, Re, I, Yb, Co) with classification 3.

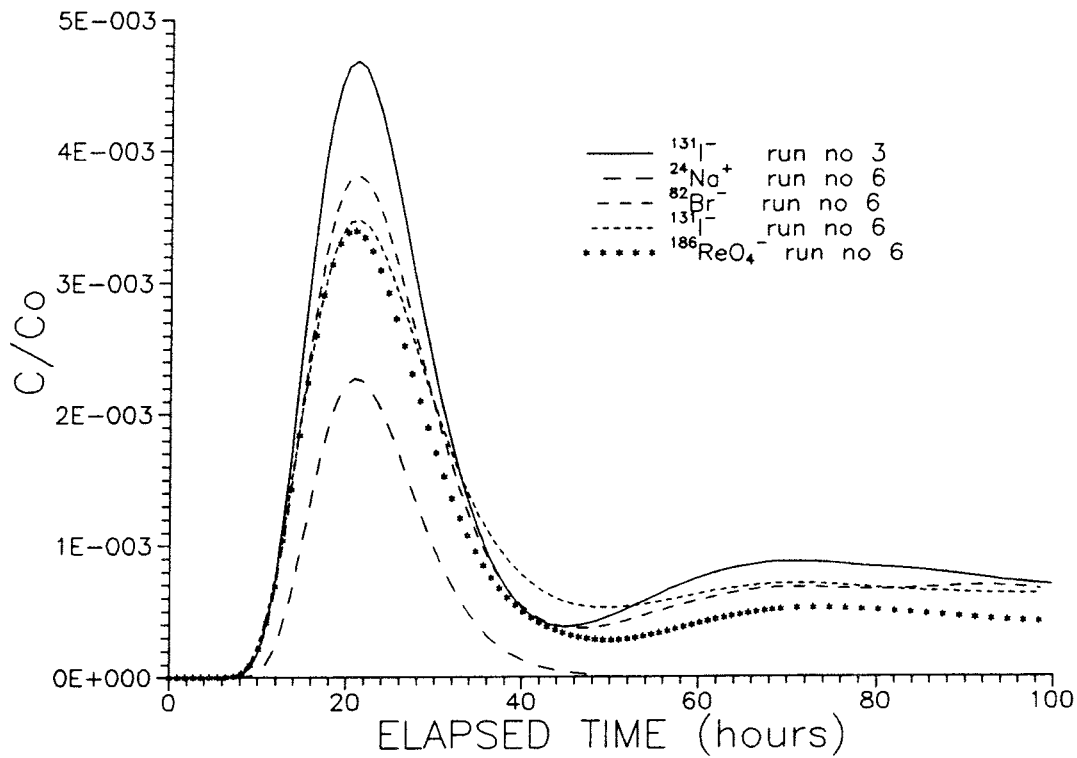


Figure 4-3. Comparison of simulations of tracer breakthrough in KFI11 for non-sorbing tracers (injections 3 and 6). Fits to experimental data is presented in Appendix A.

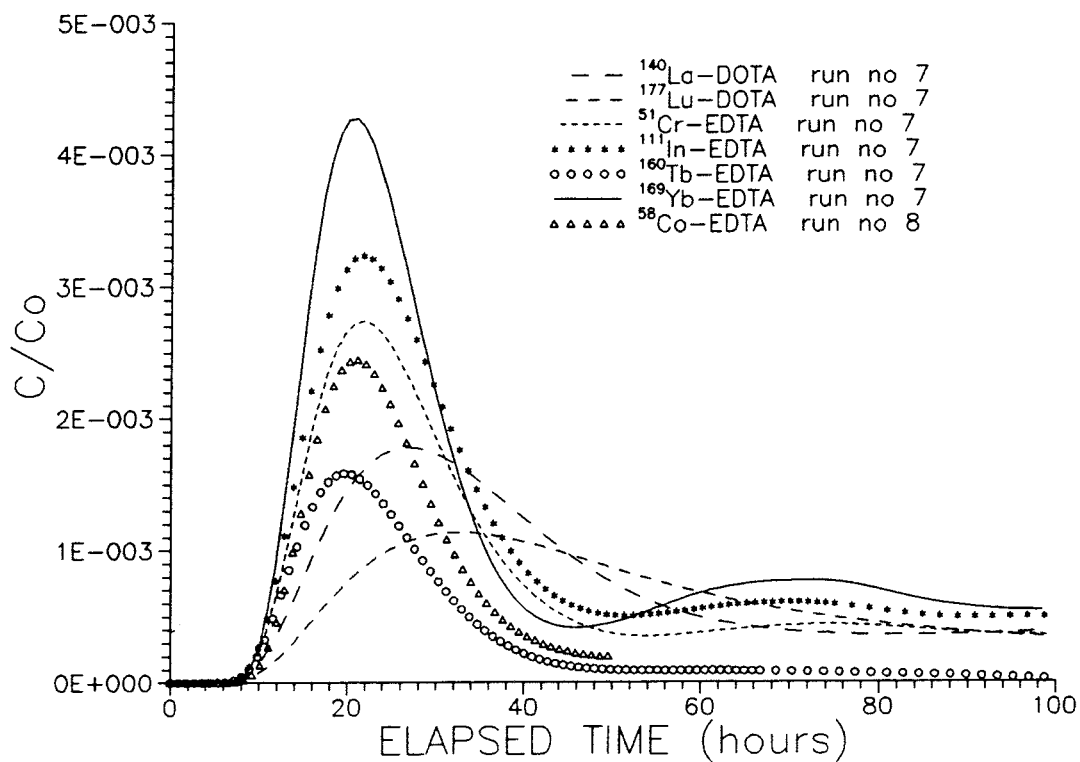


Figure 4-4. Comparison of simulations of tracer breakthrough in KFI11 for non-sorbing and weakly sorbing tracers (injection 7). Fits to experimental data is presented in Appendix A.

The simulations also included parameter estimation using 2 or 3 breakthrough curves simultaneously for determination of retardation coefficients for the sorbing tracers, see Table 4-2. A weighing factor was applied during the regression calculations for the sorbed tracers to account for the loss of mass. This was made in two different ways, i) using the peak concentrations, and ii) using the f parameter as determined from the initial runs (Table 4-1).

Table 4-2 Model simulations of the transport between BFI01 and KFI11 for determination of retardation coefficients, R.

Tracers nonsorbing-sorbing	Weight=peak		Weight=f-parameter	
	r <sup>*</sup>	R	r <sup>*</sup>	R
<sup>131</sup> I <sup>-</sup> - Rhodamine WT	0.94	1.28	0.96	1.27
<sup>169</sup> Yb-EDTA - <sup>140</sup> La-DOTA	0.95	1.30	0.96	1.29
<sup>169</sup> Yb-EDTA - <sup>177</sup> Lu-DOTA	0.95	1.72	0.97	1.62
<sup>169</sup> Yb-EDTA - <sup>140</sup> La-DOTA - <sup>177</sup> Lu-DOTA	0.94	1.38 1.71	0.95	1.30 1.63

\* Correlation coefficient (least-square sum).

Using the f-parameter as weighing factor was found to give the best fits recognized by higher correlation coefficients and lower correlations between parameters, see also Appendix A. An example of a simultaneous fit of three curves using the f-parameter as weighing factor is presented in Figure 4-5.

Although regression statistics show low estimation errors and low correlation between parameters, other considerations indicate that the assumption of linear, reversible sorption is not correct. This may be interpreted from Figure 4-5, where all tracers are forced to have the same advection parameters (average water velocity, Peclet number), but both sorbing tracers show systematic model errors in the tailing parts. In addition, a comparison of ratios of estimated f-parameters for each tracer (from individual curves), and ratios of C<sub>0</sub>-values for each, indicate that sorption is not completely reversible.

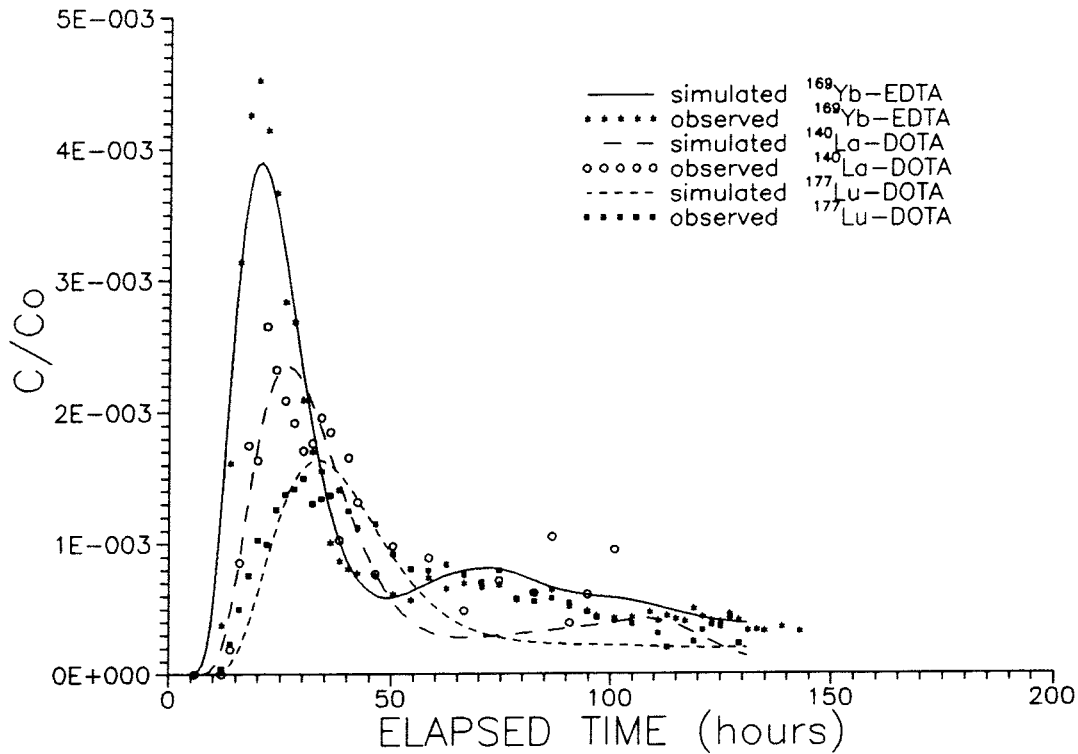


Figure 4-5. Simultaneous model simulation of breakthrough in borehole KFI11 for  $^{169}\text{Yb-EDTA}$ ,  $^{140}\text{La-DOTA}$ , and  $^{177}\text{Lu-DOTA}$ .

#### 4.2.2 Transport between BFI01 and KFI06

The breakthrough in KFI06 is markedly delayed compared to KFI11. The long residence times only enabled detection of the rising part of the breakthrough curves. These model simulations are therefore more ambiguous and consequently classified as being poor with the exception of Rhodamine WT which was monitored during a longer time interval, see Table 4-3.

Table 4-3. One-dimensional model simulations of the transport between BFI01 and KFI06 during the dipole tracer test.

Transport path	Tracer	Run	$t_b$ (h)	$D/v$ (m)	$f$	Class*
BFI01-KFI06	$^{131}\text{I}^-$	3	368	15.0	0.40	1
	$^{51}\text{Cr-EDTA}$	7	514	24.9	0.41	1
	$^{169}\text{Yb-EDTA}$	7	625	51.2	0.77	1
	$^{58}\text{Co-EDTA}$	8	481	27.7	0.27	1
	Rhodamine WT	A	622	22.8	0.27	2

Table 4-3 and Figure 4-6 also show that  $^{131}\text{I}^-$  is transported faster than the other tracers and displays a steeper rising part of the breakthrough curve.

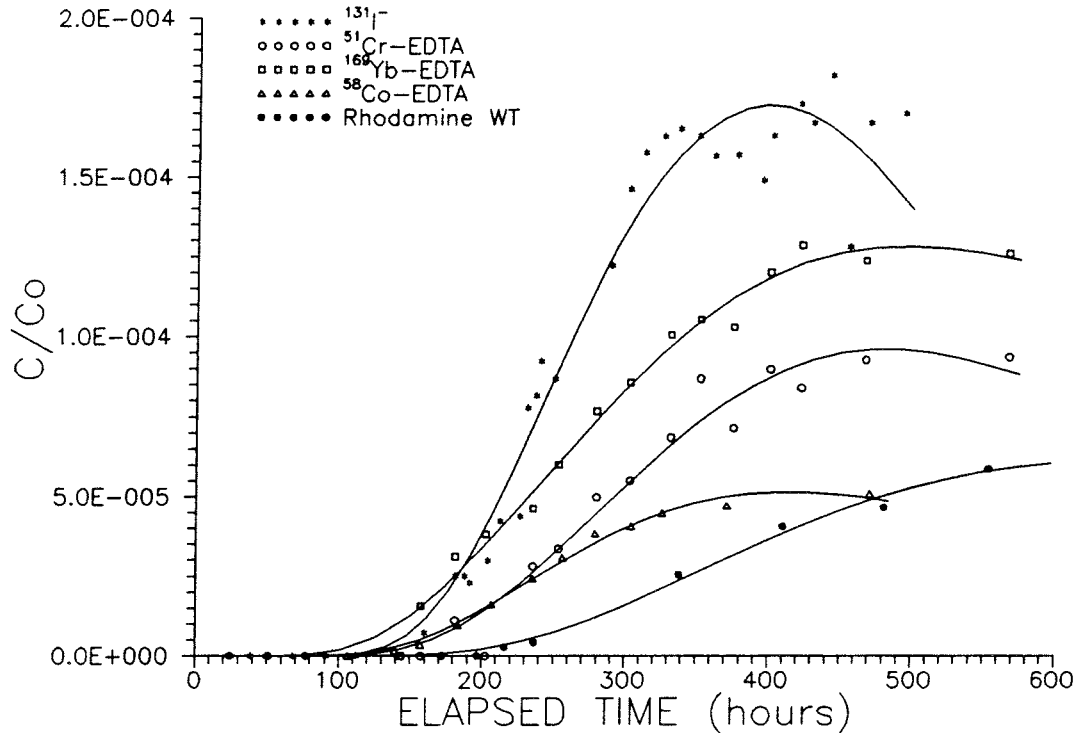


Figure 4-6. Comparison of tracer breakthrough in borehole KFI06. Solid lines represent best fit for regression estimates.

Figure 4-6 indicates that Rhodamine WT and  $^{51}\text{Cr-EDTA}$  are weakly sorbing as also indicated in KFI11.  $^{169}\text{Yb-EDTA}$  and  $^{58}\text{Co-EDTA}$  arrives approximately the same time as  $^{131}\text{I}^-$  but the peaks seem to be delayed. However, as only a few original data from the peak of  $^{131}\text{I}^-$  exist due to the interference with the second run of  $^{131}\text{I}^-$  (run no. 6) the Iodide data are somewhat uncertain after about 350 hours of elapsed time. The data from 350 hours to 500 hours were determined by subtraction of the data from run no.6 by assuming the same breakthrough as in run no.3. Thus, the model simulation of the peak is rather ambiguous.

No attempts were made to determine retardation coefficients based on breakthrough data from KFI06.

#### 4.2.3 Transport between KFI11 and BFI02

The transport between KFI11 and BFI02 has been described in two previous experiments, the combined interference test and tracer test /Andersson et al., 1989/ and the radially converging tracer experiment /Gustafsson & Nordqvist, 1993/. Both these experiments indicate that the transport cannot be described by a single path model. Therefore, also a two path model was considered.

The injection in KFI11 was made in the circulation system for "undisturbed" injection, also used in the radially converging experiment /Gustafsson et al., 1990/. In such a system the tracer is injected by dilution with the natural

groundwater flow, which means that a decaying injection function had to be applied. The results, summarized in Table 4-4 and presented in Figures 4-7 and 4-8, indicate that a single path model is not sufficient to explain the breakthrough curve. The two-path model is better but the tailing suggests that additional flow paths are needed to explain the complete breakthrough curve. Another possibility is that variations in the source term is not properly accounted for.

Table 4-4. One-dimensional model simulations of the transport between KFI11 and BFI02 during the dipole tracer test.

Transport path	Tracer	Run	$t_0$ (h)	D/v (m)	f	Class
KFI11-BFI02	$^{131}\text{I}^-$	9+10 one path	30.7	10.2	0.002	1
		9+10 two paths	29.4 120	5.5 65	0.001 0.005	1

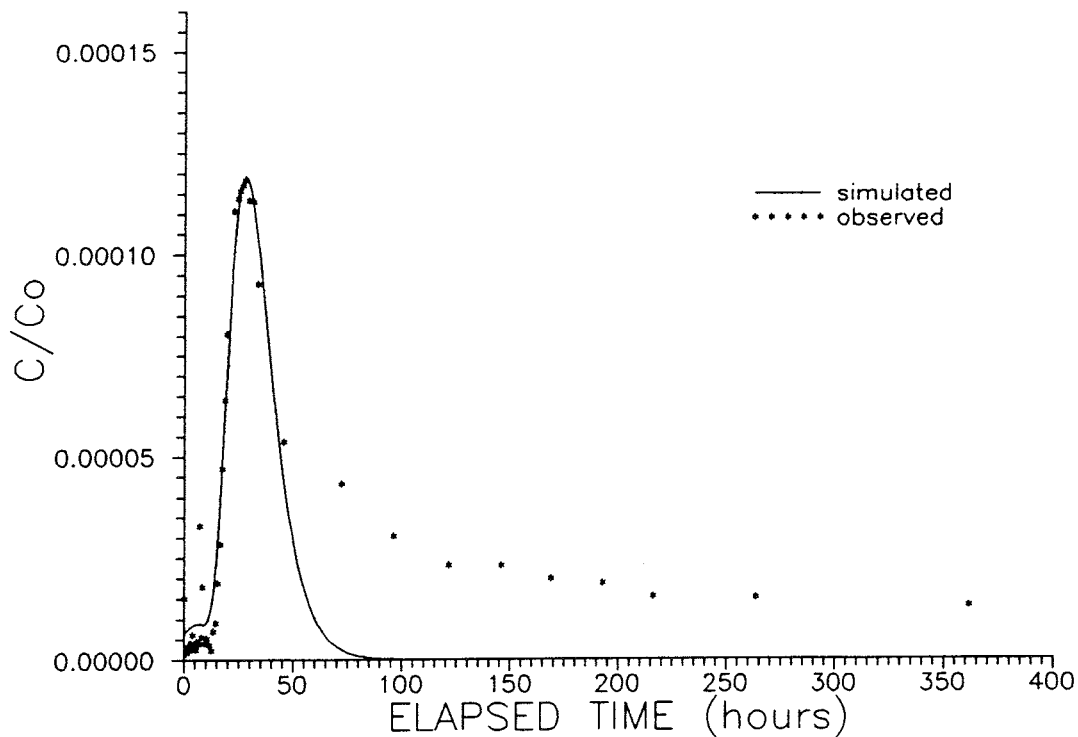


Figure 4-7. Simulation of tracer breakthrough of  $^{131}\text{I}^-$  in BFI02 from injection in KFI11 using a single path model.

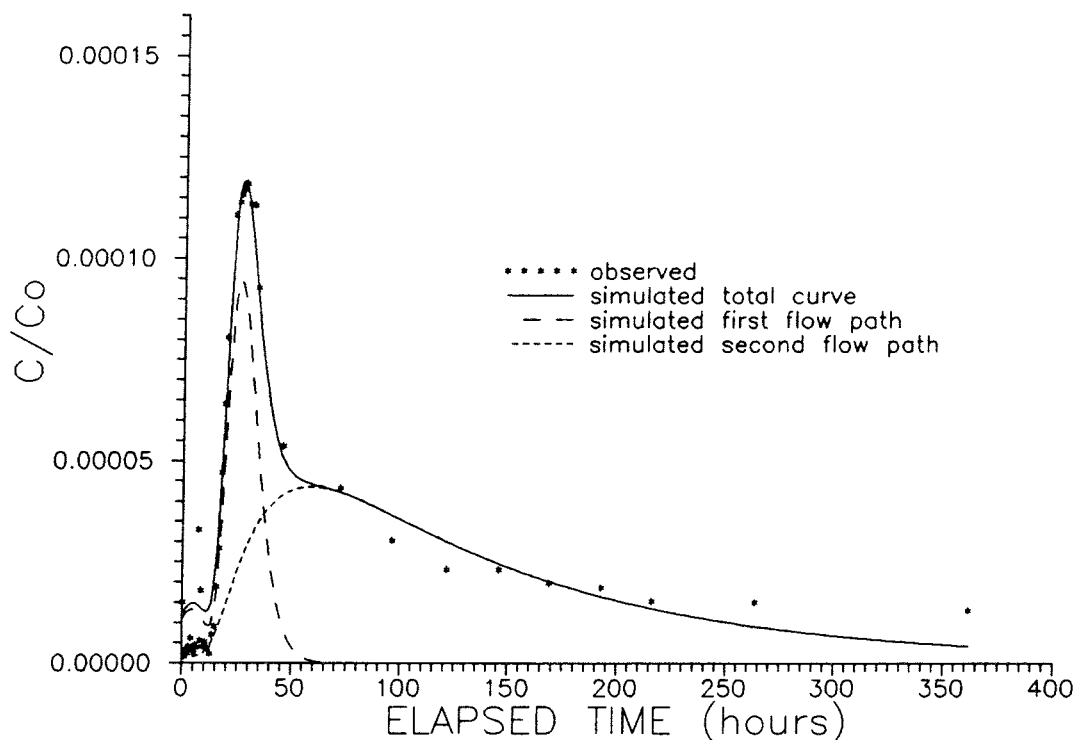


Figure 4-8. Simulation of tracer breakthrough of  $^{131}\text{I}^-$  in BFI02 from injection in KFI11 using a two path model.

### 4.3 ANALYSIS AND RESULTS OF 2-D MODELLING

#### 4.3.1 Flow Domain and Boundary Conditions

The flow domain considered for the 2-D analysis was generally defined so that the boreholes of interest (BFI01, BFI02, KFI06, and KFI11), as well as most of the theoretical dipole flow field would be included. For all inverse analysis, this amounted to an area 500 x 500 meters in size. The finite element mesh that was used for most simulations is shown in Figure 4-9, consisting of 2601 nodes and 2500 elements. Figure 4-9 also includes the locations of the boreholes.

The boundary conditions are defined so that a uniform hydraulic gradient across the flow domain is defined. For most simulations, the direction of the gradient is in the direction from BFI01 to BFI02, which is consistent with previous assumptions about the natural gradient in the zone. This is accomplished by specifying constant head along the boundaries "upstream" BFI01, and "downstream" BFI02, while the remaining boundaries parallel to the direction of the gradient are specified as no-flow boundaries.

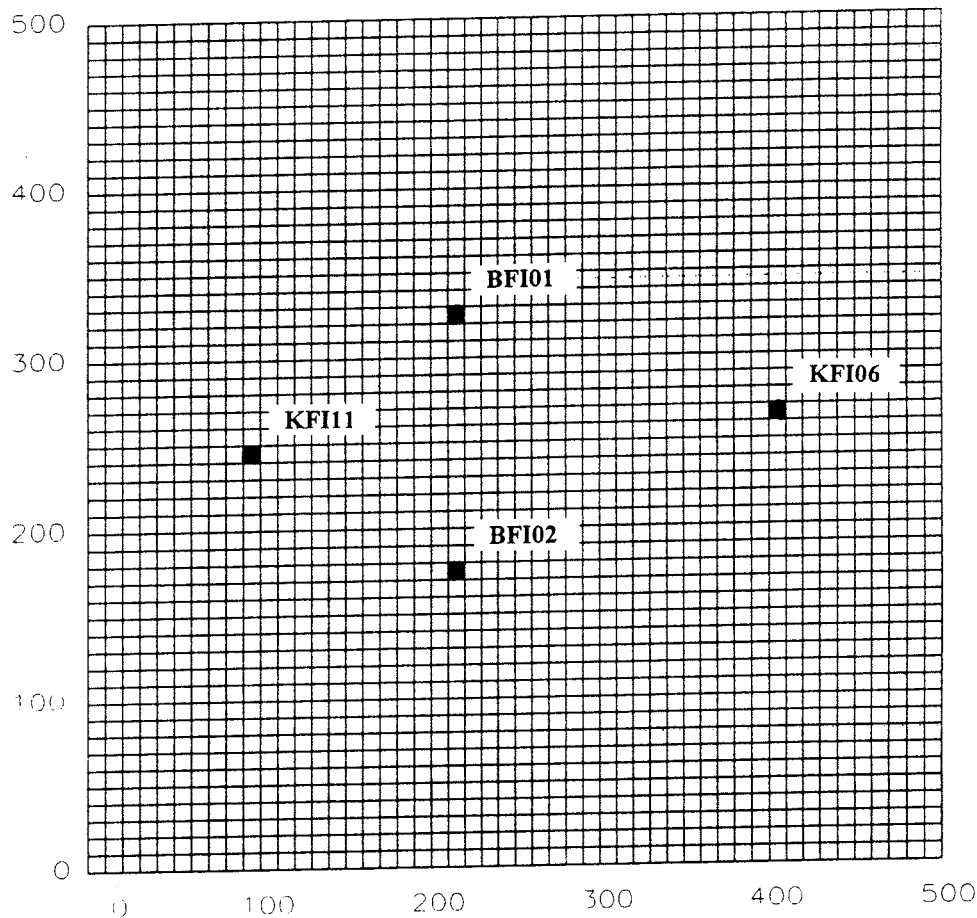


Figure 4-9. Finite element mesh used for the 2-D analysis.

#### 4.3.2 **Modelled Cases**

The simulation time steps are generally set to two hours. The initial pulse injection period of duration 4 minutes is simulated separately (with a unit inlet concentration), and the resulting concentration distribution is used as initial condition for the rest of the simulation. The re-circulation of the tracer from BFI02 into BFI01 is simulated by specifying the outlet concentration in BFI02 as the inlet concentration to BFI01, with a lag of one time step. Although this means that the time required to re-circulate is not represented exactly, the error from this should be insignificant. The 2-D analysis was carried out for only one of the injected tracers,  $^{131}\text{I}^-$ .

The 2-D inverse analysis can be divided into the following main cases:

- Isotropic fracture zone, fixed gradient direction
- Isotropic fracture zone, alternate gradient direction
- Anisotropic fracture zone, fixed gradient direction
- Anisotropic fracture zone, fixed gradient direction, vertical leakage

Thus, it was investigated to what extent the direction of the natural gradient and possible anisotropic condition in the fracture zone may explain the deviations from an ideal dipole flow field, regarding tracer transport in the zone. It should be repeated that the objective here is to explain all breakthrough curves with a single flow and transport model (although idealized), using reasonable assumptions that can be supported with independent information.

Each of the above cases are discussed separately below. The first case also includes a discussion of previously predicted breakthrough curves based on results from the radially converging tracer experiment /Nordqvist, 1988/, prior to any results from the dipole experiment being available, as the basic assumptions of isotropy and gradient direction are the same. Any discussion of parameter values and additional assumptions are discussed under each case.

#### 4.3.2.1 **Isotropic Fracture Zone, Fixed Gradient Direction**

A comparison and discussion of previous predictions /Nordqvist, 1988/, and the breakthrough in BFI02 has to some extent already been reported elsewhere /Andersson, 1993/. Such a comparison indicates that tracer transport between BFI01 and BFI02 actually is relatively well predicted, as can be seen in Figure 4–10. There is only a part of the tail that is not simulated accurately, for which a plausible explanation may be that vertical leakage around BFI02, as indicated by increasing salinity, was not accounted for in this prediction. Thus, if only two boreholes (injection and pumping) had been used for the experiment, which often is the case, this may have been considered a good model.

However, by extending the comparison to breakthrough data from KFI11 and KFI06 as well, it is apparent that the total transport pattern in the fracture is not predicted accurately. Comparisons of predicted and observed breakthrough for KFI06 and KFI11 are shown in Figures 4–11 and 4–12. The average tracer travel time is significantly over-estimated for KFI11, and significantly underestimated for KFI06. In addition, the peak values of tracer concentration are very different from the observed ones.

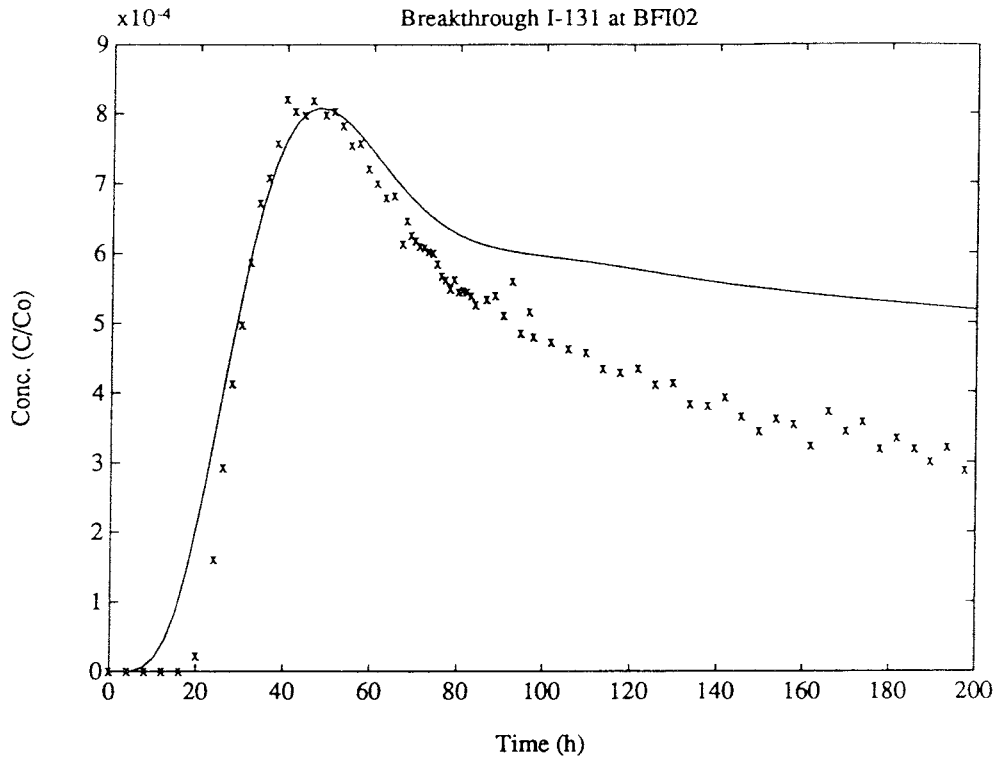


Figure 4-10. Comparison of predicted (solid line) and observed breakthrough in BFI02.

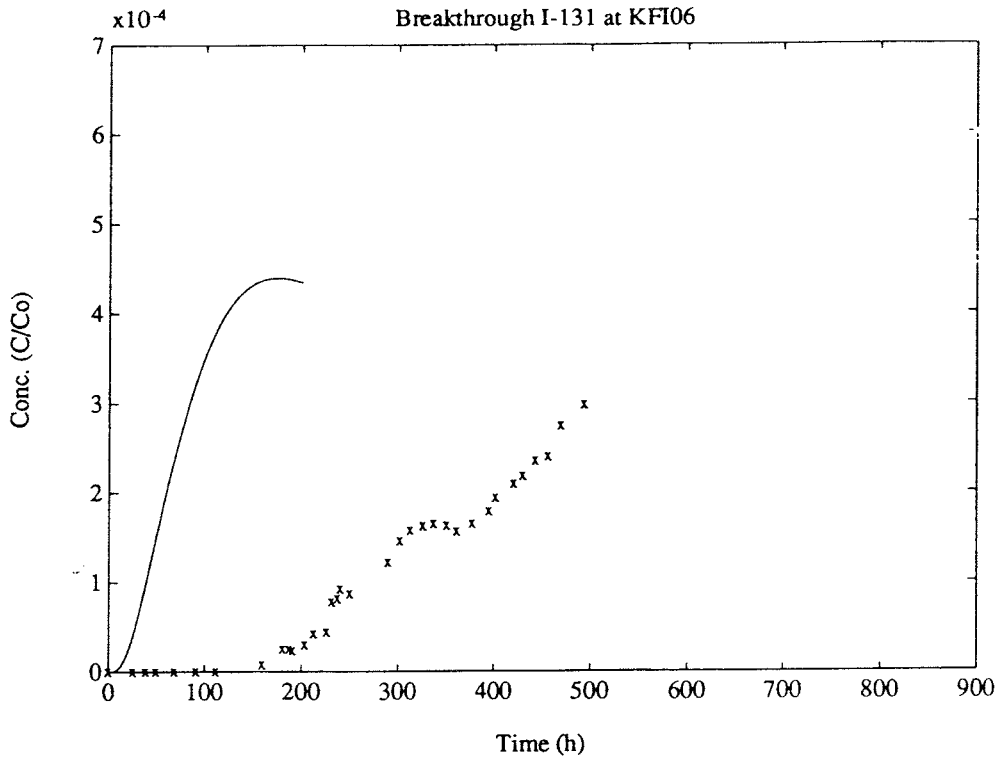


Figure 4-11. Comparison of predicted (solid line) and observed breakthrough in KFI06.

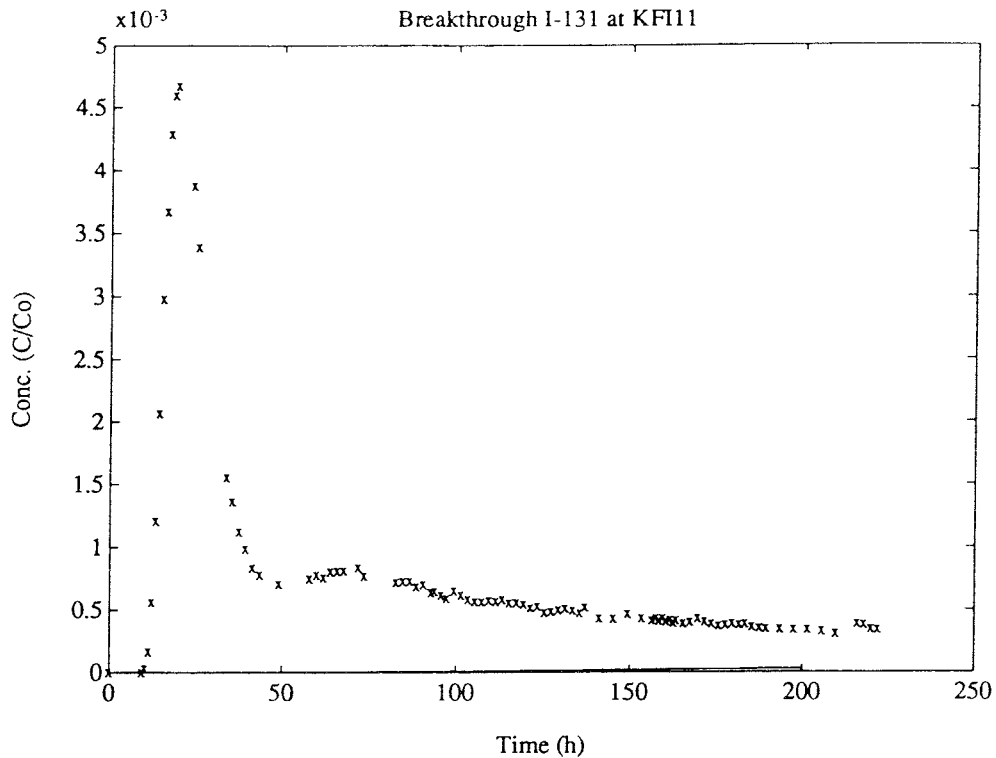


Figure 4-12. Comparison of predicted (solid line) and observed breakthrough in KFI11.

Such apparently irregular transport patterns is entirely consistent with recent notions on the effects of structural heterogeneity on transport. The transport during the dipole experiment may thus be attributed to some irregular flow connectivity pattern, created by the injection and pumping of water, in BFI01 and BFI02 respectively.

However, before concluding that the transport only can be explained by some assumptions of spatial heterogeneity, described by statistical parameters, one should show that no other idealized (deterministic) descriptions of the fracture zone also will explain the highly varying tracer arrival in the boreholes. It should again be pointed out that any considered attributes of the fracture zone that may explain tracer transport should be supported by independent data or interpretations, otherwise any analysis will only be a curve-fitting exercise without providing possibilities for a meaningful interpretation.

For the completeness of this analysis, the parameter values used for the predictions mentioned above were updated by inverse modelling. To begin with, this was done for BFI02 only, introducing a dilution factor in the sampling section, estimated from salinity measurements, as a crude approximation of an effect of leakage in the vertical direction towards the zone. This dilution factor was set to 0.8 based on salinity measurements. The estimated parameters were then porosity, longitudinal dispersivity and a proportionality factor. Estimation of the proportionality factor may actually be omitted, as the magnitude of the concentration in theory already is

simulated by the model (since  $C/C_0$  is used as observation data). Allowing estimation of this parameter is equivalent to accepting that some model error in the injection representation most likely exists.

The results from the inverse simulation in this case generally verified what was hypothesized above, that differences between predicted and observed breakthrough in BFI02 may very well be explained by introducing this crude representation of leakage in the vertical direction.

Next, the analysis was repeated adding observation data in KFI11 as well. Thus, parameter estimation on two data sets was carried out simultaneously. As expected, the results clearly showed that this flow model basically should be rejected, as a best-fit exercise did not give plausible results even when using only two of the three observation boreholes.

In summary, the tracer breakthrough data in BFI02, KFI11, and KFI06, may not be explained by a single flow and transport model that assumes homogenous isotropic hydraulic conditions and a uniform gradient directed from BFI01 to BFI02. The only mechanisms other than a heterogeneous hydraulic system that may be considered in order to modify this simple model, and that to different extent will change the flow direction, are the direction of the hydraulic gradient and anisotropic hydraulic conditions.

#### 4.3.2.2 **Isotropic Fracture Zone, Alternative Gradient Direction**

The generally reported direction and magnitude of the hydraulic gradient is based on measurements in the existing boreholes in the zone, which means that the areal coverage of measurements is relatively limited. Thus, the actual natural gradient may in reality be significantly different than what is usually assumed. As far as hypothesizing how the gradient should be changed in order to explain data better, it appears clear that it should be directed more towards KFI11, seen from BFI01, than towards BFI02.

In principle, one may estimate the direction of the gradient from the tracer test results, as any other parameter in the system by, for example, expressing it as angle from some defined coordinate axis. However, with this kind of discretized model, the practical difficulties are considerable. One method to accomplish this may be to consider the prescribed head condition in all four corner nodes to be parameters to estimate, with boundary heads defined to vary linearly between the corner nodes. However, in this analysis, uncertainty in gradient direction is simply analyzed by using a pre-determined direction change and estimate all other parameters. The parameters that were actually estimated, for a given gradient direction, were porosity, longitudinal dispersivity, magnitude of hydraulic gradient, and the proportionality factor, thus a total of four parameters. Again, a dilution factor of 0.8 was assumed. Observation data from BFI02 and KFI11 was used simultaneously for estimation.

The results from this inverse simulation is shown in Figure 4-13. The direction of the gradient was in this run defined as more or less exactly in the direction of KFI11 from BFI01, a change of about 90 degrees compared

to the documented direction. Figure 4-13 clearly shows that a change in gradient direction only will not contribute to an improved model. Although tracer breakthrough in KFI11 is simulated approximately, breakthrough in BFI02 is not simulated well. One may comment on the estimation results in this case that it seems not unlikely that multiple minima in least-square space exists, and that one just as well would be able to fit breakthrough in BFI02 better by using different starting parameter values. In that case, breakthrough in KFI11 would be fitted less well to the model. In other words, the estimation problem is ill-conditioned in this case, in spite of relatively acceptable regression statistics.

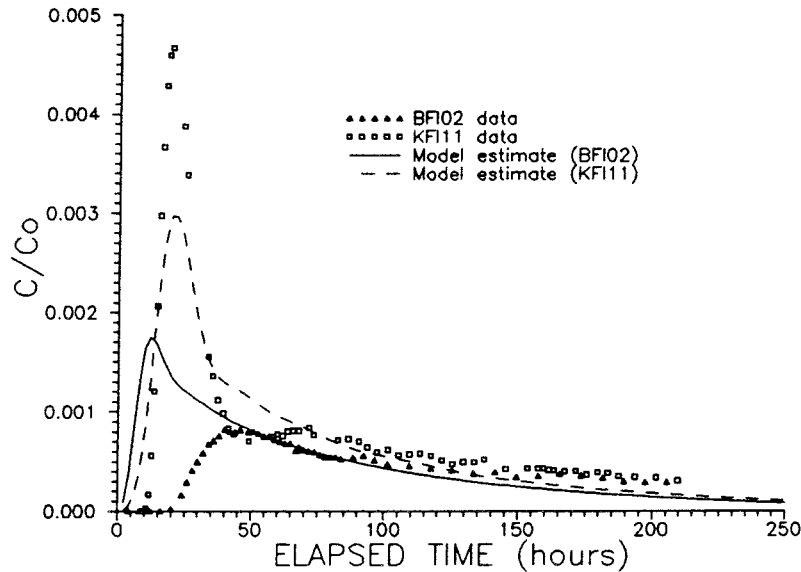


Figure 4-13. Results of estimation using data from BFI02 and KFI11 simultaneously, assuming isotropic hydraulic conditions and an alternative natural gradient direction.

The analysis in this case was simply aimed at hypothesizing the case that would give a maximal effect, as far as re-routing the main flow in the direction of KFI11 from BFI01. An independent interpretation of the uncertainty of the gradient direction based on measured head data is that such a large change in gradient seems unlikely, which confirms the already developed conclusion that a change in the natural gradient will not give a better flow and transport model.

#### 4.3.2.3 Anisotropic Fracture Zone, Fixed Gradient Direction

Supported by previous geological interpretations of the fracture zone /Andersson et al., 1989/, it may be hypothesized that anisotropic hydraulic conditions may prevail. This has not been tested in any earlier analyses of flow and transport experiments in the zone, except for some limited analysis of drawdown data from the interference tests /Andersson et al., 1989/.

The estimated parameters in this case were porosity, the direction of maximum hydraulic conductivity, the value of the minimum hydraulic

conductivity, the hydraulic head at the "upstream" boundary, and the proportionality factor. The direction of maximum hydraulic conductivity is expressed as the angle counter-clockwise from the x-direction. The value of the maximum conductivity was fixed at a value of  $3 \times 10^{-3}$  m/s. Naturally, the value of  $K_{\max}$  is also unknown in this case, but the used value is of the same magnitude as was interpreted in earlier analyses, /Andersson et al, 1989/. As mentioned in section 3.4.5, what is effectively estimated is the ratio  $K_{\max}/K_{\min}$ . In contrast to the previous simulations, the longitudinal dispersivity was set to a constant value. It was found during some preliminary runs, with anisotropy, that the value of this parameter did not have a significant impact on the interpretation of the regression results. As this model is more complex than the previous ones, there is a general interest of reducing the number of parameters to be estimated.

In this case, data from all three boreholes were used simultaneously for estimation. The data from KFI06 was cut off at approximately 470 hours, as effects from the following injection of I-131 (injection no. 6) could be noticed, and this second injection was not included in the model. In addition, the breakthrough curves for BFI02 and KFI11 was thinned by removing every other point in the tail of the curves. This was done in order to somewhat balance the contribution of each curve to the least square sum in the regression algorithm. Ideally should additional steps be taken to balance this, for example by applying weights so that the peak value of each curve would be similar magnitude, but this was not done in this analysis.

The results of the inverse modelling in this case are shown in Figure 4-14, and it is clear that the agreement between data and model estimate is remarkably good. Main features of the curves, such as travel time, dispersive effects, and magnitude of the concentration values are explained by a single flow and transport model, using single values of the porosity, the dispersivity, and the hydraulic conductivity tensor. The values of the estimated parameters in this case are:

- porosity = 0.01
- $K_{\max}$  angle = 217.6 degrees
- $K_{\max}/K_{\min}$  = 8.3
- "upstream" hydraulic head = 8.16
- proportionality factor = 1.1

It may be noted that the value of the estimated porosity, although it basically serves here as scaling factor for velocity, is very similar to previously interpreted values, for example from the radially converging tracer experiment, /Gustafsson & Nordqvist, 1993/. The estimated angle of the maximum hydraulic conductivity is counter-clockwise from the x-direction (see Figure 4-1), which means that this direction is almost directly towards KFI11 from BFI01. The direction is very close to the strike direction of Zone 2 /Tirén, 1991/. Thus, it would suggest that the highest conductivity (or transmissivity) direction should be along the strike direction of the zone. This hypothesis also seems to agree with the geological character of Zone 2 /Tirén, 1991/, where the stepwise extension along the dip direction may decrease the connectivity in this direction, while the zone may be well connected along the strike direction /Andersson et al., 1993/. The

configuration of fracture sets in Zone 2 gives intersection lineations, "channels", in an approx. NW-SE direction, i.e. along the strike of the zone /Andersson et al., 1989/.

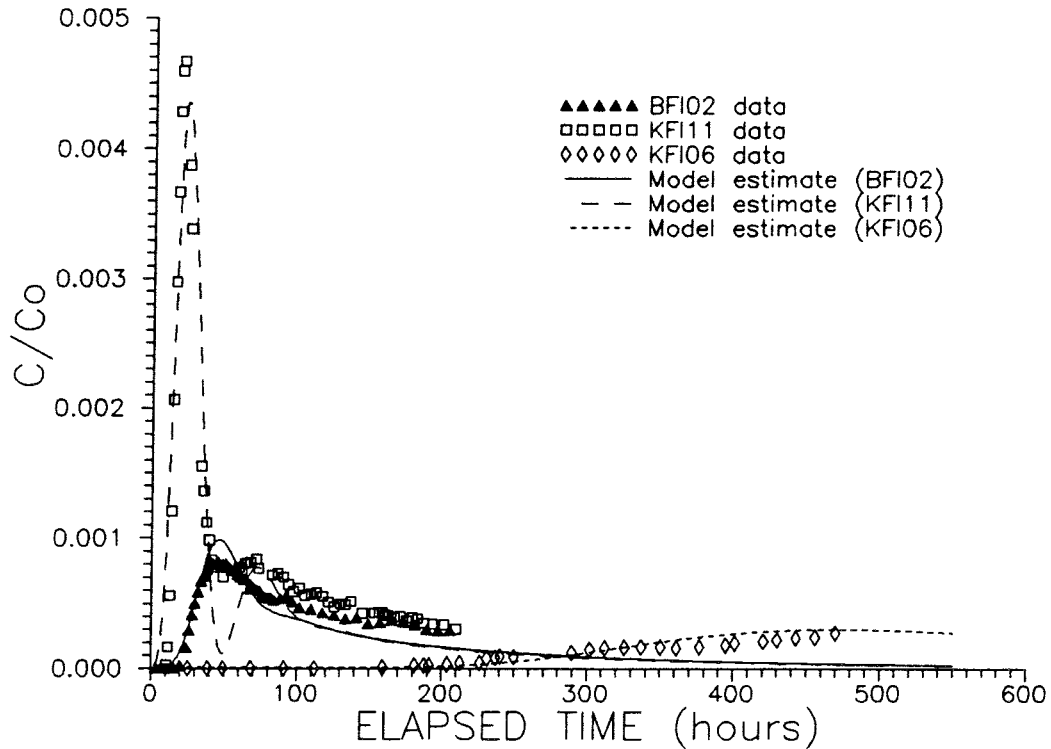


Figure 4-14. Results of estimation using data from all boreholes simultaneously, assuming anisotropic hydraulic conditions.

The estimated value of the proportionality factor is close to unity, as it should be, and confirms that the tracer injection is reasonably well accounted for by the model.

The only somewhat inconsistent result in this case is the estimated value of the hydraulic head at the "upstream" boundary. As the hydraulic head at the "downstream" boundary is set to 8.33, the results in this case would indicate that there actually is a small gradient (1/3000) in a direction opposite to what is normally assumed. However, this gradient is so small it is practically negligible, as far as having a major impact on the flow pattern. In addition, the regression statistics (standard error = 0.14) indicate that this parameter may just as well be equal to the "downstream" value, without affecting the goodness-of-fit of the model. Thus, the best-fit model indicates practically zero hydraulic gradient, in contrast to the measured gradient with a value of 1/300.

Although the estimated natural hydraulic gradient differs somewhat from the measured, it may be argued that this does not significantly affect the plausibility of the anisotropic model. The representation of the boundary condition is extremely simple in the model applied here. In reality, the

hydraulic heads along the entire boundary (all four sides) are unknown, and a slightly different representation of the boundaries may very well result in a model that more closely reproduces the measured gradient. More importantly, it seems unlikely that other boundary conditions will have a major impact on the interpretation that the major features of the overall tracer transport in the zone is remarkably well explained, supported by independent information, by the assumption of hydraulic anisotropy.

#### 4.3.2.4 **Anisotropic Fracture Zone, Fixed gradient Direction, Vertical Leakage**

Although the previous model apparently explains data relatively well, a less satisfying feature of all models applied for inverse analysis so far has been the inclusion of a dilution factor for the re-circulation of water, as a crude approximation of the indicated vertical leakage. A more conceptually appealing model would allow for aurally distributed leakage across the entire area, rather than an instantaneous loss of tracer during the re-circulation.

The simplest way to model aurally distributed vertical leakage (in or out of the zone) is to assume leakage through a semi-permeable layer, extending across the entire flow domain, where the amount of leakage is governed by an assumed value of the hydraulic head on the distant side of the layer, as expressed mathematically in equation 3-1. This introduces two additional model parameters; the leakage coefficient of the semi-permeable layer, which is the hydraulic conductivity divided by the thickness of the layer, and the hydraulic head value of the distant side of the layer. It should be pointed out the assumption of a semi-permeable layer also is a major simplification, since such a layer hardly can be defined precisely in this case, but that this is the simplest way to represent non-negligible flow through the surrounding rock towards the fracture zone.

For this inverse simulation, the value of the hydraulic head of the distant side of the semi-permeable layer was set to 8.8 m, approximately an average of the "upstream" and "downstream" boundary values. The selection of this value is somewhat arbitrary, since the thickness of the semi-permeable layer is a rather fictive one. The value is selected so that some leakage into the zone is simulated around BFI02, and some leakage out from the zone closer to BFI01.

As mentioned, no dilution factor for the re-circulation was assumed in this case. Further, the hydraulic gradient set to a fixed value (not estimated) of 1/500, in order to force the model to include a gradient of the same magnitude as the measured. Thus the model parameters that were estimated in this case were porosity, the leakage coefficient of the leaky layer, the angle of  $K_{max}$ ,  $K_{max}/K_{min}$ , and the proportionality factor.

The results of the inverse modelling are shown in Figure 4-15. The values of the estimated parameters are:

- porosity = 0.01
- leakage coefficient =  $1.2 \times 10^{-8} \text{ s}^{-1}$
- $K_{max}$  angle = 218.0 degrees

- $K_{\max}/K_{\min} = 8.3$
- proportionality factor = 1.04

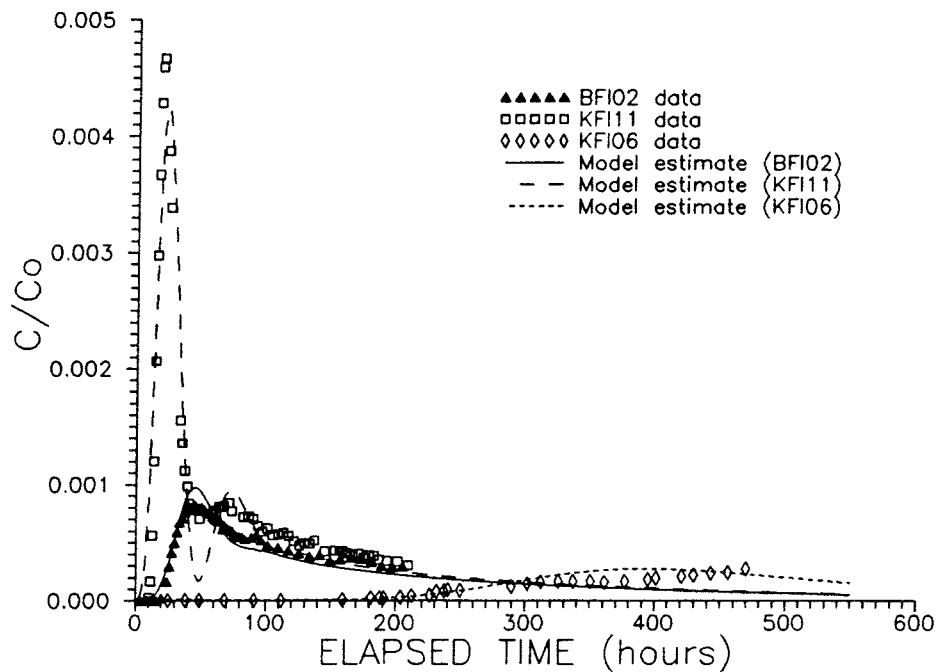


Figure 4-15. Results of estimation using data from all boreholes simultaneously, assuming anisotropic hydraulic conditions and aerially distributed vertical leakage.

Compared to Figure 4-14, the agreement between model and observed data is about the same, although a slight improvement may be seen in the tailing parts for BFI02 and BFI01. A slight improvement may also be seen in the regression statistics, where this inverse run have a slightly smaller sum of squared residuals ( $1.02 \times 10^{-5}$  compared to  $1.13 \times 10^{-5}$  for the previous case). However, by analyzing goodness-of-fit only, the improvement compared to the case without aerially distributed leakage is marginal.

It can also be noted that the estimated values are very similar to the ones in the case of no leakage. But more importantly, by introducing a very simple model of aerially distributed leakage, the somewhat dubious inclusion of a dilution factor for the re-circulation is avoided, while slightly improving the goodness-of-fit by the model. This conclusion is strengthened by the estimated value of the proportionality factor, which is closer to unity in this case (1.04 compared to 1.10). As mentioned, a value close to unity of this parameter indicate that the tracer injection is modelled approximately accurate.

It may be pointed out that the estimated value of the leakage coefficient,  $1.2 \times 10^{-8} \text{ s}^{-1}$ , is arrived at only by analyzing tracer data, and no hydraulic data in this case. Thus, the only phenomenon that governs the estimation of this parameter is dilution of the tracer in the fracture zone. The value arrived here may be compared to an independent estimate based on the results from the hydraulic interference tests /Andersson et al., 1989, Andersson et al., 1991/, using a similar type of simplified model for the leakage. From drawdown data in borehole sections along the entire thickness of Zone 2, the value of

the leakage coefficient was estimated to  $1 - 5 \times 10^{-8} \text{ s}^{-1}$ . Thus, both estimated values, based on entirely different type of data (head changes vs concentration), are very close to each other.

It has been mentioned that hydraulic head data was not utilized for the estimation of parameters. This may appear somewhat contradictory, as several of the estimated parameters may be considered as hydraulic parameters. However, the ratio of  $K_{\max}$  and  $K_{\min}$  and the direction of  $K_{\max}$  in combination with porosity, directly affects the areal distribution of tracer mass transport. Ideally, the measured head data would be used simultaneously with the tracer data in inverse modelling. In this case, assuming a fixed value of the thickness of the zone,  $K_{\max}$  would be estimated as well, since it is the transmissivity of the fracture zone that governs the hydraulic head distribution. Thus, the implication of assuming a fixed value of  $K_{\max}$  is, although breakthrough curves are well fitted by the model, that the calculated heads in the boreholes may not be accurately reproduced by the best-fit model based on tracer data only.

A qualitative check of the simulated hydraulic heads in the fracture zone, using the best-fit-model with aurally distributed leakage, was made by looking at the calculated flow field. Figure 4-16 shows a contour plot of the calculated head distribution across the area, which illustrates the distorted dipole flow field caused by the hydraulic anisotropy. It may be recalled that the prescribed value of the hydraulic head in the distant layer of the semi-permeable layer was set to 8.8 m. This means that there is an outflow of water (and tracer) from the upper left part of the flow domain, including KFI11, while there is an inflow of water in the lower right area, including KFI06, see Figure 4-16. Since water that flows out of the system does not re-enter it, the leakage causes some loss of tracer mass around BFI01, and dilution of tracer around BFI02. The calculated total net inflow of water from leakage in Figure 4-16 about 15 percent of the flow rate in the re-circulating system, of which most would be expected to enter the system close to BFI02. Thus, given the uncertainties associated with the simple leakage model, the calculated amount of leakage seems not to be unreasonable, with regard to leakage estimated from salinity measurements, see Section 4.1.5, Appendix B.

Measured head differences between BFI01, KFI11, KFI06 and BFI02 are approximately 2.74, 0.91, and 0.24 m, respectively. The corresponding simulated values are 4.70, 2.60, and 1.65 m. Except for that the simulated relation between the differences are the same, the values themselves are significantly different. One may envision several, relatively minor, changes of flow parameters that would cause the values to agree better. For example, an increase transmissivity values and an increase in the ratio between  $K_{\max}$  and  $K_{\min}$  would be likely to both decrease the overall magnitude of the differences in head between BFI02 and other boreholes, and also to affect the relation between the values. If the leakage is increased, the difference between the injection and boreholes would be decreased. Changing boundary conditions may also have an effect, especially on KFI06. Thus, in spite of the differences between the observed and simulated hydraulic head distribution, it is judged that the interpretation of the main features of the

flow system is not affected significantly. Although it would be interesting to also fit the head data better, for example the transmissivities in the system may be increased by a factor two without conflicting with interpretations from the interference tests /Andersson et al., 1989/, this option is not pursued further here.

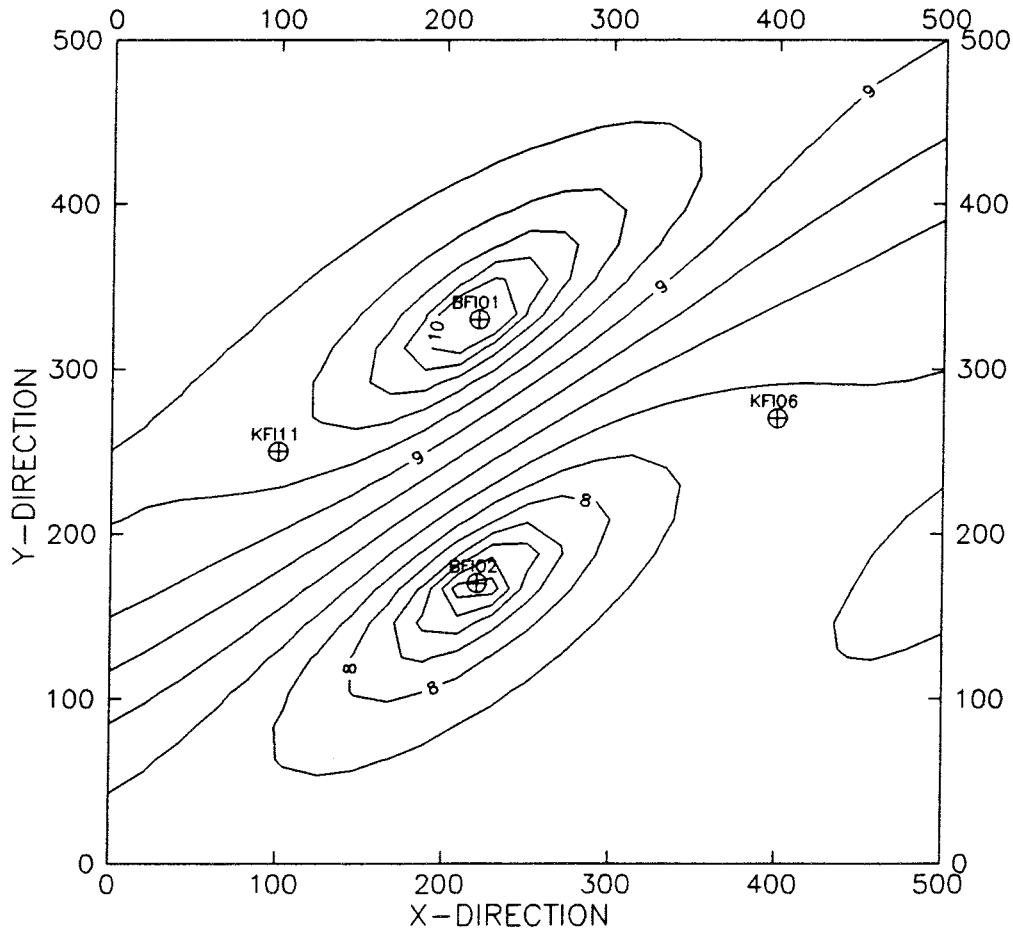


Figure 4-16. Calculated steady-state flow field for the best-fit model assuming anisotropy and leakage.

The same flow field is also illustrated in Figure 4-17, showing calculated velocity vectors. From Figure 4-17 it may be interpreted that the bulk of the transport emanating from the injection borehole is directed along direction of maximum hydraulic conductivity, and thus in the directions opposite and towards KFI11. It can also be seen that the transport directed towards KFI11 is not diluted by any other water in the fracture zone. This, in combination with the somewhat shorter velocity arrows in the direction of BFI02, explains the relative appearance of the breakthrough curves for BFI02 and KFI11 in Figure 4-15.

The reason for the low concentrations and slow arrival time in KFI06 is also clearly seen in Figure 4-17. The tracer transport from BFI01 in the direction of KFI06, although close to the injection point seemingly substantial, is

quickly diverted away from KFI06 by the hydraulic head created by the dipole and also the imposed hydraulic boundary conditions. In fact, water entering the "upstream" boundary makes a major contribution to the flow going through KFI06, causing significant effects of dilution and dispersion in the breakthrough data.

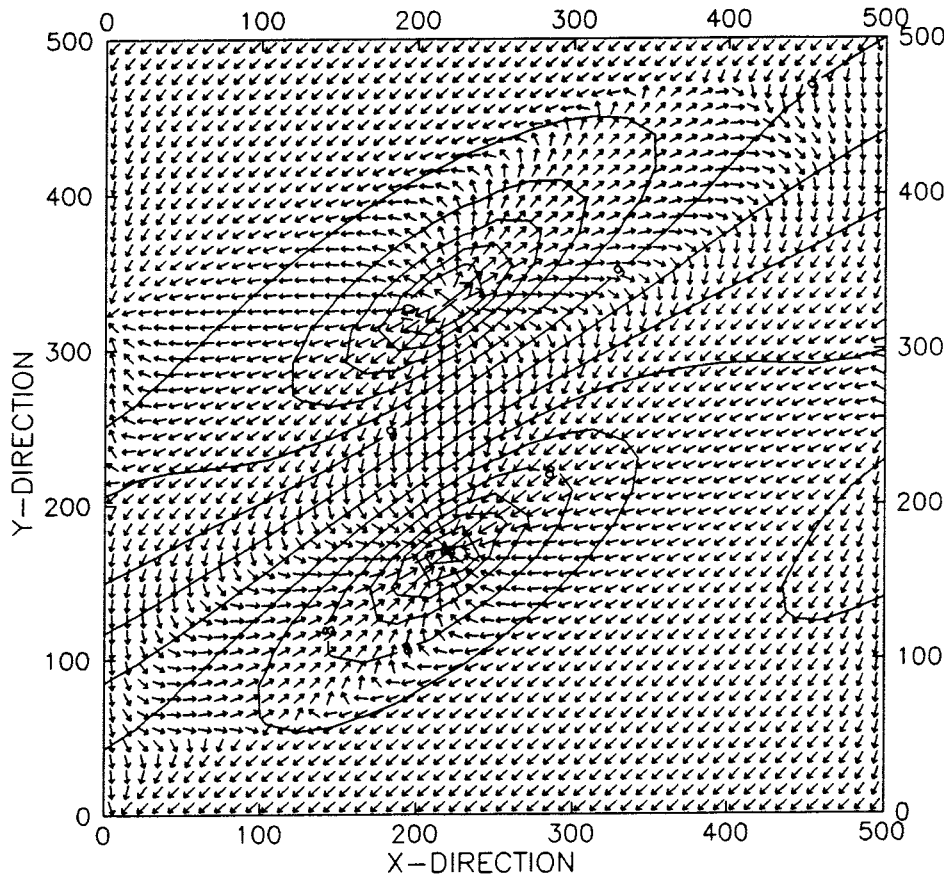


Figure 4-17. Velocity vectors of the calculated steady-state flow field.

Figure 4-17 may also be used to illustrate the importance of the boundary conditions. Assuming that the interpreted anisotropy is a feature of the real system, it seems clear that the occurrence of "open" hydraulic boundaries, modelled as specified-head boundaries, are necessary for the low concentration and slow transport times in KFI06. In Figure 4-17 only the upper and lower boundaries are open, while the boundaries in the y-direction are closed. This distinction is somewhat arbitrary, and it may easily be imagined that the estimation results might differ if also the boundaries in the y-direction were open. In such a case dilution in KFI06 by inflow across the boundaries may be even more pronounced, possibly affecting the estimation of other parameters in the system. One may also argue that the computational domain should be larger, since the extent dipole flow field, especially along the left hand side boundary, is distorted by flow being forced along the no-flow boundaries. However, although boundary effects may be interesting and

worth further study, it is here argued that the main features of the flow and transport system arrived at through the inverse modelling is not significantly altered by uncertainty about the boundaries.

In summary, the inclusion of aerially vertical leakage eliminated the need for a dilution factor during circulation, while also improving other results from the estimation. Considering that other interpreted model features identified by the inverse modelling, especially the anisotropy and leakage, agree remarkably well with other independent geological and hydrogeological interpretation, a reasonable conclusion seems to be that the upper part of Zone 2 may be described with a relatively idealized flow and transport model.

#### 4.4 **COMPARISON WITH OTHER TRACER EXPERIMENTS IN ZONE 2**

Previously, two other tracer experiments have been performed in the same borehole geometry as the dipole experiment, the interference test /Andersson et al., 1989/, and the radially converging experiment /Gustafsson & Nordqvist, 1993/. A comparison with these experiments have been made in order to establish similarities and to examine whether it is possible to draw further conclusions regarding flow and transport within the zone.

One interesting feature of these experiments in the upper part of Zone 2 is that they have been performed at three different velocities. In the interference test, a pumping rate of 500 l/min was applied, in the radially converging experiment, 82 l/min (calculated from the transmissivity distribution in borehole BFI02), and in the dipole experiment, 120 l/min. There are two routes between boreholes that have been used in all three experiments, namely KFI11–BFI02 and BFI01–BFI02.

Table 4–5 presents a comparison of some of the parameters determined from the two routes KFI11–BFI02 and BFI01–BFI02. The table shows that the test with the highest flow velocity, the interference test, yields the lowest dispersivity. This can also be seen in Figure 4–18, where tracer breakthrough in BFI02 from pulse injections in borehole KFI11 is compared for the three experiments. There may be several explanations for this. The most probable one is that the higher hydraulic gradient will tend to concentrate the flow to a fewer number of flow paths resulting in lower dispersivity.

Another explanation may be that "inertial cores" are developed as suggested by Dybbs and Edwards (1984) and discussed by Raven et al. (1988). Inertial cores have been observed in laboratory experiments at relatively high flow velocities corresponding to Reynolds numbers,  $Re$  of 1–50. In a situation where inertial cores are developed, immobile fluid zones are created resulting in transient solute storage which Raven et al. (1988) used as explanation for the tailing of breakthrough curves in high velocity tracer tests. They were not able to fit breakthrough curves from a series of dipole tests in a single fracture with an ordinary advection–dispersion model without introducing transient solute storage. Comparison of flow velocities (mean velocities) display very similar values to the dipole experiment in Zone 2 where 1D advection–dispersion models gave excellent fits. However, the main

difference between the two experiments is that Raven et al. (1988) performed their experiments in a single fracture while in Zone 2 the experiments were performed in fracture zone where velocity differences caused by flow in several fractures most likely is the dominating dispersive effect.

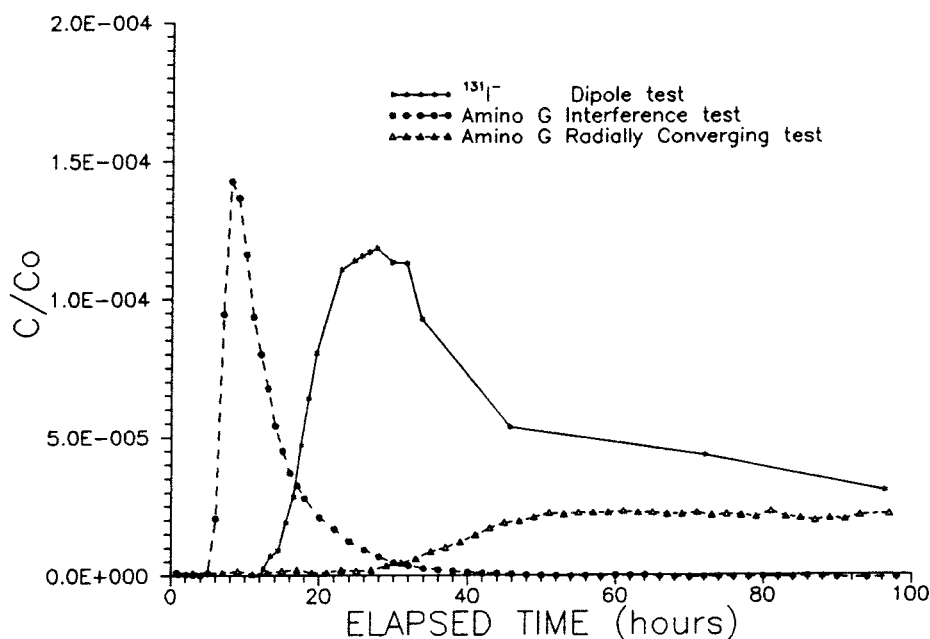


Figure 4-17. Comparison of tracer breakthrough in borehole BFI02 from pulse injections in borehole KFI11 during three different tracer experiments.

Table 4-5. Comparison of some flow and transport parameters determined from three different tracer experiments performed in the upper highly transmissive part of Zone 2.

Route	Parameter*	Interference test	Dipole experiment	Radially converging experiment
	Q (l/min)	500	120	82
KFI11-BFI02 two paths L = 157 m	$\Delta h$ (m)	3.7	0.91	0.81
	$t_a$ (h)	5	13	24
	$t_{01}$ (h)	8	27	39
	$t_{02}$ (h)	15	110	103
	$D/v_1$ (m)	2.7	5.5	3.6
	$D/v_2$ (m)	11.4	65	10.7
BFI01-BFI02 one path L = 168 m	$\Delta h$ (m)	5.3	2.7	1.1
	$t_a$ (h)	20	20	75
	$t_0$ (h)	35	45	154
	$D/v$ (m)	2.4	4	6.3

\* Q = induced flow rate,  $\Delta h$  = head difference,  $t_a$  = first arrival,  $t_0$  = mean travel time,  $D/v$  = dispersivity.

Effects of matrix diffusion in these short term, high velocity experiments are not likely. Maloszewski & Zuber (1985) show that matrix diffusion has a negligible effect when the ratio of fracture to matrix porosity,  $\gamma$ , is small (i.e.  $\gamma \leq 10^{-4}$ ).

$$\gamma = n_p (D_p / e^f)^{1/2} \quad (4-1)$$

where  $n_p$  = rock mass porosity (dimensionless)  
 $D_p$  = diffusion coefficient (m<sup>2</sup>/s)  
 $e^f$  = frictional loss fracture aperture (m)

Using reasonable values of  $n_p$  and  $D_p$  from Finnsjö granite ( $n_p = 2 \cdot 10^{-2}$ ,  $D_p = 10^{-10}$  m<sup>2</sup>/s) /Gidlund et al., 1990; Skagius & Neretnieks, 1986/ and fracture apertures determined from the upper part of Zone 2 ( $e^f = 1 \cdot 10^{-3}$ ) /Gustafsson & Nordqvist, 1993/ gives  $\gamma = 2 \cdot 10^{-10}$ , i.e. a negligible effect of matrix diffusion.

Table 4-5 also shows that the dispersivity determined from the 1-D analysis of the dipole experiment is higher than the others which is an effect of the flow geometry with a larger number of flow paths contributing to the flow in the dipole field. It should be noted that the parameter values presented in Table 4-5 are determined from 1-D model analysis except for the BFI01-BFI02 path in the dipole experiment which cannot be described in only one dimension. The values determined from 1-D and 2-D analysis may differ due to the complexity of the flow field that cannot be taken into account in the 1-D analysis. Induced flow field, natural gradients, and anisotropy may interact in such way that more, or less, dispersivity is needed to explain the results. A 2-D model also includes some transversal dispersion which contributes to the dispersivity so that less longitudinal dispersion is needed to explain data.

Notable in Table 4-5 is also that the tracer first arrival,  $t_a$ , for the transport between BFI01 and BFI02 is the same for the interference test and the dipole experiment although head differences and flow velocities are different, see Figure 4-19. This may be seen as an indication that different preferential flow paths between the boreholes are activated depending on the inferred boundary conditions for flow. Hence, channelling in the form of fixed channels where flow occurs independently of flow geometry does not seem to exist.

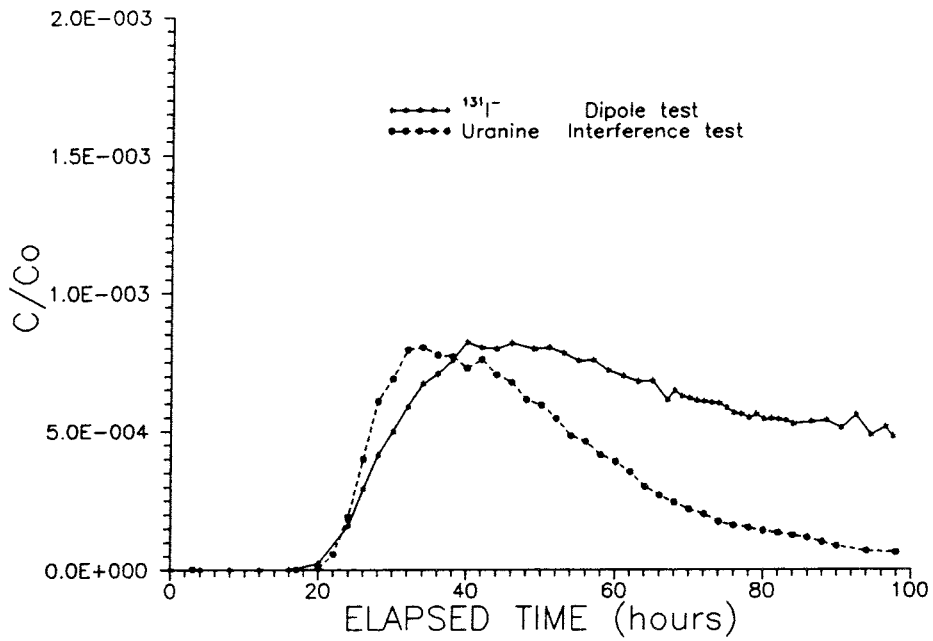


Figure 4-19. Comparison between tracer breakthrough in BFI02 of tracers injected during the interference test and the dipole experiment. Breakthrough during interference test is upscaled for easier comparison.

## 5 DISCUSSION AND CONCLUSIONS

### 5.1 EXPERIMENTAL DESIGN

Large scale tracer experiments under controlled conditions are quite rare, especially in crystalline rock. Only recently, in connection to research activities for the siting of underground repositories, such experiments have been reported. In most cases in crystalline rock, a radially converging flow geometry has been applied but a few dipole experiments (also referred to as injection-withdrawal experiments) have also been performed.

Webster et al. (1970) performed a recirculating dipole experiment in an approximately 100 m wide, gently dipping (20 degrees) fracture zone in crystalline rock with a distance of 540 m between the boreholes. The geometry of the zone was very similar to Zone 2 but with lower transmissivity ( $T = 4 \cdot 10^{-5} \text{ m}^2/\text{s}$ ) and a considerably slower flow velocity (about 1 m/day) than in the dipole experiment in Zone 2.

Olsson et al. (1991) used a dipole geometry to monitor the transport of saline water through a minor fracture zone by borehole radar measurements. Single fractures have also been investigated by means of dipole experiments over shorter distances by Raven et al. (1988) and Novakowski (1988), and in a series of small scale experiments at the Grimsel test site /Frick et al., 1992/.

The dipole geometry has the advantage compared to the more commonly used radially converging that a larger portion of the rock/fracture is tested. It has been demonstrated in this experiment that the use of passive observation boreholes inside the flow field may add substantial information regarding flow geometry and heterogeneity. A passive observation hole was also successfully used by Raven et al. (1988) and Olsson et al. (1991).

The recirculation proved to have several advantages compared to a more ordinary injection-withdrawal setup. No large supply of water had to be kept at the site with problems of maintaining water chemistry, biological growth, temperature differences, etc. Measurements of the redox potential showed that reducing conditions was obtained. Also, the closed recirculating system made it easier to use radionuclides as they remain and decay within the bedrock. The major disadvantage is coupled to the evaluation where recirculation effects have to be considered.

The dipole experiment showed that it is possible to use short-lived radionuclides as tracers in this type of high velocity, short term experiments. The tracer characteristics are further discussed in Andersson et al. (1990), Appendix B, Sections 4.1.6 and 5.2.

Technetium in the form of pertechnetate ( $\text{TcO}_4^-$ ) is very soluble and has a low sorption on rock mineral surfaces. Under oxidizing (air) conditions

technetium will form pertechnetate. However, laboratory experiments indicate that pertechnetate will become reduced to tetravalent Tc(IV) under normal reducing deep groundwater conditions /Eriksen & Cui, 1991/, /Byegård et al., 1992/. This was confirmed by the dipole experiment at Finnsjön. The redox potential monitored during the experiment showed stable reducing conditions and no breakthrough of  $^{99m}\text{Tc}$  was registered despite the fact that it was injected as pertechnetate. This can only be explained by an in-situ reduction of mobile  $\text{TcO}_4^-$  to immobile Tc(IV) /Byegård et al., 1992/. Natural geochemical conditions at depth in granitic rock will therefore act as a barrier against technetium dissolution and migration. Until the dipole experiment, this has only been indicated by laboratory experiments where it is difficult to simulate reducing conditions.

## 5.2 FLOW AND TRANSPORT WITHIN ZONE 2

A general observation from all experiments using passive observation holes is that tracer breakthrough has been monitored in all observation holes. This may be an indication that flow is relatively homogeneously distributed within the fractures/fracture zones in crystalline rock. However, based on the results of this experiment, it is clear that preferential **directions** exist but it is not likely that these are channels of finite width. In a fracture zone like Zone 2 flow occurs within a number of well interconnected fractures. Depending on the boundary conditions, different preferential flow paths will be activated.

The main feature of the dipole experiment is the fast transport to borehole KFI11. The data suggests that a preferential flow direction exists and the objective of the numerical 2-D modelling was to investigate to what extent the direction of the natural gradient and possible anisotropic condition in the fracture zone may explain the deviations from an ideal dipole flow field, regarding tracer transport in the zone.

The modelling performed has showed that it is possible to explain the observed breakthrough without assumptions of spatial heterogeneity, that need to be described statistically.

In summary the modelling showed that:

- The variation in residence times and dispersivities is small for the non-sorbing tracers ( $^{82}\text{Br}^-$ ,  $^{186}\text{ReO}_4^-$ ,  $^{131}\text{I}^-$ ,  $^{169}\text{Yb-EDTA}$  while  $^{58}\text{Co-EDTA}$ ).  $^{140}\text{La-DOTA}$ ,  $^{177}\text{Lu-DOTA}$  and Rhodamine WT are markedly delayed.  $^{51}\text{Cr-EDTA}$ ,  $^{111}\text{In-EDTA}$ , and In-EDTA (stable) also show minor delays. Some of the tracers, e.g.  $^{24}\text{Na}^+$  and  $^{160}\text{Tb-EDTA}$ , are not delayed but shows lower peak values and less recovery than others.
- Tracer transport between BFI01 and BFI02 was relatively well predicted. However, significant deviations from the predictions occurred when observation holes KFI06 and KFI11 were included in the analysis.
- A change of the gradient direction does not contribute to an improved model.

- Including an anisotropy factor ( $K_{\max}/K_{\min}$ ) of about 8 directed approximately along the strike of the zone, gives a remarkably good agreement between data and model.
- The model estimated anisotropy direction agrees well with the geological character of Zone 2 where the configuration of fracture sets gives intersection lineations, "channels", in an approximately NW-SE direction, i.e. parallel to the strike direction of the zone.
- Flow during the dipole experiment is dominated by advection. The only other mechanism needed to explain breakthrough curves is dispersion. Matrix diffusion or other effects like transient solute storage is likely to have negligible effects.
- Including leakage from the lower parts of Zone 2, as indicated by independent information such as head and electrical conductivity data, gives slightly better fits than by assuming tracer losses.
- Estimated leakage coefficient agree well with independent data from the interference tests /Andersson et al., 1989/

Comparison of tracer breakthrough data and derived transport parameters from all three tracer experiments performed in the upper part of the zone indicates a velocity dependent dispersivity with the lowest values for the highest flow rates. One explanation for this may be that a higher hydraulic gradient tend to concentrate the flow to fewer flow paths. The comparison also shows that transport between BFI01 and BFI02 gives very similar travel times for the dipole test and the interference test although pumping rates were quite different. This may be seen as an indication that different preferential flow paths between the boreholes are activated depending on the inferred boundary conditions for flow. Hence, channelling in the form of fixed channels where flow occurs independently of flow geometry does not seem to exist.

**REFERENCES**

- Ahlbom K, Andersson P, Ekman L, Gustafsson E, Smellie J, and Tullborg E-L 1986. Preliminary investigations of fracture zones in the Brändan area, Finnsjön study site. SKB Technical Report 86-05.
- Ahlbom K, Andersson P, Ekman L, and Tirén S 1988. Characterization of fracture zones in the Brändan area, Finnsjön study site. SKB Progress Report 88-09.
- Ahlbom K, and Smellie J.A.T (editors) 1989. Characterization of fracture zone 2, Finnsjön study site, Part 1-6. SKB Technical Report 89-19.
- Andersson J-E, Ekman L, Gustafsson E, Nordqvist R, and Tirén S 1989. Hydraulic interference tests within the Brändan area, Finnsjön study site. The Fracture Zone Project Phase 3. SKB Technical Report 89-12.
- Andersson P, Eriksson C-O, Gustafsson E, and Ittner T 1990. Dipole Tracer Experiment in a Low-Angle Fracture Zone at the Finnsjön Site, Central Sweden- Experimental Design and Preliminary Results. SKB Progress Report 90-24.
- Andersson P 1993. The Fracture Zone Project - Final Report. SKB Technical Report in prep.
- Byegård J, Albinsson Y, Skarnemark G, and Skålberg M 1992. Field and laboratory studies of the reduction and sorption of technetium (VII). *Radiochemica Acta* 58/59, pp 239-244.
- Byegård J, Skarnemark G, and Skålberg M in prep. Radioactive tracer experiments performed at the Finnsjö area and at Äspö. Dept. of Nuclear Chemistry, Chalmers University of Technology, Göteborg.
- Carlsson L, Gentschein B, Gidlund G, Hansson K, Svensson T, and Thoregren U 1980. Kompletterande permeabilitetsmätningar i finnsjöområdet. SKBF/KBS Technical Report 80-10.
- Carlsson L, and Gidlund G 1983. Evaluation of the hydrogeological conditions at Finnsjön. SKBF/KBS Technical Report 83-56.
- Cooley R L 1979. A method for estimating parameters and assessing reliability for models of steady state ground-water flow. 2. Application of statistical analysis. *Water Resources Research*, vol. 15, no. 3.
- Cooley R L 1985. A comparison of several methods of solving nonlinear regression groundwater flow problems. *Water Resources Research*, vol. 21, no. 10.

- Dybbs A, and Edwards R V 1984. A new look at porous media fluid mechanics – Darcy to turbulent. Fundamentals of Transport Phenomena in Porous Media, Proc. NATO Advanced Study Institute on Mechanics of Fluids in Porous Media, pp 201–256, University of Delaware, Newark.
- Eriksen T, and Cui D 1991. On the interaction of granite with Tc(IV) and Tc(VII) in aqueous solution. SKB Technical Report TR 91–47.
- Freeze J A, and Cherry J F 1979. Groundwater. Prentice–Hall, Englewood Cliffs, N. J.
- Frick U, Alexander W R, Bayens B, Bossart P, Bradbury M H, Bühler Ch, Eikenberg J, Fierz Th, Heer W, Hoehn E, McKinley I G, and Smith P A 1991. Grimsel Test Site. The radionuclide migration experiment – Overview of investigations 1985–1990. NAGRA Technical Report 91–04.
- Gidlund J, Moreno M, and Neretnieks I 1990. Porosity and diffusivity measurements of samples from Finnsjön. SKB Progress Report 90–34.
- Gustafsson E, Andersson P, Eriksson C–O, and Nordqvist R 1990. Radially Converging Tracer Experiment in a Low Angle Fracture Zone at the Finnsjön Site, Central Sweden. The Fracture Zone Project Phase 3. SKB Progress Report 90–27.
- Gustafsson E, and Nordqvist R 1993. Radially Converging Tracer Experiment in a Low Angle Fracture Zone at the Finnsjön Site, Central Sweden. The Fracture Zone Project Phase 3. SKB Technical Report in prep.
- Maloszewski P, and Zuber A 1985. On the theory of tracer experiments in fissured rock with a porous matrix. Journal of Hydrology, Vol 79, pp 333–358.
- Marquardt D W 1963. An algorithm for least squares estimation of nonlinear parameters. J. Soc. Ind. Appl. Math., 11(2).
- Nordqvist R, and Andersson J–E 1988. Transient Flow Simulations in a Fracture Zone in the Brändan Area, Finnsjön. SKB Progress Report 88–11.
- Nordqvist R 1989. Numerical predictions of a dipole tracer test in a fracture zone in the Brändan area, Finnsjön. SKB Progress Report 89–34.
- Novakowski K S 1988. Comparison of fracture aperture widths determined from hydraulic measurements and tracer experiments. Proc. Fourth Canadian/American Conference on Hydrogeology. Fluid Flow, Heat Transfer and Mass Transport in Fractured Rocks, Banff, Alberta, pp 68–80.
- Olkiewicz A, Scherman S, and Kornfält K–A 1979. Kompletterande berggrundsundersökningar inom Finnsjö- och Karlshamnsområdena. SKBF/KBS Technical Report 79–05.

- Olsson O, Andersson P, and Gustafsson E 1991. Site characterization and validation – Monitoring of saline tracer transport by borehole radar measurements, final report. Stripa Project Technical Report 91-18.
- Raven K G, Novakowski K S, and Lapcevic P A 1988. Interpretation of field tracer tests of a single fracture using a transient solute storage model. *Water Resources Research*, Vol 24, No 12, pp 2019-2032.
- Skagius K, and Neretnieks I 1986. Porosities and diffusivities of some non-sorbing species in crystalline rock. *Water Resources Research* Vol 22, no 3, pp 389-398.
- Smellie J, Gustafsson E, and Wikberg P 1987. Groundwater sampling during and subsequent to air-flush rotary drilling: Hydrochemical investigations at depth in fractured crystalline rock. SKB Progress Report 87-31.
- Smellie J A T, and Wikberg P 1991. Hydrochemical investigations at Finnsjön, Sweden. *Journal of Hydrology*, Vol 126, pp 129-158.
- Van Genuchten M Th, and Alves W J 1982. Analytical solutions of the one-dimensional convective-dispersive solute transport equation, U. S. Dep. Agric. Tech. Bull., 1661.
- Webster D S, Proctor J F, and Marine I W 1970. Two-well tracer test in fractured crystalline rock. U. S. Geological Survey Water-Supply Paper 1544-1.
- Voss C I 1990. SUTRA – A finite-element simulation model for saturated-unsaturated, fluid-density-dependent groundwater flow with energy transport or chemically-reactive single-species solute transport. Version V06902D. U.S. Geological Survey Water-Resources Investigations Report 84-4369.
- Zuber A 1984. Theoretical possibilities of the two-well pulse method. *Isotope Techniques in Groundwater Hydrology*, Vol II, pp 277-294. IAEA Vienna, Austria.



## APPENDIX A

### ONE-DIMENSIONAL MODELLING OF TRACER BREAKTHROUGH

	CONTENTS	page
A1	MODELLING OF TRACER BREAKTHROUGH IN BFI02	A: 1
A2	MODELLING OF TRACER BREAKTHROUGH IN KFI11	A: 3
A3	MODELLING OF TRACER BREAKTHROUGH IN KFI06	A:14
A4	MODELLING OF SORBING TRACER BREAKTHROUGH IN KFI11 WITH WEIGHING FACTOR FROM PEAK CONCENTRATIONS	A:18
A5	MODELLING OF SORBING TRACER BREAKTHROUGH IN KFI11 WITH WEIGHING FACTOR FROM F-PARAMETER	A:21

Table A-1. List of explanations for the regression summary and regression statistics in Appendix A1-A3.

---

Final estimate for parameter 1: mean velocity first flow path, $v_1$ (m/s)
Final estimate for parameter 2: dispersion coeff. first flow path, $D_1$ ( $m^2/s$ )
Final estimate for parameter 3: f-parameter first flow path, $f_1$ (dim.less)
Final estimate for parameter 4: mean velocity second flow path, $v_2$ (m/s)
Final estimate for parameter 5: dispersion coeff. second flow path, $D_2$ ( $m^2/s$ )
Final estimate for parameter 6: f-parameter second flow path, $f_2$ (dim.less)

---

\*\*\*\*\* REGRESSION SUMMARY \*\*\*\*\*

TRANSPORT PATH: KFI11-BFI02  
 TRACER: I-131

FINAL ESTIMATE FOR PARAMETER 1 = 0.1421E-02  
 FINAL ESTIMATE FOR PARAMETER 2 = 0.1444E-01  
 FINAL ESTIMATE FOR PARAMETER 3 = 0.2010E-02

\*\*\*\*\*

REGRESSION STATISTICS

NO. OF OBSERVATIONS: 42

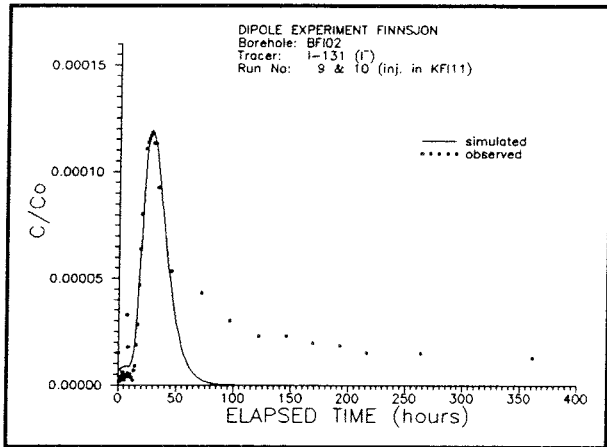
SUM OF SQUARED DIFFERENCES = 0.708E-08

ERROR VARIANCE = 0.181E-09

CORRELATION COEFFICIENT = .95440E+00

STANDARD ERROR FOR PARAMETER 1 = 0.614E-04  
 STANDARD ERROR FOR PARAMETER 2 = 0.192E-02  
 STANDARD ERROR FOR PARAMETER 3 = 0.189E-03

CORRELATION BETWEEN PARAM. 1 AND 2 = -.6155E+00  
 CORRELATION BETWEEN PARAM. 1 AND 3 = -.8826E+00  
 CORRELATION BETWEEN PARAM. 2 AND 3 = 0.7129E+00



\*\*\*\*\* REGRESSION SUMMARY \*\*\*\*\*

TRANSPORT PATH: KFI11-BFI02  
 TRACER: I-131

FINAL ESTIMATE FOR PARAMETER 1 = 0.1486E-02  
 FINAL ESTIMATE FOR PARAMETER 2 = 0.8161E-02  
 FINAL ESTIMATE FOR PARAMETER 3 = 0.1179E-02  
 FINAL ESTIMATE FOR PARAMETER 4 = 0.3617E-03  
 FINAL ESTIMATE FOR PARAMETER 5 = 0.2340E-01  
 FINAL ESTIMATE FOR PARAMETER 6 = 0.4733E-02

\*\*\*\*\*

REGRESSION STATISTICS

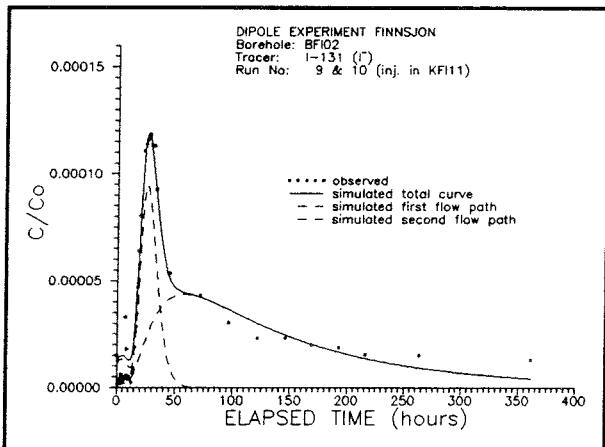
NO. OF OBSERVATIONS: 42

SUM OF SQUARED DIFFERENCES = 0.269E-08

ERROR VARIANCE = 0.747E-10

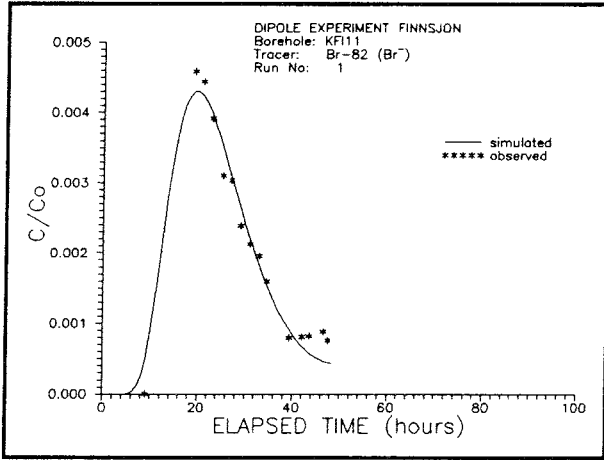
CORRELATION COEFFICIENT = .98471E+00

STANDARD ERROR FOR PARAMETER 1 = 0.540E-04  
 STANDARD ERROR FOR PARAMETER 2 = 0.222E-02  
 STANDARD ERROR FOR PARAMETER 3 = 0.418E-03  
 STANDARD ERROR FOR PARAMETER 4 = 0.677E-04  
 STANDARD ERROR FOR PARAMETER 5 = 0.154E-01  
 STANDARD ERROR FOR PARAMETER 6 = 0.114E-02



CORRELATION BETWEEN PARAM. 1 AND 2 = -.7943E+00  
 CORRELATION BETWEEN PARAM. 1 AND 3 = -.7960E+00  
 CORRELATION BETWEEN PARAM. 1 AND 4 = 0.5167E+00  
 CORRELATION BETWEEN PARAM. 1 AND 5 = 0.6310E+00  
 CORRELATION BETWEEN PARAM. 1 AND 6 = 0.4353E+00  
 CORRELATION BETWEEN PARAM. 2 AND 3 = 0.9525E+00  
 CORRELATION BETWEEN PARAM. 2 AND 4 = -.4011E+00  
 CORRELATION BETWEEN PARAM. 2 AND 5 = -.8941E+00  
 CORRELATION BETWEEN PARAM. 2 AND 6 = -.6564E+00  
 CORRELATION BETWEEN PARAM. 3 AND 4 = -.4652E+00  
 CORRELATION BETWEEN PARAM. 3 AND 5 = -.9463E+00  
 CORRELATION BETWEEN PARAM. 3 AND 6 = -.6839E+00  
 CORRELATION BETWEEN PARAM. 4 AND 5 = 0.2458E+00  
 CORRELATION BETWEEN PARAM. 4 AND 6 = -.2524E+00  
 CORRELATION BETWEEN PARAM. 5 AND 6 = 0.7685E+00

A2      MODELLING OF TRACER BREAKTHROUGH IN KFI11



\*\*\*\*\* REGRESSION SUMMARY \*\*\*\*\*

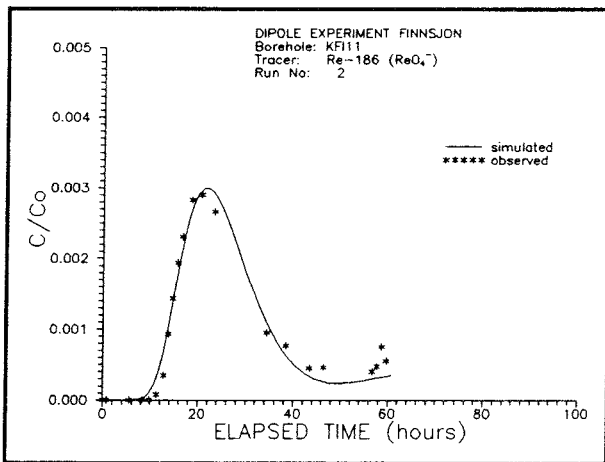
TRANSPORT PATH: BFI01-KFI11  
TRACER: BR-82

FINAL ESTIMATE FOR PARAMETER 1 = 0.2009E-02  
FINAL ESTIMATE FOR PARAMETER 2 = 0.2711E-01  
FINAL ESTIMATE FOR PARAMETER 3 = 0.1071E+00

\*\*\*\*\*

REGRESSION STATISTICS

NO. OF OBSERVATIONS: 15  
SUM OF SQUARED DIFFERENCES = 0.103E-05  
ERROR VARIANCE = 0.857E-07  
CORRELATION COEFFICIENT = .98301E+00  
STANDARD ERROR FOR PARAMETER 1 = 0.525E-04  
STANDARD ERROR FOR PARAMETER 2 = 0.380E-02  
STANDARD ERROR FOR PARAMETER 3 = 0.598E-01  
CORRELATION BETWEEN PARAM. 1 AND 2 = 0.5221E+00  
CORRELATION BETWEEN PARAM. 1 AND 3 = 0.4180E+00  
CORRELATION BETWEEN PARAM. 2 AND 3 = 0.8403E+00



\*\*\*\*\* REGRESSION SUMMARY \*\*\*\*\*

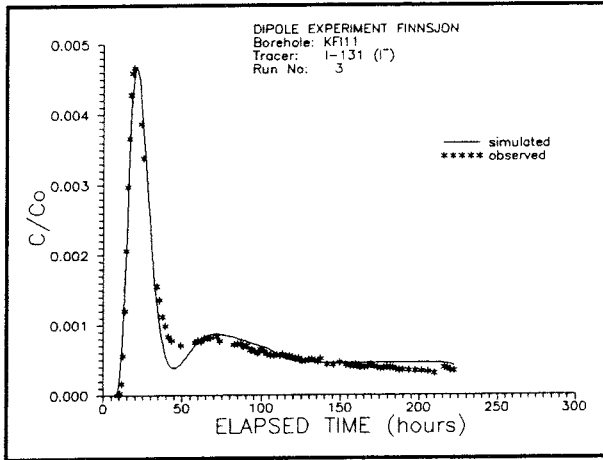
TRANSPORT PATH: BFI01-KFI11  
TRACER: RE-186

FINAL ESTIMATE FOR PARAMETER 1 = 0.1904E-02  
FINAL ESTIMATE FOR PARAMETER 2 = 0.1690E-01  
FINAL ESTIMATE FOR PARAMETER 3 = 0.8257E+00

\*\*\*\*\*

REGRESSION STATISTICS

NO. OF OBSERVATIONS: 22  
SUM OF SQUARED DIFFERENCES = 0.718E-06  
ERROR VARIANCE = 0.378E-07  
CORRELATION COEFFICIENT = .98275E+00  
STANDARD ERROR FOR PARAMETER 1 = 0.360E-04  
STANDARD ERROR FOR PARAMETER 2 = 0.127E-02  
STANDARD ERROR FOR PARAMETER 3 = 0.432E-01  
CORRELATION BETWEEN PARAM. 1 AND 2 = -.4130E+00  
CORRELATION BETWEEN PARAM. 1 AND 3 = -.7932E+00  
CORRELATION BETWEEN PARAM. 2 AND 3 = 0.4094E+00



\*\*\*\*\* REGRESSION SUMMARY \*\*\*\*\*

TRANSPORT PATH: BFI01-KFI11  
TRACER: I-131

FINAL ESTIMATE FOR PARAMETER 1 = 0.2002E-02  
FINAL ESTIMATE FOR PARAMETER 2 = 0.1539E-01  
FINAL ESTIMATE FOR PARAMETER 3 = 0.1153E+01

\*\*\*\*\*  
REGRESSION STATISTICS

NO. OF OBSERVATIONS: 91

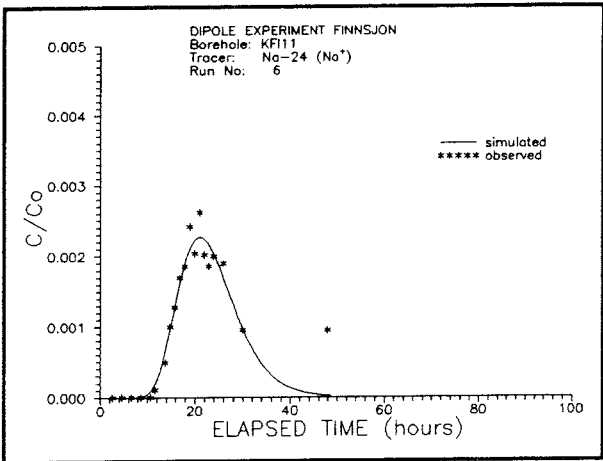
SUM OF SQUARED DIFFERENCES = 0.241E-05

ERROR VARIANCE = 0.274E-07

CORRELATION COEFFICIENT = .98583E+00

STANDARD ERROR FOR PARAMETER 1 = 0.140E-04  
STANDARD ERROR FOR PARAMETER 2 = 0.580E-03  
STANDARD ERROR FOR PARAMETER 3 = 0.214E-01

CORRELATION BETWEEN PARAM. 1 AND 2 = -.3247E+00  
CORRELATION BETWEEN PARAM. 1 AND 3 = -.6436E+00  
CORRELATION BETWEEN PARAM. 2 AND 3 = 0.3665E+00



\*\*\*\*\* REGRESSION SUMMARY \*\*\*\*\*

TRANSPORT PATH: BFI01-KFI11  
TRACER: NA-24

FINAL ESTIMATE FOR PARAMETER 1 = 0.2033E-02  
FINAL ESTIMATE FOR PARAMETER 2 = 0.1272E-01  
FINAL ESTIMATE FOR PARAMETER 3 = 0.5028E+00

\*\*\*\*\*  
REGRESSION STATISTICS

NO. OF OBSERVATIONS: 20

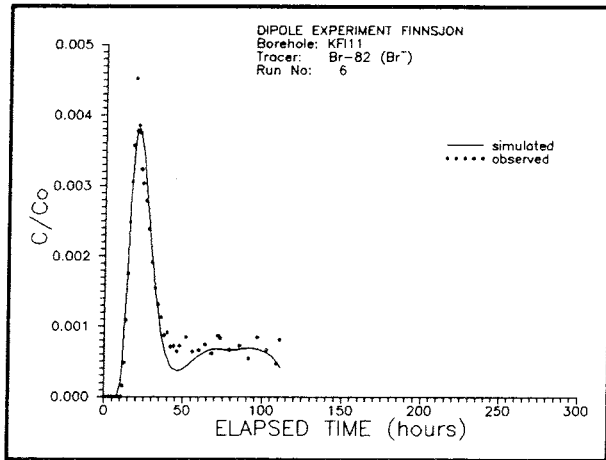
SUM OF SQUARED DIFFERENCES = 0.134E-05

ERROR VARIANCE = 0.790E-07

CORRELATION COEFFICIENT = .95936E+00

STANDARD ERROR FOR PARAMETER 1 = 0.597E-04  
STANDARD ERROR FOR PARAMETER 2 = 0.219E-02  
STANDARD ERROR FOR PARAMETER 3 = 0.471E-01

CORRELATION BETWEEN PARAM. 1 AND 2 = -.6164E+00  
CORRELATION BETWEEN PARAM. 1 AND 3 = -.7942E+00  
CORRELATION BETWEEN PARAM. 2 AND 3 = 0.7975E+00



\*\*\*\*\* REGRESSION SUMMARY \*\*\*\*\*

TRANSPORT PATH: BFI01-KFI11  
TRACER: BR-82

FINAL ESTIMATE FOR PARAMETER 1 = 0.1974E-02  
FINAL ESTIMATE FOR PARAMETER 2 = 0.1651E-01  
FINAL ESTIMATE FOR PARAMETER 3 = 0.9881E+00

\*\*\*\*\*

REGRESSION STATISTICS

NO. OF OBSERVATIONS: 45

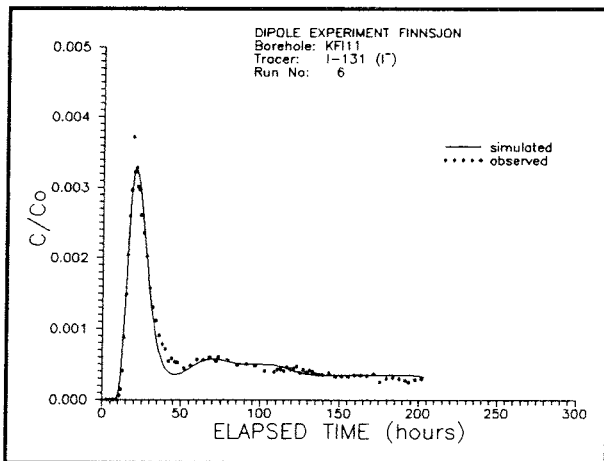
SUM OF SQUARED DIFFERENCES = 0.335E-05

ERROR VARIANCE = 0.798E-07

CORRELATION COEFFICIENT = .97617E+00

STANDARD ERROR FOR PARAMETER 1 = 0.248E-04  
STANDARD ERROR FOR PARAMETER 2 = 0.112E-02  
STANDARD ERROR FOR PARAMETER 3 = 0.328E-01

CORRELATION BETWEEN PARAM. 1 AND 2 = -.2769E+00  
CORRELATION BETWEEN PARAM. 1 AND 3 = -.5698E+00  
CORRELATION BETWEEN PARAM. 2 AND 3 = 0.5666E+00



\*\*\*\*\* REGRESSION SUMMARY \*\*\*\*\*

TRANSPORT PATH: BFI01-KFI11  
TRACER: I-131

FINAL ESTIMATE FOR PARAMETER 1 = 0.2035E-02  
FINAL ESTIMATE FOR PARAMETER 2 = 0.1444E-01  
FINAL ESTIMATE FOR PARAMETER 3 = 0.7452E+00

\*\*\*\*\*

REGRESSION STATISTICS

NO. OF OBSERVATIONS: 74

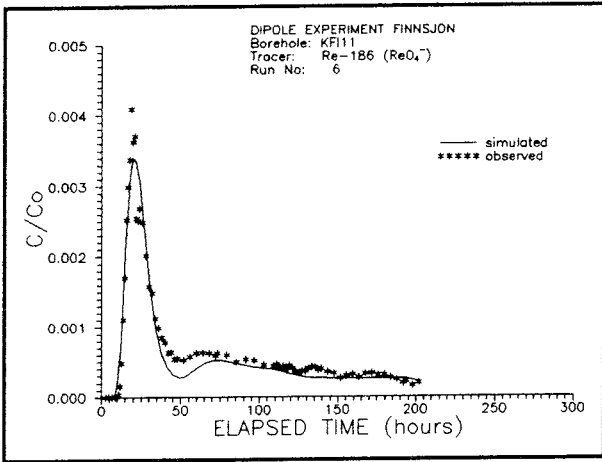
SUM OF SQUARED DIFFERENCES = 0.131E-05

ERROR VARIANCE = 0.185E-07

CORRELATION COEFFICIENT = .98889E+00

STANDARD ERROR FOR PARAMETER 1 = 0.137E-04  
STANDARD ERROR FOR PARAMETER 2 = 0.573E-03  
STANDARD ERROR FOR PARAMETER 3 = 0.134E-01

CORRELATION BETWEEN PARAM. 1 AND 2 = -.2439E+00  
CORRELATION BETWEEN PARAM. 1 AND 3 = -.5210E+00  
CORRELATION BETWEEN PARAM. 2 AND 3 = 0.5549E+00



\*\*\*\*\* REGRESSION SUMMARY \*\*\*\*\*

TRANSPORT PATH: BFI01-KFI11  
TRACER: RE-186

FINAL ESTIMATE FOR PARAMETER 1 = 0.2012E-02  
FINAL ESTIMATE FOR PARAMETER 2 = 0.1739E-01  
FINAL ESTIMATE FOR PARAMETER 3 = 0.8744E+00

\*\*\*\*\*

REGRESSION STATISTICS

NO. OF OBSERVATIONS: 74

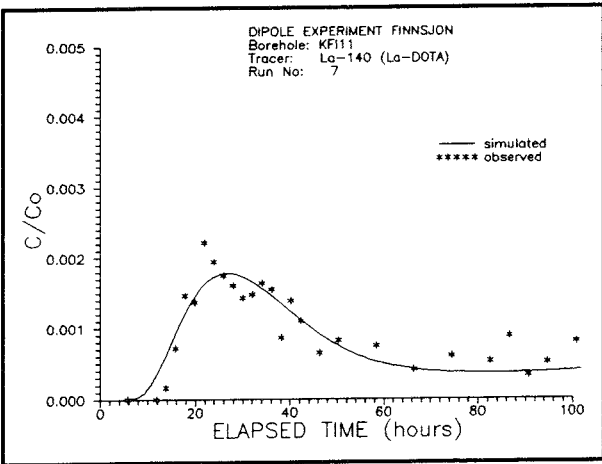
SUM OF SQUARED DIFFERENCES = 0.404E-05

ERROR VARIANCE = 0.569E-07

CORRELATION COEFFICIENT = .97191E+00

STANDARD ERROR FOR PARAMETER 1 = 0.244E-04  
STANDARD ERROR FOR PARAMETER 2 = 0.112E-02  
STANDARD ERROR FOR PARAMETER 3 = 0.272E-01

CORRELATION BETWEEN PARAM. 1 AND 2 = -.2729E+00  
CORRELATION BETWEEN PARAM. 1 AND 3 = -.5628E+00  
CORRELATION BETWEEN PARAM. 2 AND 3 = 0.5693E+00



\*\*\*\*\* REGRESSION SUMMARY \*\*\*\*\*

TRANSPORT PATH: BFI01-KFI11  
TRACER: LA-140

FINAL ESTIMATE FOR PARAMETER 1 = 0.1386E-02  
FINAL ESTIMATE FOR PARAMETER 2 = 0.2729E-01  
FINAL ESTIMATE FOR PARAMETER 3 = 0.9286E+00

\*\*\*\*\*

REGRESSION STATISTICS

NO. OF OBSERVATIONS: 27

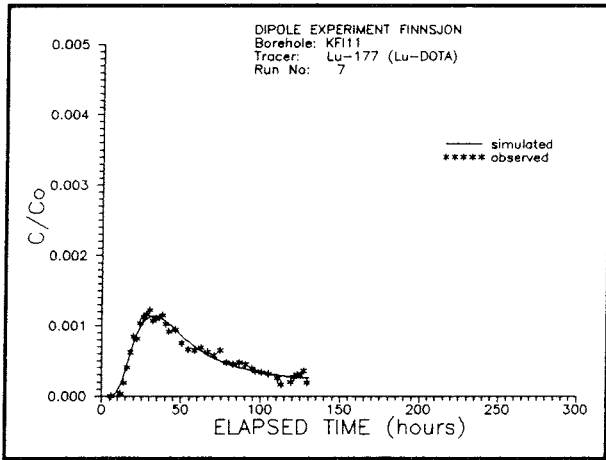
SUM OF SQUARED DIFFERENCES = 0.190E-05

ERROR VARIANCE = 0.792E-07

CORRELATION COEFFICIENT = .89625E+00

STANDARD ERROR FOR PARAMETER 1 = 0.654E-04  
STANDARD ERROR FOR PARAMETER 2 = 0.434E-02  
STANDARD ERROR FOR PARAMETER 3 = 0.761E-01

CORRELATION BETWEEN PARAM. 1 AND 2 = -.4465E+00  
CORRELATION BETWEEN PARAM. 1 AND 3 = -.7205E+00  
CORRELATION BETWEEN PARAM. 2 AND 3 = 0.6527E+00



\*\*\*\*\* REGRESSION SUMMARY \*\*\*\*\*

TRANSPORT PATH: BFI01-KF111  
TRACER: LU-177

FINAL ESTIMATE FOR PARAMETER 1 = 0.1041E-02  
FINAL ESTIMATE FOR PARAMETER 2 = 0.3047E-01  
FINAL ESTIMATE FOR PARAMETER 3 = 0.9080E+00

\*\*\*\*\*

REGRESSION STATISTICS

NO. OF OBSERVATIONS: 41

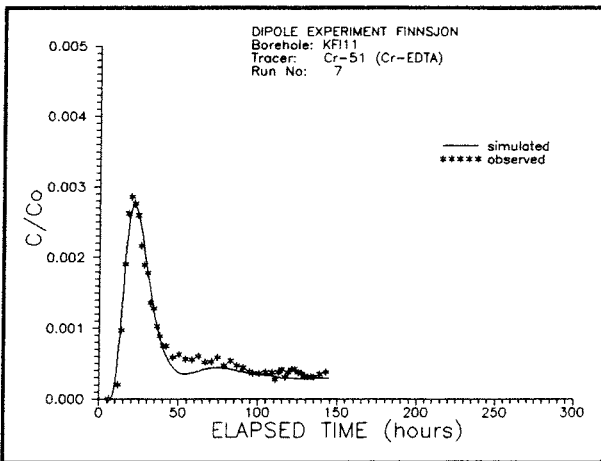
SUM OF SQUARED DIFFERENCES = 0.195E-06

ERROR VARIANCE = 0.513E-08

CORRELATION COEFFICIENT = .98013E+00

STANDARD ERROR FOR PARAMETER 1 = 0.174E-04  
STANDARD ERROR FOR PARAMETER 2 = 0.148E-02  
STANDARD ERROR FOR PARAMETER 3 = 0.220E-01

CORRELATION BETWEEN PARAM. 1 AND 2 = -.2488E+00  
CORRELATION BETWEEN PARAM. 1 AND 3 = -.6823E+00  
CORRELATION BETWEEN PARAM. 2 AND 3 = 0.4587E+00



\*\*\*\*\* REGRESSION SUMMARY \*\*\*\*\*

TRANSPORT PATH: BFI01-KF111  
TRACER: CR-51

FINAL ESTIMATE FOR PARAMETER 1 = 0.1864E-02  
FINAL ESTIMATE FOR PARAMETER 2 = 0.2117E-01  
FINAL ESTIMATE FOR PARAMETER 3 = 0.8567E+00

\*\*\*\*\*

REGRESSION STATISTICS

NO. OF OBSERVATIONS: 49

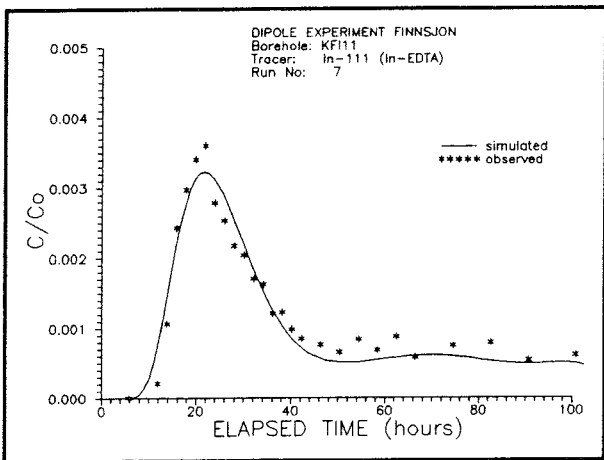
SUM OF SQUARED DIFFERENCES = 0.922E-06

ERROR VARIANCE = 0.200E-07

CORRELATION COEFFICIENT = .98502E+00

STANDARD ERROR FOR PARAMETER 1 = 0.203E-04  
STANDARD ERROR FOR PARAMETER 2 = 0.121E-02  
STANDARD ERROR FOR PARAMETER 3 = 0.205E-01

CORRELATION BETWEEN PARAM. 1 AND 2 = -.1658E+00  
CORRELATION BETWEEN PARAM. 1 AND 3 = -.3909E+00  
CORRELATION BETWEEN PARAM. 2 AND 3 = 0.5398E+00



\*\*\*\*\* REGRESSION SUMMARY \*\*\*\*\*

TRANSPORT PATH: BFI01-KFI11  
TRACER: IN-111

FINAL ESTIMATE FOR PARAMETER 1 = 0.1857E-02  
FINAL ESTIMATE FOR PARAMETER 2 = 0.2150E-01  
FINAL ESTIMATE FOR PARAMETER 3 = 0.1021E+01

\*\*\*\*\*

REGRESSION STATISTICS

NO. OF OBSERVATIONS: 27

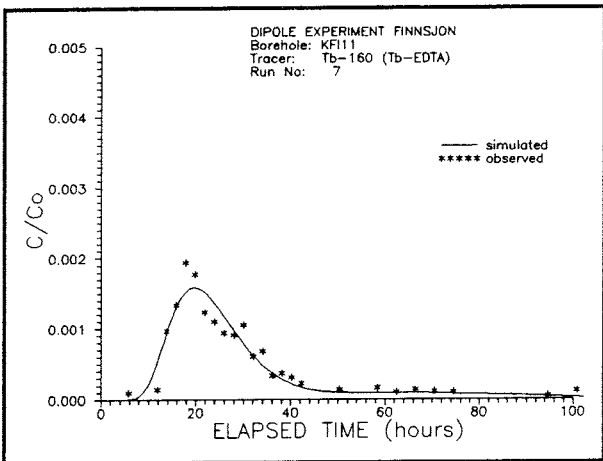
SUM OF SQUARED DIFFERENCES = 0.161E-05

ERROR VARIANCE = 0.672E-07

CORRELATION COEFFICIENT = .97028E+00

STANDARD ERROR FOR PARAMETER 1 = 0.318E-04  
STANDARD ERROR FOR PARAMETER 2 = 0.192E-02  
STANDARD ERROR FOR PARAMETER 3 = 0.390E-01

CORRELATION BETWEEN PARAM. 1 AND 2 = -.1843E+00  
CORRELATION BETWEEN PARAM. 1 AND 3 = -.4112E+00  
CORRELATION BETWEEN PARAM. 2 AND 3 = 0.5533E+00



\*\*\*\*\* REGRESSION SUMMARY \*\*\*\*\*

TRANSPORT PATH: BFI01-KFI11  
TRACER: TB-160

FINAL ESTIMATE FOR PARAMETER 1 = 0.2062E-02  
FINAL ESTIMATE FOR PARAMETER 2 = 0.2226E-01  
FINAL ESTIMATE FOR PARAMETER 3 = 0.4378E+00

\*\*\*\*\*

REGRESSION STATISTICS

NO. OF OBSERVATIONS: 25

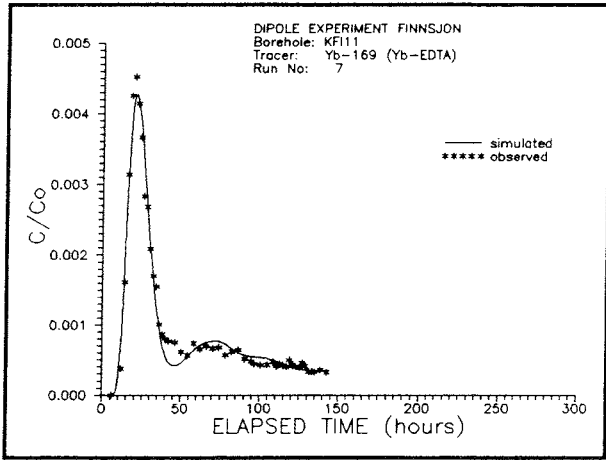
SUM OF SQUARED DIFFERENCES = 0.743E-06

ERROR VARIANCE = 0.338E-07

CORRELATION COEFFICIENT = .95129E+00

STANDARD ERROR FOR PARAMETER 1 = 0.510E-04  
STANDARD ERROR FOR PARAMETER 2 = 0.321E-02  
STANDARD ERROR FOR PARAMETER 3 = 0.267E-01

CORRELATION BETWEEN PARAM. 1 AND 2 = -.1474E+00  
CORRELATION BETWEEN PARAM. 1 AND 3 = -.3731E+00  
CORRELATION BETWEEN PARAM. 2 AND 3 = 0.5811E+00



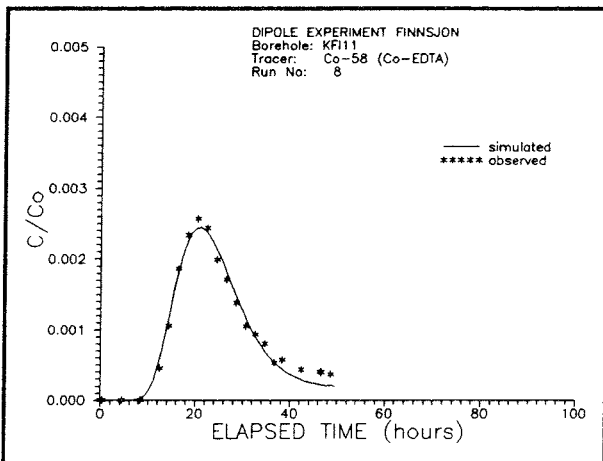
\*\*\*\*\* REGRESSION SUMMARY \*\*\*\*\*

TRANSPORT PATH: BFI01-KFI11  
TRACER: YB-169

FINAL ESTIMATE FOR PARAMETER 1 = 0.2011E-02  
FINAL ESTIMATE FOR PARAMETER 2 = 0.1766E-01  
FINAL ESTIMATE FOR PARAMETER 3 = 0.1110E+01

\*\*\*\*\*  
REGRESSION STATISTICS

NO. OF OBSERVATIONS: 49  
SUM OF SQUARED DIFFERENCES = 0.141E-05  
ERROR VARIANCE = 0.307E-07  
CORRELATION COEFFICIENT = .98875E+00  
STANDARD ERROR FOR PARAMETER 1 = 0.160E-04  
STANDARD ERROR FOR PARAMETER 2 = 0.844E-03  
STANDARD ERROR FOR PARAMETER 3 = 0.223E-01  
CORRELATION BETWEEN PARAM. 1 AND 2 = -.1197E+00  
CORRELATION BETWEEN PARAM. 1 AND 3 = -.3254E+00  
CORRELATION BETWEEN PARAM. 2 AND 3 = 0.5264E+00



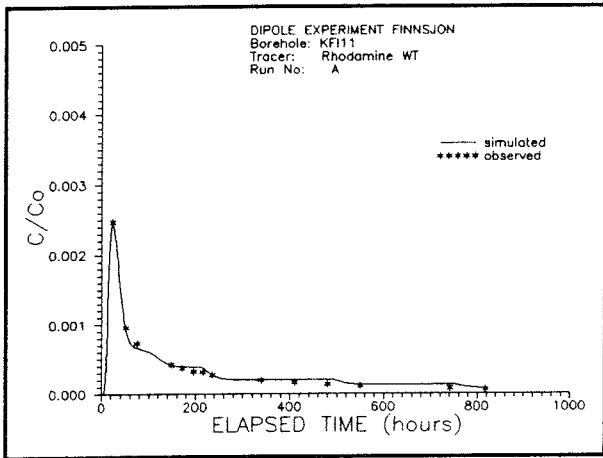
\*\*\*\*\* REGRESSION SUMMARY \*\*\*\*\*

TRANSPORT PATH: BFI01-KFI11  
TRACER: CO-58

FINAL ESTIMATE FOR PARAMETER 1 = 0.1998E-02  
FINAL ESTIMATE FOR PARAMETER 2 = 0.1665E-01  
FINAL ESTIMATE FOR PARAMETER 3 = 0.6248E+00

\*\*\*\*\*  
REGRESSION STATISTICS

NO. OF OBSERVATIONS: 22  
SUM OF SQUARED DIFFERENCES = 0.265E-06  
ERROR VARIANCE = 0.139E-07  
CORRELATION COEFFICIENT = .99188E+00  
STANDARD ERROR FOR PARAMETER 1 = 0.188E-04  
STANDARD ERROR FOR PARAMETER 2 = 0.978E-03  
STANDARD ERROR FOR PARAMETER 3 = 0.158E-01  
CORRELATION BETWEEN PARAM. 1 AND 2 = -.1423E+00  
CORRELATION BETWEEN PARAM. 1 AND 3 = -.3412E+00  
CORRELATION BETWEEN PARAM. 2 AND 3 = 0.5546E+00



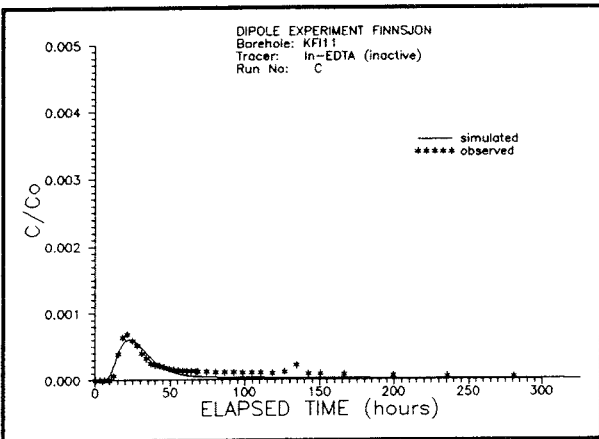
\*\*\*\*\* REGRESSION SUMMARY \*\*\*\*\*

TRANSPORT PATH: BFI01-KFI11  
 TRACER: RHODAMINE WT

FINAL ESTIMATE FOR PARAMETER 1 = 0.1500E-02  
 FINAL ESTIMATE FOR PARAMETER 2 = 0.3515E-01  
 FINAL ESTIMATE FOR PARAMETER 3 = 0.1263E+01

\*\*\*\*\*  
 REGRESSION STATISTICS

NO. OF OBSERVATIONS: 14  
 SUM OF SQUARED DIFFERENCES = 0.244E-07  
 ERROR VARIANCE = 0.222E-08  
 CORRELATION COEFFICIENT = .99841E+00  
 STANDARD ERROR FOR PARAMETER 1 = 0.829E-04  
 STANDARD ERROR FOR PARAMETER 2 = 0.984E-02  
 STANDARD ERROR FOR PARAMETER 3 = 0.402E-01  
 CORRELATION BETWEEN PARAM. 1 AND 2 = 0.9534E+00  
 CORRELATION BETWEEN PARAM. 1 AND 3 = 0.5949E+00  
 CORRELATION BETWEEN PARAM. 2 AND 3 = 0.7533E+00



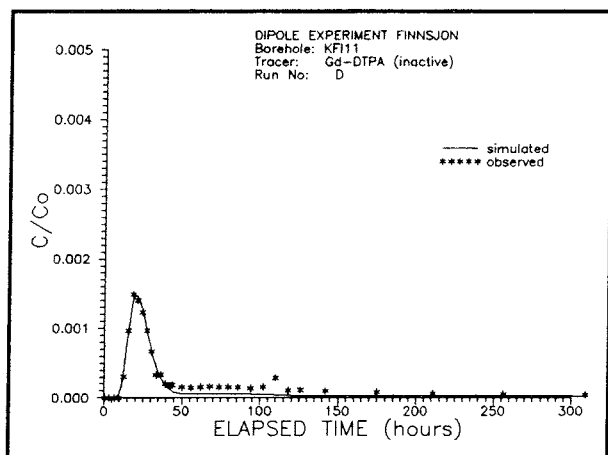
\*\*\*\*\* REGRESSION SUMMARY \*\*\*\*\*

TRANSPORT PATH: BFI01-KFI11  
 TRACER: IN-EDTA

FINAL ESTIMATE FOR PARAMETER 1 = 0.1674E-02  
 FINAL ESTIMATE FOR PARAMETER 2 = 0.2785E-01  
 FINAL ESTIMATE FOR PARAMETER 3 = 0.2462E+00

\*\*\*\*\*  
 REGRESSION STATISTICS

NO. OF OBSERVATIONS: 41  
 SUM OF SQUARED DIFFERENCES = 0.206E-06  
 ERROR VARIANCE = 0.541E-08  
 CORRELATION COEFFICIENT = .93965E+00  
 STANDARD ERROR FOR PARAMETER 1 = 0.538E-04  
 STANDARD ERROR FOR PARAMETER 2 = 0.389E-02  
 STANDARD ERROR FOR PARAMETER 3 = 0.153E-01  
 CORRELATION BETWEEN PARAM. 1 AND 2 = -.1472E+00  
 CORRELATION BETWEEN PARAM. 1 AND 3 = -.4152E+00  
 CORRELATION BETWEEN PARAM. 2 AND 3 = 0.5000E+00



\*\*\*\*\* REGRESSION SUMMARY \*\*\*\*\*

TRANSPORT PATH: BFI01-KFI11  
TRACER: GD-DTPA

FINAL ESTIMATE FOR PARAMETER 1 = 0.2019E-02  
FINAL ESTIMATE FOR PARAMETER 2 = 0.1692E-01  
FINAL ESTIMATE FOR PARAMETER 3 = 0.3751E+00

\*\*\*\*\*

REGRESSION STATISTICS

NO. OF OBSERVATIONS: 33

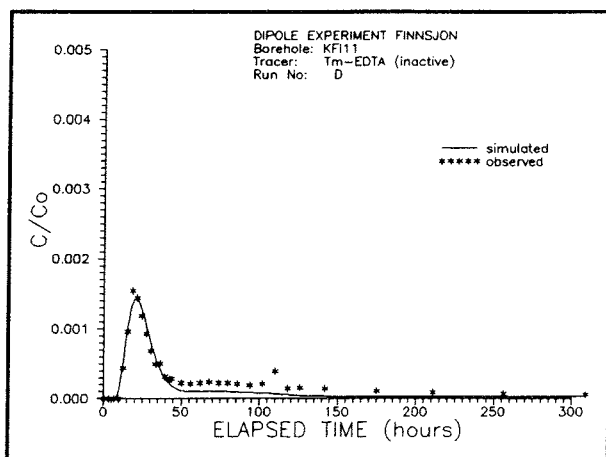
SUM OF SQUARED DIFFERENCES = 0.220E-06

ERROR VARIANCE = 0.732E-08

CORRELATION COEFFICIENT = .98775E+00

STANDARD ERROR FOR PARAMETER 1 = 0.271E-04  
STANDARD ERROR FOR PARAMETER 2 = 0.140E-02  
STANDARD ERROR FOR PARAMETER 3 = 0.137E-01

CORRELATION BETWEEN PARAM. 1 AND 2 = -.1193E+00  
CORRELATION BETWEEN PARAM. 1 AND 3 = -.3250E+00  
CORRELATION BETWEEN PARAM. 2 AND 3 = 0.5340E+00



\*\*\*\*\* REGRESSION SUMMARY \*\*\*\*\*

TRANSPORT PATH: BFI01-KFI11  
TRACER: TM-EDTA

FINAL ESTIMATE FOR PARAMETER 1 = 0.1957E-02  
FINAL ESTIMATE FOR PARAMETER 2 = 0.2195E-01  
FINAL ESTIMATE FOR PARAMETER 3 = 0.4236E+00

\*\*\*\*\*

REGRESSION STATISTICS

NO. OF OBSERVATIONS: 33

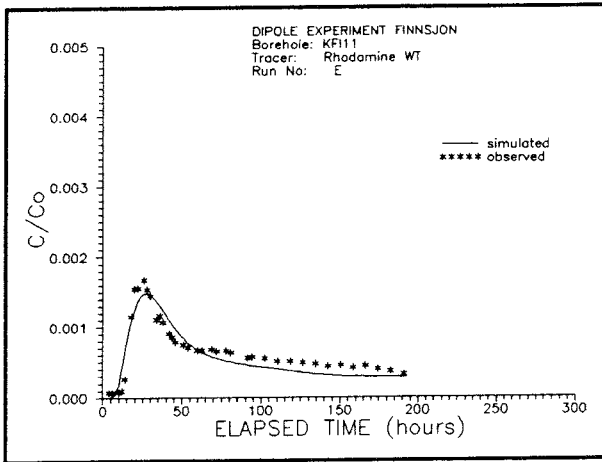
SUM OF SQUARED DIFFERENCES = 0.398E-06

ERROR VARIANCE = 0.133E-07

CORRELATION COEFFICIENT = .97489E+00

STANDARD ERROR FOR PARAMETER 1 = 0.397E-04  
STANDARD ERROR FOR PARAMETER 2 = 0.236E-02  
STANDARD ERROR FOR PARAMETER 3 = 0.201E-01

CORRELATION BETWEEN PARAM. 1 AND 2 = -.1380E+00  
CORRELATION BETWEEN PARAM. 1 AND 3 = -.3683E+00  
CORRELATION BETWEEN PARAM. 2 AND 3 = 0.5262E+00



\*\*\*\*\* REGRESSION SUMMARY \*\*\*\*\*

TRANSPORT PATH: BFI01-KF111  
TRACER: RHODAMINE WT

FINAL ESTIMATE FOR PARAMETER 1 = 0.1129E-02  
FINAL ESTIMATE FOR PARAMETER 2 = 0.2666E-01  
FINAL ESTIMATE FOR PARAMETER 3 = 0.9268E+00

\*\*\*\*\*  
REGRESSION STATISTICS

NO. OF OBSERVATIONS: 39

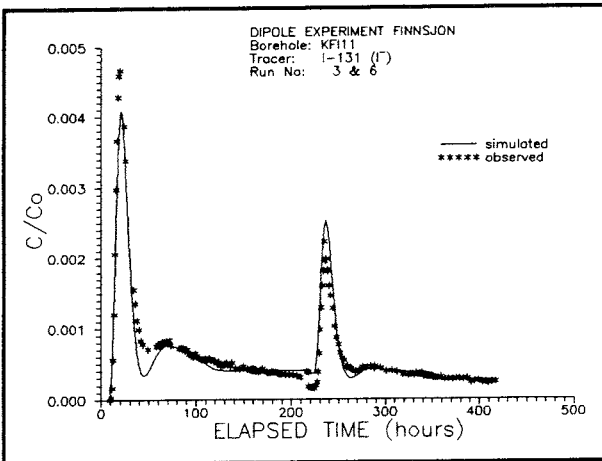
SUM OF SQUARED DIFFERENCES = 0.950E-06

ERROR VARIANCE = 0.264E-07

CORRELATION COEFFICIENT = .93614E+00

STANDARD ERROR FOR PARAMETER 1 = 0.378E-04  
STANDARD ERROR FOR PARAMETER 2 = 0.271E-02  
STANDARD ERROR FOR PARAMETER 3 = 0.426E-01

CORRELATION BETWEEN PARAM. 1 AND 2 = -.2399E+00  
CORRELATION BETWEEN PARAM. 1 AND 3 = -.6085E+00  
CORRELATION BETWEEN PARAM. 2 AND 3 = 0.5021E+00



\*\*\*\*\* REGRESSION SUMMARY \*\*\*\*\*

TRANSPORT PATH: BFI01-KF111  
TRACER: I-131

FINAL ESTIMATE FOR PARAMETER 1 = 0.2014E-02  
FINAL ESTIMATE FOR PARAMETER 2 = 0.1574E-01  
FINAL ESTIMATE FOR PARAMETER 3 = 0.1006E+01

\*\*\*\*\*  
REGRESSION STATISTICS

NO. OF OBSERVATIONS: 163

SUM OF SQUARED DIFFERENCES = 0.895E-05

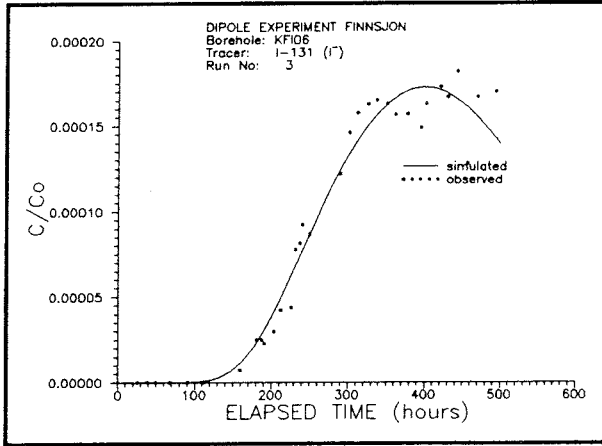
ERROR VARIANCE = 0.560E-07

CORRELATION COEFFICIENT = .95608E+00

STANDARD ERROR FOR PARAMETER 1 = 0.189E-04  
STANDARD ERROR FOR PARAMETER 2 = 0.799E-03  
STANDARD ERROR FOR PARAMETER 3 = 0.235E-01

CORRELATION BETWEEN PARAM. 1 AND 2 = -.2955E+00  
CORRELATION BETWEEN PARAM. 1 AND 3 = -.6039E+00  
CORRELATION BETWEEN PARAM. 2 AND 3 = 0.4145E+00

A3            MODELLING OF TRACER BREAKTHROUGH IN KFI06



\*\*\*\*\* REGRESSION SUMMARY \*\*\*\*\*

TRANSPORT PATH: BFI01-KFI06  
TRACER: I-131

FINAL ESTIMATE FOR PARAMETER 1 = 0.1684E-03  
FINAL ESTIMATE FOR PARAMETER 2 = 0.2525E-02  
FINAL ESTIMATE FOR PARAMETER 3 = 0.3999E+00

\*\*\*\*\*  
REGRESSION STATISTICS

NO. OF OBSERVATIONS: 33

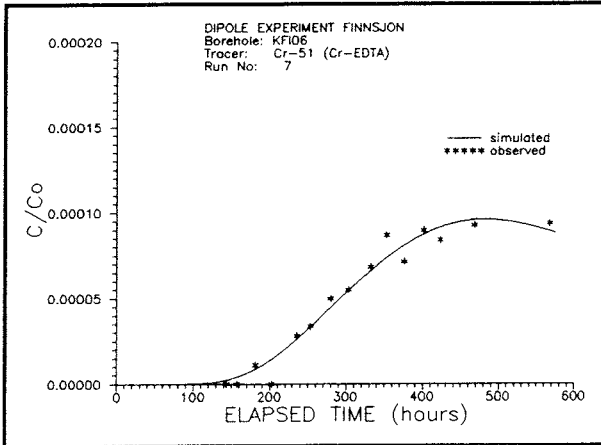
SUM OF SQUARED DIFFERENCES = 0.482E-08

ERROR VARIANCE = 0.161E-09

CORRELATION COEFFICIENT = .98429E+00

STANDARD ERROR FOR PARAMETER 1 = 0.538E-05  
STANDARD ERROR FOR PARAMETER 2 = 0.323E-03  
STANDARD ERROR FOR PARAMETER 3 = 0.265E-01

CORRELATION BETWEEN PARAM. 1 AND 2 = -.8166E+00  
CORRELATION BETWEEN PARAM. 1 AND 3 = -.9326E+00  
CORRELATION BETWEEN PARAM. 2 AND 3 = 0.8855E+00



\*\*\*\*\* REGRESSION SUMMARY \*\*\*\*\*

TRANSPORT PATH: BFI01-KFI06  
TRACER: CR-51

FINAL ESTIMATE FOR PARAMETER 1 = 0.1205E-03  
FINAL ESTIMATE FOR PARAMETER 2 = 0.3003E-02  
FINAL ESTIMATE FOR PARAMETER 3 = 0.4148E+00

\*\*\*\*\*  
REGRESSION STATISTICS

NO. OF OBSERVATIONS: 15

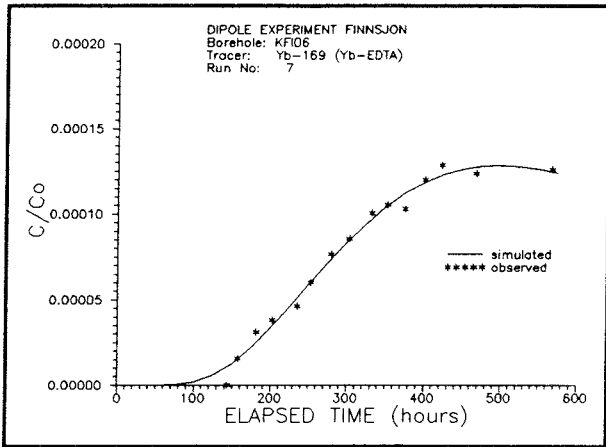
SUM OF SQUARED DIFFERENCES = 0.626E-09

ERROR VARIANCE = 0.522E-10

CORRELATION COEFFICIENT = .98335E+00

STANDARD ERROR FOR PARAMETER 1 = 0.105E-04  
STANDARD ERROR FOR PARAMETER 2 = 0.527E-03  
STANDARD ERROR FOR PARAMETER 3 = 0.696E-01

CORRELATION BETWEEN PARAM. 1 AND 2 = -.8647E+00  
CORRELATION BETWEEN PARAM. 1 AND 3 = -.9832E+00  
CORRELATION BETWEEN PARAM. 2 AND 3 = 0.8640E+00



\*\*\*\*\* REGRESSION SUMMARY \*\*\*\*\*

TRANSPORT PATH: BFI01-KFI06  
TRACER: YB-169

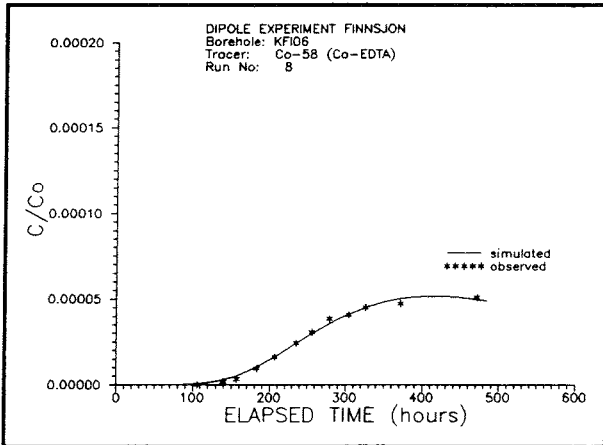
FINAL ESTIMATE FOR PARAMETER 1 = 0.9913E-04  
FINAL ESTIMATE FOR PARAMETER 2 = 0.5071E-02  
FINAL ESTIMATE FOR PARAMETER 3 = 0.7713E+00

\*\*\*\*\*  
REGRESSION STATISTICS

NO. OF OBSERVATIONS: 15  
SUM OF SQUARED DIFFERENCES = 0.347E-09  
ERROR VARIANCE = 0.289E-10  
CORRELATION COEFFICIENT = .99332E+00

STANDARD ERROR FOR PARAMETER 1 = 0.111E-04  
STANDARD ERROR FOR PARAMETER 2 = 0.522E-03  
STANDARD ERROR FOR PARAMETER 3 = 0.135E+00

CORRELATION BETWEEN PARAM. 1 AND 2 = -.9075E+00  
CORRELATION BETWEEN PARAM. 1 AND 3 = -.9958E+00  
CORRELATION BETWEEN PARAM. 2 AND 3 = 0.8990E+00



\*\*\*\*\* REGRESSION SUMMARY \*\*\*\*\*

TRANSPORT PATH: BFI01-KFI06  
TRACER: CO-58

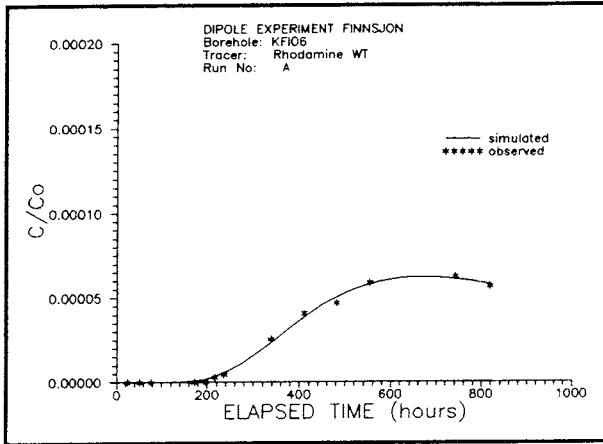
FINAL ESTIMATE FOR PARAMETER 1 = 0.1287E-03  
FINAL ESTIMATE FOR PARAMETER 2 = 0.3562E-02  
FINAL ESTIMATE FOR PARAMETER 3 = 0.2741E+00

\*\*\*\*\*  
REGRESSION STATISTICS

NO. OF OBSERVATIONS: 12  
SUM OF SQUARED DIFFERENCES = 0.261E-10  
ERROR VARIANCE = 0.290E-11  
CORRELATION COEFFICIENT = .99695E+00

STANDARD ERROR FOR PARAMETER 1 = 0.688E-05  
STANDARD ERROR FOR PARAMETER 2 = 0.299E-03  
STANDARD ERROR FOR PARAMETER 3 = 0.273E-01

CORRELATION BETWEEN PARAM. 1 AND 2 = -.8979E+00  
CORRELATION BETWEEN PARAM. 1 AND 3 = -.9875E+00  
CORRELATION BETWEEN PARAM. 2 AND 3 = 0.8820E+00



\*\*\*\*\* REGRESSION SUMMARY \*\*\*\*\*

TRANSPORT PATH: BFI01-KFI06  
TRACER: RHODAMINE WT

FINAL ESTIMATE FOR PARAMETER 1 = 0.9961E-04  
FINAL ESTIMATE FOR PARAMETER 2 = 0.2267E-02  
FINAL ESTIMATE FOR PARAMETER 3 = 0.2693E+00

\*\*\*\*\*

REGRESSION STATISTICS

NO. OF OBSERVATIONS: 13

SUM OF SQUARED DIFFERENCES = 0.337E-10

ERROR VARIANCE = 0.337E-11

CORRELATION COEFFICIENT = .99806E+00

STANDARD ERROR FOR PARAMETER 1 = 0.255E-05  
STANDARD ERROR FOR PARAMETER 2 = 0.197E-03  
STANDARD ERROR FOR PARAMETER 3 = 0.120E-01

CORRELATION BETWEEN PARAM. 1 AND 2 = -.7502E+00  
CORRELATION BETWEEN PARAM. 1 AND 3 = -.9254E+00  
CORRELATION BETWEEN PARAM. 2 AND 3 = 0.8106E+00

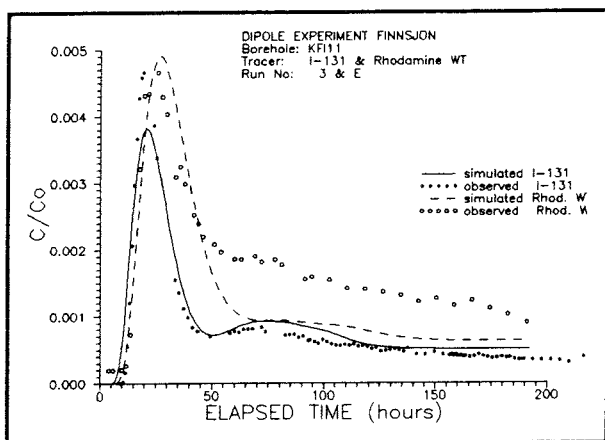
A4            **MODELLING OF SORBING TRACER BREAKTHROUGH IN KFI11  
WITH WEIGHING FACTOR FROM PEAK CONCENTRATIONS**

Table A-2. List of explanations for the regression summary and regression statistics in Appendix A4-A5.

---

Final estimate for parameter 1: mean velocity,  $v$  (m/s)  
Final estimate for parameter 2: dispersion coefficient,  $D$  (m<sup>2</sup>/s)  
Final estimate for parameter 3: f-parameter non-sorbing tracer,  $f_1$  (dim.less)  
Final estimate for parameter 4: retardation coeff. sorbing tracer,  $R_1$  (dim.less)  
Final estimate for parameter 5: f-parameter sorbing tracer,  $f_2$  (dim.less)  
Final estimate for parameter 6: retardation coeff. sorbing tracer,  $R_2$  (dim.less)  
Final estimate for parameter 7: f-parameter sorbing tracer,  $f_3$  (dim.less)

---



\*\*\*\*\* REGRESSION SUMMARY \*\*\*\*\*

TRANSPORT PATH: BFI01-KFI11  
NON-SORBING TRACER: I-131  
SORBING TRACER: RHODAMINE WT

FINAL ESTIMATE FOR PARAMETER 1 = 0.1652E-02  
FINAL ESTIMATE FOR PARAMETER 2 = 0.1979E-01  
FINAL ESTIMATE FOR PARAMETER 3 = 0.1276E+01  
FINAL ESTIMATE FOR PARAMETER 4 = 0.1282E+01  
FINAL ESTIMATE FOR PARAMETER 5 = 0.1641E+01

\*\*\*\*\*  
REGRESSION STATISTICS

NO. OF OBSERVATIONS: 130  
SUM OF SQUARED DIFFERENCES = 0.208E-04  
ERROR VARIANCE = 0.167E-06  
CORRELATION COEFFICIENT = .93768E+00

STANDARD ERROR FOR PARAMETER 1 = 0.350E-04  
STANDARD ERROR FOR PARAMETER 2 = 0.136E-02  
STANDARD ERROR FOR PARAMETER 3 = 0.545E-01  
STANDARD ERROR FOR PARAMETER 4 = 0.347E-01  
STANDARD ERROR FOR PARAMETER 5 = 0.851E-01

CORRELATION BETWEEN PARAM. 1 AND 2 = -.3251E-01  
CORRELATION BETWEEN PARAM. 1 AND 3 = -.5711E+00  
CORRELATION BETWEEN PARAM. 1 AND 4 = 0.7124E+00  
CORRELATION BETWEEN PARAM. 1 AND 5 = 0.3625E+00  
CORRELATION BETWEEN PARAM. 2 AND 3 = 0.1059E+00  
CORRELATION BETWEEN PARAM. 2 AND 4 = 0.1824E+00  
CORRELATION BETWEEN PARAM. 2 AND 5 = 0.2325E+00  
CORRELATION BETWEEN PARAM. 3 AND 4 = -.3889E+00  
CORRELATION BETWEEN PARAM. 3 AND 5 = -.7346E+00  
CORRELATION BETWEEN PARAM. 4 AND 5 = 0.4278E+00

\*\*\*\*\* REGRESSION SUMMARY \*\*\*\*\*

TRANSPORT PATH: BFI01-KFI11  
NON-SORBING TRACER:  
SORBING TRACER:

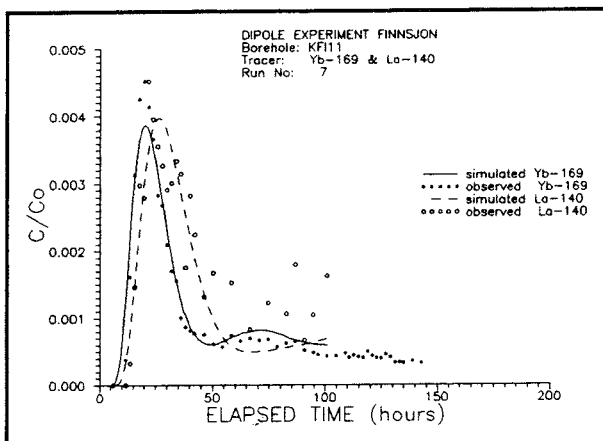
FINAL ESTIMATE FOR PARAMETER 1 = 0.1722E-02  
FINAL ESTIMATE FOR PARAMETER 2 = 0.1906E-01  
FINAL ESTIMATE FOR PARAMETER 3 = 0.1201E+01  
FINAL ESTIMATE FOR PARAMETER 4 = 0.1302E+01  
FINAL ESTIMATE FOR PARAMETER 5 = 0.1338E+01

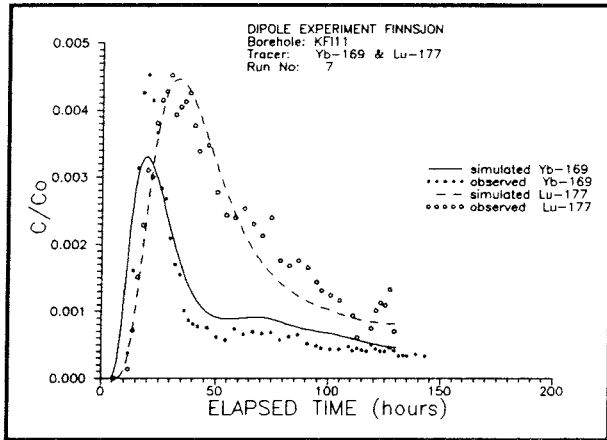
\*\*\*\*\*  
REGRESSION STATISTICS

NO. OF OBSERVATIONS: 76  
SUM OF SQUARED DIFFERENCES = 0.124E-04  
ERROR VARIANCE = 0.174E-06  
CORRELATION COEFFICIENT = .94673E+00

STANDARD ERROR FOR PARAMETER 1 = 0.399E-04  
STANDARD ERROR FOR PARAMETER 2 = 0.166E-02  
STANDARD ERROR FOR PARAMETER 3 = 0.540E-01  
STANDARD ERROR FOR PARAMETER 4 = 0.400E-01  
STANDARD ERROR FOR PARAMETER 5 = 0.741E-01

CORRELATION BETWEEN PARAM. 1 AND 2 = 0.4024E-01  
CORRELATION BETWEEN PARAM. 1 AND 3 = -.3185E+00  
CORRELATION BETWEEN PARAM. 1 AND 4 = 0.6866E+00  
CORRELATION BETWEEN PARAM. 1 AND 5 = 0.1516E+00  
CORRELATION BETWEEN PARAM. 2 AND 3 = 0.3733E+00  
CORRELATION BETWEEN PARAM. 2 AND 4 = 0.3228E+00  
CORRELATION BETWEEN PARAM. 2 AND 5 = 0.1639E+00  
CORRELATION BETWEEN PARAM. 3 AND 4 = -.1046E+00  
CORRELATION BETWEEN PARAM. 3 AND 5 = -.5950E+00  
CORRELATION BETWEEN PARAM. 4 AND 5 = 0.3085E+00





\*\*\*\*\* REGRESSION SUMMARY \*\*\*\*\*

TRANSPORT PATH: BF01-KF11  
NON-SORBING TRACER: YB-169  
SORBING TRACER: LU-177

FINAL ESTIMATE FOR PARAMETER 1 = 0.1649E-02  
FINAL ESTIMATE FOR PARAMETER 2 = 0.3197E-01  
FINAL ESTIMATE FOR PARAMETER 3 = 0.1328E+01  
FINAL ESTIMATE FOR PARAMETER 4 = 0.1717E+01  
FINAL ESTIMATE FOR PARAMETER 5 = 0.2318E+01

\*\*\*\*\*  
REGRESSION STATISTICS

NO. OF OBSERVATIONS: 90  
SUM OF SQUARED DIFFERENCES = 0.141E-04  
ERROR VARIANCE = 0.166E-06  
CORRELATION COEFFICIENT = .9554E+00

STANDARD ERROR FOR PARAMETER 1 = 0.544E-04  
STANDARD ERROR FOR PARAMETER 2 = 0.238E-02  
STANDARD ERROR FOR PARAMETER 3 = 0.586E-01  
STANDARD ERROR FOR PARAMETER 4 = 0.657E-01  
STANDARD ERROR FOR PARAMETER 5 = 0.117E+00

CORRELATION BETWEEN PARAM. 1 AND 2 = 0.2977E+00  
CORRELATION BETWEEN PARAM. 1 AND 3 = -.3478E+00  
CORRELATION BETWEEN PARAM. 1 AND 4 = 0.8223E+00  
CORRELATION BETWEEN PARAM. 1 AND 5 = 0.2454E+00  
CORRELATION BETWEEN PARAM. 2 AND 3 = 0.1909E+00  
CORRELATION BETWEEN PARAM. 2 AND 4 = 0.4931E+00  
CORRELATION BETWEEN PARAM. 2 AND 5 = 0.1790E+00  
CORRELATION BETWEEN PARAM. 3 AND 4 = -.2058E+00  
CORRELATION BETWEEN PARAM. 3 AND 5 = -.7354E+00  
CORRELATION BETWEEN PARAM. 4 AND 5 = 0.3777E+00

\*\*\*\*\* REGRESSION SUMMARY \*\*\*\*\*

TRANSPORT PATH: BF101-KF11  
NON-SORBING TRACER: YB-169  
SORBING TRACERS: LA-140, LU-177

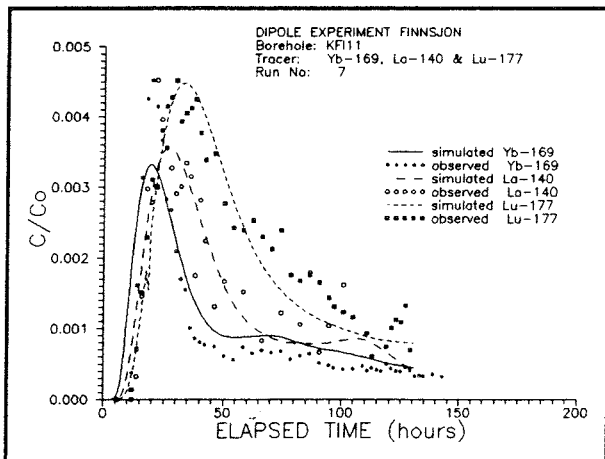
FINAL ESTIMATE FOR PARAMETER 1 = 0.1652E-02  
FINAL ESTIMATE FOR PARAMETER 2 = 0.3129E-01  
FINAL ESTIMATE FOR PARAMETER 3 = 0.1323E+01  
FINAL ESTIMATE FOR PARAMETER 4 = 0.1383E+01  
FINAL ESTIMATE FOR PARAMETER 5 = 0.1482E+01  
FINAL ESTIMATE FOR PARAMETER 6 = 0.1713E+01  
FINAL ESTIMATE FOR PARAMETER 7 = 0.2309E+01

\*\*\*\*\*  
REGRESSION STATISTICS

NO. OF OBSERVATIONS: 117  
SUM OF SQUARED DIFFERENCES = 0.221E-04  
ERROR VARIANCE = 0.201E-06  
CORRELATION COEFFICIENT = .94425E+00

STANDARD ERROR FOR PARAMETER 1 = 0.588E-04  
STANDARD ERROR FOR PARAMETER 2 = 0.230E-02  
STANDARD ERROR FOR PARAMETER 3 = 0.631E-01  
STANDARD ERROR FOR PARAMETER 4 = 0.648E-01  
STANDARD ERROR FOR PARAMETER 5 = 0.936E-01  
STANDARD ERROR FOR PARAMETER 6 = 0.709E-01  
STANDARD ERROR FOR PARAMETER 7 = 0.128E+00

CORRELATION BETWEEN PARAM. 1 AND 2 = 0.3558E+00  
CORRELATION BETWEEN PARAM. 1 AND 3 = -.3397E+00  
CORRELATION BETWEEN PARAM. 1 AND 4 = 0.7254E+00  
CORRELATION BETWEEN PARAM. 1 AND 5 = 0.2058E+00  
CORRELATION BETWEEN PARAM. 1 AND 6 = 0.8289E+00  
CORRELATION BETWEEN PARAM. 1 AND 7 = 0.2460E+00  
CORRELATION BETWEEN PARAM. 2 AND 3 = 0.1363E+00  
CORRELATION BETWEEN PARAM. 2 AND 4 = 0.4985E+00  
CORRELATION BETWEEN PARAM. 2 AND 5 = 0.2220E+00  
CORRELATION BETWEEN PARAM. 2 AND 6 = 0.5096E+00  
CORRELATION BETWEEN PARAM. 2 AND 7 = 0.1795E+00  
CORRELATION BETWEEN PARAM. 3 AND 4 = -.1756E+00  
CORRELATION BETWEEN PARAM. 3 AND 5 = -.6367E+00  
CORRELATION BETWEEN PARAM. 3 AND 6 = -.2184E+00  
CORRELATION BETWEEN PARAM. 3 AND 7 = -.7523E+00  
CORRELATION BETWEEN PARAM. 4 AND 5 = 0.4104E+00  
CORRELATION BETWEEN PARAM. 4 AND 6 = 0.6604E+00  
CORRELATION BETWEEN PARAM. 4 AND 7 = 0.2038E+00  
CORRELATION BETWEEN PARAM. 5 AND 6 = 0.2072E+00  
CORRELATION BETWEEN PARAM. 5 AND 7 = 0.5916E+00  
CORRELATION BETWEEN PARAM. 6 AND 7 = 0.3743E+00



A5      **MODELLING OF SORBING TRACER BREAKTHROUGH IN KFI11  
WITH WEIGHING FACTOR FROM F-PARAMETER**

\*\*\*\*\* REGRESSION SUMMARY \*\*\*\*\*

TRANSPORT PATH: BFI01-KFI11  
 NON-SORBING TRACER: I-131  
 SORBING TRACER: RHODAMINE WT

FINAL ESTIMATE FOR PARAMETER 1 = 0.1726E-02  
 FINAL ESTIMATE FOR PARAMETER 2 = 0.1384E-01  
 FINAL ESTIMATE FOR PARAMETER 3 = 0.1199E+01  
 FINAL ESTIMATE FOR PARAMETER 4 = 0.1270E+01  
 FINAL ESTIMATE FOR PARAMETER 5 = 0.6820E+00

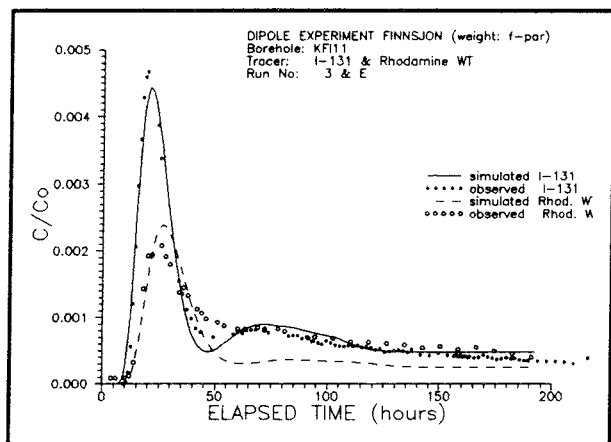
\*\*\*\*\*

REGRESSION STATISTICS

NO. OF OBSERVATIONS: 130  
 SUM OF SQUARED DIFFERENCES = 0.731E-05  
 ERROR VARIANCE = 0.584E-07  
 CORRELATION COEFFICIENT = .96080E+00

STANDARD ERROR FOR PARAMETER 1 = 0.184E-04  
 STANDARD ERROR FOR PARAMETER 2 = 0.691E-03  
 STANDARD ERROR FOR PARAMETER 3 = 0.314E-01  
 STANDARD ERROR FOR PARAMETER 4 = 0.278E-01  
 STANDARD ERROR FOR PARAMETER 5 = 0.328E-01

CORRELATION BETWEEN PARAM. 1 AND 2 = -.2324E+00  
 CORRELATION BETWEEN PARAM. 1 AND 3 = -.6151E+00  
 CORRELATION BETWEEN PARAM. 1 AND 4 = 0.4317E+00  
 CORRELATION BETWEEN PARAM. 1 AND 5 = 0.2269E+00  
 CORRELATION BETWEEN PARAM. 2 AND 3 = 0.2780E+00  
 CORRELATION BETWEEN PARAM. 2 AND 4 = 0.1761E-01  
 CORRELATION BETWEEN PARAM. 2 AND 5 = 0.1041E+00  
 CORRELATION BETWEEN PARAM. 3 AND 4 = -.2487E+00  
 CORRELATION BETWEEN PARAM. 3 AND 5 = -.4456E+00  
 CORRELATION BETWEEN PARAM. 4 AND 5 = 0.2979E+00



\*\*\*\*\* REGRESSION SUMMARY \*\*\*\*\*

TRANSPORT PATH: BFI01-KFI11  
 NON-SORBING TRACER: YB-169  
 SORBING TRACER: LA-140

FINAL ESTIMATE FOR PARAMETER 1 = 0.1745E-02  
 FINAL ESTIMATE FOR PARAMETER 2 = 0.1609E-01  
 FINAL ESTIMATE FOR PARAMETER 3 = 0.1156E+01  
 FINAL ESTIMATE FOR PARAMETER 4 = 0.1287E+01  
 FINAL ESTIMATE FOR PARAMETER 5 = 0.7640E+00

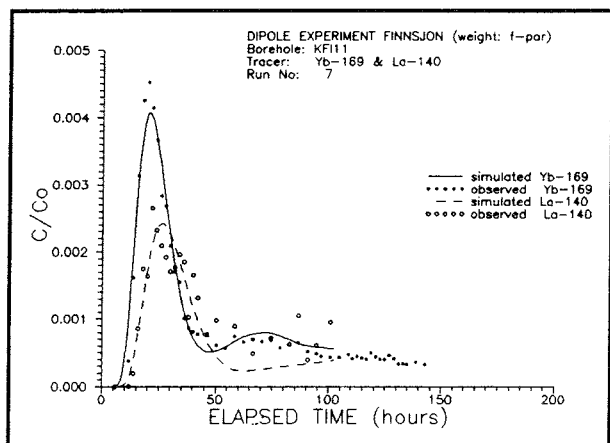
\*\*\*\*\*

REGRESSION STATISTICS

NO. OF OBSERVATIONS: 76  
 SUM OF SQUARED DIFFERENCES = 0.566E-05  
 ERROR VARIANCE = 0.797E-07  
 CORRELATION COEFFICIENT = .96331E+00

STANDARD ERROR FOR PARAMETER 1 = 0.247E-04  
 STANDARD ERROR FOR PARAMETER 2 = 0.110E-02  
 STANDARD ERROR FOR PARAMETER 3 = 0.363E-01  
 STANDARD ERROR FOR PARAMETER 4 = 0.328E-01  
 STANDARD ERROR FOR PARAMETER 5 = 0.388E-01

CORRELATION BETWEEN PARAM. 1 AND 2 = -.5907E-01  
 CORRELATION BETWEEN PARAM. 1 AND 3 = -.3238E+00  
 CORRELATION BETWEEN PARAM. 1 AND 4 = 0.4954E+00  
 CORRELATION BETWEEN PARAM. 1 AND 5 = 0.9705E-01  
 CORRELATION BETWEEN PARAM. 2 AND 3 = 0.4629E+00  
 CORRELATION BETWEEN PARAM. 2 AND 4 = 0.1976E+00  
 CORRELATION BETWEEN PARAM. 2 AND 5 = 0.1070E+00  
 CORRELATION BETWEEN PARAM. 3 AND 4 = -.5937E-01  
 CORRELATION BETWEEN PARAM. 3 AND 5 = -.4118E+00  
 CORRELATION BETWEEN PARAM. 4 AND 5 = 0.2891E+00

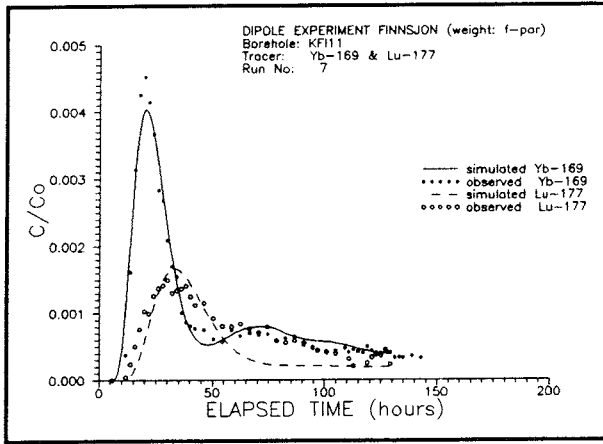


## **APPENDIX B**

**DIPOLE TRACER EXPERIMENT IN A LOW-ANGLE FRACTURE  
ZONE AT THE FINNSJÖN SITE, CENTRAL SWEDEN.**  
Experimental design and preliminary results.

The Fracture Zone Project - Phase 3

SKB Progress Report AR 90-24



\*\*\*\*\* REGRESSION SUMMARY \*\*\*\*\*

TRANSPORT PATH: BFI01-KFI11  
 NON-SORBING TRACER: YB-169  
 SORBING TRACER: LU-177

FINAL ESTIMATE FOR PARAMETER 1 = 0.1741E-02  
 FINAL ESTIMATE FOR PARAMETER 2 = 0.1660E-01  
 FINAL ESTIMATE FOR PARAMETER 3 = 0.1165E+01  
 FINAL ESTIMATE FOR PARAMETER 4 = 0.1617E+01  
 FINAL ESTIMATE FOR PARAMETER 5 = 0.6661E+00

\*\*\*\*\*  
 REGRESSION STATISTICS

NO. OF OBSERVATIONS: 90  
 SUM OF SQUARED DIFFERENCES = 0.486E-05  
 ERROR VARIANCE = 0.572E-07  
 CORRELATION COEFFICIENT = .9686E+00

STANDARD ERROR FOR PARAMETER 1 = 0.214E-04  
 STANDARD ERROR FOR PARAMETER 2 = 0.102E-02  
 STANDARD ERROR FOR PARAMETER 3 = 0.314E-01  
 STANDARD ERROR FOR PARAMETER 4 = 0.460E-01  
 STANDARD ERROR FOR PARAMETER 5 = 0.373E-01

CORRELATION BETWEEN PARAM. 1 AND 2 = -.8107E-01  
 CORRELATION BETWEEN PARAM. 1 AND 3 = -.3363E+00  
 CORRELATION BETWEEN PARAM. 1 AND 4 = 0.3745E+00  
 CORRELATION BETWEEN PARAM. 1 AND 5 = 0.7057E-01  
 CORRELATION BETWEEN PARAM. 2 AND 3 = 0.4850E+00  
 CORRELATION BETWEEN PARAM. 2 AND 4 = 0.1715E+00  
 CORRELATION BETWEEN PARAM. 2 AND 5 = 0.9729E-01  
 CORRELATION BETWEEN PARAM. 3 AND 4 = -.3290E-01  
 CORRELATION BETWEEN PARAM. 3 AND 5 = -.3021E+00  
 CORRELATION BETWEEN PARAM. 4 AND 5 = 0.3866E+00

\*\*\*\*\* REGRESSION SUMMARY \*\*\*\*\*

TRANSPORT PATH: BFI01-KFI11  
 NON-SORBING TRACER: YB-169  
 SORBING TRACERS: LA-140, LU-177

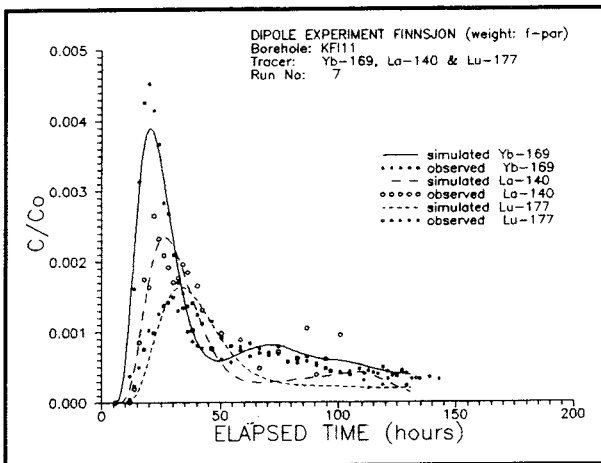
FINAL ESTIMATE FOR PARAMETER 1 = 0.1725E-02  
 FINAL ESTIMATE FOR PARAMETER 2 = 0.1862E-01  
 FINAL ESTIMATE FOR PARAMETER 3 = 0.1195E+01  
 FINAL ESTIMATE FOR PARAMETER 4 = 0.1300E+01  
 FINAL ESTIMATE FOR PARAMETER 5 = 0.7816E+00  
 FINAL ESTIMATE FOR PARAMETER 6 = 0.1634E+01  
 FINAL ESTIMATE FOR PARAMETER 7 = 0.6848E+00

\*\*\*\*\*  
 REGRESSION STATISTICS

NO. OF OBSERVATIONS: 117  
 SUM OF SQUARED DIFFERENCES = 0.837E-05  
 ERROR VARIANCE = 0.761E-07  
 CORRELATION COEFFICIENT = .9540E+00

STANDARD ERROR FOR PARAMETER 1 = 0.262E-04  
 STANDARD ERROR FOR PARAMETER 2 = 0.119E-02  
 STANDARD ERROR FOR PARAMETER 3 = 0.364E-01  
 STANDARD ERROR FOR PARAMETER 4 = 0.354E-01  
 STANDARD ERROR FOR PARAMETER 5 = 0.392E-01  
 STANDARD ERROR FOR PARAMETER 6 = 0.566E-01  
 STANDARD ERROR FOR PARAMETER 7 = 0.442E-01

CORRELATION BETWEEN PARAM. 1 AND 2 = -.1796E-01  
 CORRELATION BETWEEN PARAM. 1 AND 3 = -.3314E+00  
 CORRELATION BETWEEN PARAM. 1 AND 4 = 0.4965E+00  
 CORRELATION BETWEEN PARAM. 1 AND 5 = 0.1040E+00  
 CORRELATION BETWEEN PARAM. 1 AND 6 = 0.3906E+00  
 CORRELATION BETWEEN PARAM. 1 AND 7 = 0.8184E-01  
 CORRELATION BETWEEN PARAM. 2 AND 3 = 0.4276E+00  
 CORRELATION BETWEEN PARAM. 2 AND 4 = 0.2304E+00  
 CORRELATION BETWEEN PARAM. 2 AND 5 = 0.1240E+00  
 CORRELATION BETWEEN PARAM. 2 AND 6 = 0.1804E+00  
 CORRELATION BETWEEN PARAM. 2 AND 7 = 0.9140E-01  
 CORRELATION BETWEEN PARAM. 3 AND 4 = -.6360E-01  
 CORRELATION BETWEEN PARAM. 3 AND 5 = -.4141E+00  
 CORRELATION BETWEEN PARAM. 3 AND 6 = -.5041E-01  
 CORRELATION BETWEEN PARAM. 3 AND 7 = -.3234E+00  
 CORRELATION BETWEEN PARAM. 4 AND 5 = 0.3236E+00  
 CORRELATION BETWEEN PARAM. 4 AND 6 = 0.2388E+00  
 CORRELATION BETWEEN PARAM. 4 AND 7 = 0.6287E-01  
 CORRELATION BETWEEN PARAM. 5 AND 6 = 0.6421E-01  
 CORRELATION BETWEEN PARAM. 5 AND 7 = 0.2240E+00  
 CORRELATION BETWEEN PARAM. 6 AND 7 = 0.4043E+00



SWEDISH GEOLOGICAL CO  
Division of Engineering Geology  
Uppsala  
Sweden

REPORT  
Id no: IRAP 90 206  
Date: 1990-04-17

DIPOLE TRACER EXPERIMENT IN A LOW-ANGLE  
FRACTURE ZONE AT THE FINNSJÖN SITE,  
CENTRAL SWEDEN

Experimental design and preliminary results

The Fracture Zone Project - Phase 3

Peter Andersson  
Carl-Olof Eriksson  
Erik Gustafsson  
Thomas Ittner

Swedish Geological Co., Uppsala, Sweden

March 1990

## ABSTRACT

As a part of the Fracture Zone Project at the Finnsjön study site, central Sweden, a large scale tracer experiment in a dipole flow geometry was performed. The objectives of the experiment was primarily to determine transport parameters from a major fracture zone. Secondly, the applicability of the method in a large scale and in highly conductive rock was tested and thirdly, the use of short-lived radioisotopes was tested.

This report describes the experimental design and a qualitative evaluation of the tracer breakthrough data. A more quantitative evaluation including model runs and comparison with the predictive modelling will be reported separately.

The experiment was performed in the Brändan area, Finnsjön study site, using the same borehole configuration as the previously performed radially converging experiment (Gustafsson et al., 1989). The dipole flow field was created in a sealed off interval of the highly conductive upper part of Zone 2. Water was recirculated between the injection borehole and the pumping borehole in a closed system over a distance of 168 m. Tracers slugs were injected and detected in the pumping borehole and also in two observation boreholes along the flow direction. In total 15 injections including 14 radiotracers and 5 non-radioactive tracers were made. Both sorbing and non-sorbing tracers were injected.

Tracer breakthrough was registered in all three boreholes with mean residence times ranging between 18-400 hours. The large spread in mean residence times indicates that the upper part of Zone 2 is more heterogeneous than expected from the hydraulic tests. It was also found that about 30 % of the mass of tracer was lost, possibly due to the heterogeneity of the system in combination with the natural gradient in the area.

Based on the breakthrough data including first arrival, mean residence time, peak concentration, and tracer recovery, a classification of the tracers was made. The data showed four different types of tracers:

- Conservative tracers with high recovery.
- Conservative tracers with irreversible losses.
- Weakly sorbing tracers (reversible losses).
- Strongly sorbing tracers.

The results also shows that it is possible to use short-lived radioisotopes as tracers in large scale field experiments. The method enables very fast and simple tracer analyses in situ.

	<u>Page</u>
<u>CONTENTS</u>	
<u>ABSTRACT</u>	i
<u>CONTENTS</u>	ii
1. <u>INTRODUCTION</u>	1
1.1 BACKGROUND	1
1.2 OBJECTIVES	2
2. <u>SITE CHARACTERIZATION</u>	3
2.1 GEOLOGY	3
2.2 GEOHYDROLOGY	3
2.3 HYDROCHEMISTRY	7
3. <u>EXPERIMENTAL DESIGN</u>	10
3.1 CONCEPTUAL MODEL	10
3.2 EXPERIMENTAL SET-UP	11
3.2.1 <u>Equipment and procedures</u>	11
3.2.2 <u>Tracer injections</u>	13
3.3 TRACER SAMPLING AND ANALYSIS	17
3.4 SUPPORTING MEASUREMENTS	18
4. <u>EXPERIMENTAL RESULTS</u>	20
4.1 TRACER BREAKTHROUGH	20
4.1.1 <u>Breakthrough in borehole BFI02</u>	20
4.1.2 <u>Breakthrough in borehole KFI11</u>	25
4.1.3 <u>Breakthrough in borehole KFI06</u>	27
4.1.4 <u>Dilution measurement and tracer injection in borehole KFI11</u>	28
4.1.5 <u>Recovery calculations</u>	30
4.1.6 <u>Classification of tracers</u>	33
4.2 SUPPORTING MEASUREMENTS	34
4.2.1 <u>Head measurements</u>	34
4.2.2 <u>Pumping rate and physical parameters</u>	36

5.	<u>DISCUSSION AND CONCLUSIONS</u>	40
5.1	EXPERIMENTAL DESIGN	40
5.2	EXPERIMENTAL RESULTS	41
6.	<u>REFERENCES</u>	43

APPENDICES

APPENDIX A: Tracer breakthrough in borehole BFI02.

APPENDIX B: Tracer breakthrough in borehole KFI11.

APPENDIX C: Tracer breakthrough in borehole KFI06.

APPENDIX D: Supporting measurements.

## 1. INTRODUCTION

### 1.1 BACKGROUND

In crystalline rock the flow of groundwater through the intact rock matrix is very low. The rate at which radionuclides in groundwater can migrate through the rock is chiefly dependent upon the fracture system. Hence, fractures and fracture zones represent the primary flow paths along which radionuclides may migrate from a nuclear waste repository to the biosphere.

Lacking a deeper knowledge about the properties and the influence these major fracture zones have regarding radionuclide transport in crystalline bedrock, the distance between the repository and a major fracture zone was decided not to be shorter than 100 metres in the KBS 3 safety analysis. It is thus of great importance to enhance the knowledge about the transport conditions in major fracture zones to get a better basis in determining the distance required from a repository to a major fracture zone. If the distance can be reduced or must be increased this will directly influence the rock volume usable for excavation of the repository. The following is to be answered:

- How are radionuclides transported in major fracture zones ?
- How do the major fracture zones interact with the surrounding rock regarding radionuclide transport ?

In order to answer the above stated questions, detailed investigations have been carried out in a major fracture zone at the Finnsjön study site (Ahlbom et al., 1986, 1987, 1989). The study was focused on the geologic/tectonic and hydrogeologic character of the extensive low-angle fracture zone, Zone 2, which was encountered at depths ranging from 100 to 250 metres. Results from hydrochemical investigations in the area (Ahlbom et al., 1986; Smellie et al., 1987) show that Zone 2 represents a structural boundary between non-saline and saline groundwater. The salinity increases distinctly in the upper part of the zone and remains nearly constant further below.

The characterization of Zone 2 in Phase 1 and 2 of the Fracture Zone Project constitutes the basis for previously performed radially converging tracer experiment (RCT) and the here described dipole tracer experiment in Phase 3 of the study. An extensive amount of background information regarding the hydrogeological and hydrochemical properties have been gathered during the first two phases of the project. Phase 3 also includes three large-scale interference tests performed in the same radial geometry as the radially converging tracer experiment (Andersson et al., 1988b).

## 1.2 OBJECTIVES

The objectives of the dipole tracer experiment are primarily to determine parameters essential for the understanding of radionuclide transport in major fracture zones and to utilize the results for calibration and verification of radionuclide transport models. Secondly, the applicability of the method in a large scale and in a highly conductive rock, is tested. The test geometry also enables the results to be directly compared to the results obtained at the radially converging experiment. Finally, the use of radiotracers with short half lives (6 hours to 71 days) in a closed recirculating system, is tested.

## 2. SITE CHARACTERIZATION

### 2.1 GEOLOGY

The general geological, geophysical and hydrogeological characterization of the Finnsjön study site are given by Ahlbom et al., (1986), (1987) and summarized by Ahlbom and Smellie (1989). Figure 2-1 and 2-2 show the dominant structural features of the Brändan area within the Finnsjön study site. Location of the boreholes in relation to the main investigation site at Brändan are also shown.

The tectonic block within the main investigation site is dominated by granodiorite. The rock is medium grained, grey to reddish grey, and is generally foliated (strike NW, dipping steeply to the E). The granodiorite brecciates the older leptites and basites. Xenolites of these rocktypes are frequent within the granodiorite. Dikes of younger rocktypes, i.e. granite, pegmatite and aplite, are common. Red-coloured granodiorite is often associated with tectonism in areas where mylonites are common.

At the main investigation site two major fracture zones have been identified and characterized. The Brändan fracture zone (Fig. 2-1; Zone 1) has a NNE strike with a dip of about 75 degrees to the east. The second fracture zone, the low-angle Zone 2, is defined from borehole data (Fig. 2-2). Zone 2 is trending north with a dip of about 16 degrees to the west and consists of sections with high fracture frequency and tectonisation. The colour of the rock is red within the tectonized sections and the fracture infillings are dominated by calcite and chlorite. Other common minerals within the low-angle zone are hematite, laumontite, asphaltite and clay minerals.

### 2.2 GEOHYDROLOGY

The geohydrology of the Brändan area is dominated by the two highly conductive fracture zones, the Brändan zone (Zone 1) and the low angle zone (Zone 2).

Zone 1, the Brändan fracture zone, strikes NNE and dips 75 degrees to the east. The thickness of the zone is about 20 m and the lineament representing the fracture zone is well defined from surface geophysical measurements for more than one km of length. The hydraulic conductivity of Zone 1 ranges between  $1 \text{ E-6} - 5 \text{ E-5 m/s}$  (2 m intervals) as compared to  $1 \text{ E-7 m/s}$  in the country rock.

Zone 2, the low-angle fracture zone, is well defined in seven boreholes located within an area of approx.  $500 \times 500 \text{ m}$ , see Figure 2-2. In this area the fracture zone is almost planar with the upper surface located between 100 to 240 m below the ground surface. The orientation of Zone 2 is  $28^{\circ} \text{W}$  with a dip of 16 degrees to the southwest. The location of the lower boundary

of the zone is somewhat uncertain. However, in general the zone has a thickness of about 100 m. Representative values of the hydraulic conductivity, measured in 2 m sections by single hole water injection tests (Andersson et al., 1988a), above and below the fracture zone are  $5 \times 10^{-8}$  and  $1 \times 10^{-9}$  m/s, respectively. Within the fracture zone the mean value is  $5 \times 10^{-6}$  m/s, but the conductivity is enhanced in the upper and lower margins of the fracture zone, where the values are  $2 \times 10^{-4}$  and  $1 \times 10^{-5}$  m/s respectively, while other parts have conductivities similar to the country rock.

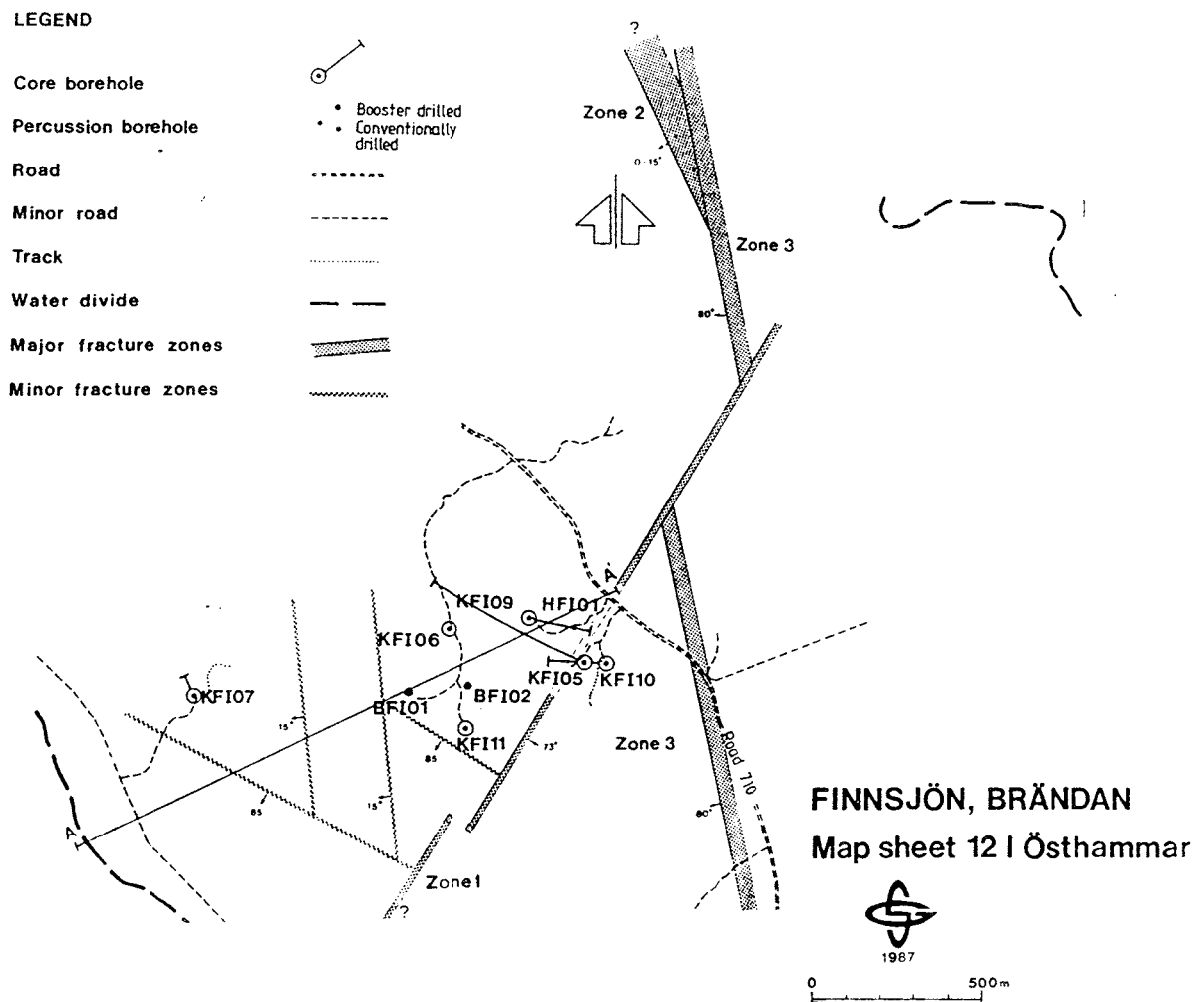


Figure 2-1 Map of the Brändan area showing borehole locations and fracture zones. The location of profile A - A' illustrated in Figure 2-2 is also marked.

The salinity shows an abrupt increase of more than 5000 mg/l of equivalent chlorine at the uppermost part of Zone 2, as measured in all boreholes intersecting the zone. The salinity remains high from the upper part of the fracture zone and downward.

The natural groundwater flow distribution in the Brändan area is most likely governed by Zone 1 and Zone 2. Piezometric measurements have simultaneously been made in packed-off intervals of the boreholes penetrating the low-angle zone and also in the Brändan zone. In the boreholes, up to five sections have been measured above and within the zones. The measurements of the groundwater table indicate a weak groundwater gradient varying between 1 m/350 m in the western part of the area to 1 m/150 m in the eastern part and directed towards ENE, see Figure 2-3. Within Zone 2, the direction and the gradients are roughly the same, see Figure 2-3. Zone 2 seems to act as a drain in the part of the area where it is deepest below the ground surface, while in the shallow parts, near the Brändan zone, it seems to be discharging water to the Brändan zone. A tentative model of groundwater flow in Zone 2 is presented in Figure 2-4.

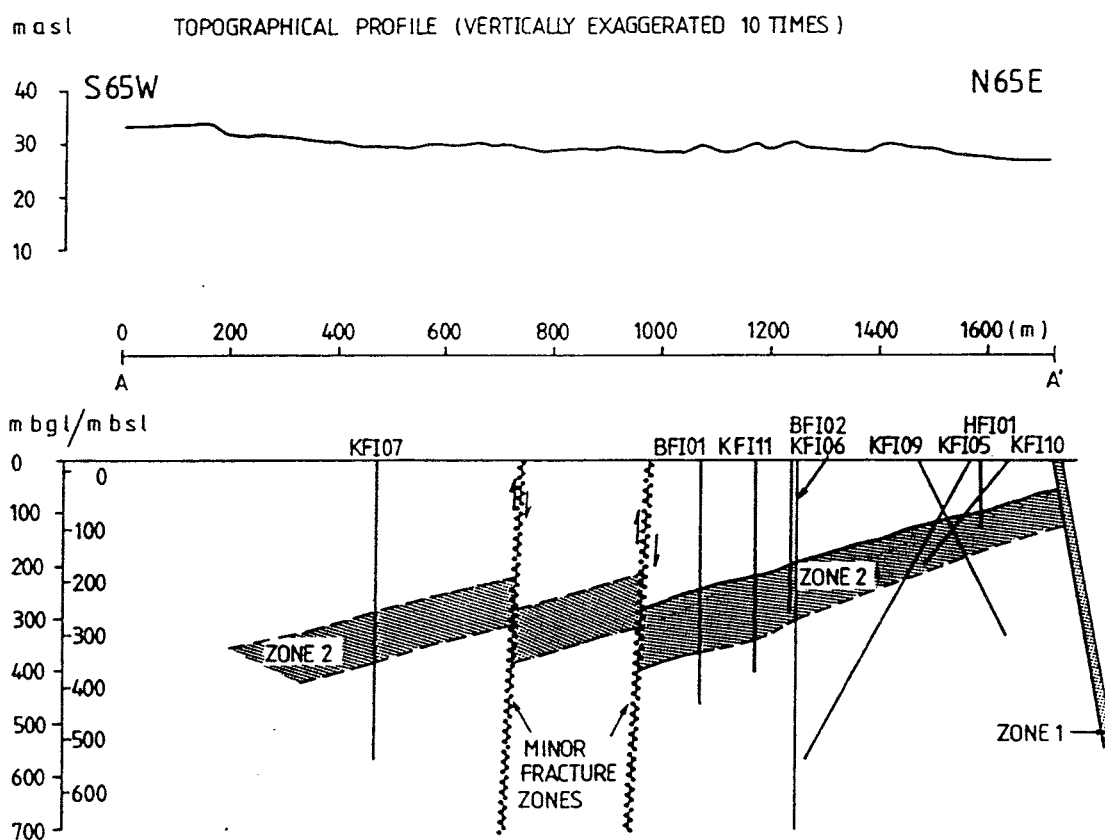


Figure 2-2 Structural profile through the Brändan area showing the location of Zone 2. The boreholes are projected into the profile.

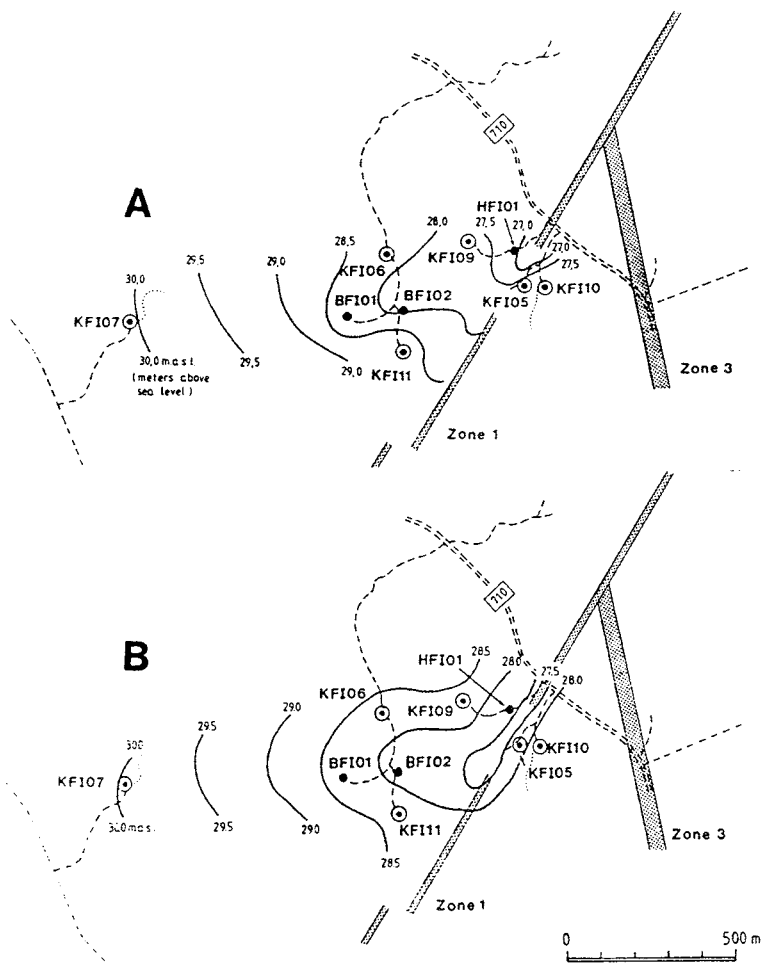


Figure 2-3 Map of the Brändan area illustrating A) the elevation of the groundwater table and B) the distribution of the hydraulic head in the upper part of Zone 2.

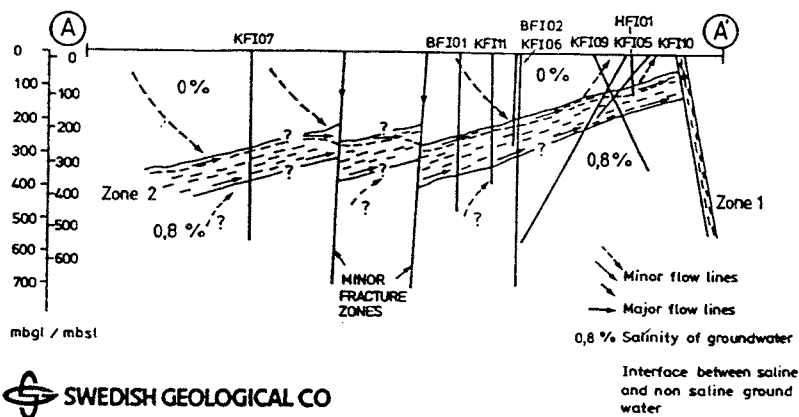


Figure 2-4 Tentative model of groundwater flow during undisturbed conditions. The location of the profile is shown in Figure 2-1.

### 2.3 HYDROCHEMISTRY

The groundwater at the study site in Finnsjön can be divided into two different types based on the chemistry of the waters. An old saline water in the lower parts and a younger near-surface water on top. The fairly sharp interface between these two waters corresponds to the highly conductive part of Zone 2 (Smellie et al., 1987; Ahlbom et al., 1988; Ahlbom and Smellie, 1989). The old saline water is characterized by a high content of dissolved species. Notable differences between the two waters are the low content of  $\text{HCO}_3$  and the high content of Na, Ca and Cl in the saline water.

The water in Zone 2 is a mixture of these two waters. The mixing of waters of different origin creates a highly super-saturated water and this results in the precipitation of calcite. This is most pronounced in the upper part of Zone 2 and it seems as if the calcite precipitation strengthens the separation between the old saline water and the younger surface-like water

During the dipole tracer test, water was circulated and injected into the low angle fracture zone to create a two-dimensional dipole field in the upper highly conductive part of Zone 2. The tracer test included elements in ionic form and consequently the chemistry of the circulating water played an important role due to the expected sorption of these elements. The physio-chemical parameters of the water from Zone 2 are presented by Ahlbom and Smellie, 1989. A rather complete chemical analysis of the sampled water was made at the end of the dipole tracer experiment, see Table 2-1. During the test the oxidation-reduction potential was measured showing that the conditions were stable and reducing ( -200 mV).

Water sampling for chemical analyses from Zone 2 in boreholes BFI01 and BFI02 has previously been performed (Smellie et al., 1987; Ahlbom et al., 1988; Ahlbom and Smellie, 1989). Water sampling for elemental analyses was made after the finish of the field test. A more complete analysis was made at the main sampling point, borehole BFI02, while at boreholes KFI06 and KFI11 only the major elements were analyzed, see Table 2-1.

Table 2-1 Chemical analyses of water sampled in the borehole sections

Element	BF102 (1)	BF102 (2)	KFI06	KFI11
Al ppb	1.5	0.5	11	1.5
As ppb	25	24	30	2
Ba ppb	71	81	45	89
Ca ppm	400	200	210	180
Cd ppb	<0.2	<0.2	<0.2	<0.2
Co ppb	0.5	0.5	0.5	0.5
Cr ppb	1.1	1.3	2.4	1.4
Cu ppb	120	160	2.7	6.2
Fe ppm	2.8	2.4	2.4	2.2
Hg ppb	<0.2	0.3	1.1	0.3
K ppm	12	7.2	7.2	7.5
Mn ppb	360	460	430	440
Mg ppm	48	35	38	35
Na ppm	580	370	370	330
Ni ppb	4.1	6.9	7.5	6.2
Pb ppb	3.4	3.8	0.3	0.2
V ppb	36	37	49	50
Zn ppb	39	100	5.2	18
Sr ppb		3800		
Rb ppb		12		
In ppb		<0.2		
La ppb		0.3		
Tb ppb		<0.1		
Yb ppb		0.4		
Lu ppb		<0.1		
Li ppb		<0.1		
Si ppb		7500		
Cs ppb		0.7		
Mo ppb		3.5		
Re ppb		<0.1		
B ppb		430		
Fe ppm	0.35	0.14	0.53	
PO <sub>4</sub> ppm	<0.1	0.04	0.03	0.03
SO <sub>4</sub> ppm	150	130	120	120
Cl ppm	1800	1600	1600	1600
F ppm	1.8	1.8	1.6	1.8
I ppm	0.17	0.13	12	0.15
Br ppm	24	19	190	22
HCO <sub>3</sub> ppm	230	240	230	240
NH <sub>4</sub> ppm		<0.05		0.91
P ppm		0.013		0.010
NO <sub>2</sub> ppm		<0.01		<0.01
NO <sub>3</sub> ppm		0.16		0.06
SO <sub>4</sub> ppm		140		160
B ppm		0.48		0.40

Table 2-1 continued

Element	BFI02 (1)	BFI02 (2)	KFI06	KFI11
pH		7.6		7.4
Cond. mS/m		525		537
KMnO <sub>4</sub> ppm		30		29
TOC ppm		7.4		6.0

(1) 890613

(2) 890526

### 3. EXPERIMENTAL DESIGN

#### 3.1 CONCEPTUAL MODEL

The dipole experiment (also referred to as a doublet or two-well test) was performed in a recirculating system between boreholes BFI01 (injection) and BFI02 (withdrawal), see Figure 3-1. A recirculating system had to be used because of the high flow rates and thereby large volumes needed to create a dipole flow field in the scale of 168 meters. The recirculation also made it easier to get permission to use short-lived radio-nuclides as tracers.

Boreholes BFI01 and BFI02 were also used in the radially converging tracer experiment (RCT) as injection and withdrawal boreholes, respectively. However, in the dipole experiment, only the upper highly conductive part of Zone 2 was pumped. Boreholes KFI06 and KFI11, also used as injection boreholes in RCT, were used as observation boreholes in the dipole experiment.

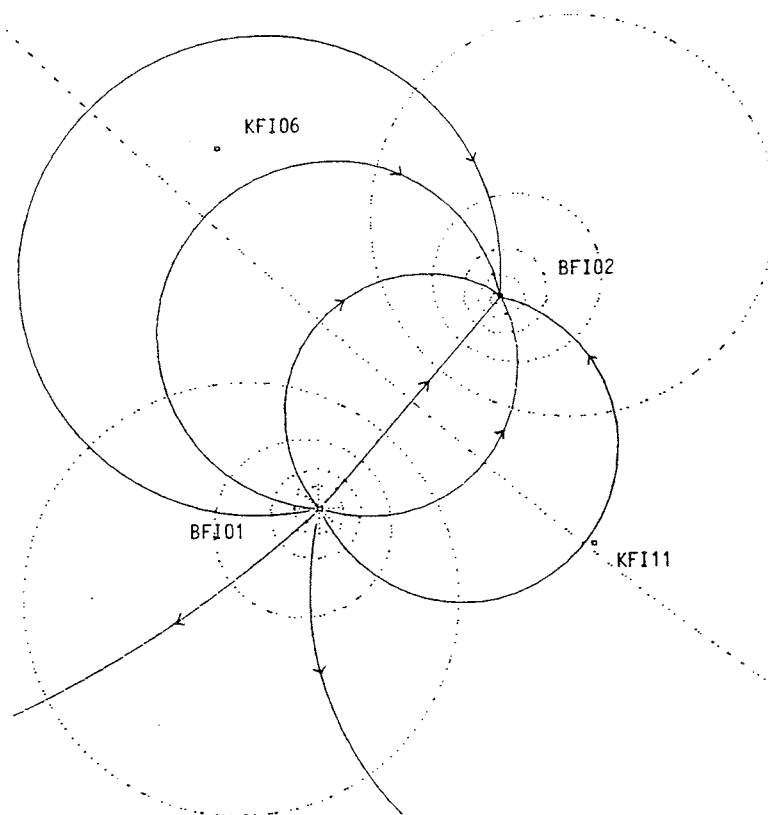


Figure 3-1 Conceptual model of the dipole experiment.

## 3.2 EXPERIMENTAL SET-UP

### 3.2.1 Equipment and procedures

Boreholes BFI01 and BFI02 are air-percussion drilled boreholes at a diameter of 165 mm. Both boreholes are drilled through the entire thickness of Zone 2. In the dipole experiment, the upper highly conductive interval was packed-off using water-inflatable packers. The borehole intervals used are given in Table 3-1 together with the transmissivities as determined from hydraulic injection tests in 2 m and 0.11 m intervals (Andersson et al., 1988a). Notable is that the upper intervals in boreholes BFI01, KFI06, and KFI11 are identical with the intervals used for tracer injection in RCT.

Table 3-1 Borehole intervals used in the dipole experiment.

Borehole	Interval (m)	Length (m)	Transmissivity (m <sup>2</sup> /s)	Remarks
BFI01	241.5-246.5	5	1.29 E-3	injection
BFI02	193.0-217.0	24	1.84 E-3	withdrawal
KFI06	212.0-217.0	5	5.60 E-4	observation
KFI11	221.5-226.5	5	3.71 E-4	observation

The choice of a longer isolated interval in borehole BFI02 was due to practical aspects. However, the transmissivity of the interval is limited to a much shorter interval as shown in earlier investigations (Andersson et al., 1988a). The effective thickness of the upper highly conductive interval is only in the order of 0.5 meters, between 203.87-204.42 m. This 0.5 m interval contributes with 99% to the total transmissivity of the 24 m interval in BFI02.

The water from the pumped interval in borehole BFI02 was withdrawn with a submersible pump through 193 m of steel pipes with an inner diameter of 80 mm. The water was then re-circulated to the injection interval in BFI01 through 495 m of plastic pipes (Polyethylene) with an inner diameter of 44 mm, see Figure 3-2. The total volume of the pipe system and the borehole intervals was 2150 litres.

The two 56 mm diameter observation boreholes, KFI06 and KFI11, were both packed-off in the same manner as in RCT, i.e. in three intervals within Zone 2 (Gustafsson et al., 1989). The intervals were circulated with pumps exactly in the same way as in RCT in order to achieve a homogeneous distribution of tracer within the intervals.

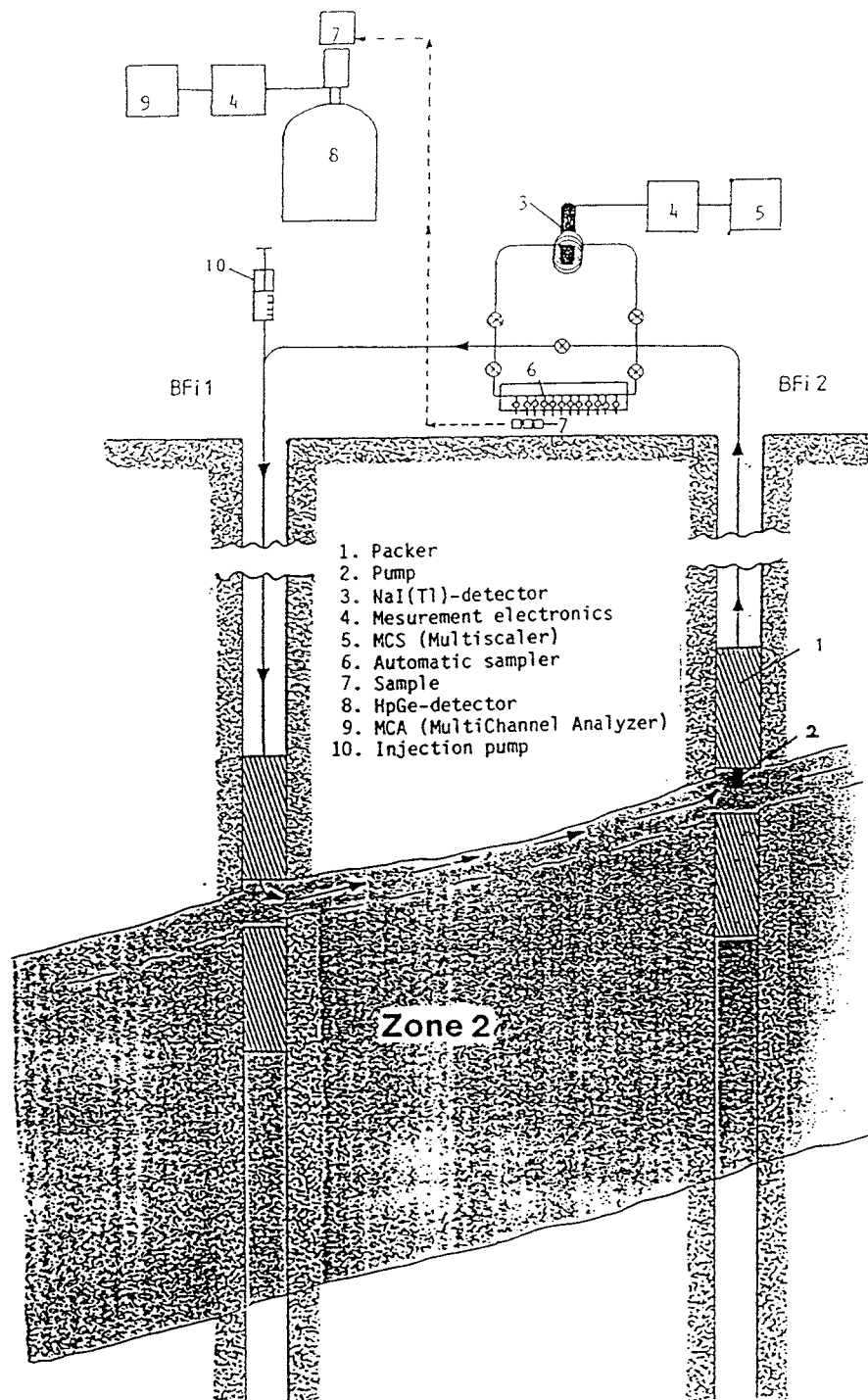


Figure 3-2 Experimental design of the dipole experiment.

3.2.2 Tracer injections

The tracer injections in the recirculating system were made at the point where the plastic pipe enters borehole BFI01, i.e. 243 meters before entering Zone 2 in borehole BFI01. Two injections were also made in the upper interval of borehole KFI11. In total 15 injections including 14 radiotracers and 5 non-radioactive tracers were made during the 7 week period of the experiment. Some tracers were also injected several times. In Table 3-2 the injection schedule for the radiotracers is presented. The table also includes half-lives and chemical form of the nuclides. Table 3-3 includes the non-radioactive tracer injections.

Table 3-2 Radiotracer injection schedule.

Inj.	Date	Time	Nuclide	Radiotracer Half-life	Chem. form
1	890504	13.30	Br-82	1.47 d	Br(I)-
2	890505	23.30	Tc-99m	6.01 h	Tc(VII)O <sub>4</sub> <sup>-</sup>
			Re-186	3.78 d	Re(VII)O <sub>4</sub> <sup>-</sup>
3	890507	22.30	I-131	8.04 d	I(I)-
4	890512	00.30	Tc-99m	6.01 h	Tc(VII)O <sub>4</sub> <sup>-</sup>
5	890513	23.40	Co-58	70.92 d	Co(II) <sup>+</sup>
			Rb-86	18.66 d	Rb(I) <sup>+</sup>
6	890516	22.08	Na-24	14.66 h	Na(I) <sup>+</sup>
			Br-82	1.47 d	Br(I)-
			Tc-99m	6.01 h	Tc(VII)O <sub>4</sub> <sup>-</sup>
			I-131	8.04 d	I(I)-
			Re-186	3.78 d	Re(VII)O <sub>4</sub> <sup>-</sup>
			Tl-201	3.05 d	Tl(I) <sup>+</sup>
7	890520	23.14	Cr-51	27.70 d	Cr(III)-EDTA-
			In-111	2.81 d	In(III)-EDTA-
			La-140	1.68 d	La(III)-DOTA-
			Tb-160	72.1 d	Tb(III)-EDTA-
			Yb-169	32.0 d	Yb(III)-EDTA-
			Lu-177	6.71 d	Lu(III)-DOTA-
8	890524	23.40	Co-58	70.92 d	Co(III)-EDTA-
9*	890528	16.00	I-131	8.04 d	I(I)-
10*	890529	13.31	I-131	8.04 d	I(I)-

\* Injection in borehole KFI11, Upper interval.

The radiotracers used in this experiment included both non-sorbing (anions, metal complexes and metallic anions) and sorbing (cations) tracers. The combination of tracers in the different injections was mainly based on practical reasons, e.g. that the most short-lived nuclides had to be injected soon after the activity was delivered to the research area. Another aspect was that tracers containing complexing agents (EDTA, DOTA) had to be injected at the end of the experiment to avoid interference between the complexing agents and other tracers.

Details regarding the radiotracers are given by Byegård et al., in prep.

Table 3-3 Injection schedule for the non radioactive tracers.

Inj.	Date	Time	Tracer	Remarks
A	890425	12.39	Rhodamine WT	Dye tracer
B	890526	15.00	Blue Dextran 2000	Macro molecule
C	890530	16.30	In-EDTA	Metal complex
D	890531	17.00	Gd-DTPA Tm-EDTA	Metal complex Metal complex
E	890605	15.03	Rhodamine WT	Dye tracer

Each injection of non-radioactive tracers had a special purpose. The purposes and some comments on the tracers are given below.

#### **Inj. A and E, Rhodamine WT (RdWT)**

The first pulse of RdWT was injected two weeks after the start of pumping and one week prior to the first injection of radiotracers with the primary purpose of optimising the sampling procedure for the radiotracers. Secondly, this first pulse of RdWT could be compared with a second injection of RdWT (Inj.E) made at the end of the experiment in order to reveal any eventual changes in the dipole flow field. Thirdly, as most of the radionuclides were short-lived, it might have been difficult to detect them in the observation boreholes KFI06 and KFI11 and therefore this non-radioactive tracer was injected at an early stage.

RdWT is a well known tracer which has been widely used in groundwater studies and has also been used in earlier investigations at the Finnsjön research area (Gustafsson and Klockars, 1981).

### Inj. B, Blue Dextran 2000 (BD 2000)

BD 2000 is a macromolecular complex with an atomic weight of about 2 000 000. The purpose of the injection of BD 2000 was to study any possible effects of matrix diffusion. This large molecule, having an effective diffusivity in the order of 2-3 magnitudes lower than c.f. Iodide has earlier been used for similar purposes at the Finnsjön research area (Gustafsson and Klockars, 1981) and in the Stripa mine (Gustafsson and Andersson, in press).

### Inj. C and D, In-EDTA, Gd-DTPA and Tm-EDTA

These three metal complexes were injected to study any possible effects of the initial concentration of the complexes. In-EDTA was also injected as radionuclide (In-111) with much lower initial concentration. The difference in concentration was a factor of 4000. These three metal complexes were also used as tracers in RCT with concentrations similar to this experiment.

The tracer injections in borehole BFI01 were made with a duration of approximately 4 minutes. Immediately after each injection period of 4 minutes, the tubing was rinsed for 8 minutes with water from BFI01.

In Tables 3-4 and 3-5 below, initial tracer concentrations,  $C_{00}$ , tracer concentrations after mixing during the injection period,  $C_0$ , duration of the injections,  $t_{inj}$ , and injected volumes of  $C_{00}$ ,  $V_{inj}$ , are given.

The concentration of tracer after mixing,  $C_0$ , was calculated using a simple mass balance assuming complete mixing at the inlet of the injection tube:

$$C_0 = \frac{q_{inj} \cdot C_{00} + Q \cdot C_b}{Q + q_{inj}} \quad (3.1)$$

where  $q_{inj}$  is the injection flow rate ( $V_{inj}/t_{inj}$ ),  $Q$  is the pumping rate of the circulating system, and  $C_b$  is the background concentration.

As  $C_b \ll C_{00}$  and  $q \ll Q$ , Equation 3.1 may be approximated by:

$$C_0 = \frac{q_{inj} \cdot C_{00}}{Q} \quad (3.2)$$

The values of  $C_0$  given in Tables 3-4 and 3-5 are all calculated from Equation 3.2 assuming a constant pumping rate,  $Q=120$  l/min. Hence, minor variations of the pumping rate are neglected.

Table 3-4 Radiotracer injection data in borehole BFI01.

Inj. No	Tracer	C <sub>00</sub> (Bq/l)	C <sub>0</sub> (Bq/l)	t <sub>inj</sub> (min)	V <sub>inj</sub> (l)
1	Br-82	7.75E+6	1.47E+4	4.42	1.00
2	Tc-99m Re-186	7.46E+6 6.30E+7	1.51E+4 1.27E+5	4.13	1.00
3	I-131	1.83E+8	3.90E+5	3.92	1.00
4	Tc-99m	3.52E+8	7.30E+5	4.03	1.00
5	Co-58 Rb-86	9.31E+7 1.36E+8	1.95E+5 2.85E+5	4.00	1.00
6	Na-24 Br-82 Tc-99m I-131 Re-186 Tl-201	9.26E+6 2.42E+7 7.27E+7 1.06E+8 6.31E+8 2.38E+7	1.90E+4 4.98E+4 1.50E+5 2.18E+5 1.30E+6 4.98E+4	4.07	1.00
7	Cr-51 In-111 La-140 Tb-160 Yb-169 Lu-177	1.68E+8 5.35E+6 9.98E+6 4.71E+7 3.89E+7 1.42E+8	3.43E+5 1.09E+4 2.04E+4 9.61E+4 7.94E+4 2.90E+5	4.08	1.00
8	Co-58	8.10E+7	1.71E+5	4.00	1.00

Table 3-5 Tracer injection data for the non-radioactive tracer injections in borehole BFI01.

Inj. No	Tracer	C <sub>00</sub> (mg/l)	C <sub>0</sub> (mg/l)	t <sub>inj</sub> (min)	V <sub>inj</sub> (l)
A	Rhodamine WT	20 000	165.6	4.00	3.975
B	BD 2000	20 000	495.8	3.95	11.750
C	In-EDTA	22 000	44.3	4.05	0.994
D	Gd-DTPA Tm-EDTA	22 000 1 724	114.8 9.0	3.97	2.487
E	Rhodamine WT	20 000	144.7	4.10	3.560

Injections 9 and 10 were made in borehole KFI11 aiming at; 1) measure the groundwater flow rate with the dilution method (Inj. 9) and 2) study the transport between KFI11 and BFI02 in the dipole flow field (Inj. 10). The injections were made by labelling the entire borehole interval volume during one cycle of circulation, i.e. exactly in the same way as in RCT (Gustafsson et al., 1989). Hereby the tracer was homogeneously or nearly homogeneously distributed in the borehole interval within a short time period. The injection data for the injections in borehole KFI11 are given in Table 3-6 below.

Table 3-6 Tracer injection data for radionuclide injections in borehole KFI11.

Inj. No	Tracer	$C_{00}$ (Bq/l)	$C_0$ (Bq/l)	$t_{inj}$ (min)	$V_{inj}$ (l)
9	I-131	7.93E+6	2.67E+5	60.0	0.91
10	I-131	9.66E+7	3.47E+6	62.0	0.97

The values of  $C_0$  in Table 3-6 are calculated from Equation (3.3) assuming complete mixing in the borehole interval volume:

$$C_0 = C_{00} \cdot V_{inj} / V \quad (3.3)$$

where  $V$  is the total volume of borehole interval KFI11:U.

### 3.3 TRACER SAMPLING AND ANALYSIS

The radiotracers were sampled in the upper part of Zone 2 at boreholes BFI02 and KFI11 with automatic samplers and also occasionally in borehole KFI06. A few samples were also taken in the lower intervals of boreholes KFI06 and KFI11. The samples were immediately analyzed at the field laboratory with a High Purity Germanium (HPGe) detector connected to a multi-channel analyzer and a computer.

The sampling equipment, which was identical with the one used at RCT, was also used for sampling the inactive tracers. The volumes of the radionuclide samples was 1 l and for the inactive tracers, 100 ml.

In addition to the sampling, a continuous measurement was made at borehole BFI02 with a NaI-detector connected on-line by a flow-through cell (Fig. 3-2). Because of the relatively small volume of the measuring cell the efficiency was rather poor and evaluations could only be made for some of the injections with the on-line equipment. Further details regarding the radio-tracer analyses are given by Byegård et al, in prep.

The non-radioactive tracers were analyzed at the SGAB Laboratories in Uppsala and Luleå. The metals were analyzed with a ICP/MS equipment (Inductively Coupled Plasma Mass Spectroscopy) capable of detecting metal concentrations down to 0.01 ppb and the fluorescent dyes were analyzed with a Sequoia-Turner Fluorometer.

### 3.4 SUPPORTING MEASUREMENTS

The supporting measurements made before, during and after the dipole experiment were:

- pumping rate
- hydraulic head distribution
- electrical conductivity of the pumped water
- temperature of the pumped water
- oxidation-reduction potential of the pumped water

The **pumping rate** was measured with a volumetric flow meter with manual registration once a day during the pumping period which lasted between April 12 and June 13, 1989.

The **hydraulic head distribution** was measured almost each day during the pumping period. Measurements were also made prior to the start of the dipole pumping and immediately before the end of the RCT pumping which was stopped on April 3, 1989. One measurement was also made on June 21, i.e. one week after finishing the dipole pumping. The hydraulic heads were manually registered in 9 different boreholes including totally 19 different borehole intervals. The measured boreholes and intervals are listed in Table 3-7 below. The borehole locations are shown in Figure 2-1. From the head data, head differences relative to the pumped interval (BF102:U) were calculated, see section 4.2.

The **electrical conductivity**, and the **temperature** of the pumped water was measured at borehole BF102 (on the ground surface). The temperature was also measured at borehole BF101 (on the ground surface) together with the **oxidation-reduction potential (Eh)**. All measured values were manually registered once every day.

Table 3-7 Boreholes and borehole intervals used for hydraulic head measurements (gw1=groundwater level).

Borehole	Interval (vertical depths)	Remarks
BFI01	gw1 ; 0 -240.5 m upper; 241.5-246.5 m lower; 247.5-459.1 m	injection interval
BFI02	gw1 ; 0 -192.0 m upper; 193.0-217.0 m lower; 218.0-288.0 m	pumping interval
KFI06	gw1 ; 0 -211.0 m upper; 212.0-217.0 m middle; 236.5-239.5 m lower; 252.5-271.5 m	sampled interval
KFI11	gw1 ; 0 -220.5 m upper; 221.5-226.5 m middle; 287.5-294.5 m lower; 329.5-338.5 m	sampled interval
HFI01	gw1 ; 0 -129.0 m	
KFI05	gw1 ; 0 -575* m	
KFI07	gw1 ; 0 -550 m	
KFI09	gw1 ; 0 -325* m	
KFI10	gw1 ; 0 -196* m	

\* Inclined borehole

## 4. EXPERIMENTAL RESULTS

### 4.1 TRACER BREAKTHROUGH

The breakthrough curves of the 19 different tracers injected shows very different shapes and irregularities, some of them are easy to explain while others are more difficult to understand. Tracers were detected in both the withdrawal borehole BF102 and in the two observation boreholes, KF106 and KF111. In general, the hydraulic conditions have been stable during the experiment as shown by the graphs of the groundwater levels and hydraulic heads, section 4.2, although there are some indications of leakage from the lower parts of Zone 2.

During the experiment, a very fast and distinct transport was found between the injection borehole BF101 and observation borehole KF111. Therefore, the sampling of KF111 was intensified and extra breakthrough curves than those expected were obtained. Comments on the breakthrough curves are given below for each borehole and each injection. A summary of first arrivals, peak times, and maximum concentrations are presented in Table 4-1.

For the radiotracers in general, the detection uncertainties are dependent on the length of the counting period for the gamma radiation and the amount of injected activity. The injected activity together with the counting periods and the decay energies of the different radionuclides determines the detection limits. The dashed lines on the plotted graphs representing the detection limits are based on the mean measuring time and for the case of BF102 and KF111 it is 40 minutes. For KF106 the dashed line represents an overnight measurement (9 hours). The actual position of the dashed detection limit is therefore a result of practical considerations and a reasonable low detection limit. Details of the calculation of detection limits and uncertainties are given by Byegård et al., in prep..

All breakthrough curves are given as relative concentration,  $C/C_0$ , versus elapsed time after injection in Appendix A, B, and C. The data has not been corrected for background concentrations but the background concentration is negligible in all breakthrough data except for I-131 (Inj. 6) and Rhodamine WT (Inj. E). All data has been corrected for radioactive decay.

#### 4.1.1 Breakthrough in borehole BF102

The first breakthrough in borehole BF102 is in general registered after about 20-25 hours and the peak concentration is achieved after about 40-45 hours of elapsed time, see Table 4-1, Figure 4-1 and Appendix A. The concentrations then slowly decreases as the tracers are recirculated and thus more and more dispersed. In a closed system, the concentration would

eventually level out at a constant level as the tracer is homogeneously distributed within the flow field.

Below, a short comment of the breakthrough curves from each injection is given. Injections no. 4 and 5 are not included as no breakthrough of these tracers could be observed in any of the boreholes. Hence Tc-99m, Co-58, Rb-86 and Tl-201 are either completely sorbed or sorbed so much that the breakthrough concentration gets below the detection limit.

#### **Inj. 1, Br-82.**

The breakthrough curve of Br-82 (Appendix A:1) show a very irregular shape. The main reason for this is the short half-life of Br-82 giving high detection uncertainty which is clearly shown by the large oscillations. The detection limit, indicated by the dashed line depends strongly on the decay constant of Br-82 ( $t_{1/2} = 1.47$  days) and after about 80 hours the tracer is not detectable. First arrival and peak times could not be determined due to these uncertainties. The conclusion of the discussion above is that the breakthrough curve is not suited for further analysis.

#### **Inj. 2, Tc-99m, Re-186.**

No breakthrough of Tc-99m was registered in BF102. The breakthrough of Re-186 (Appendix A:2) is well above the detection limit. The first arrival is registered after 24 hours and the peak concentration is reached somewhere between 40-50 hours. The curve may not be suited for further analysis as the detection uncertainty is rather high (Byegård et al., in prep.). There is also a peak at about 80 hours which most likely is an effect of the increasing uncertainty with time.

#### **Inj. 3, I-131.**

The breakthrough curve for I-131 (Appendix A:3 and Figure 4-1) has a very regular shape and should be possible to use for further analysis. The concentration is well above the detection limit and the uncertainty is very low. The tracer is first detected after 20 hours and the peak concentration is registered after 45 hours. The curve then seem to level out at about 200 hours, indicating steady-state or close to steady-state conditions. The rising part of the curve at the very end (230 hours) corresponds to the second injection of I-131 (Inj. 6).

#### **Inj. 6, Na-24, Br-82, Tc-99m, I-131, Re-186, Tl-201.**

Br-82 was injected with about 3 times higher concentration than the previous injection. The breakthrough curve is therefore of somewhat better quality although measurements after about 100 hours of elapsed time are below the detection limit (Appendix A:4). Br-82 together with I-131 and Re-186 (Appendices A:4-6) all seem to have the same first arrivals, 20 hours, time to peak concentration, 45 hours, and also the same shape. However, the Re-186 curve have a somewhat lower peak concentration which

also is consistent with the previous injection of Re-186 (Inj. 2). The high background concentration of I-131 is due to Iodide remaining from the previous injection (Inj. 3). The background activity of I-131 has not been subtracted from the data. The three possibly sorbing tracers, Na-24, Tc-99m, and Tl-201 were not detected at BFI02 although there are some traces of Na-24. The short half life of Na-24 together with the low activity made it impossible to detect the tracer at BFI02 as the concentration would be below the detection limit. The detection limits for the sorbing tracers are given in Byegård et al., in prep.

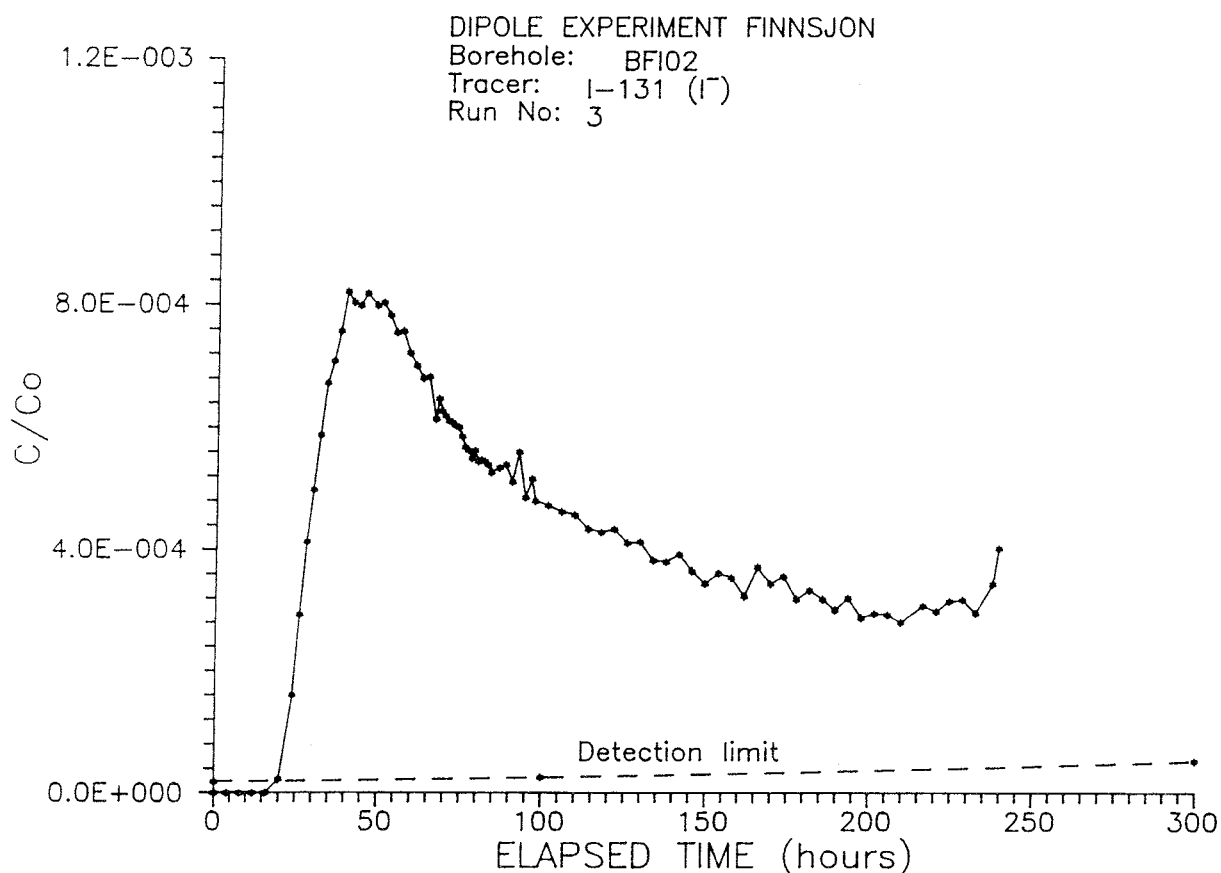


Figure 4-1 Breakthrough curve for I-131 (Inj. 3) in borehole BFI02.

**Inj. 7, Cr-51, In-111, La-140, Tb-160, Yb-169, Lu-177.**

All tracers injected in this run were in the form of metal complexes, EDTA or DOTA-complex, and should be acting as conservative tracers, according to laboratory tests (Byegård et al., in prep.) and results from RCT (Gustafsson et al., 1989). However, the breakthrough of the DOTA complexes (La and Lu, Appendix A:7-A:8) diverges somewhat from the others (Appendix A:9-A:12). Both tracers arrive slower and have lower peak concentrations than the others. This indicates that the DOTA complexes are slightly sorbed in a reversible way which is rather surprising as the DOTA complex is considered to be very stable. Laboratory sorption tests on crushed Finnsjö granite

showed no sorption at all for Tb-DOTA (Byegård et al., in prep.).

The EDTA complexes, except for Tb-EDTA, have first arrivals and peak concentrations similar to I-131 and are acting as conservative tracers. Tb-EDTA is not delayed but has a much lower peak concentration which indicates irreversible losses.

All six tracers have relatively high uncertainties and detection limits and it might therefore be difficult to use the breakthrough curves for deeper quantitative analysis.

#### **Inj. 8, Co-58**

Co-58 was injected as EDTA complex in a separate injection. The reason for not including Co-58 in Inj. 7 was the addition of H<sub>2</sub>O<sub>2</sub> to the solution which may interfere with the other complexes. The breakthrough curve (Appendix A:13) shows a lower peak concentration than the other conservative tracers while the first arrival and peak times are the same. This indicates that Co-EDTA has a conservative behaviour although some irreversible losses may occur.

#### **Inj. A and E, Rhodamine WT**

The first pulse of Rhodamine WT was made primarily in order to optimize the sampling procedure of the succeeding radiotracers. The result of the second injection, performed at the end of the dipole experiment, would by comparison with the first pulse exhibit whether the flow conditions had been stable during the time of the experiment or not. This tracer was also intended to be used to determine if any losses of tracer occurred. In a perfect recirculating dipole field, the concentration of tracer should become constant after a while if no losses occur. However, the breakthrough curves of Rhodamine WT (Appendix A:14 and A:18) are slightly delayed in time both regarding first arrival and peak times, 22 and 50 hours, respectively and the peak concentration is lower than for I-131. These facts indicate that Rhodamine WT is weakly sorbed in a reversible way. This is also further strengthened by comparing the breakthrough curves for borehole KFI06 (section 4.1.3). A weak sorption of Rhodamine WT compared to Iodide was also previously found at the Finnsjön site, involving residence times of about 25 hours and a distance of 30 meters (Gustafsson and Klockars, 1981).

The sorbing behaviour of Rhodamine WT therefore makes it difficult to use the data to determine if tracer losses occur due to influences from hydraulic boundaries and/or the natural gradient.

A comparison between the two curves shows a slightly lower peak concentration of Rhodamine WT for the second curve (Inj. E). The high background concentration at early times for the second curve are due to remnants of tracer from the first injection.

**Inj. B, Blue Dextran 2000**

The breakthrough data have not yet been analyzed.

**Inj. C and D, In-EDTA, Gd-DTPA and Tm-EDTA**

The breakthrough curves (Appendix A:14-16) shows a significantly lower peak concentration than the other conservative tracers. This is in contrast to the results of the radially converging experiment where very high recoveries of these tracers were measured (Gustafsson et al., 1989). The tracer first arrival and peak times are the same compared to I-131 for Gd-DTPA and Tm-EDTA while In-EDTA are slightly delayed and having the lowest recovery of these three tracers. The delay of In-EDTA is also clearly seen in borehole KFI11 (see Section 4.1.2). There is currently no explanation for the low recovery of the non-radioactive metal complexes.

Table 4-1 Tracer first arrivals,  $t_a$ , mean residence times,  $t_o$ , peak concentrations,  $c/c_o$  (peak) for breakthrough in BFI02.

Inj.	Tracer	$t_a$ (h)	$t_o$ (h)	$c/c_o$ (peak) * $10^{-4}$
1	Br-82	FD	FD	FD
2	Re-186	(24)	(51)	(6.3)
3	I-131	20	45	8.2
6	Br-82	20	46	8.6
	I-131	20	44	8.2
	Re-186	20	45	6.5
7	Cr-51	20	42	6.0
	In-111	20	45	7.0
	La-140	(34)	FD	(6.4)
	Tb-160	(24)	(36)	2.5
	Yb-169	(24)	(40)	8.6
	Lu-177	30	49	3.8
8	Co-58	20	(37)	5.3
A	RdWT	22	50	5.3
C	In-EDTA	20	45	1.4
D	Gd-DTPA	20	41	2.0
	Tm-EDTA	20	41	2.8
E	RdWT	22	50	4.8

FD= Few Data points  
( ) Uncertain values

#### 4.1.2. Breakthrough in borehole KFI11

The breakthrough in borehole KFI11 is faster, higher in concentration and more distinct when compared to the breakthrough curves at BFI02. The first breakthrough in KFI11 is in general registered after about 10-13 hours and the peak concentration is achieved after about 20 hours of elapsed time (Table 4-2, Figure 4-2, and Appendix B). This fast breakthrough was not expected from the geometry of the experiment as the distance between BFI01 and KFI11 is almost the same (165 m) as the distance between BFI01 and BFI02 (168 m). However, based on the results from RCT (Gustafsson et al., 1989), where tracers were injected in the same intervals in BFI01 and KFI11, this good hydraulic connection in the direction of KFI11 was not totally surprising. In RCT, the first arrival and mean residence time between KFI11 and BFI02 was 3-4 times faster than between BFI01 and BFI02 although the distance is approximately the same.

A few samples from the middle and lower parts of Zone 2 were also analyzed and gave no indications of tracer breakthrough.

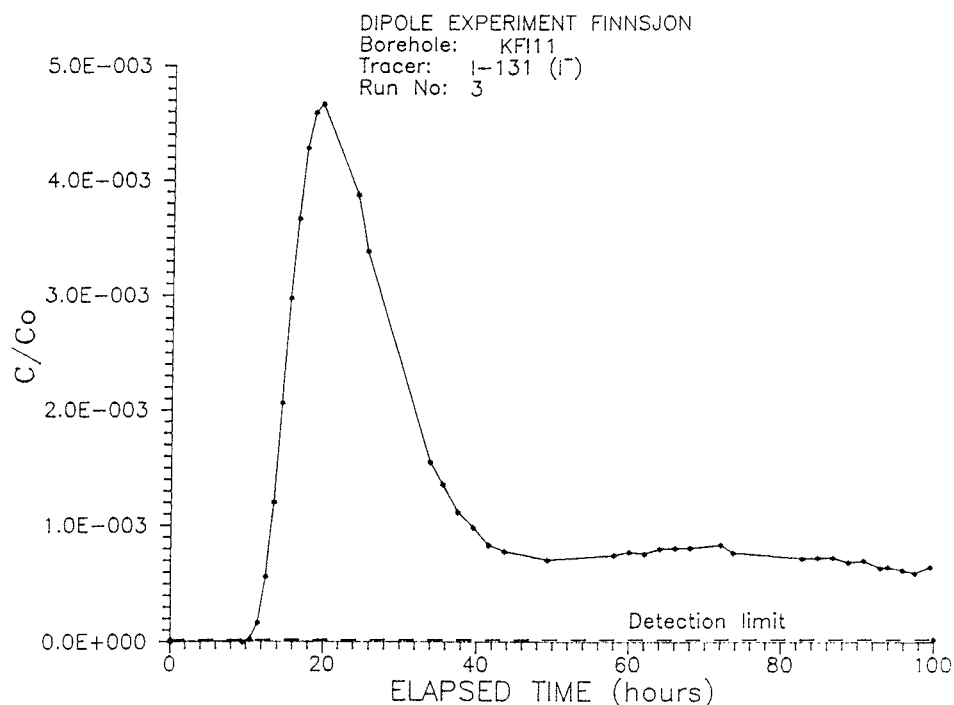


Figure 4-2 Breakthrough curve for I-131 (Inj. 3) in borehole KFI11.

As no pumping, except for the small sample volumes, was made at KFI11 during the dipole experiment, the peak represents a point sample in the flow field between BFI01 and BFI02. The very fast transport to KFI11 indicates that the main flow is diverted towards KFI11 instead of directly between BFI01 and BFI02. The curves also shows a second peak at about 60 hours as the tracer is recirculated once. Further peaks may not be distinguished as the dilution and dispersion levels out the concentration.

The comments on the breakthrough curves for BFI02 above also applies for the breakthrough in KFI11 (Appendix B). Therefore only some specific features of the breakthrough curves for KFI11 are discussed below.

The short residence time for the transport to KFI11 made it possible to get better and more accurate breakthrough curves for the most short-lived radiotracers such as **Br-82 (Appendix B:1)** and **Na-24 (Appendix B:4)**. The latter, injected as a cation and therefore believed to be sorbing, was found to be only very weakly sorbing with residence time almost as the conservative tracers (Na-24 could not be measured in BFI02 due to the short half-life in combination with the relatively low injected activity).

Table 4-2 Tracer first arrivals,  $t_a$ , mean residence times,  $t_o$ , peak concentrations,  $c/c_o$  (peak) for breakthrough in KFI11.

Inj.	Tracer	$t_a$ (h)	$t_o$ (h)	$c/c_o$ (peak) * $10^{-3}$
1	Br-82	FD	FD	FD
2	Re-186	10	21	2.9
3	I-131	10	20	4.7
6	Na-24	12	21	2.6
	Br-82	11	20	4.5
	I-131	10	19	4.0
	Re-186	10	19	4.1
7	Cr-51	(10)	20	2.9
	In-111	(10)	22	3.6
	La-140	13	22	2.2
	Tb-160	(10)	18	1.9
	Yb-169	(10)	20	4.5
	Lu-177	12	30	1.2
8	Co-58	(10)	20	2.6
A	RdWT	FD	FD	FD
C	In-EDTA	11	21	0.7
D	Tm-EDTA	10	19	1.6
	Gd-DTPA	10	19	1.5
E	RdWT	12	26	1.7

FD= Few Data points  
( ) Uncertain values

### 4.1.3 Breakthrough in borehole KFI06

The breakthrough in observation borehole KFI06, which is situated at the opposite side in the dipole field compared to KFI11 and also somewhat further peripheral, was much slower than in KFI11. The time of first arrivals were around 130-150 hours and mean residence times were in the order of 400 hours (Table 4-3, Figure 4-3 and Appendix C). Due to the long residence times, only a few of the radiotracers and one of the non-radioactive tracers could be registered in KFI06. The peak concentrations are about 6 times lower than in BFI02.

The only difference from the conclusions regarding the radiotracer breakthrough in BFI02 and KFI11 is that Cr-51 (EDTA complex) seems to be somewhat delayed compared to Yb-169 which was injected simultaneously. This may indicate a very weak sorption of Cr-51.

Analyses of samples from the middle and lower parts of Zone 2 in KFI06 showed no indications of tracer breakthrough.

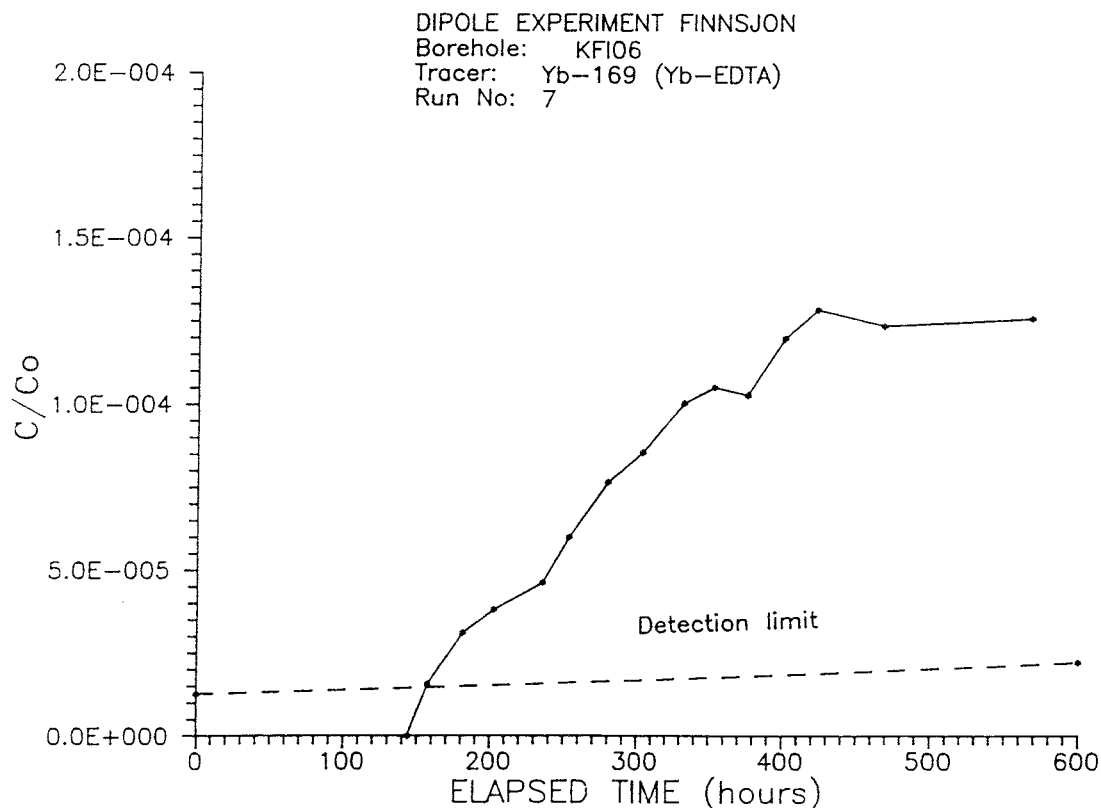


Figure 4-3 Breakthrough curve for Yb-169 (Inj. 7) in borehole KFI06.

Table 4-3 Tracer first arrivals,  $t_a$ , mean residence times,  $t_o$ , peak concentrations,  $c/c_o$  (peak) for breakthrough in KFI06.

Inj.	Tracer	$t_a$ (h)	$t_o$ (h)	$c/c_o$ (peak) * $10^{-4}$
3	I-131	150	(330)	1.65
7	Cr-51	(170)	FD	(1.0)
	Tb-160	FD	FD	(0.4)
	Yb-169	150	(420)	1.30
8	Co-58	150	FD	(0.5)
A	RdWT	200	FD	(0.6)

FD= Few Data points  
( ) Uncertain values

#### 4.1.4 Dilution measurement and tracer injection in borehole KFI11

Due to the very fast transport between BFI01 and KFI11 it was decided to include a tracer injection in borehole KFI11 to the programme. Also, a tracer dilution test was made in order to determine the groundwater flow through the borehole interval.

The dilution measurement, presented as  $\ln C/C_o$  versus time in Figure 4-4, showed that the groundwater flow rate through the sealed off borehole interval, was quite high, 519 ml/min. This is in good agreement with the dilution measurements performed prior to RCT (Gustafsson et al., 1989) where a groundwater flow of 376 ml/min was measured. The higher value at this test is due to an increased hydraulic gradient which also is indicated by the head difference to the pumping hole BFI02, 0.91 m compared to 0.81 m during RCT.

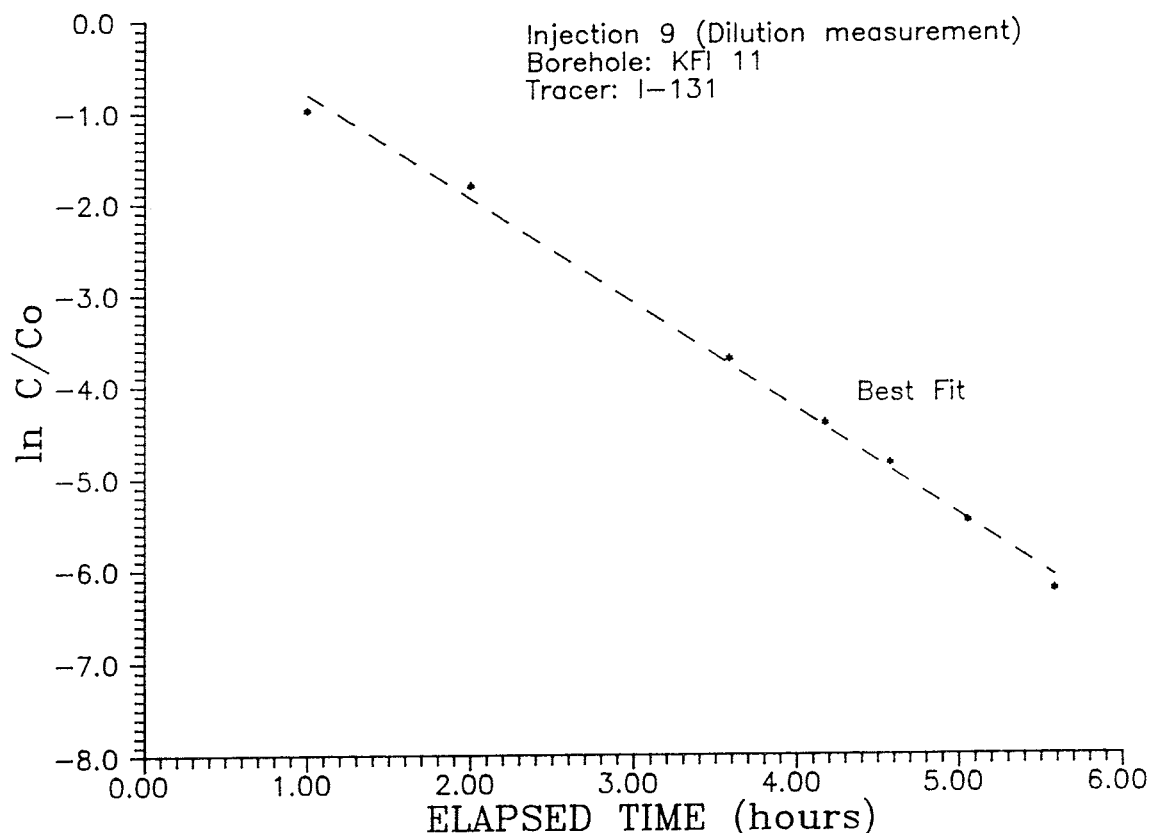


Figure 4-4 Plot of  $\ln C/C_0$  versus time from dilution measurement in borehole KFI11 (Inj. 9).

The last injection of I-131 (Inj. 10) was primarily made in order to determine if the breakthrough in borehole KFI11 represents a sampling point in the fastest flow path between BFI01 and BFI02.

The breakthrough curve (Figure 4-5) shows a first arrival of 12 hours and a mean residence time of 27 hours. Hence, addition of the mean residence times BFI01-KFI11 and KFI11-BFI02 gives a total time of about 47 hours which is very close to the mean residence times (41-50 hours) actually measured in BFI02 as a result of the injections in BFI01. Hence, these results indicate that the fracture system geometry together with the direction of the natural gradient has a great impact on the obtained dipole flow field.

The high background level is resulting from the injection of I-131 in BFI01 (Inj. 6) and the early peak at about 6 hours of elapsed time is the breakthrough of I-131 from the dilution measurement in KFI11 (Inj. 9) which was performed the day before, see Table 3-2.

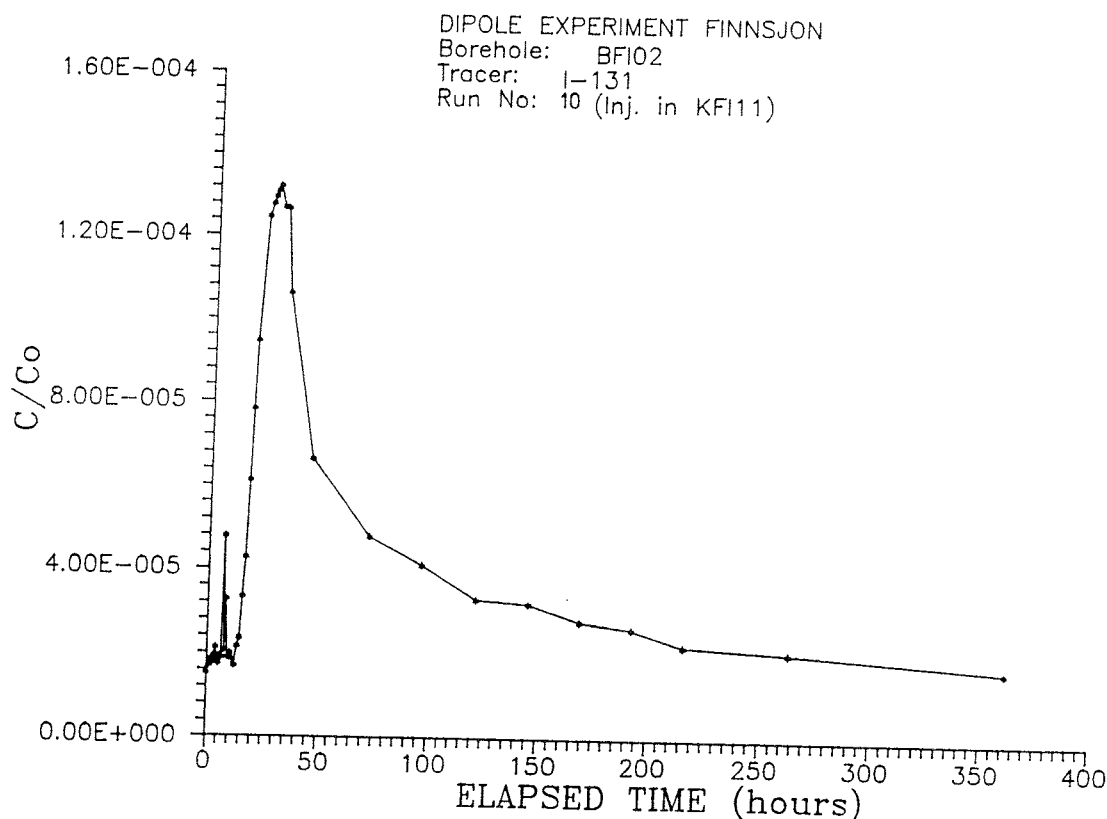


Figure 4-5 Breakthrough of I-131 in borehole BFI02 from injection in borehole KFI11 (Inj. 10).

#### 4.1.5 Recovery calculations

The tracer recovery was calculated both for the pumping hole BFI02 and for the observation boreholes KFI06 and KFI11. As the experiment was made by recirculating the water, the absolute recovery was difficult to determine. However, comparison with model calculations with the SUTRA code (Nordqvist, 1989) made for the predictions of the dipole experiment (Figure 4-6) shows that more tracer than the predicted 10% is lost. This 10% loss is due to the natural gradient influencing the dipole flow field (c.f. Nordqvist, 1989, Fig. 4.3 and 4.4). Mass balance calculations based on the electrical conductivity measurements (see Section 4.2.2) indicate tracer losses of about 30%.

In this case, the recovery was calculated at different times to be able to directly compare the recoveries of the different tracers to each other. The times were chosen in such manner that the first calculation should give the recovery at a time (40 hours) when no recirculation of tracer possibly could have occurred. Then, the recoveries at 100, 200, 300 hours, etc. was calculated. For these times the recoveries may exceed 100% due to the recirculation.

In addition to the recoveries (given as % of injected mass) the ratio between the recovery of the most conservative tracer, I-131, and the recovery of the other tracers, was calculated. For

a good conservative tracer, this ratio should be close to 1.0 at each time during the experiment. If initial irreversible losses of the tracer occur, the ratio should be less than 1.0, but remain constant at each time. An increasing ratio versus time should indicate reversible sorption of the tracer.

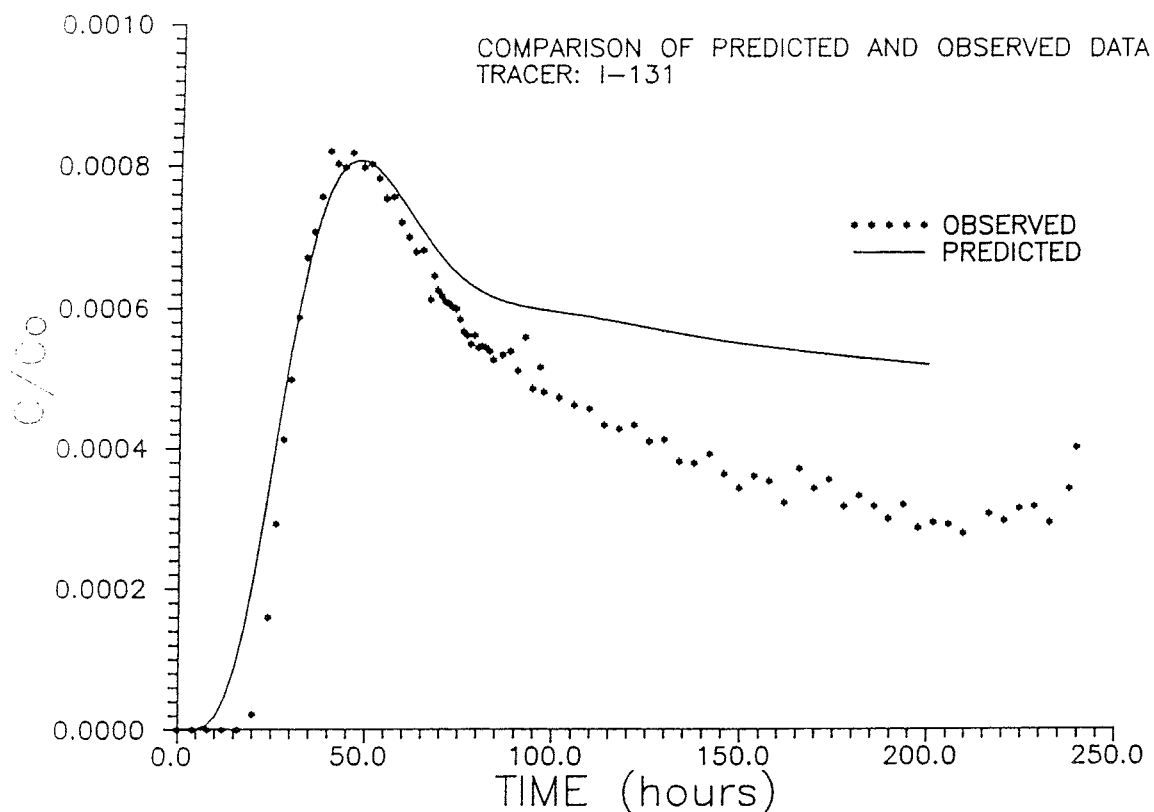


Figure 4-6 Comparison of model predictions (2-D) and experimental results from the dipole tracer experiment

The recoveries in the pumping borehole BFI02 and the observation boreholes KFI06 and KFI11 are given in Tables 4-4 to 4-6 below. The relative recoveries are calculated as the recovery relative to I-131 in Inj. 3.

For the observation boreholes KFI06 and KFI11, which are not pumped, the recovery calculations were made based on the groundwater flow determined from the dilution test in borehole KFI11 (Inj. 9). This means that the calculated values, presented in Tables 4-5 and 4-6, are measures of the mass of tracer passing through the boreholes.

Table 4-4 Tracer recovery, R (%), and relative recovery,  $R_r$  ( ), at different times in borehole BFI02.

Tracer	Inj.	R (0-40 h)	$R_r$	R (0-100 h)	$R_r$	R (0-200 h)	$R_r$
I-131	3	13.9	1.00	73.6	1.00	130.7	1.00
Cr-51	7	9.6	0.69	48.5	0.66	87.8	0.67
Co-58	8	8.6	0.62	38.0	0.52	83.2	0.64
Br-82	6	12.6	0.91	67.1	0.91	-	-
In-111	7	11.7	0.84	59.3	0.81	-	-
La-140	7	2.3	0.17	41.9	0.57	-	-
Tb-160	7	4.1	0.29	-	-	-	-
Yb-169	7	10.5	0.76	58.3	0.79	104.6	0.80
Lu-177	7	1.6	0.12	24.3	0.33	52.0	0.40
Re-186	6	10.7	0.77	56.6	0.77	97.6	0.75
RdWT	A	7.0	0.50	49.4	0.67	93.9	0.72
RdWT	E	6.7	0.48	42.0	0.57	83.1	0.64
In-EDTA	C	2.3	0.17	12.1	0.16	21.3	0.16
Gd-DTPA	D	3.5	0.25	15.8	0.21	27.0	0.21
Tm-EDTA	D	4.8	0.35	22.5	0.31	39.3	0.30

Table 4-5 Tracer recovery, R (%), and relative recovery,  $R_r$  ( ), at different times in borehole KFI06.

Tracer	Inj.	R (0-300 h)	$R_r$	R (0-500 h)	$R_r$
I-131	3	0.06	1.00	0.25*	1.00
Cr-51	7	0.02	0.37	0.13	0.50
Co-58	8	0.02	0.35	0.09	0.33
Tb-160	7	0.003	0.05	0.02	0.08
Yb-169	7	0.05	0.76	0.19	0.76
RdWT	A	0.005	0.08	0.05	0.20

\* calculated value based on constant relation with Yb-169.

Table 4-6 Tracer recovery, R (%), and relative recovery,  $R_r$  ( ), at different times in borehole KFI11.

Tracer	Inj.	R (0-40 h)	$R_r$	R (0-100 h)	$R_r$	R (0-200 h)	$R_r$
I-131	3	0.55	1.00	0.80	1.00	1.09	1.00
Na-24	6	0.18	0.33	0.22	0.28	-	-
Cr-51	7	0.32	0.58	0.53	0.66	-	-
Co-58	8	0.27	0.49	-	-	-	-
Br-82	6	0.45	0.82	0.68	0.85	-	-
In-111	7	0.38	0.69	0.65	0.81	-	-
La-140	7	0.24	0.44	0.49	0.61	-	-
Tb-160	7	0.18	0.33	0.22	0.28	-	-
Yb-169	7	0.46	0.84	0.69	0.86	-	-
Lu-177	7	0.16	0.29	0.25	0.31	-	-
Re-186	6	0.36	0.65	0.58	0.73	0.79	0.72
RdWT	E	0.20	0.36	0.41	0.51	0.65	0.60
In-EDTA	C	0.07	0.13	0.12	0.15	0.19	0.17
Gd-DTPA	D	0.15	0.27	0.21	0.26	0.29	0.27
Tm-EDTA	D	0.17	0.31	0.26	0.33	0.36	0.33

The calculated recovery values for KFI06 and KFI11 are evidently very low. As the recovery value at 40 hours in KFI11 represents the main part of the peak, this value should be about the same as the relation between the measured groundwater flow rate through the interval and the total dipole flow, 0.52 l/min and 120 l/min, respectively. These values indicate that 0.43% of the flow passes through KFI11 and the recovery calculations give a similar value, 0.55%. The difference is probably an effect of some recirculation.

#### 4.1.6 Classification of tracers

The tracers may be classified into four different groups based on the first arrivals, mean residence times, peak concentrations, and recoveries;

1. Conservative tracers with high recovery (> 75 %); Br-82, I-131 and Re-186 (anions), In-111 and Yb-169 (EDTA complexes).
2. Conservative tracers with irreversible losses; Cr-51, Tb-160 and Co-58 (EDTA complexes), In-EDTA, Tm-EDTA and Gd-DTPA (non-radioactive tracers).
3. Weakly sorbing tracers; Na-24 (cation), La-140 and Lu-177 (DOTA complexes), Rhodamine WT (dye).

4. Strongly sorbing tracers; Tc-99m (anion), Rb-86 and Tl-201 (cations).

## 4.2 SUPPORTING MEASUREMENTS

### 4.2.1 Head measurements

The head and groundwater level measurements were made in 9 boreholes divided into 19 different borehole intervals given in Table 3-7, Section 3.4. The plots of the groundwater levels and heads are given in Appendix D together with the head differences to the pumped interval in BFI02 (BFI02:U). All data is given versus elapsed time since start of pumping in BFI02.

The data, which is exemplified in Figures 4-7 and 4-8, shows that the hydraulic conditions have been very stable during the entire experiment. The groundwater levels and heads in both the upper and lower parts of Zone 2 shows a slowly sinking trend throughout the pumping period. This trend is quite normal for the period which was very dry.

The groundwater levels (Figure 4-7) for the boreholes clustered towards east (KFI05, KFI09, KFI10, and HFI01) shows a very large increase between the two first measurement points at about -210 hours and -30 hours, respectively. This is a result of the stop of the pumping for RCT. The measurement point at about -210 hours was taken just before pump stop. The same pattern can also be seen in the head plots (Appendix D:2 and D:3). Also borehole KFI06 behaves in the same manner although the borehole is sealed off with packers above Zone 2. This is in contrast to the other sealed off boreholes, BFI01, BFI02, and KFI11, where the groundwater levels are much more unaffected by the pumping in BFI02. This is also clearly seen at the start of the dipole pumping ( $t=0$ ) where there are almost no changes of the groundwater levels in BFI01, BFI02, and KFI11 while in KFI06 there is a significant response from the pumping in BFI02.

The measurement point at about 1500 hours of elapsed time was taken immediately before finishing the dipole pumping and the point at about 1700 hours was measured 8 days after pump stop.

The head differences, presented in Figure 4-8 and Appendix D:4-D:6, are stable throughout the experiment except for a slightly sinking trend for the upper interval in KFI06. Mean values and standard deviations of the head difference relative to the pumped interval (BFI02:U) are given in Table 4-7 below.

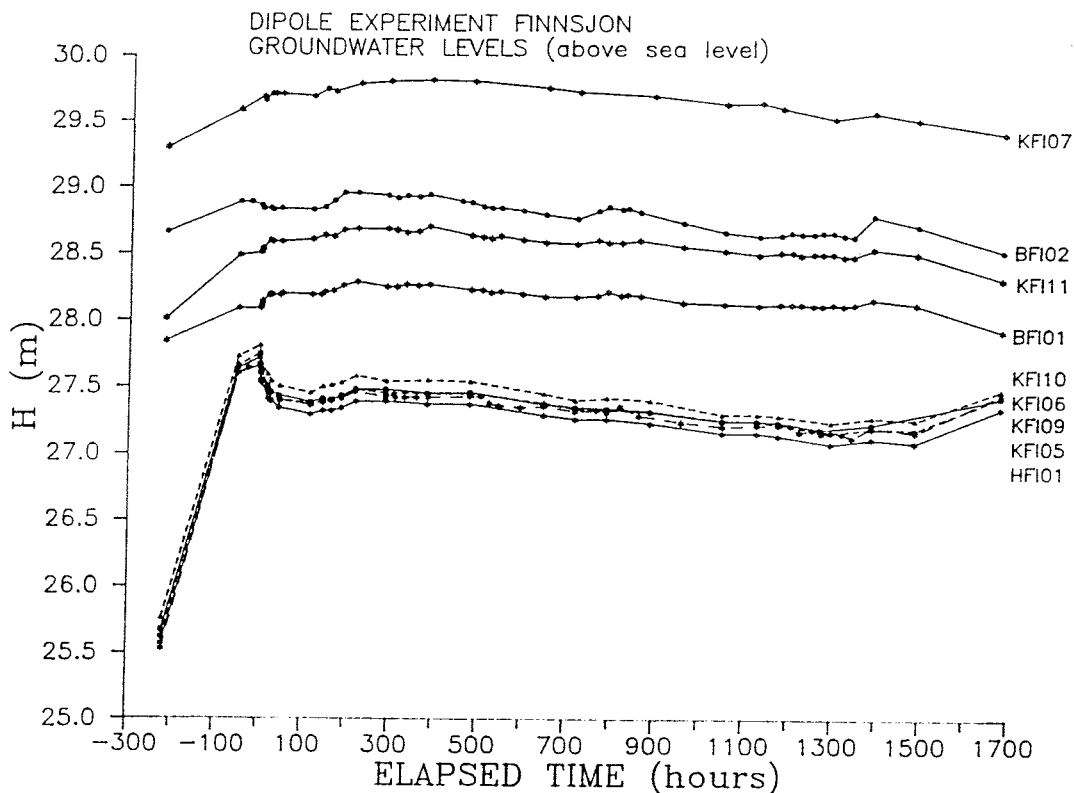


Figure 4-7 Groundwater levels versus elapsed time after start of pumping in BFI02.

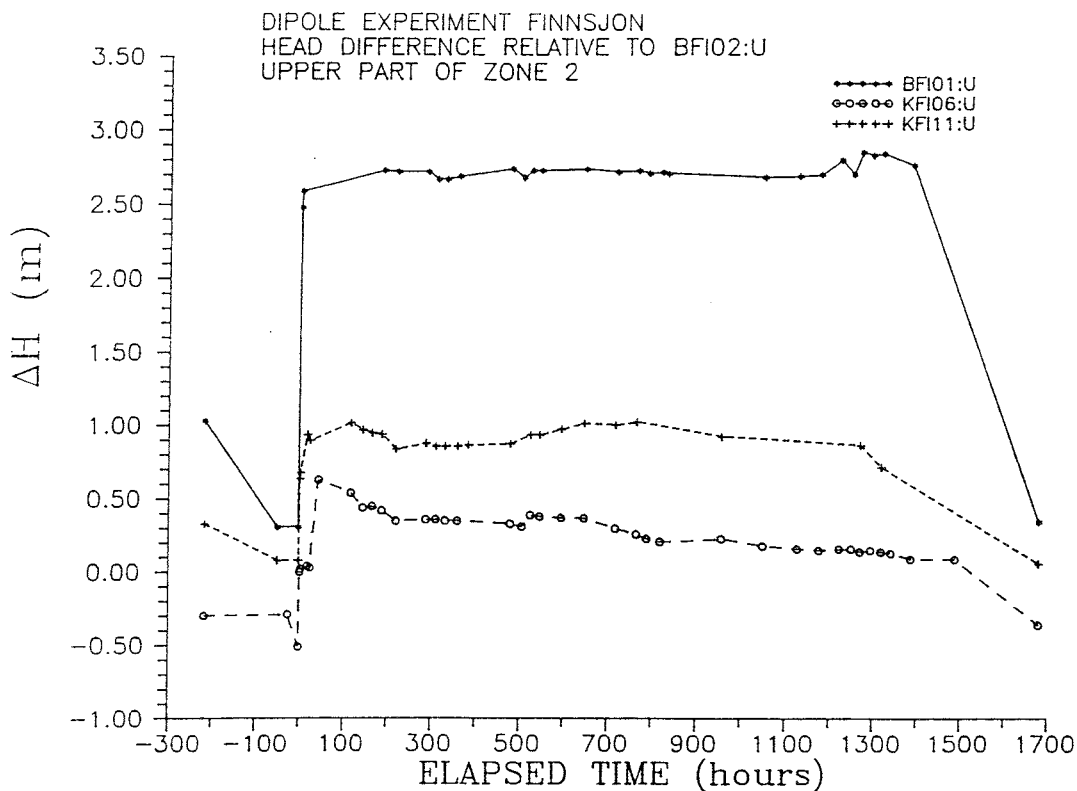


Figure 4-8 Head differences relative to the pumped interval in BFI02 for the injection interval (BFI01:U) and the observation intervals (KFI06:U and KFI11:U).

Table 4-7 Mean head differences relative to the pumped interval in BFI02 for the period 300-1485 hours of elapsed time.

Borehole interval	H (m)	st. dev. (m)
Upper part of Zone 2:		
BFI01:U	2.74	0.06
KFI06:U	0.24	0.10
KFI11:U	0.91	0.08
Middle and lower parts of Zone 2:		
BFI01:L	1.71	0.05
BFI02:L	0.37	0.01
KFI06:M	0.56	0.02
KFI06:L	-0.17	0.01
KFI11:M	0.69	0.04
KFI11:L	0.17	0.15
Groundwater levels:		
BFI01	1.44	0.05
BFI02	2.05	0.04
KFI06	0.56	0.01
KFI11	1.85	0.04
KFI05	0.57	0.01
KFI07	2.95	0.02
KFI09	0.58	0.01
KFI10	0.64	0.03
HFI01	0.49	0.02

#### 4.2.2 Pumping rate and physical parameters

The pumping in borehole BFI02 was performed without any major disturbances and at an almost constant rate. A very slightly increasing trend from about 119 l/min, at the beginning of the tracer injections, to about 121 l/min at the end of the pumping can be seen in Figure 4-8. The mean value over the period 0-1485 hours was 120.2 l/min ( $s=1.4$ ). Only a few shorter pump stops occurred between 814-820 hours of elapsed time with a total duration of less than one hour due to power failure. This can also be seen in Figure 4-9 as a "dip" in the plot. It should also be noted that each data point represents an average flow over a period of 1-3 days.

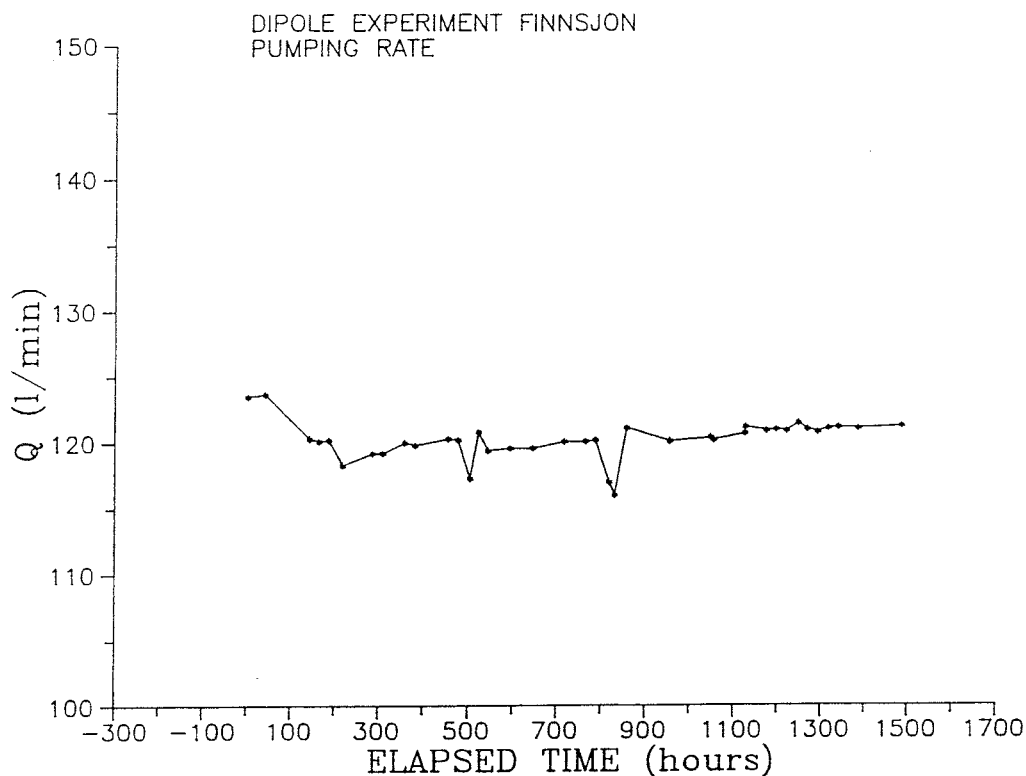


Figure 4-9 Dipole pumping/injection rate versus elapsed time after start of pumping.

The physical parameters measured during the experiment were: electrical conductivity, temperature, and oxidation-reduction potential of the pumped water. The temperature was measured both in the pumping hole and before entering the injection borehole.

The temperature of the pumped water at BF101 (Figure 4-10) shows no significant trend. Measurements were also made at borehole BF102 but unfortunately with an erroneous temperature probe. The mean value of the temperature at BF101 was  $8.7^{\circ}\text{C}$  ( $s=0.6^{\circ}\text{C}$ ).

The electrical conductivity of the pumped water (Figure 4-11) shows a significantly increasing trend from about  $360\text{ mS/m}$  at the very beginning of the pumping, to almost  $600\text{ mS/m}$  at the end. This increase is due to leakage of saline water from deeper parts of Zone 2 which also has been noted during the previous interference tests (Andersson et al., 1988b). The leakage rate could be estimated by mass balance calculations, see Section 5.2. The large increase around 120 hours is most probably due to an erroneous reading of the electrical conductivity meter.

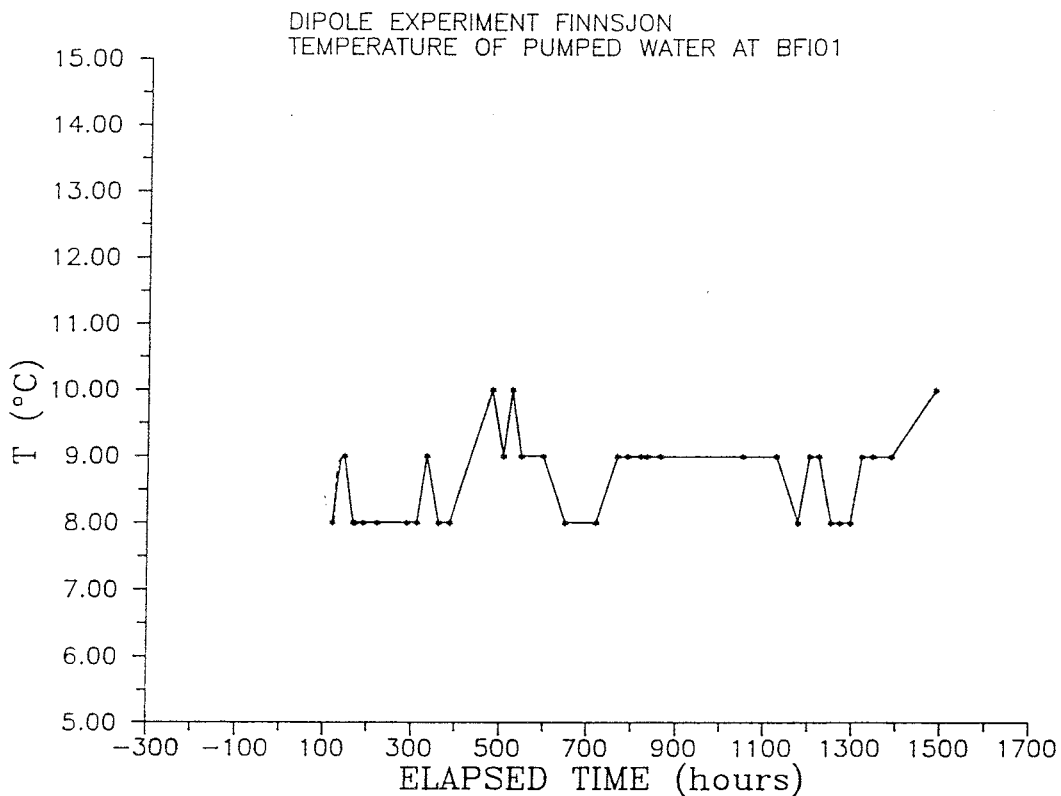


Figure 4-10 Temperature of pumped/injected water at BFI01.

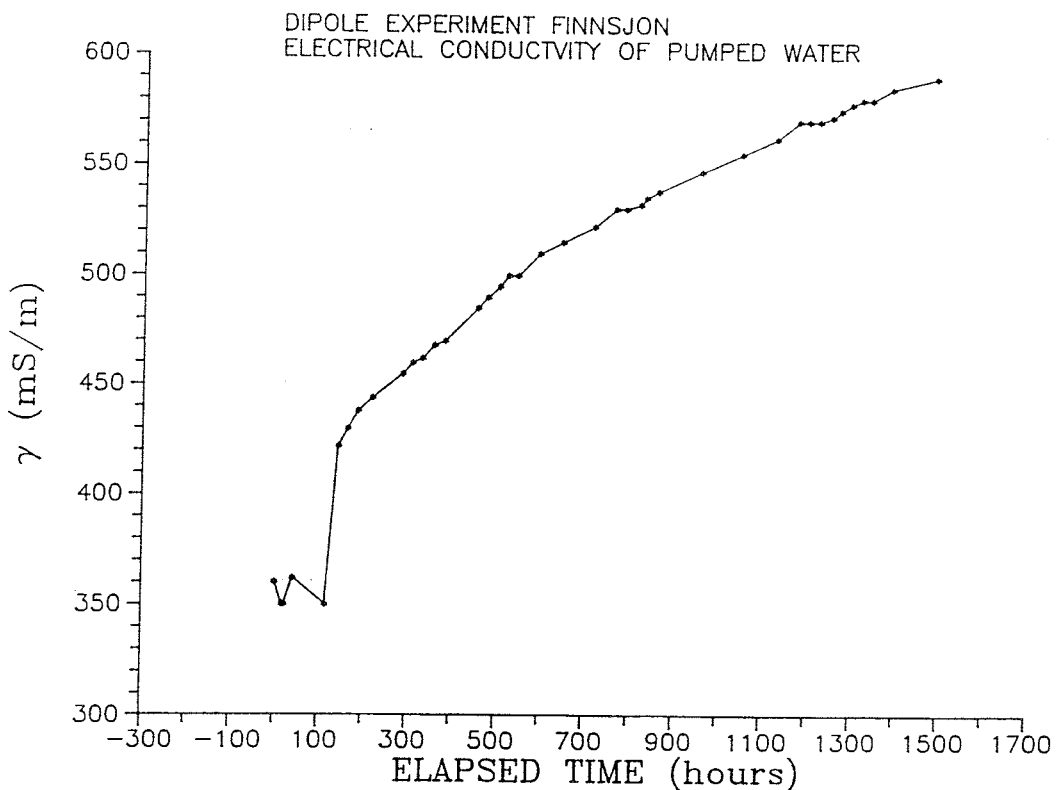


Figure 4-11 Electrical conductivity of pumped water during the dipole experiment.

The oxidation-reduction potential (Figure 4-12) was negative (-150 - -220 mV) during most of the time of the tracer injections (300-1500 hours). The only positive values were registered at the very beginning of the pumping and in conjunction with the short pump stops between 814-820 hours.

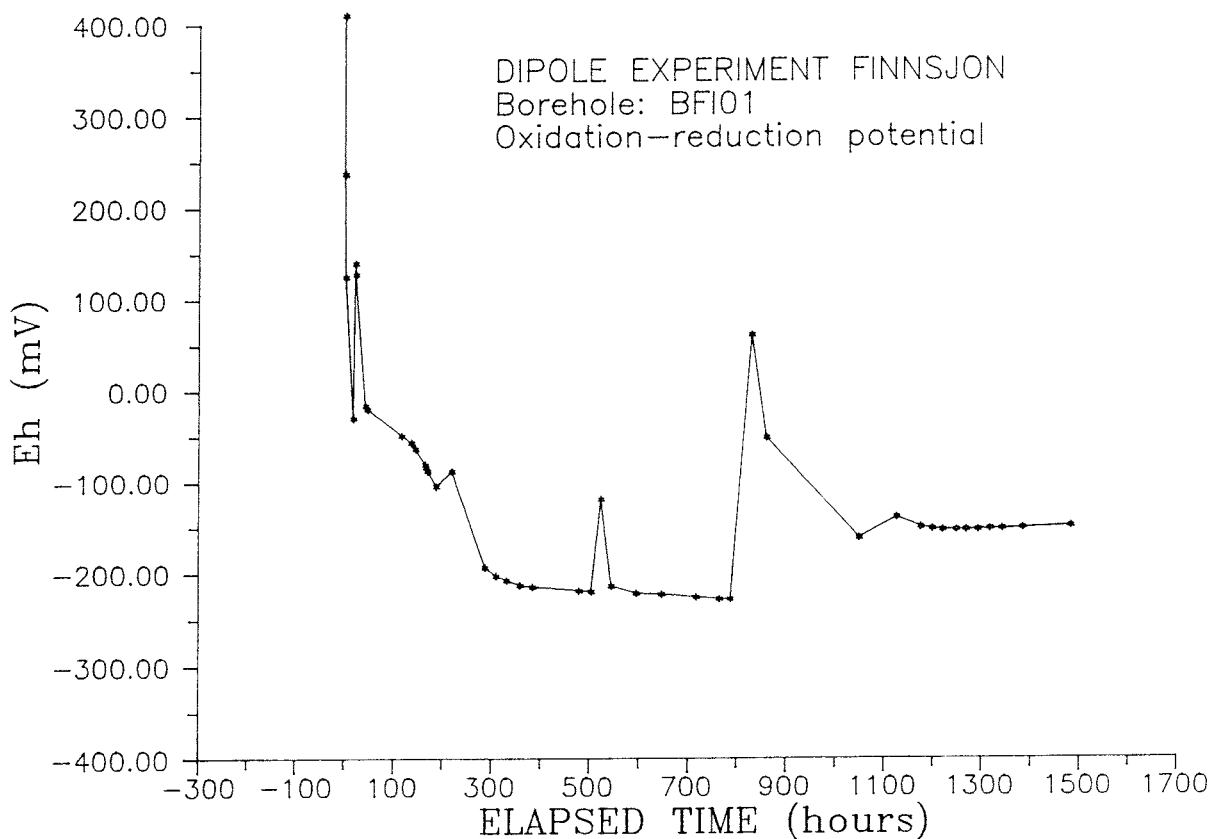


Figure 4-12 Oxidation-reduction potential of the pumped water at BFI01.

## 5 DISCUSSION AND CONCLUSIONS

### 5.1 EXPERIMENTAL DESIGN

The design of the dipole experiment was made in order to create a dipole field in the upper highly conductive subzone of the major low angle Zone 2. This implied a virtually two-dimensional flow field. The high transmissivity of the upper subzone made it necessary to use a recirculating flow.

The dipole experiment was performed in the same borehole geometry as the preceding radially converging experiment. The idea was to directly compare the values of the transport parameters determined from the two experiments. One advantage of the dipole geometry compared to the radially converging is that a much larger rock surface is accessible for the tracers. This may be favorable when sorbing or macromolecular tracers are used.

The recirculation has some advantages as well as some disadvantages. The major advantage was that no large supply of water had to be kept at the site with all the problems of maintaining the chemistry of the water, avoiding biological growth, temperature differences, oxidation, etc. Also the closed recirculating system made it possible to use radio-nuclides as there are no problems with the discharge from the pumping. The system is also favorable from a practical point of view as only one pump and one capacity regulation system is needed. It is also possible to use the recirculation as a check of the stability of the dipole field as the tracer concentration should stabilize at a constant level in a perfect dipole field.

The major disadvantage is in the evaluation as the effects of the recirculation must be taken into account in the model fitting of the tails of the breakthrough curves.

The use of observation boreholes proved to be very valuable. In this experiment, the heterogeneity of the system was displayed and the system with constantly mixed observation intervals made it possible to obtain breakthrough data of high quality. Another valuable aspect is that the use of observation boreholes expands the time scale of the experiment, in this case from one breakthrough at 45 hours to three breakthroughs at 20-200 hours.

A large number of tracer injections were made during a relatively short period of time. This might create some problems with interference from previously injected tracers if not great care is taken to optimize the injection schedule. In this experiment only minor problems with high background concentrations occurred as a result of several injections of I-131.

In summary, the experimental design was made in such way that good reproducible data could be obtained throughout the whole time period of the experiment.

## 5.2 EXPERIMENTAL RESULTS

The injection of the 19 different tracers resulted in about 50 breakthrough curves in the pumping holes and the two observation holes. This is a large number of data to analyze and evaluate and this will be made separately. This report is limited to a qualitative interpretation of the breakthrough data and some calculations of recovery and tracer losses.

The breakthrough data is mostly of good quality, both in the pumping hole and in the observation holes. The stable conditions prevailing during the experiment (pumping rate, head differences) makes it possible to directly compare the transport of different tracers to each other. Based on the breakthrough data including first arrival, mean residence time, peak concentration and tracer recovery, a classification of the tracers was made (see Section 4.1.5). The data showed four different types of tracers:

- Conservative tracers with high recovery.
- Conservative tracers with irreversible losses.
- Weakly sorbing tracers (reversible losses).
- Strongly sorbing tracers.

Most of the tracers were behaving in an expected manner, e.g. that the ions were conservative and the cations were sorbing. There are also some more unexpected results which can not be easily explained. The most prominent feature of the breakthrough is that most tracers are lost to some degree as compared to I-131 (anion). Even a tracer like Cr-51 (EDTA-complex), which is considered as conservative and earlier has showed recoveries close to that of Iodide at the Finnsjön site (Gustafsson and Klockars, 1981), were found to have losses. For the EDTA-complexes, the losses may be due to the high content of Fe (2-3 ppm).

The surprisingly low recovery of the non-radioactive metal complexes (In-EDTA, Gd-DTPA, and Tm-EDTA) does not agree with the results of the radially converging experiment where recoveries of 72-98% were found for these tracers. Currently, no good explanation can be given for the observed behaviour. However, it should also be noted that no reversible sorption can be observed from the breakthrough data.

The sorbing tracers were either completely sorbed (or much delayed), as Tc-99m ( $TcO_4^-$ ), Co-58 ( $Co^{2+}$ ), Rb-86 ( $Rb^+$ ), Tl-201 ( $Tl^+$ ), or weakly sorbed. The sorption of Tc-99m is of special interest as this is one of the fission products. Laboratory data has indicated that Tc-99 is sorbing under reducing conditions (as  $TcO_2$ ), while under oxidizing conditions it is mobile (as  $TcO_4^-$ ) (Eriksen, 1988). This is also indicated by

the breakthrough of the chemical analogue Re-186 ( $\text{ReO}_4^-$ ) where no delay was observed. One problem with the injection of Tc-99m is the very short half-life (6 hours) which of course limits the detectability. The detectability was somewhat improved by the high activity injected but a slow breakthrough with a low peak concentration may be difficult to detect even in the nearest borehole (KFI11).

No transport of the cations can be observed, except for Na. The retention of  $\text{Rb}^+$  and  $\text{Tl}^+$  compared to the fast transport of  $\text{Na}^+$  can be explained by the high background concentration (300-600 ppm) of Na in the groundwater.

Based on predictions with the SUTRA-code (Nordqvist, 1987) a tracer loss of about 10% was expected due to the disturbance of the dipole flow field caused by the natural gradient in the area. The natural gradient was estimated to be in the order of 1m/300m (Ahlbom et al., 1987). However, the increasing trend of the electrical conductivity during the experiment (Figure 4-11) indicated that saline water from deeper parts of Zone 2 was withdrawn. Simple mass balance calculations indicated that about 30% of the water pumped from the upper part of BFI02 was leaking from lower parts of Zone 2 and hence, the loss of tracer from the dipole field should be approximately the same (30 %).

In summary, the experimental results show that even though the upper highly conductive subzone of Zone 2 is considered to be fairly homogeneous, judging from single hole tests and large scale interference tests, there are considerable differences regarding the transport in different directions. The results also show that it is possible to use short-lived radioisotopes as tracers in large scale field experiments. The method enables very fast and simple tracer analyses in situ.

## 6. REFERENCES

- Ahlbom K, Andersson P, Ekman L, Gustafsson E, Smellie J, and Tullborg E-L 1986. Preliminary investigations of fracture zones in the Brändan area, Finnsjön study site. SKB Technical Report 86-05.
- Ahlbom K, Andersson P, Ekman L, and Tirén S 1987. Characterization of fracture zones in the Brändan area, Finnsjön study site. SKB Progress Report 88-09.
- Ahlbom K, and Smellie, J.A.T (editors) 1989. Characterization of fracture zone 2, Finnsjön study site, Part 1-6. SKB Technical Report 89-19.
- Andersson J-E, Ekman L, and Winberg A 1988a. Detailed investigations of fracture zones in the Brändan area, Finnsjön study site. Single hole water injection tests in detailed sections. Analysis of conductive fracture frequency. SKB Progress Report 88-08.
- Andersson J-E, Ekman L, Gustafsson E, Nordqvist R, and Tirén S 1988b. Hydraulic interference tests within the Brändan area, Finnsjön study site. The Fracture Zone Project Phase 3. SKB Technical Report 89-12.
- Byegård J, Skarnemark G, and Skålberg M in prep. Tracer experiments in a dipole geometry in a fracture zone at the Finnsjön area. Results from radioactive tracer test. The Fracture Zone Project Phase 3. Dep. of Nuclear Chemistry Chalmers University of Technology.
- Eriksen T E 1988. Radionuclide transport in a single fissure. A laboratory flow system for transport under reducing conditions. SKB Technical Report 88-28.
- Gustafsson E, and Klockars C-E 1981. Studies on groundwater transport in fractured crystalline rock under controlled conditions using non-radioactive tracers. SKB Technical Report 81-07.
- Gustafsson E, Andersson P, Eriksson C-O, and Nordqvist R 1989. Radially converging tracer experiment in a low angle fracture zone at the Finnsjön site, central Sweden. The Fracture Zone Project Phase 3. SKB Technical Report, in prep.
- Gustafsson E, and Andersson P 1990. Small scale tracer experiments in the Stripa mine using a macromolecular compound. SKB Progress Report, in prep.
- Nordqvist R 1989. Numerical predictions of a dipole tracer test in a fracture zone in the Brändan area, Finnsjön. SKB Progress Report 89-34.

Smellie J, Gustafsson E, and Wikberg P 1987. Groundwater sampling during and subsequent to air-flush rotary drilling: Hydrochemical investigations at depth in fractured crystalline rock. SKB Progress Report 87-31.

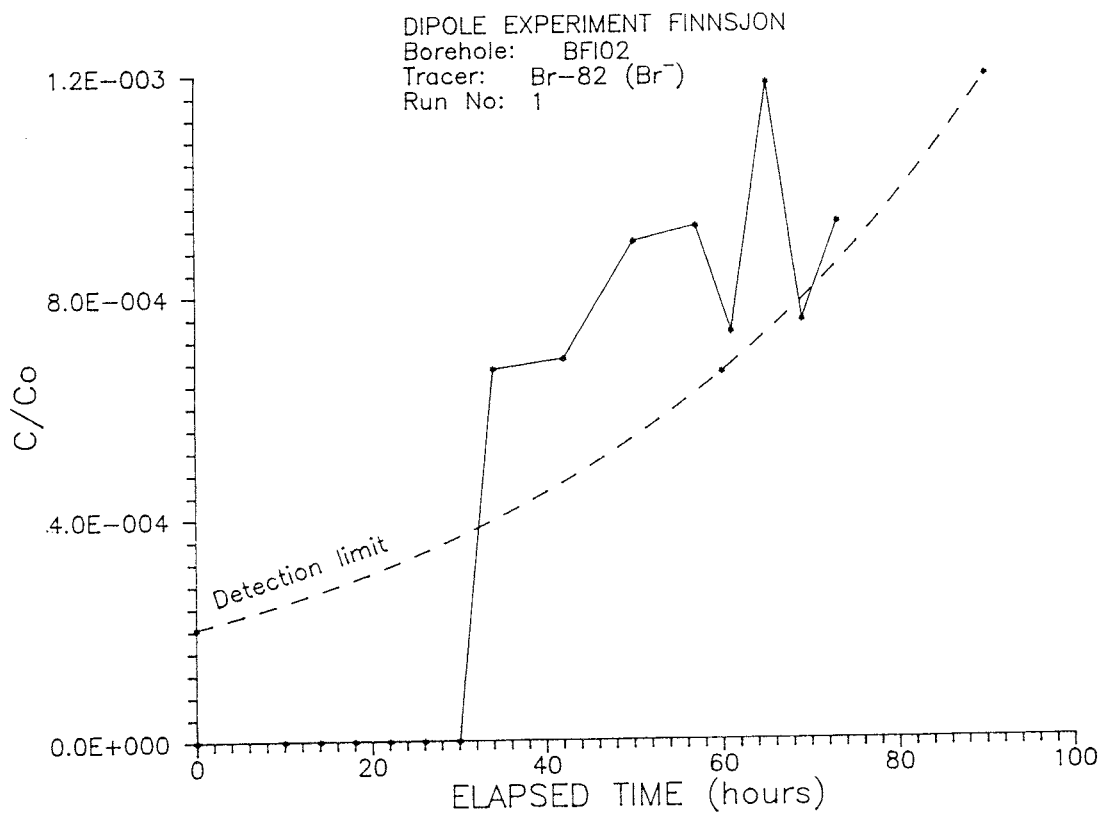
## APPENDIX A

## TRACER BREAKTHROUGH IN BOREHOLE BF102

CONTENTS	Page
Breakthrough curve for Br-82 (Inj. 1) in BF102, 0-100 h.	A:1
Breakthrough curve for Re-186 (Inj. 2) in BF102, 0-100 and 0-300 h.	A:2
Breakthrough curve for I-131 (Inj. 3) in BF102, 0-100 and 0-300 h.	A:3
Breakthrough curve for Br-82 (Inj. 6) in BF102, 0-100 h.	A:4
Breakthrough curve for I-131 (Inj.6) in BF102, 0-100 and 0-300 h.	A:5
Breakthrough curve for Re-186 (Inj. 6) in BF102, 0-100 and 0-300 h.	A:6
Breakthrough curve for La-140 (Inj. 7) in BF102, 0-100 h.	A:7
Breakthrough curve for Lu-177 (Inj. 7) in BF102, 0-100 and 0-300 h.	A:8
Breakthrough curve for Cr-51 (Inj. 7) in BF102, 0-100 and 0-300 h.	A:9
Breakthrough curve for In-111 (Inj. 7) in BF102, 0-100 h.	A:10
Breakthrough curve for Tb-160 (Inj. 7) in BF102, 0-100 h.	A:11
Breakthrough curve for Yb-169 (Inj. 7) in BF102, 0-100 and 0-300 h.	A:12
Breakthrough curve for Co-58 (Inj. 8) in BF102, 0-100 and 0-300 h.	A:13
Breakthrough curve for Rhodamine WT (Inj. A) in BF102, 0-100 and 0-1000 h.	A:14
Breakthrough curve for In-EDTA (Inj. C) in BF102, 0-100 and 0-300 h.	A:15

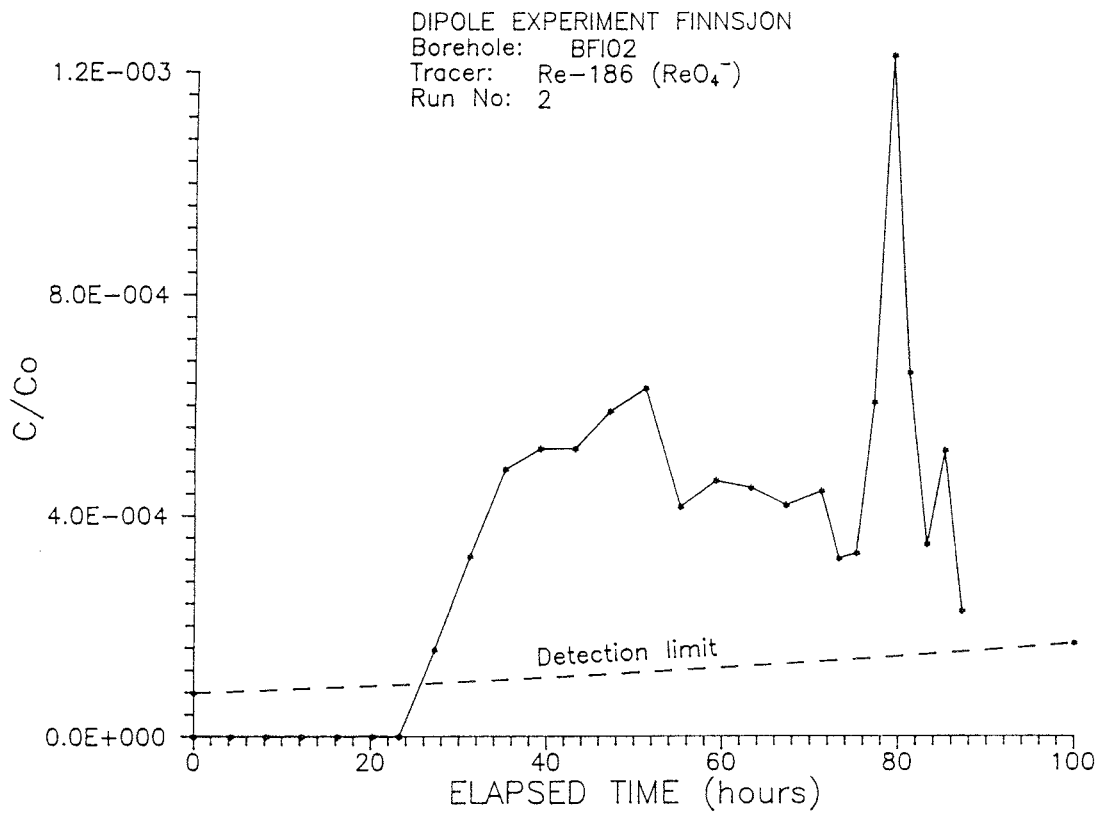
CONTENTS (Continued)	Page
Breakthrough curve for Gd-DTPA (Inj. D) in BFI02, 0-100 and 0-300 h.	A:16
Breakthrough curve for Tm-EDTA (Inj. D) in BFI02, 0-100 and 0-300 h.	A:17
Breakthrough curve for Rhodamine WT (Inj. E) in BFI02, 0-100 and 0-300 h.	A:18

A: 1



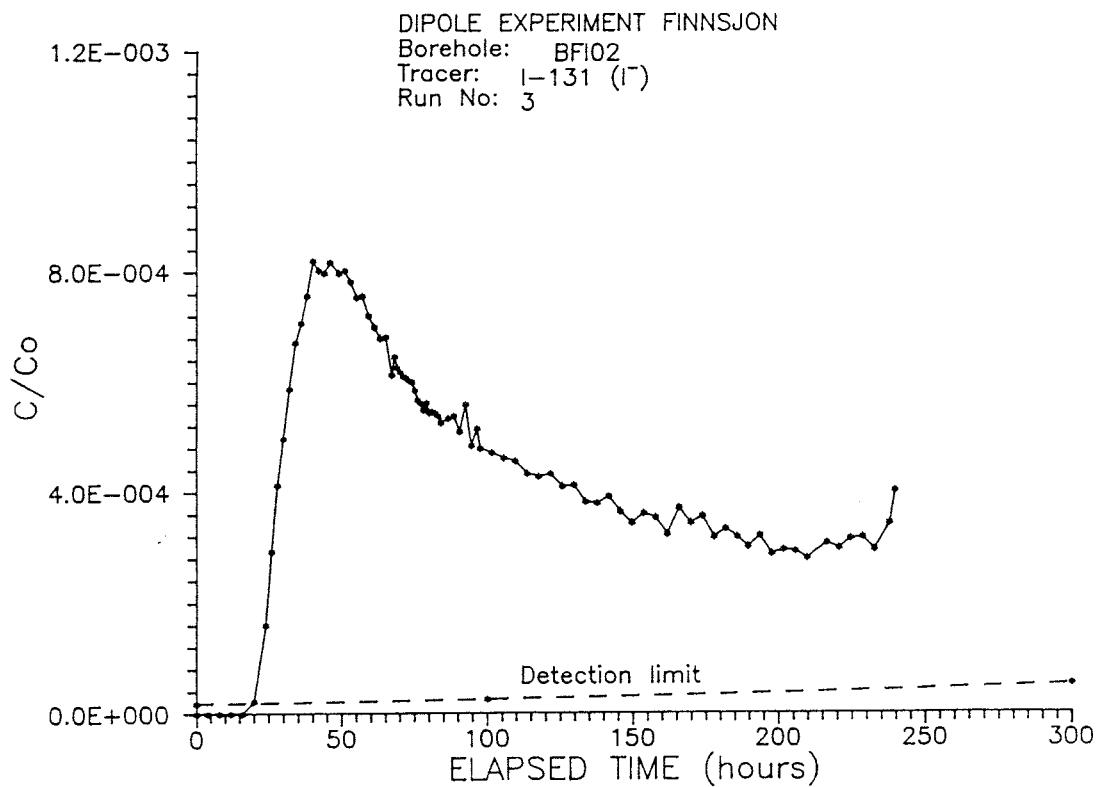
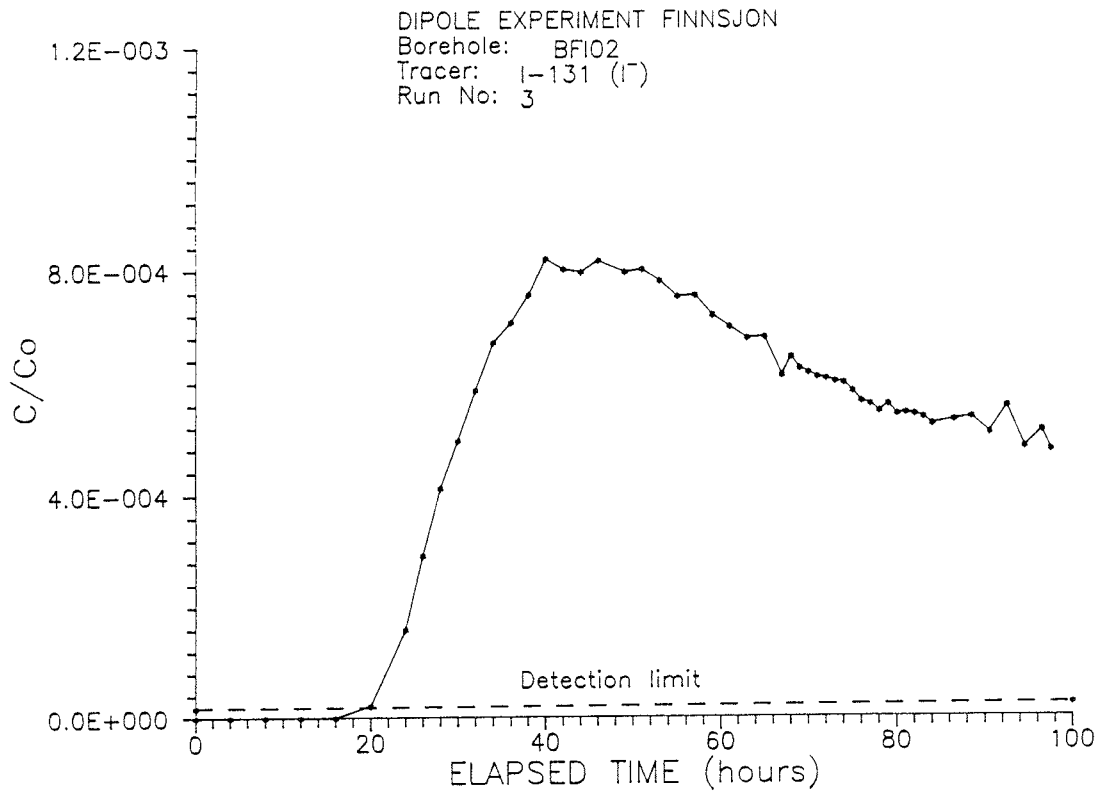
Breakthrough curve for Br-82 (Inj. 1) in BFI02, 0-100 h.

A: 2



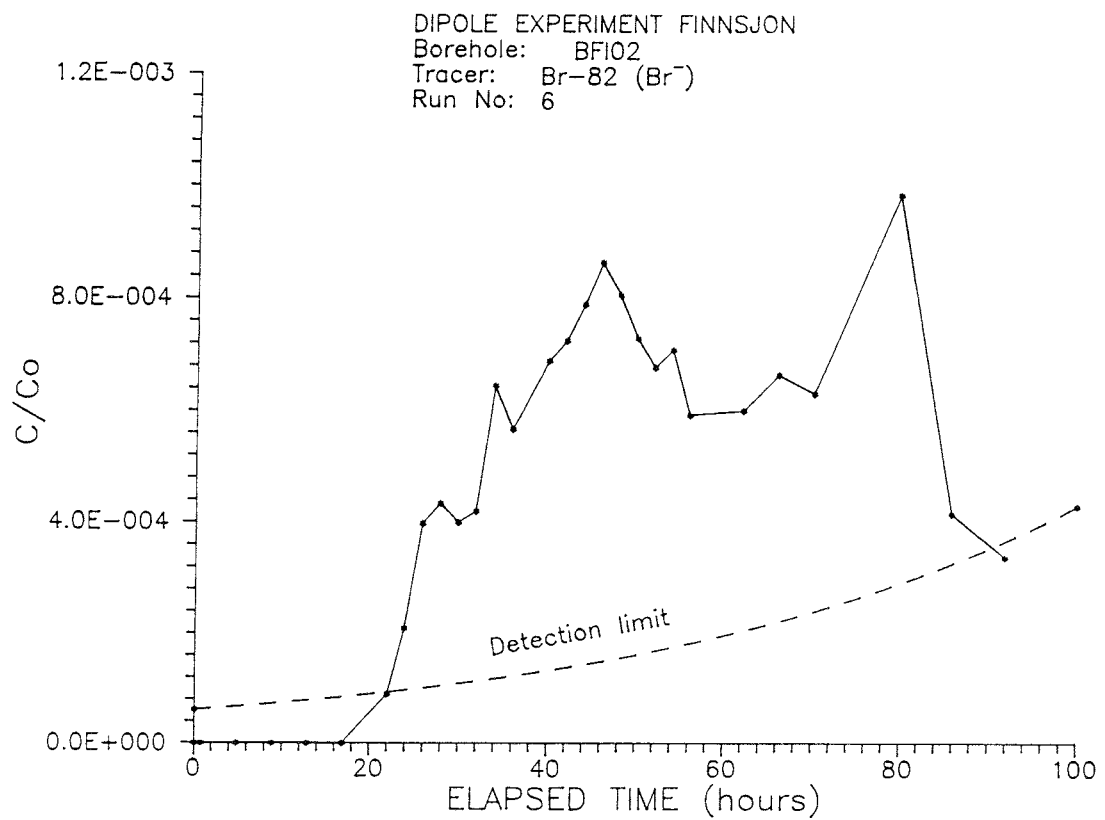
Breakthrough curve for Re-186 (Inj. 2) in BF102, 0-100 h.

A: 3



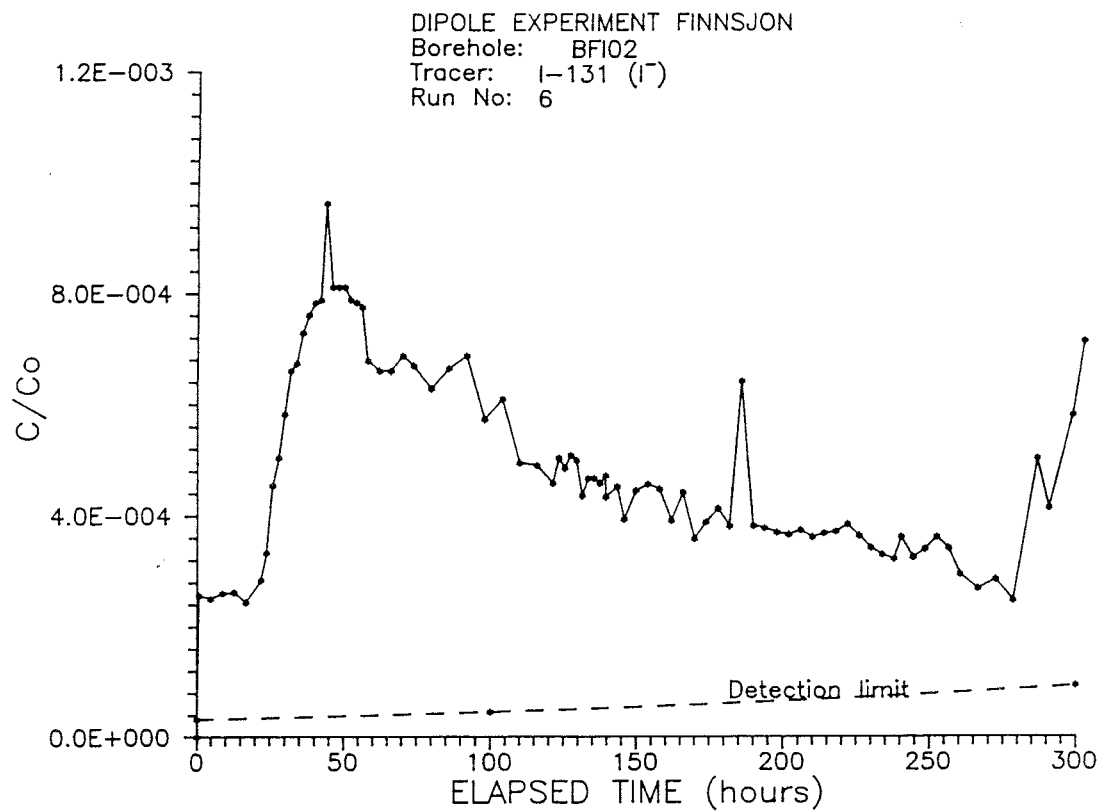
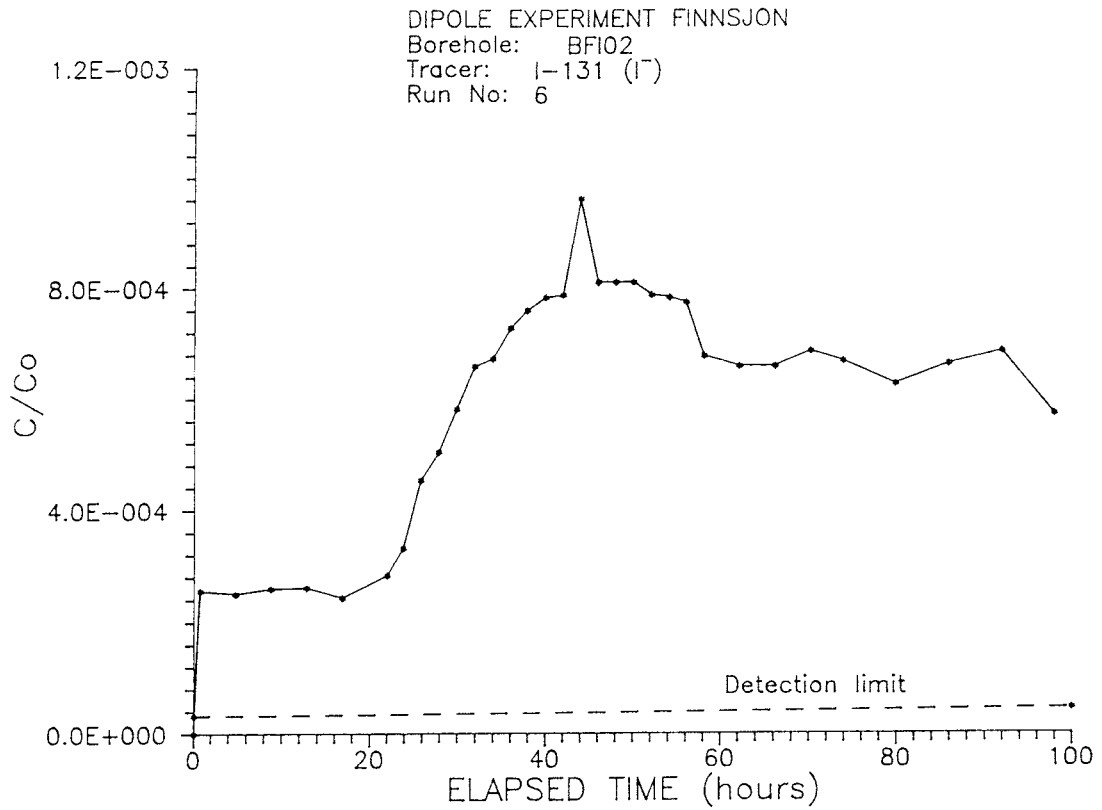
Breakthrough curve for I-131 (Inj. 3) in BFI02,  
 0-100 and 0-300 h.

A: 4



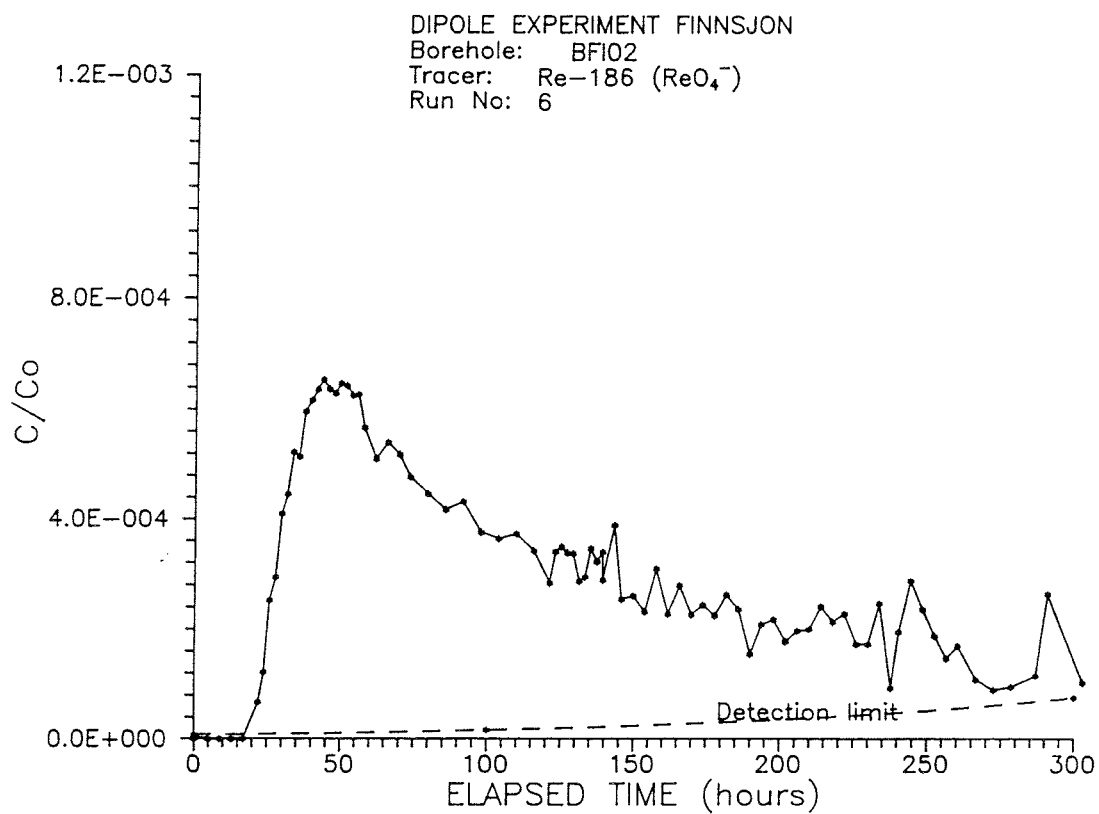
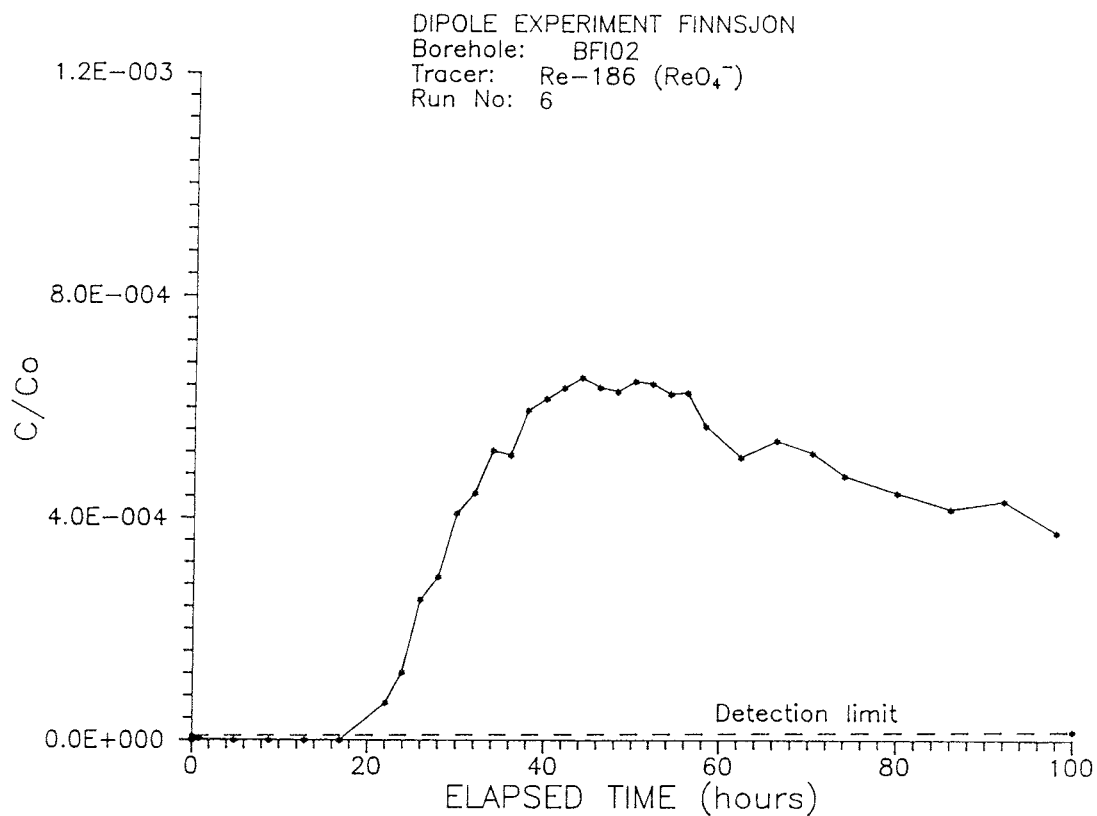
Breakthrough curve for Br-82 (Inj. 6) in BFI02, 0-100 h.

A: 5



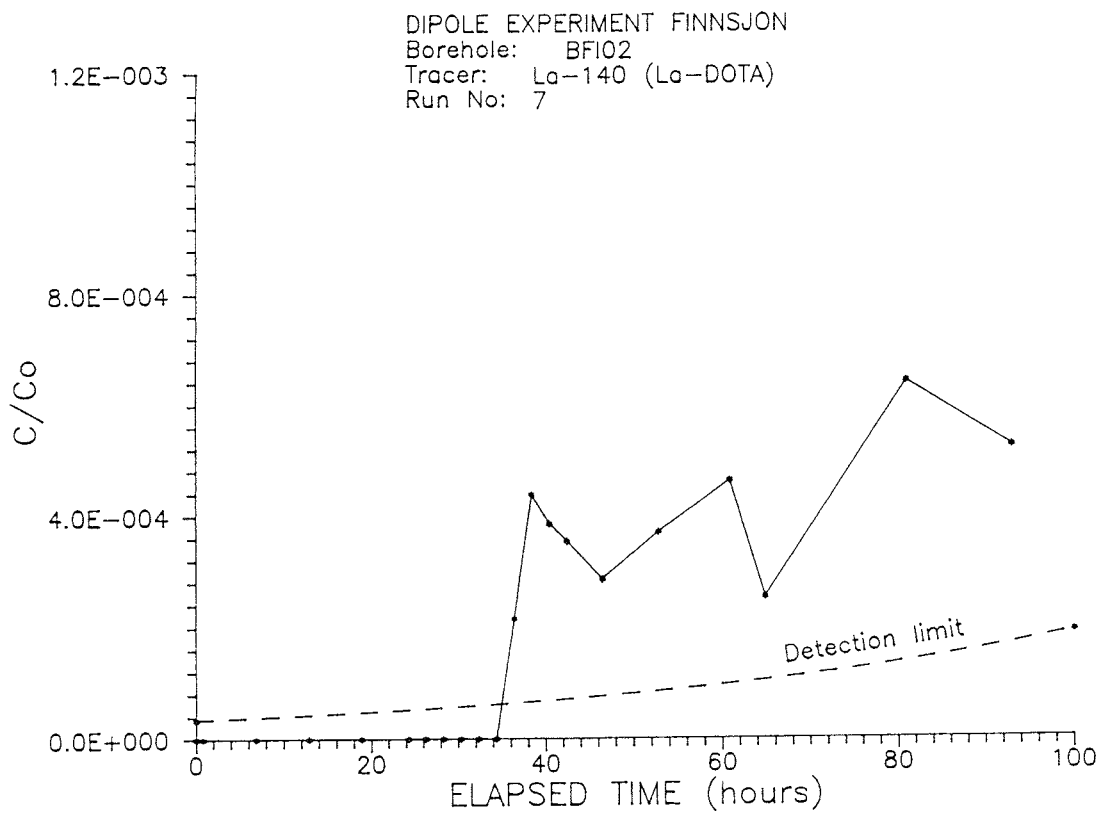
Breakthrough curve for I-131 (Inj.6) in BFI02, 0-100 and 0-300 h.

A: 6



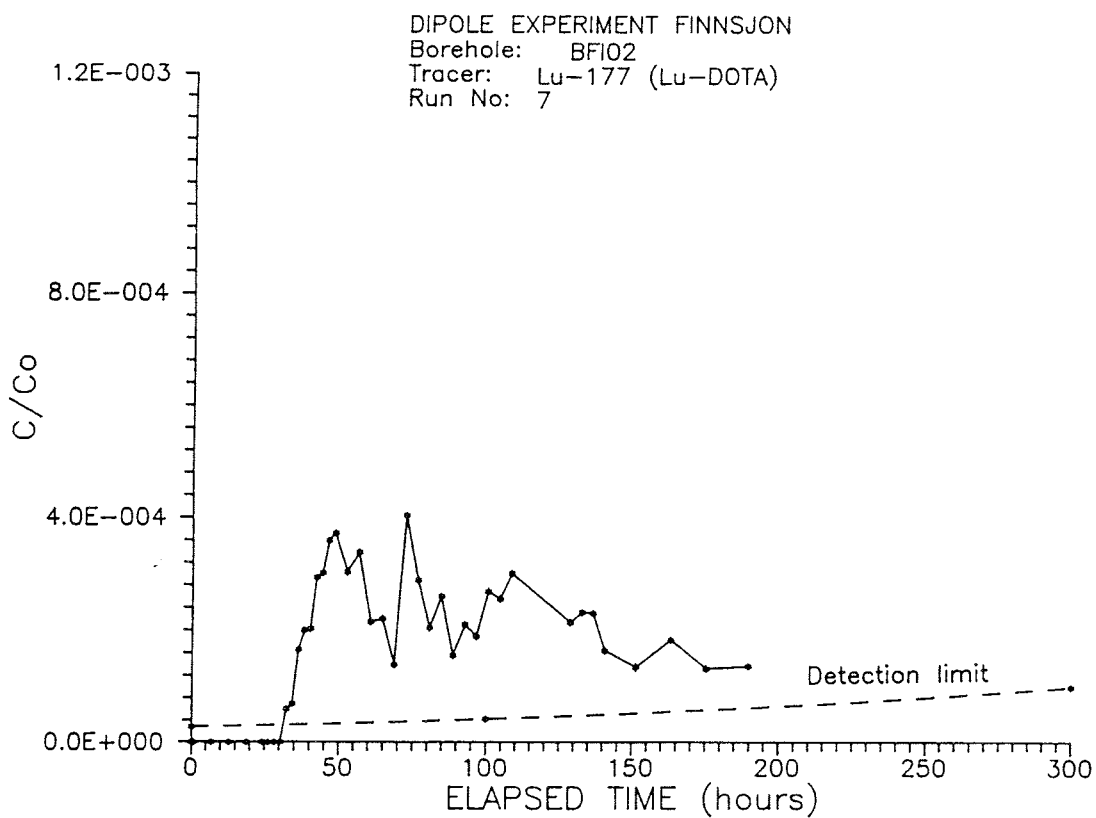
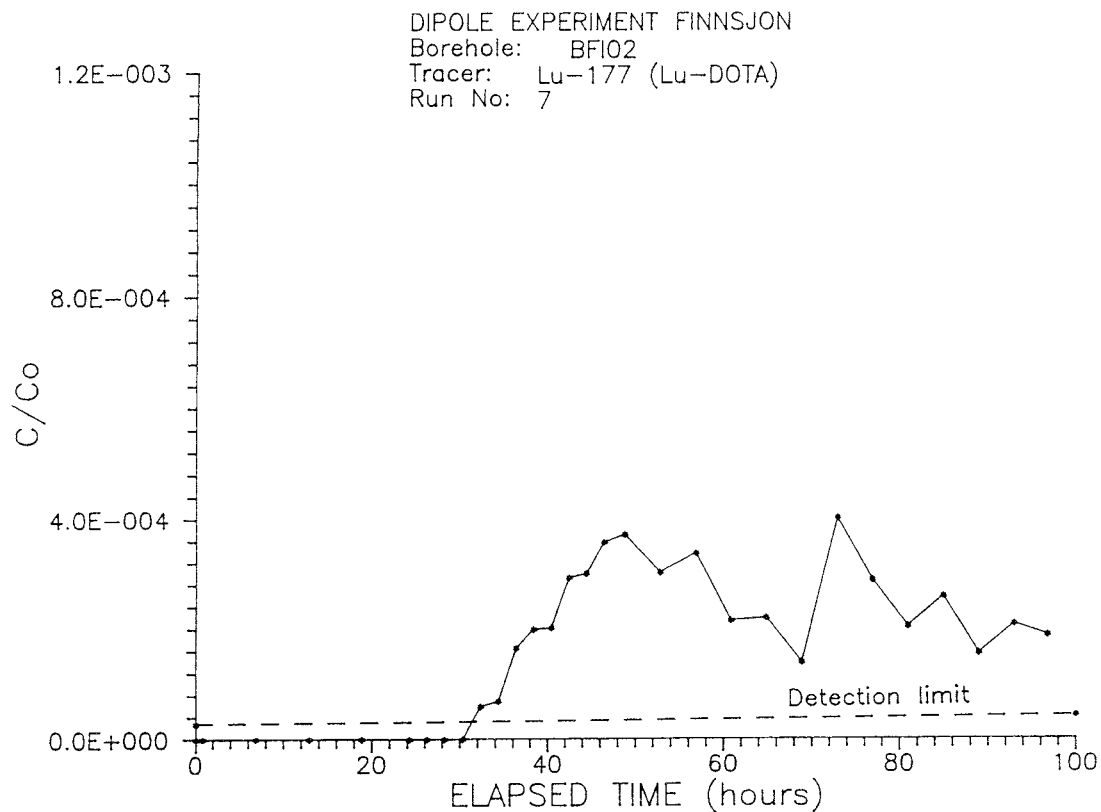
Breakthrough curve for Re-186 (Inj. 6) in BFI02,  
0-100 and 0-300 h.

A: 7



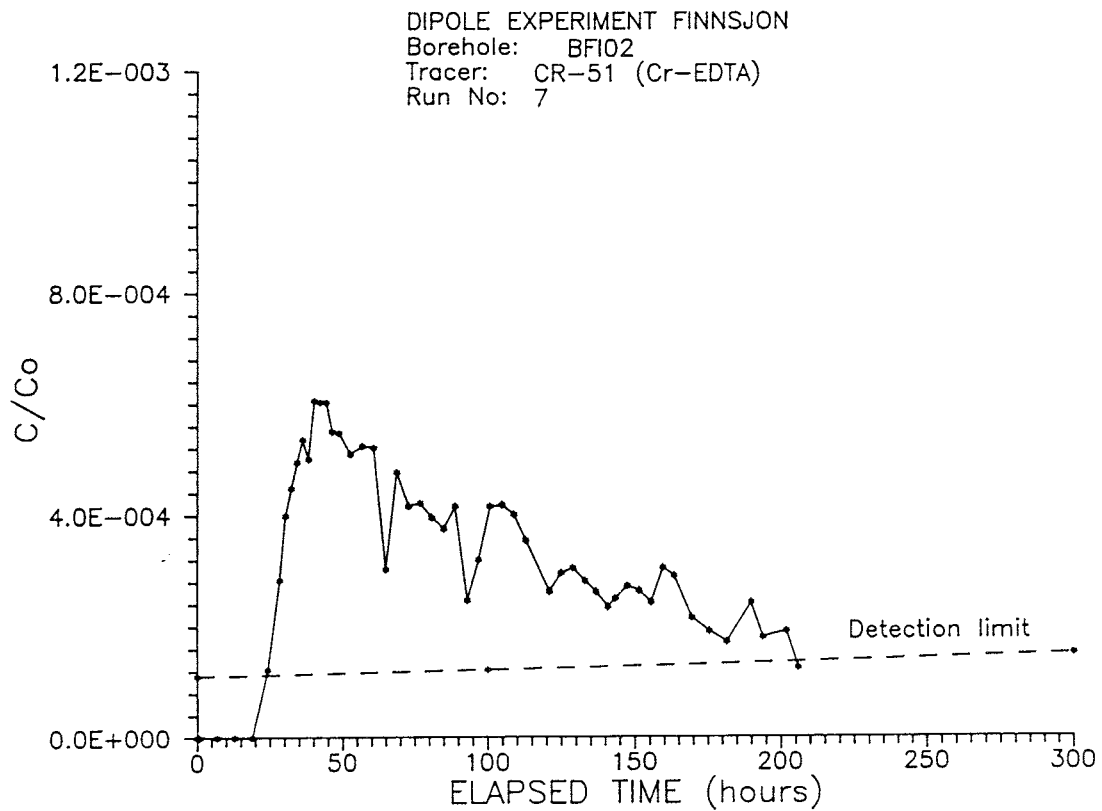
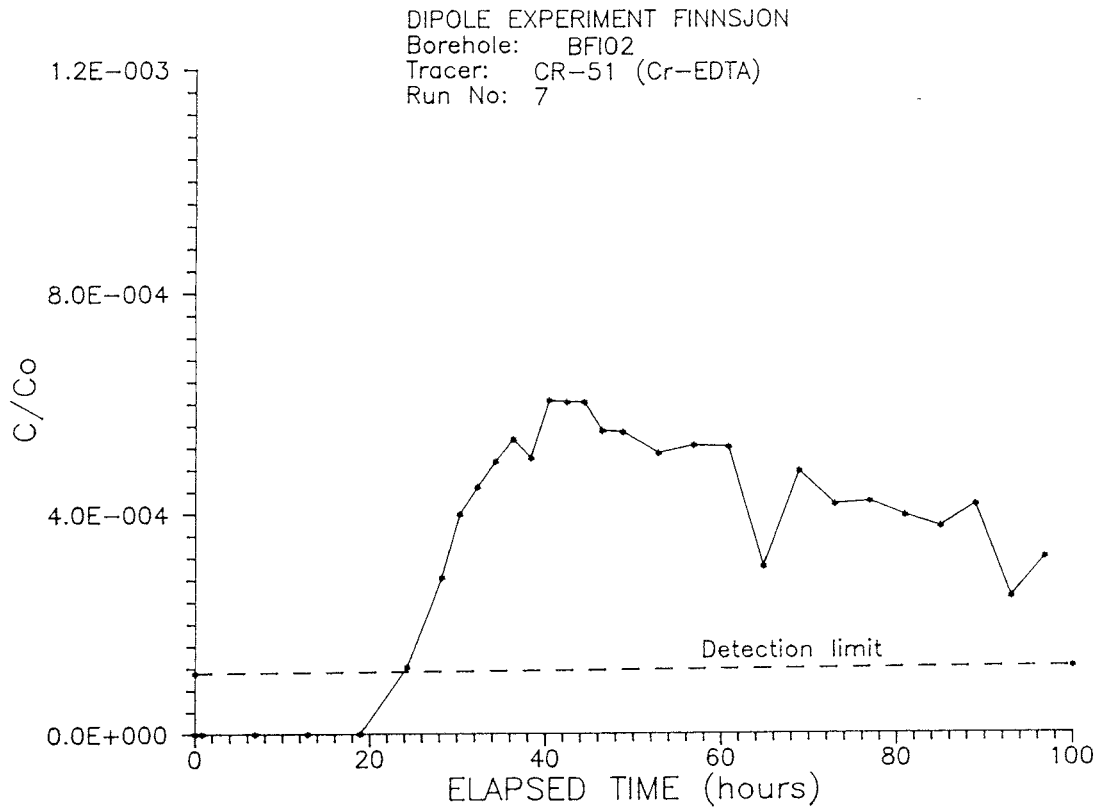
Breakthrough curve for La-140 (Inj. 7) in BF102, 0-100 h.

A: 8



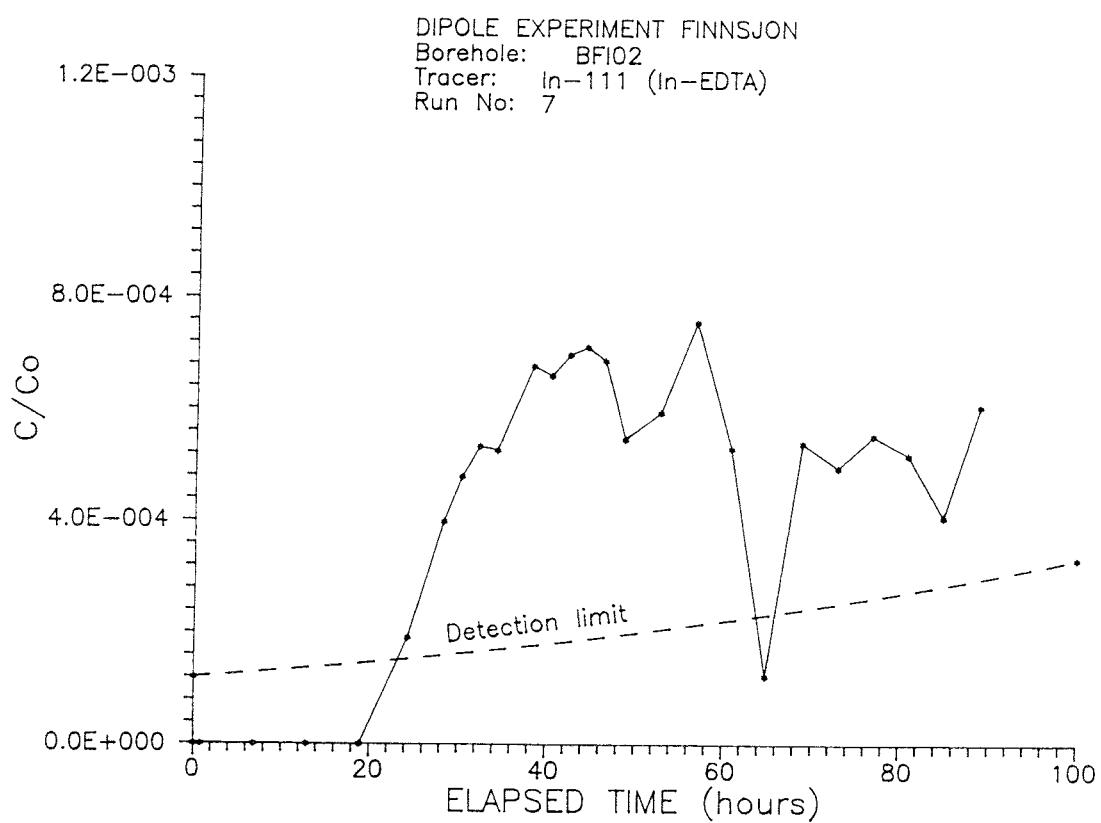
Breakthrough curve for Lu-177 (Inj. 7) in BFI02, 0-100 and 0-300 h.

A: 9



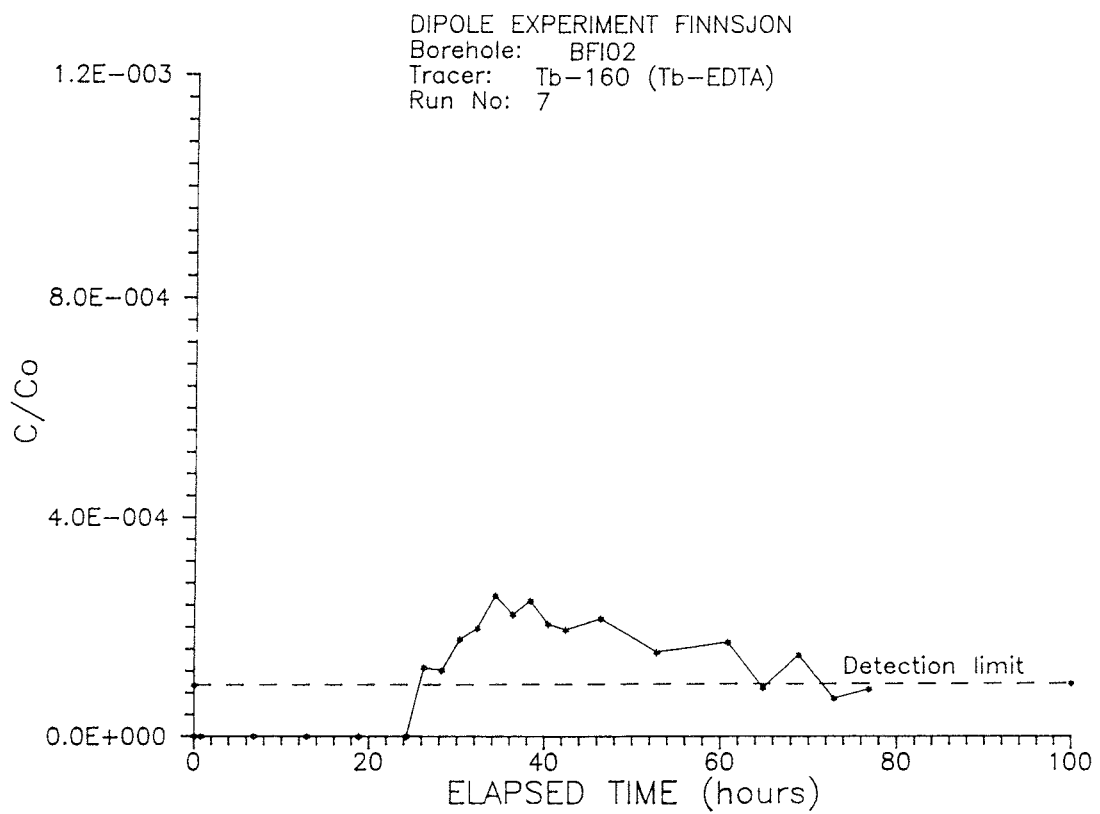
Breakthrough curve for Cr-51 (Inj. 7) in BFI02,  
 0-100 and 0-300 h.

A: 10



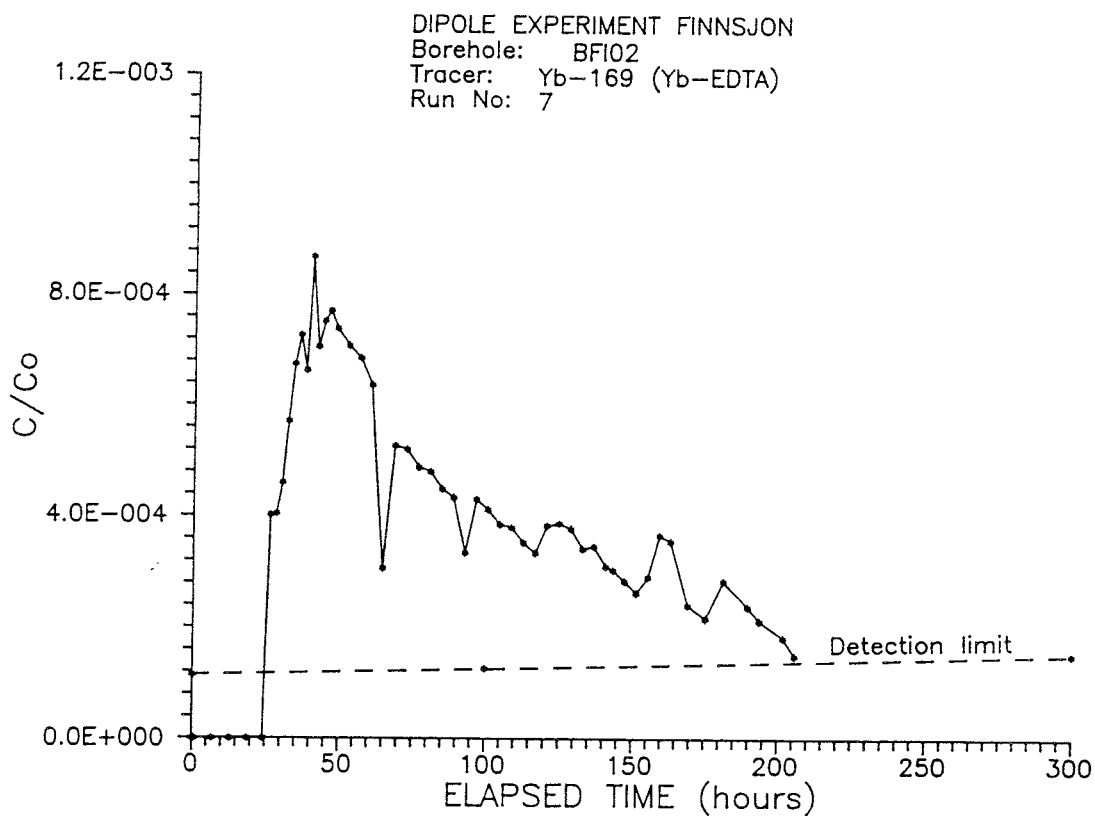
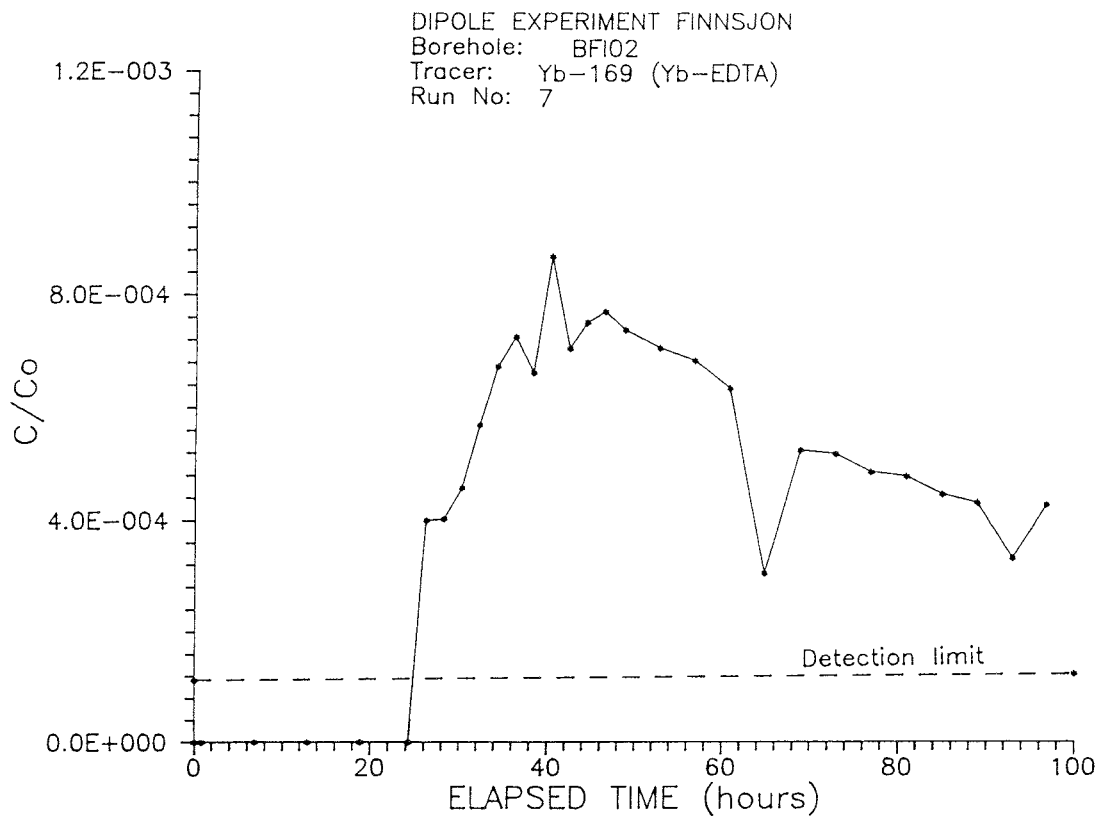
Breakthrough curve for In-111 (Inj. 7) in BFI02, 0-100 h.

A: 11



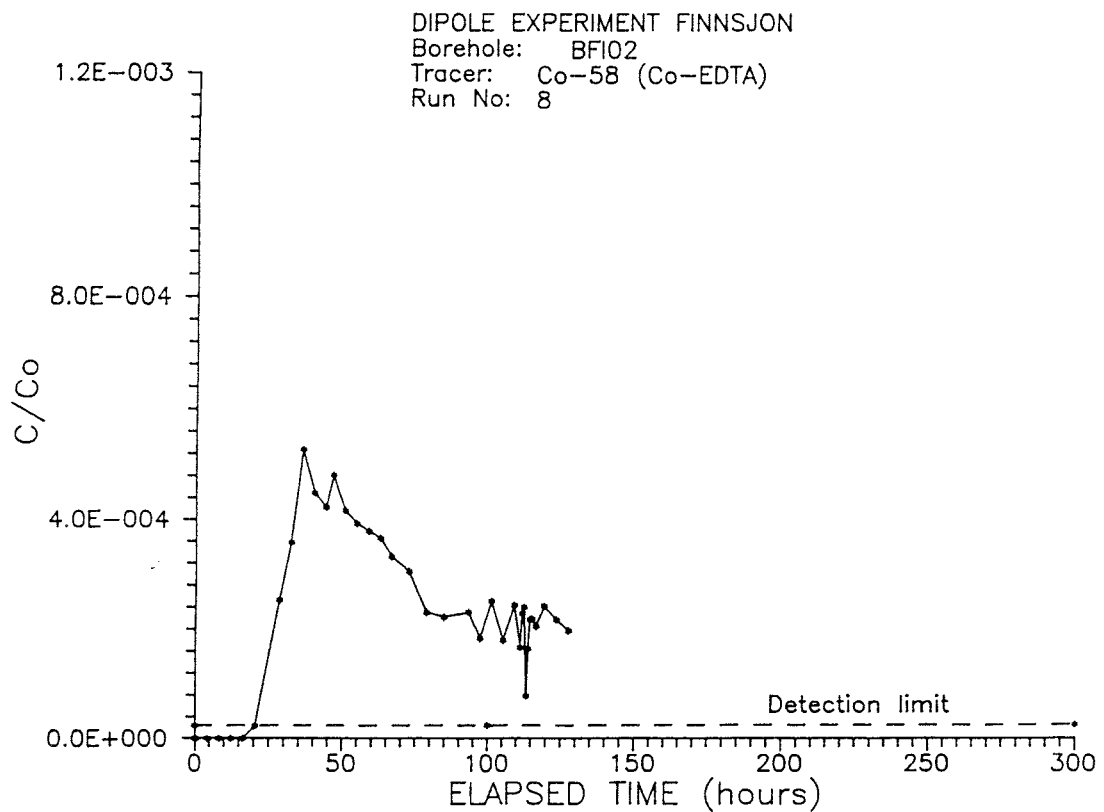
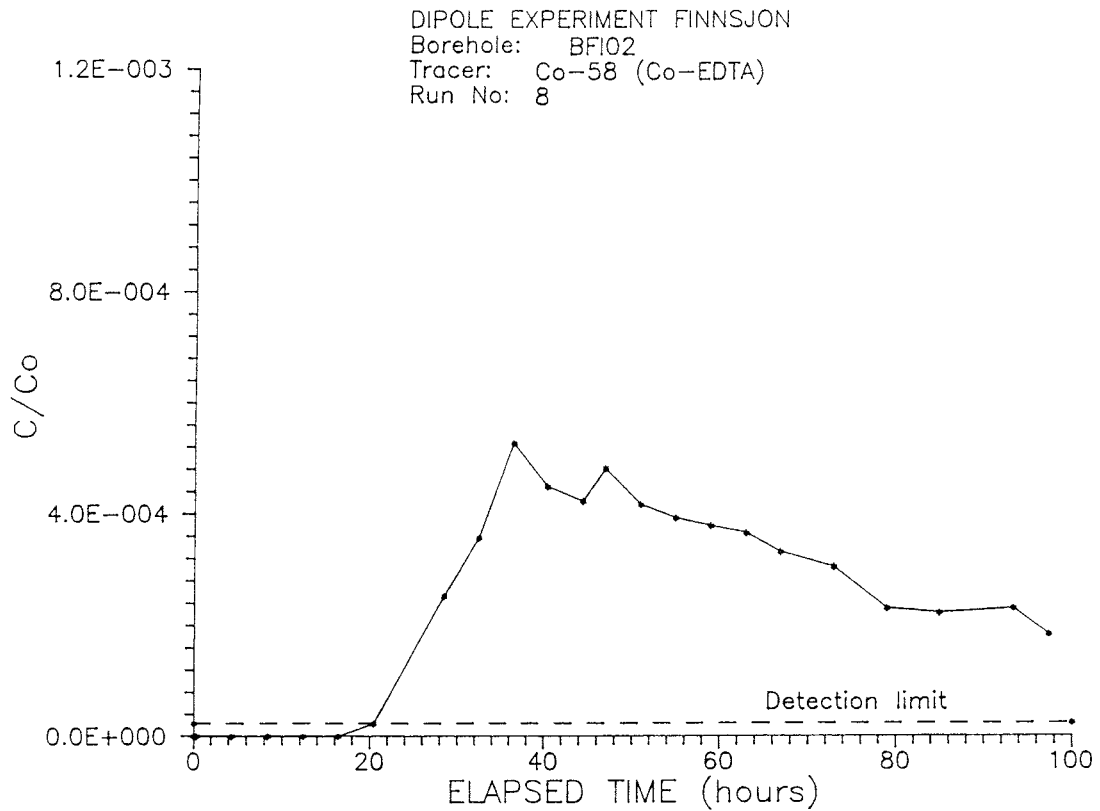
Breakthrough curve for Tb-160 (Inj. 7) in BFI02, 0-100 h.

A: 12



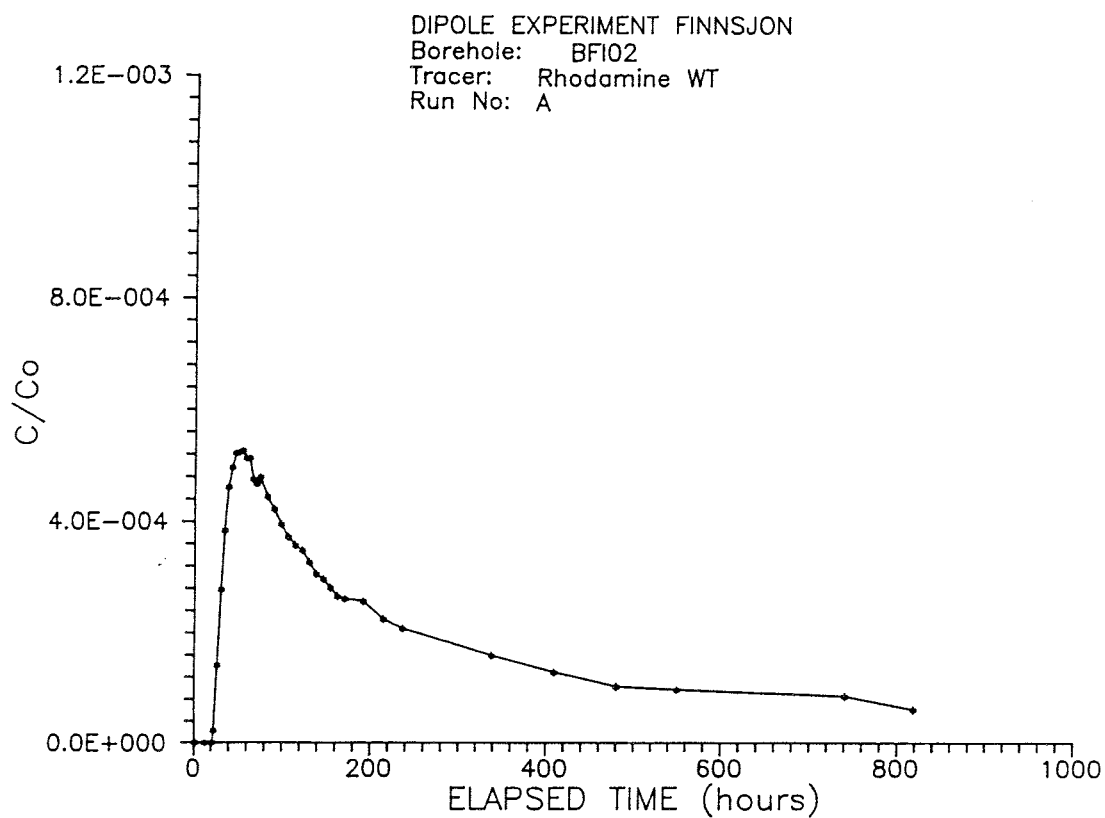
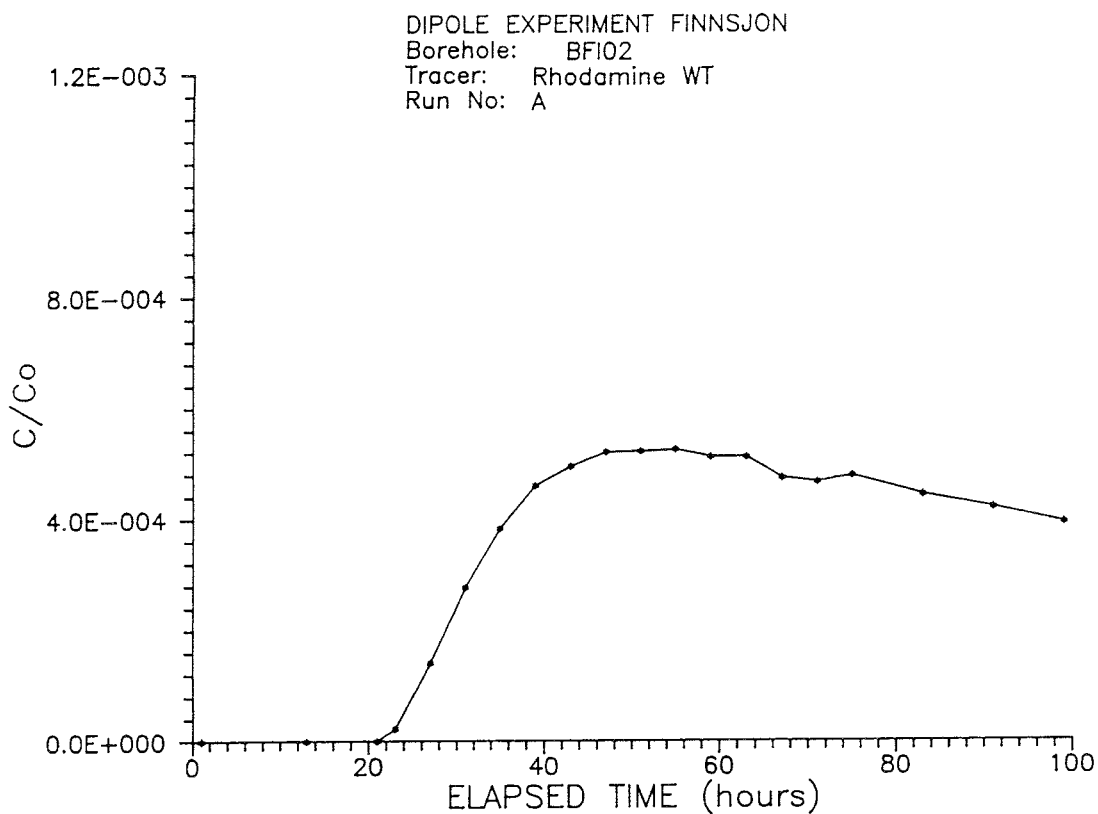
Breakthrough curve for Yb-169 (Inj. 7) in BF102, 0-100 and 0-300 h.

A: 13



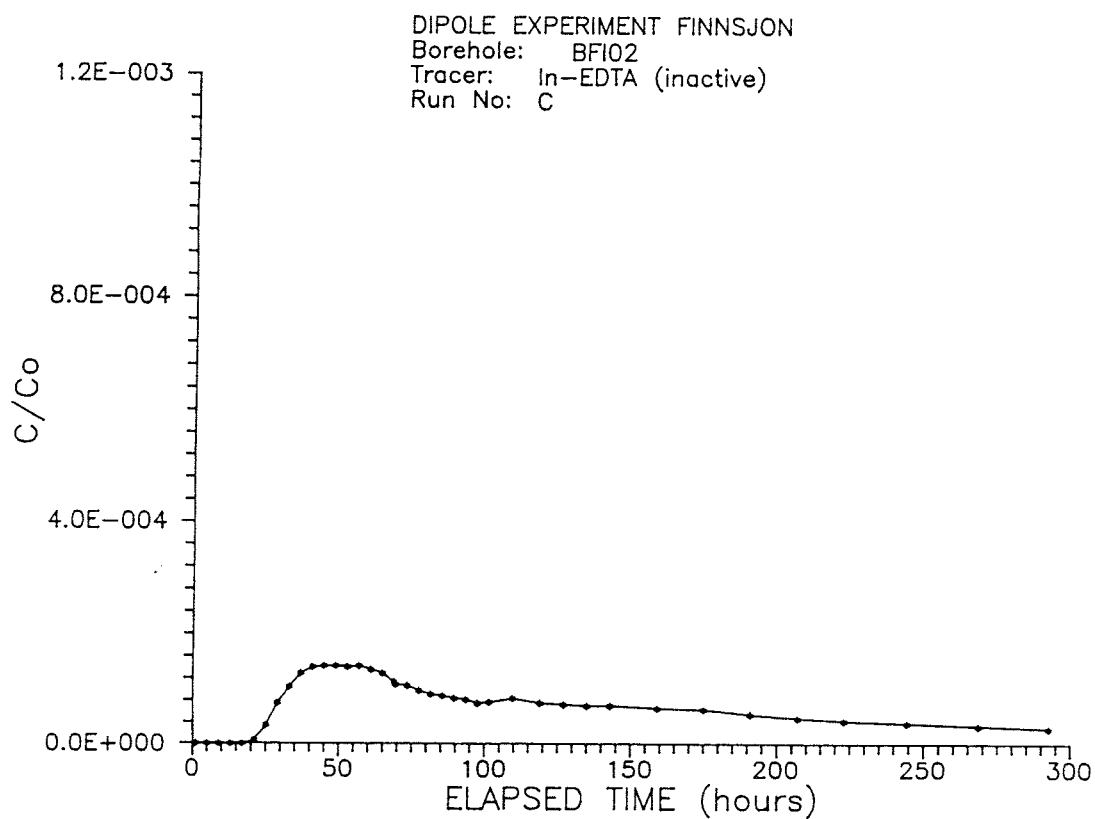
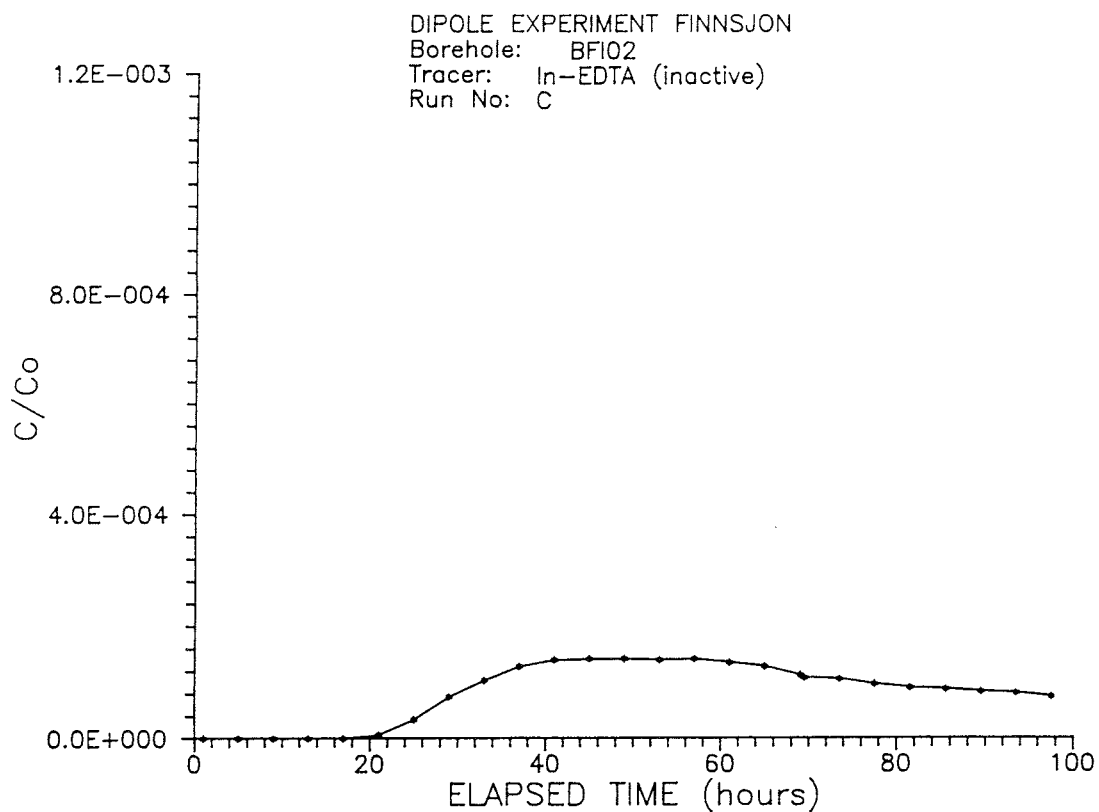
Breakthrough curve for Co-58 (Inj. 8) in BFI02,  
0-100 and 0-300 h.

A: 14



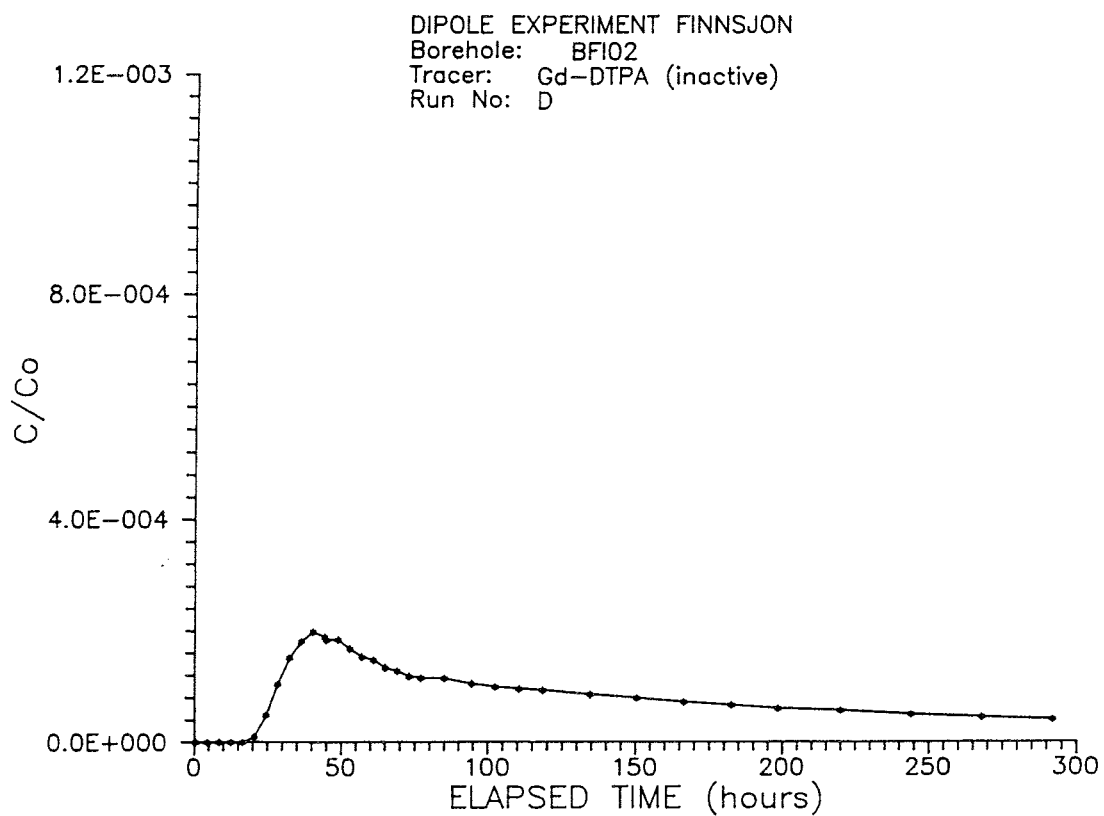
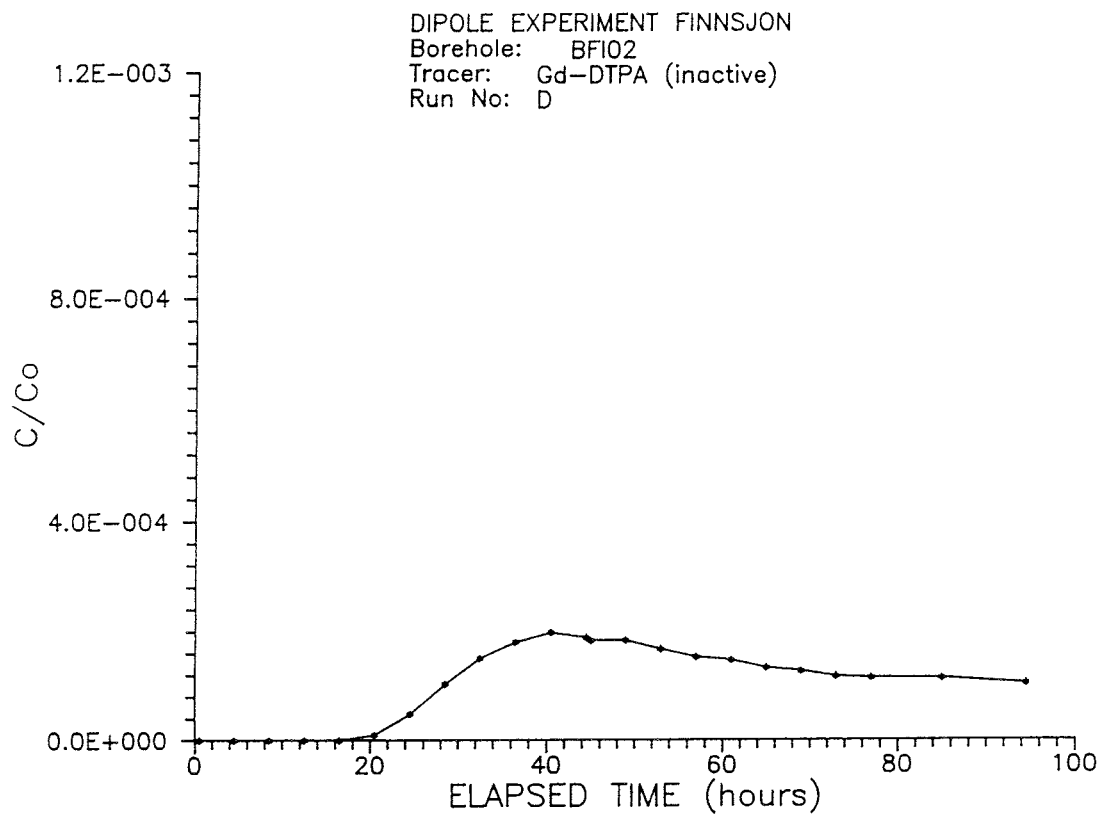
Breakthrough curve for Rhodamine WT (Inj. A) in BF102,  
0-100 and 0-1000 h.

A: 15



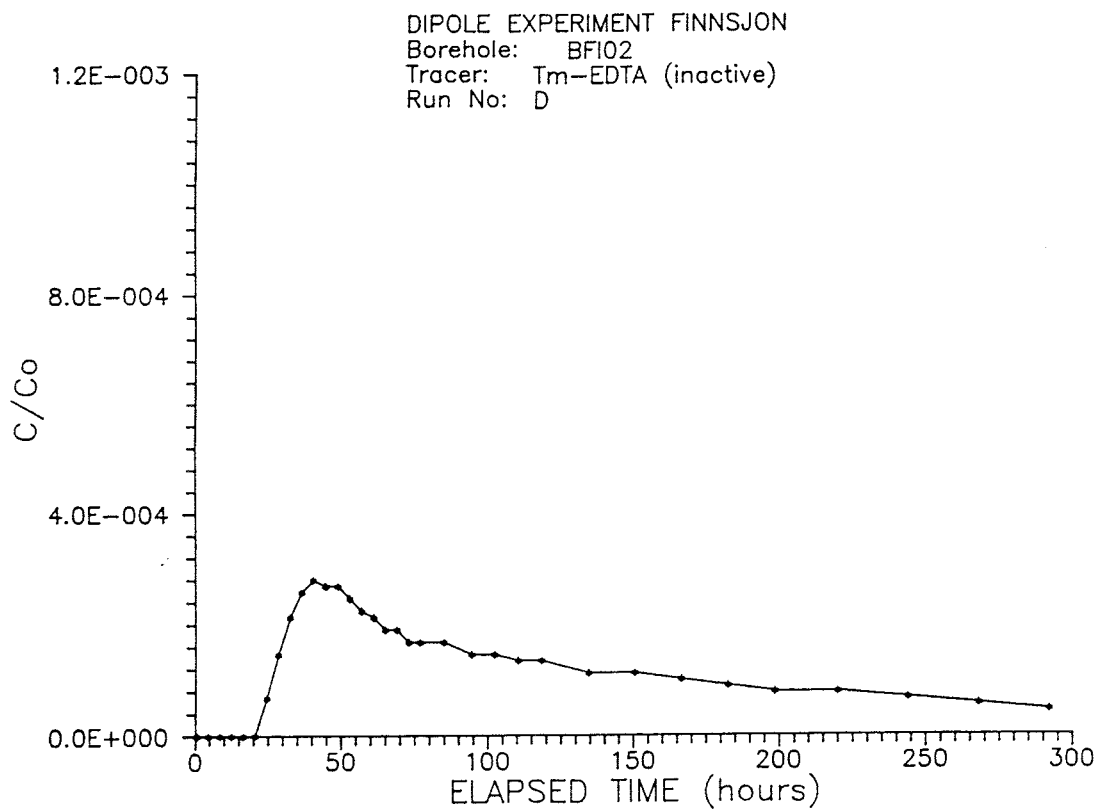
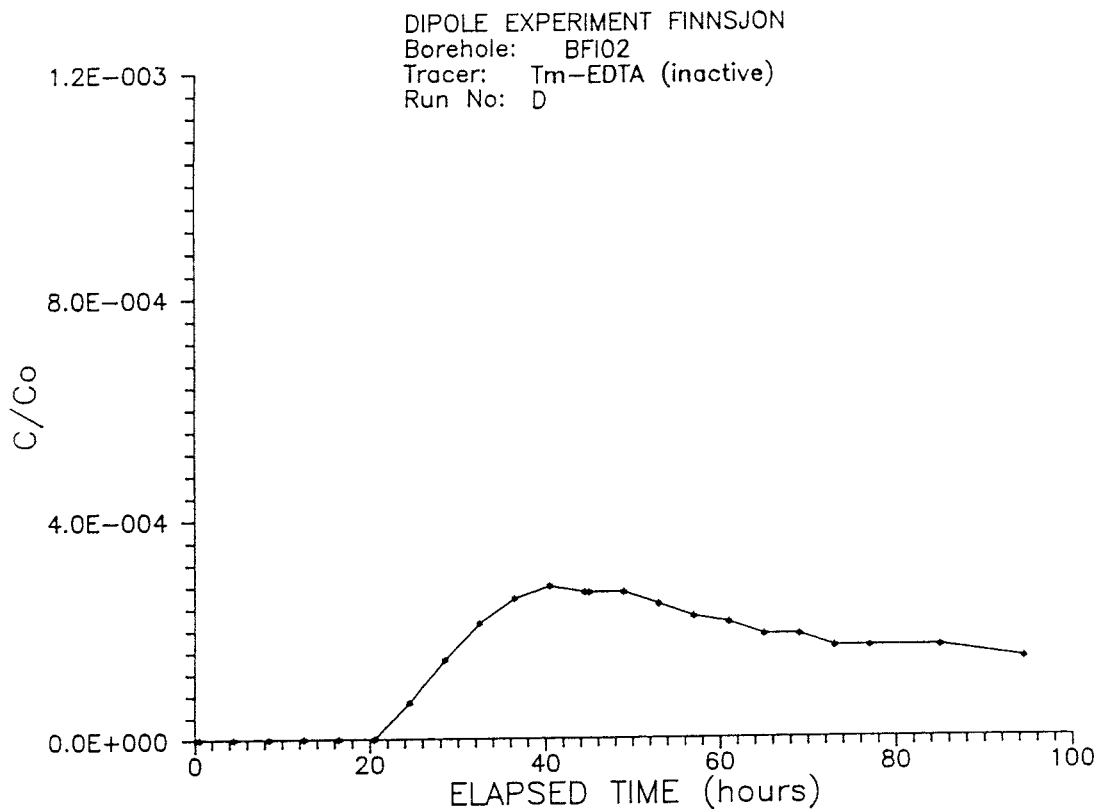
Breakthrough curve for In-EDTA (Inj. C) in BF102,  
0-100 and 0-300 h.

A: 16



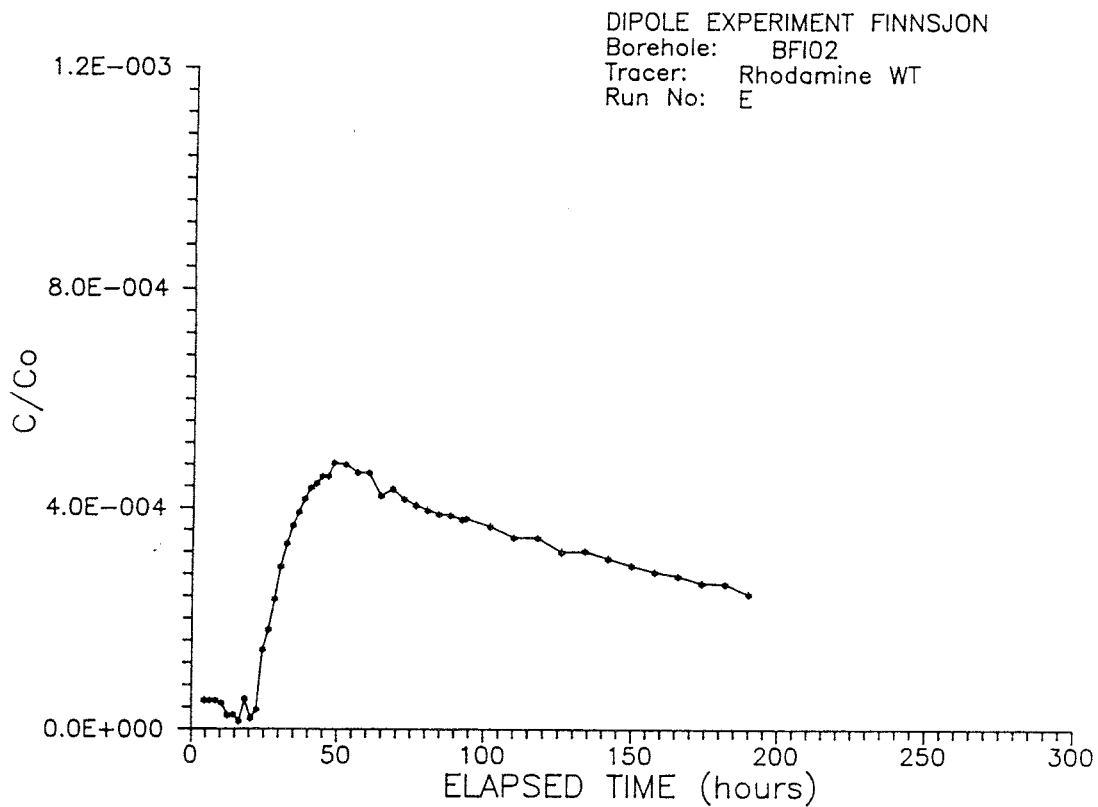
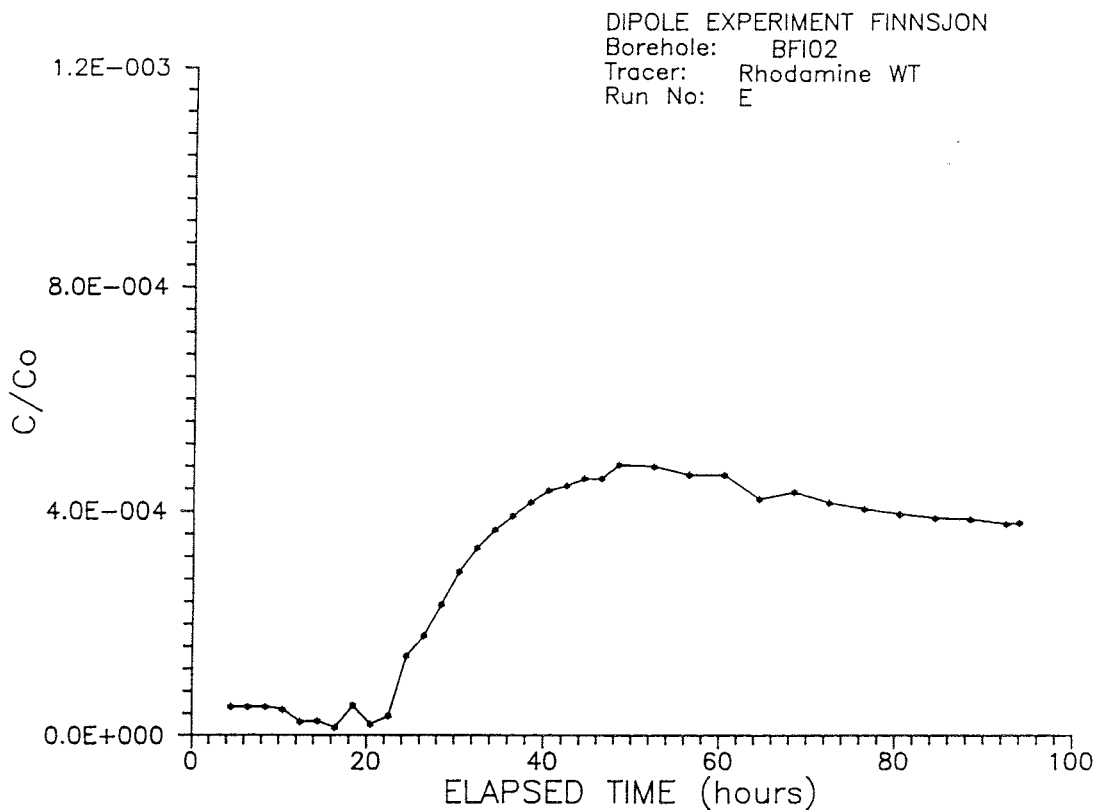
Breakthrough curve for Gd-DTPA (Inj. D) in BFI02,  
0-100 and 0-300 h.

A: 17



Breakthrough curve for Tm-EDTA (Inj. D) in BF102, 0-100 and 0-300 h.

A: 18



Breakthrough curve for Rhodamine WT (Inj. E) in BFI02, 0-100 and 0-300 h.

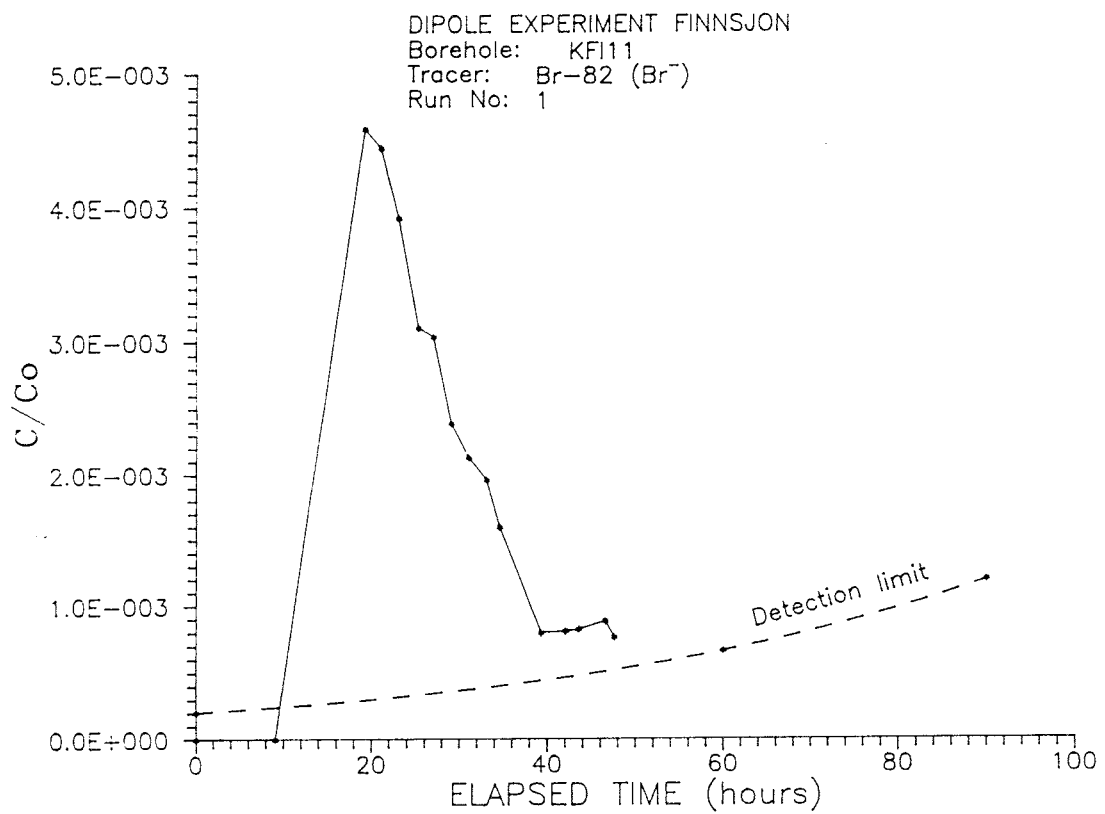
## APPENDIX B

## TRACER BREAKTHROUGH IN BOREHOLE KFI11

CONTENTS	Page
Breakthrough curve for Br-82 (Inj. 1) in KFI11, 0-100 h.	B:1
Breakthrough curve for Re-186 (Inj. 2) in KFI11, 0-100 h.	B:2
Breakthrough curve for I-131 (Inj. 3) in KFI11, 0-100 and 0-300 h.	B:3
Breakthrough curve for Na-24 (Inj. 6) in KFI11, 0-100 h.	B:4
Breakthrough curve for Br-82 (Inj. 6) in KFI11, 0-100 h.	B:5
Breakthrough curve for I-131 (Inj.6) in KFI11, 0-100 and 0-300 h.	B:6
Breakthrough curve for Re-186 (Inj. 6) in KFI11, 0-100 and 0-300 h.	B:7
Breakthrough curve for La-140 (Inj. 7) in KFI11, 0-100 h.	B:8
Breakthrough curve for Lu-177 (Inj. 7) in KFI11, 0-100 and 0-300 h.	B:9
Breakthrough curve for Cr-51 (Inj. 7) in KFI11, 0-100 and 0-300 h.	B:10
Breakthrough curve for In-111 (Inj. 7) in KFI11, 0-100 h.	B:11
Breakthrough curve for Tb-160 (Inj. 7) in KFI11, 0-100 h.	B:12
Breakthrough curve for Yb-169 (Inj. 7) in KFI11, 0-100 and 0-300 h.	B:13
Breakthrough curve for Co-58 (Inj. 8) in KFI11, 0-100 h.	B:14
Breakthrough curve for Rhodamine WT (Inj. A) in KFI11, 0-1000 h.	B:15
Breakthrough curve for In-EDTA (Inj. C) in KFI11, 0-100 and 0-300 h.	B:16

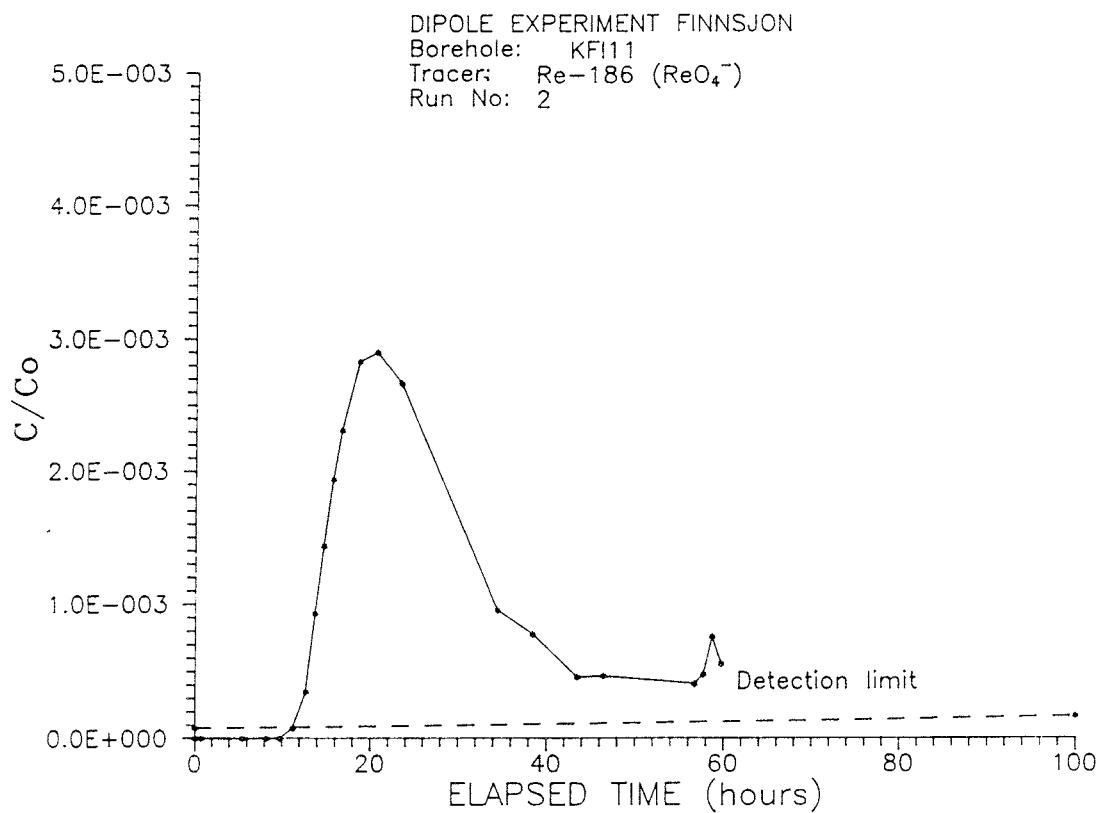
CONTENTS (Continued)	Page
Breakthrough curve for Gd-DTPA (Inj. D) in KFI11, 0-100 and 0-300 h.	B:17
Breakthrough curve for Tm-EDTA (Inj. D) in KFI11, 0-100 and 0-300 h.	B:18
Breakthrough curve for Rhodamine WT (Inj. E) in KFI11, 0-100 and 0-300 h.	B:19

B: 1



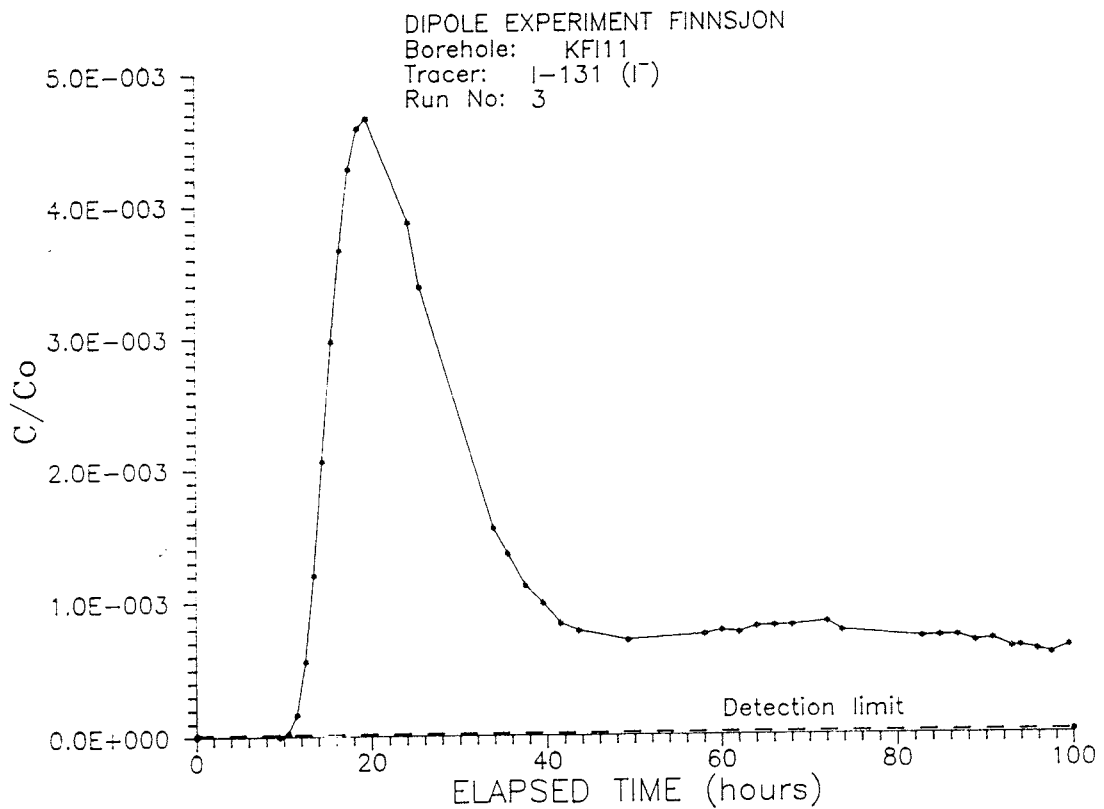
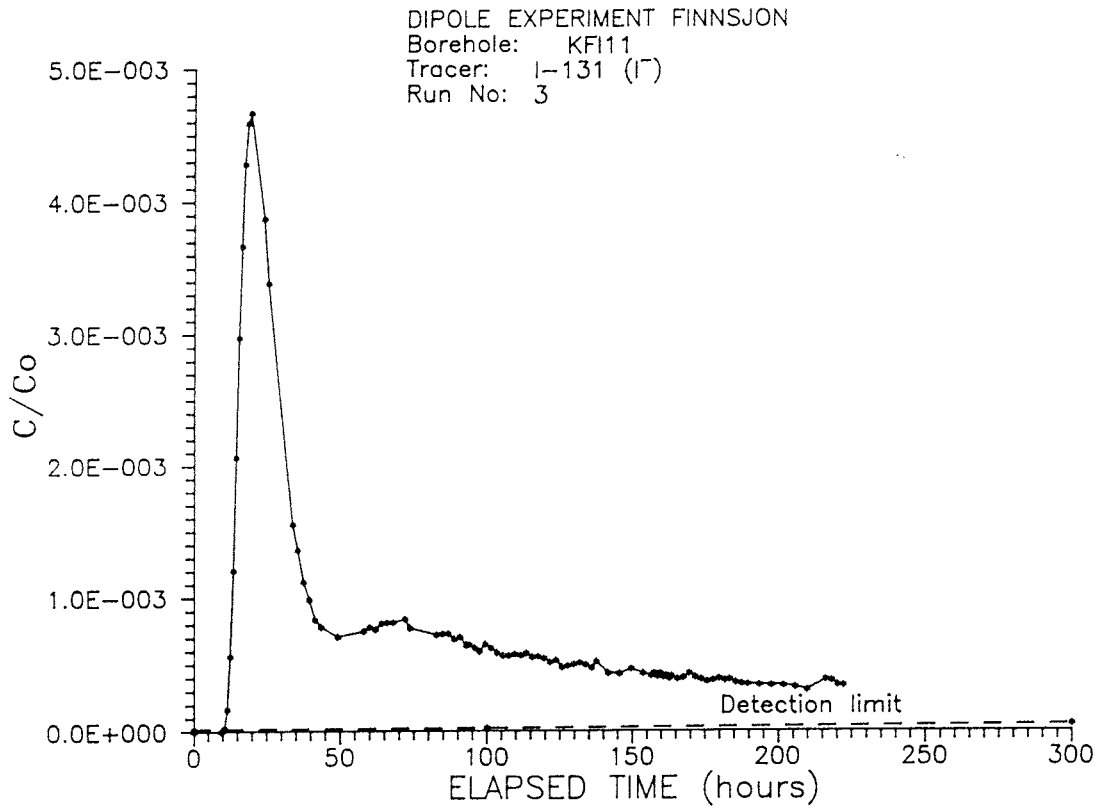
Breakthrough curve for Br-82 (Inj. 1) in KFI11, 0-100 h.

B: 2



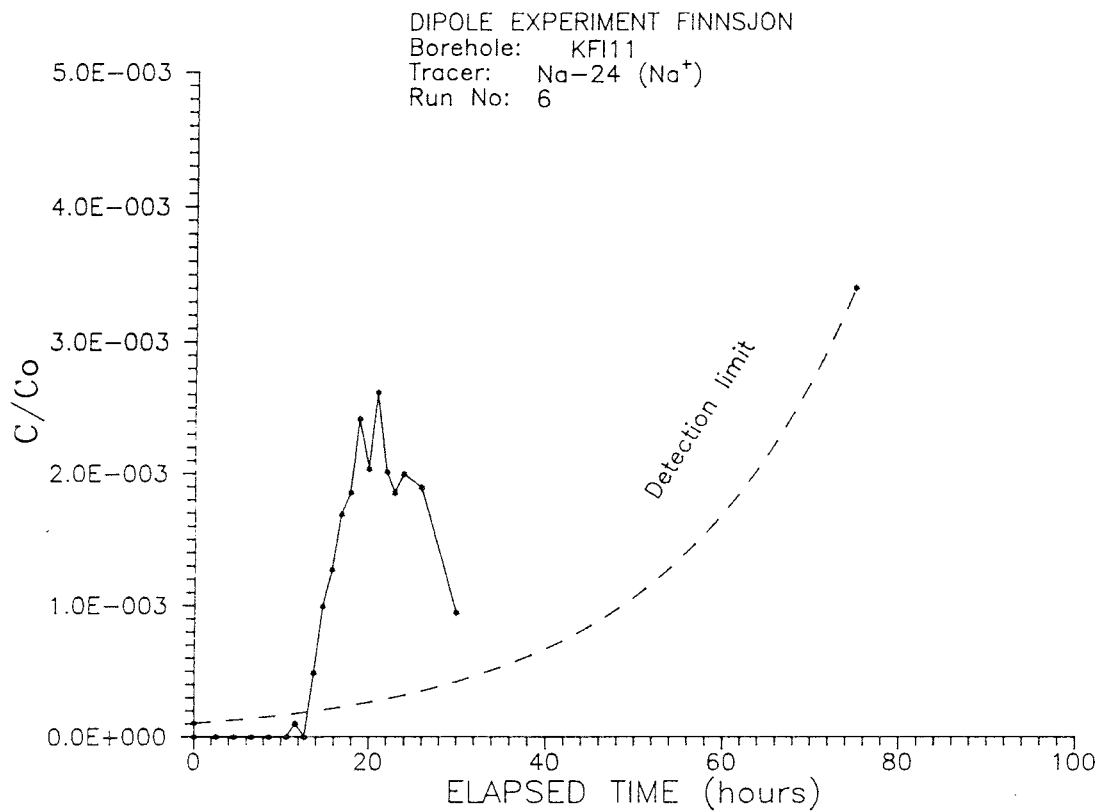
Breakthrough curve for Re-186 (Inj. 2) in KFI11, 0-100 h.

B: 3



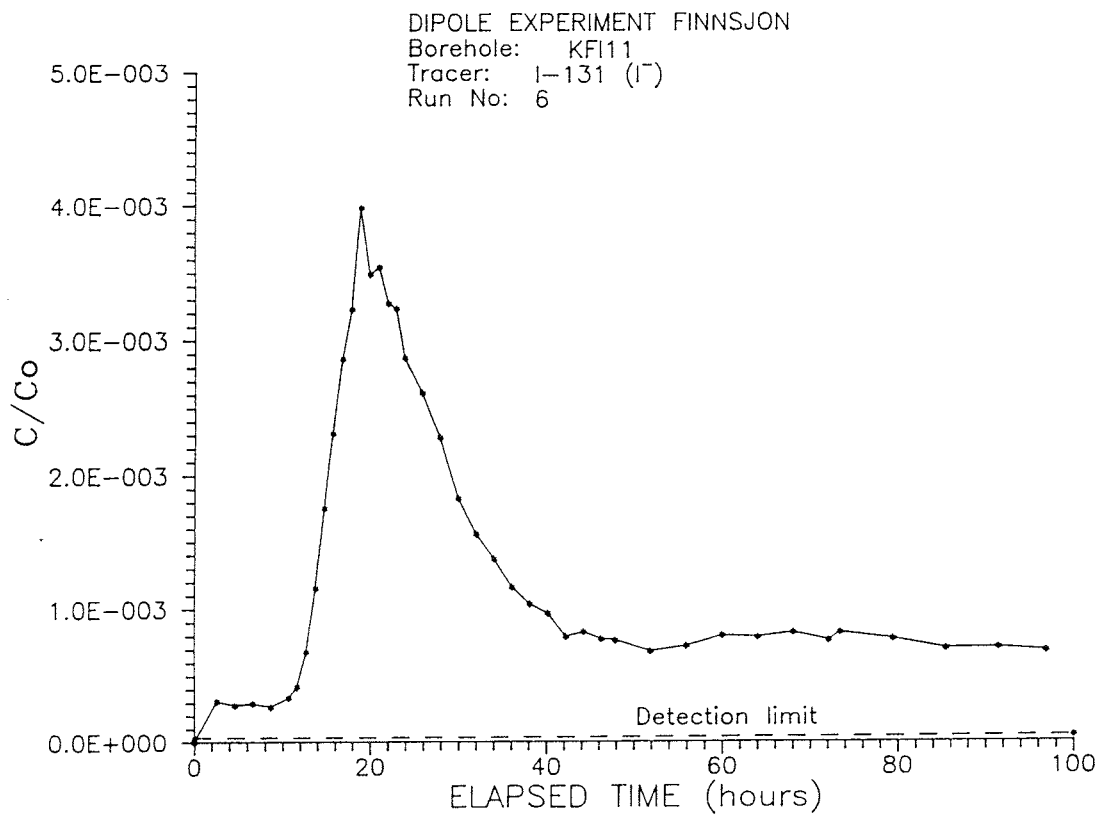
Breakthrough curve for I-131 (Inj. 3) in KFI11,  
 0-100 and 0-300 h.

B: 4



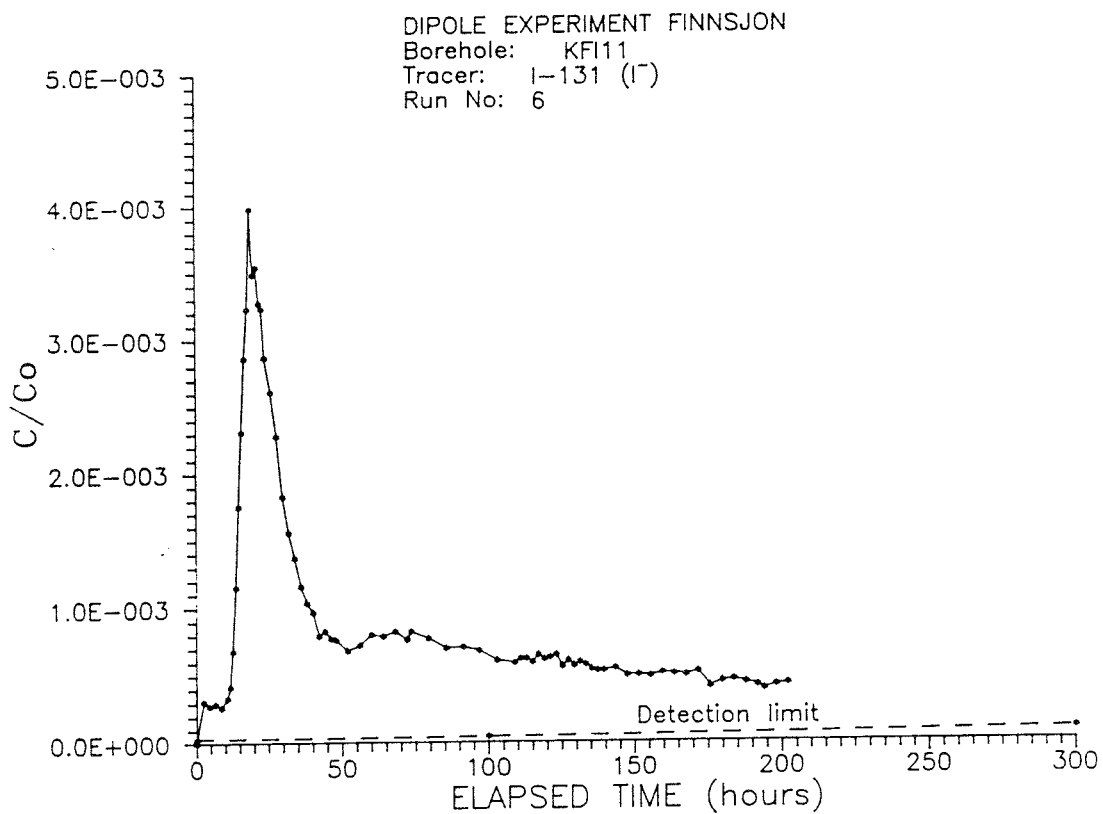
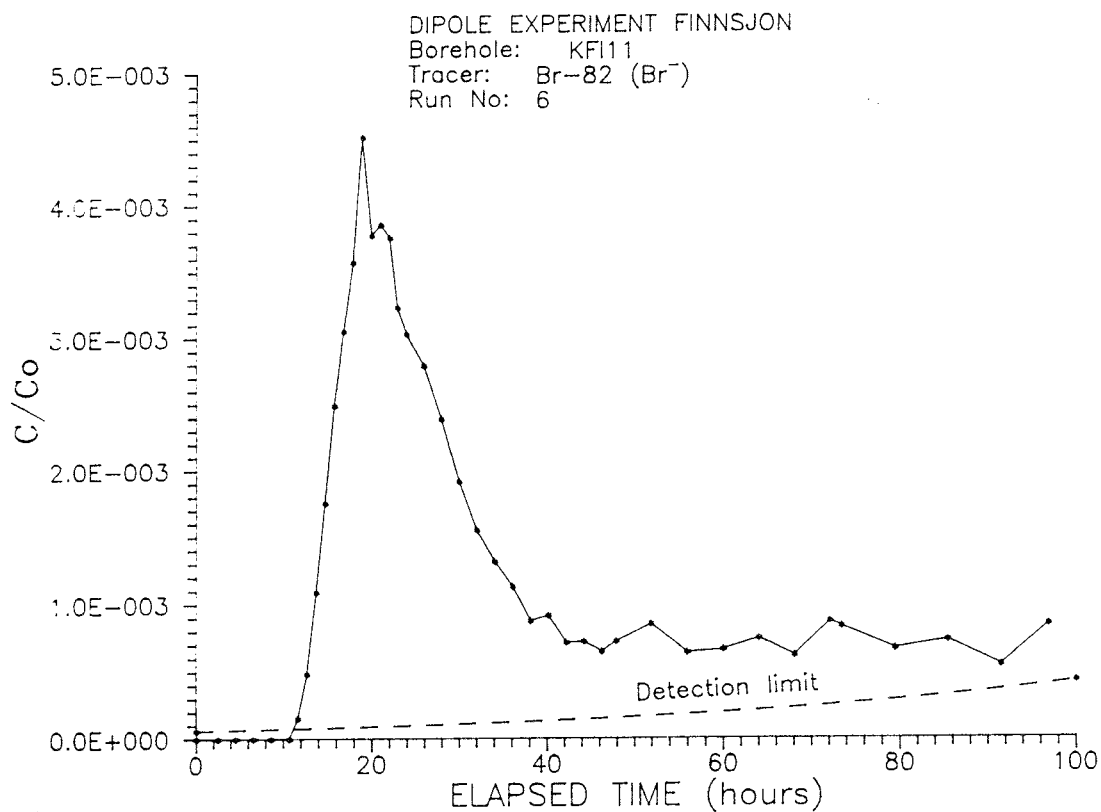
Breakthrough curve for Na-24 (Inj. 6) in KFI11, 0-100 h.

B: 5



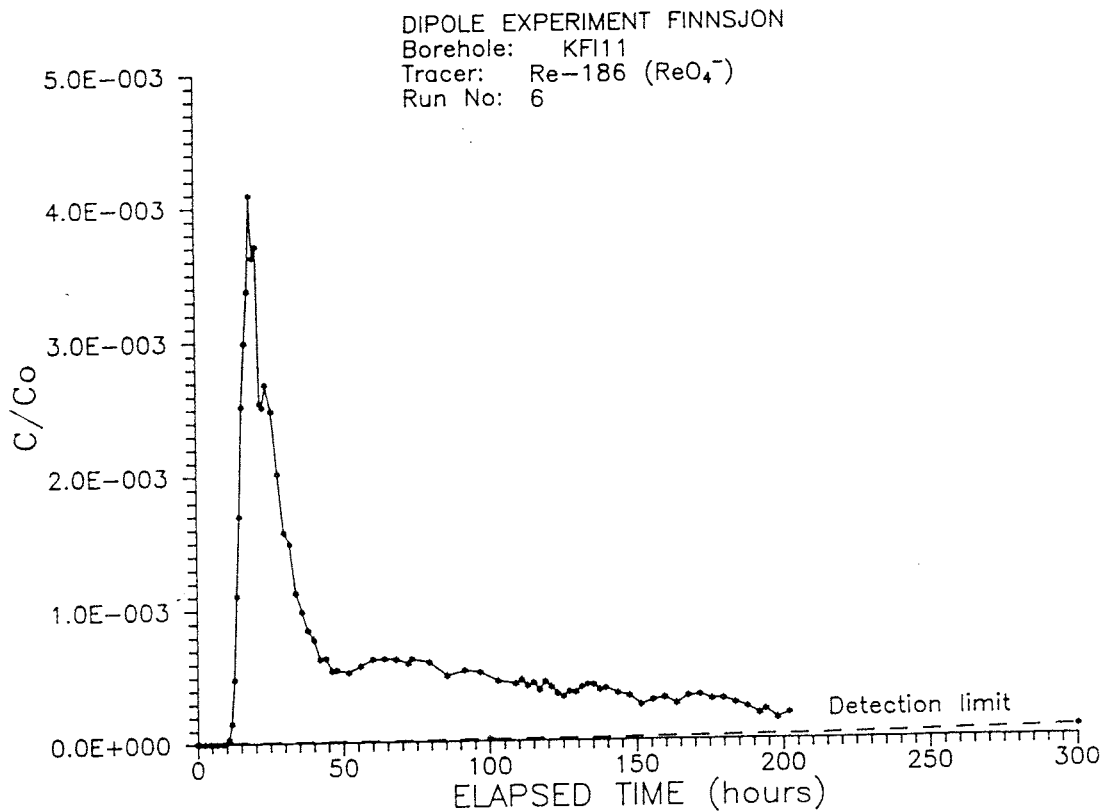
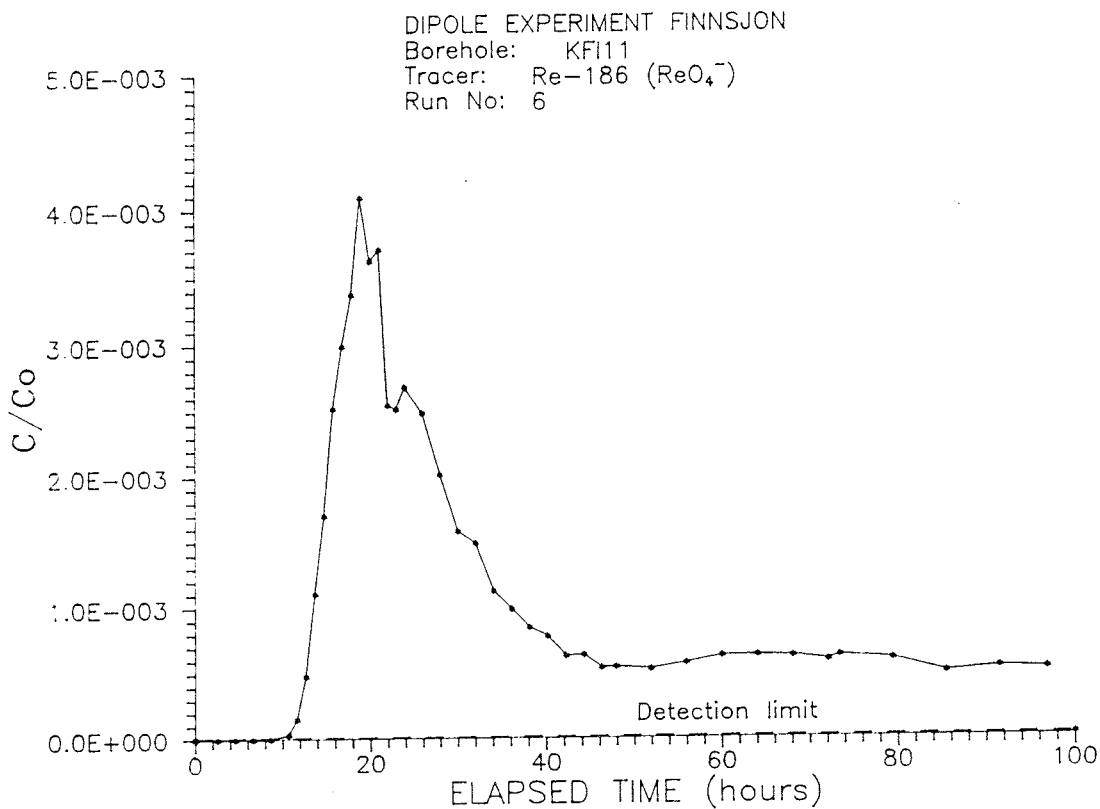
Breakthrough curve for Br-82 (Inj. 6) in KFI11, 0-100 h.

B: 6



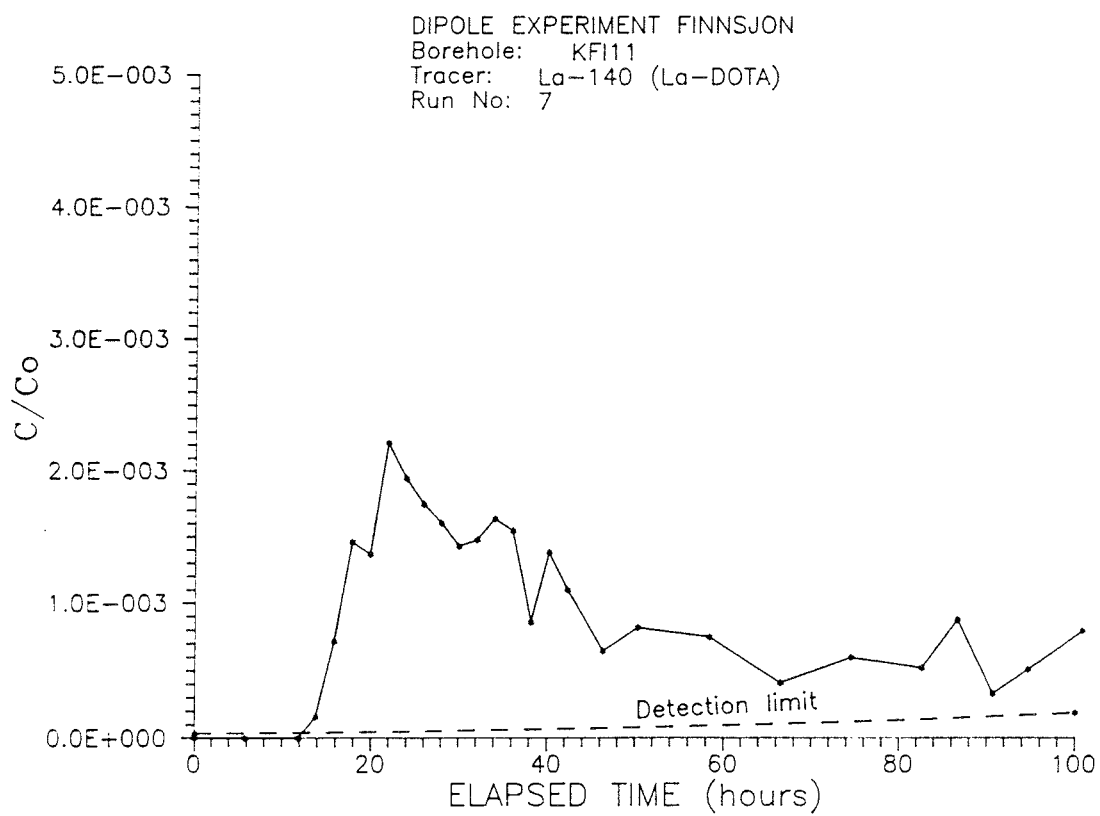
Breakthrough curve for I-131 (Inj.6) in KFI11, 0-100 and 0-300 h.

B: 7



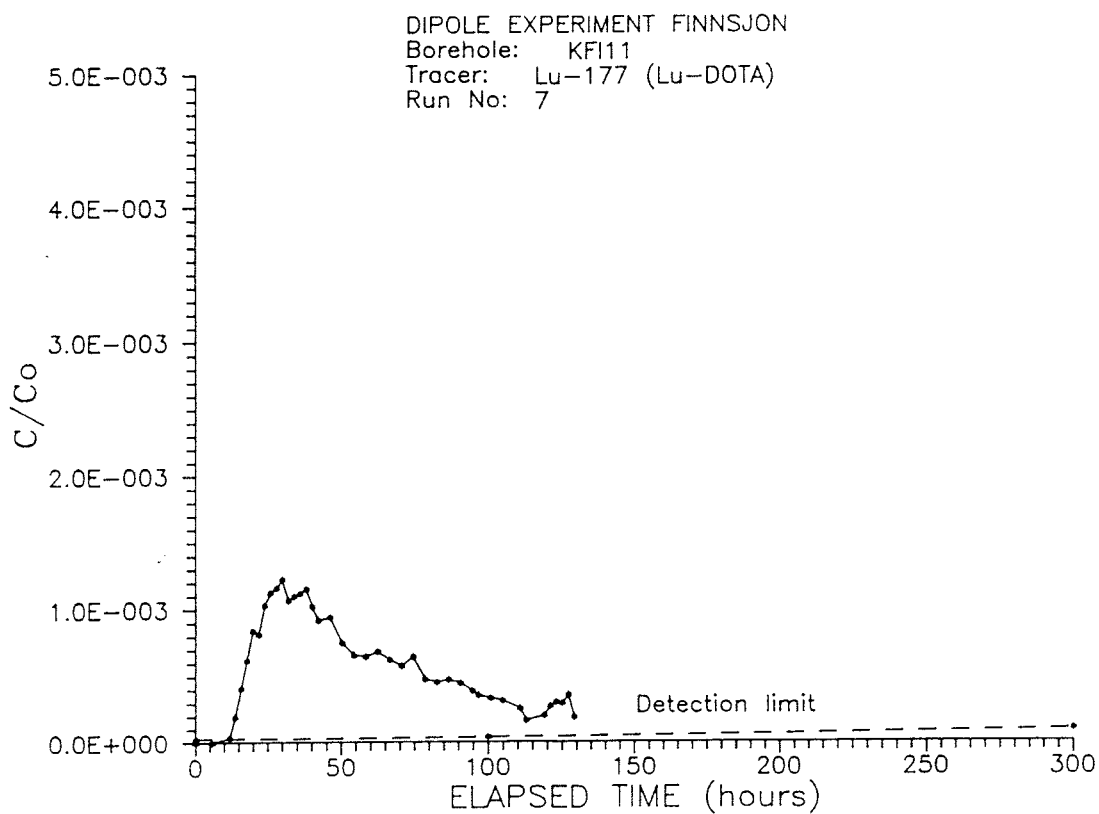
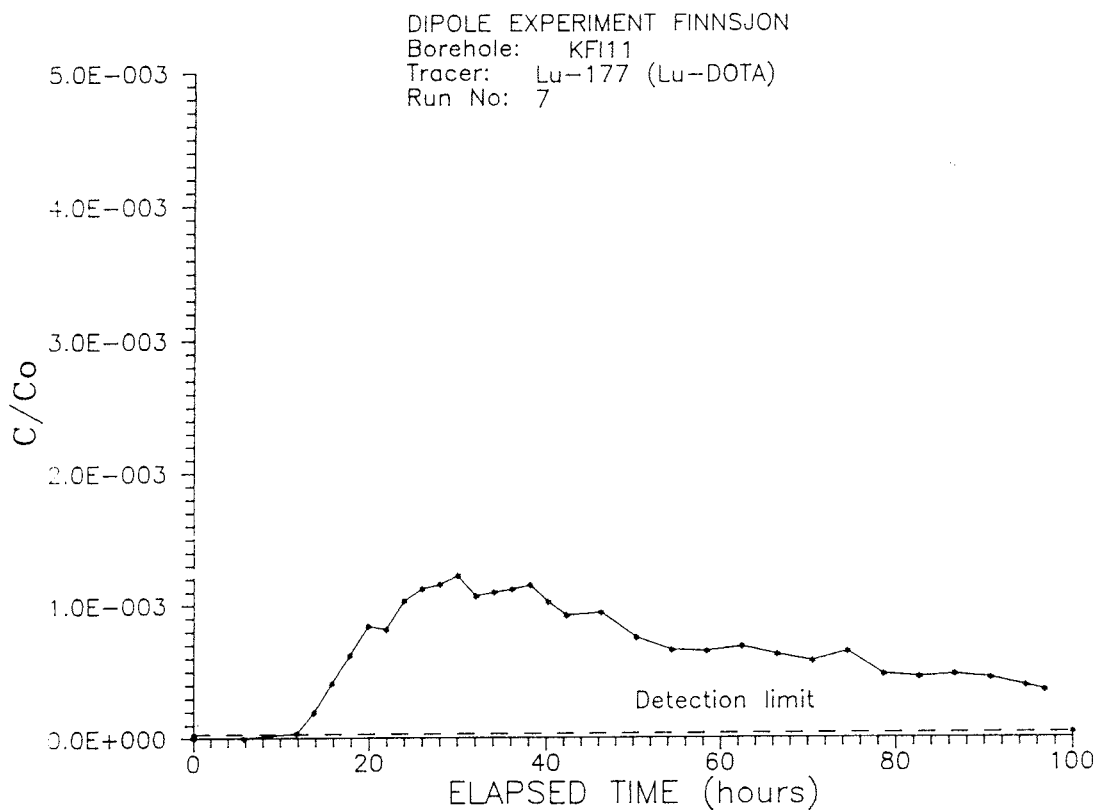
Breakthrough curve for Re-186 (Inj. 6) in KFI11, 0-100 and 0-300 h.

B: 8



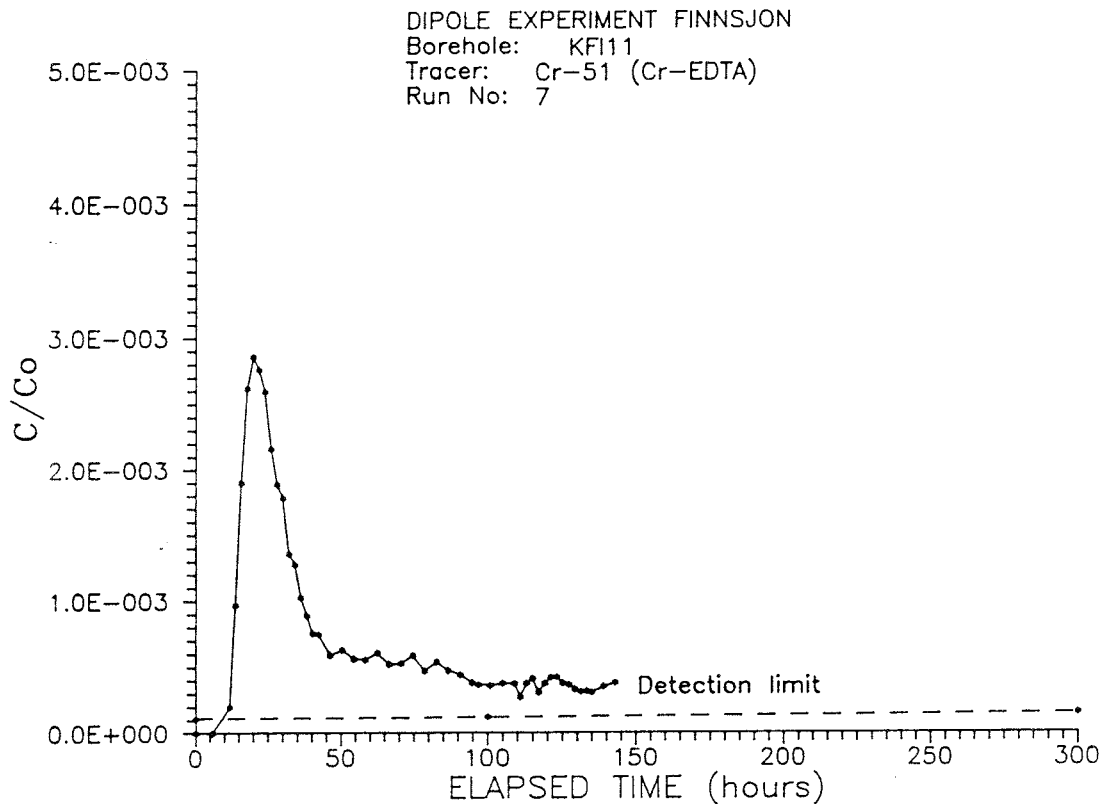
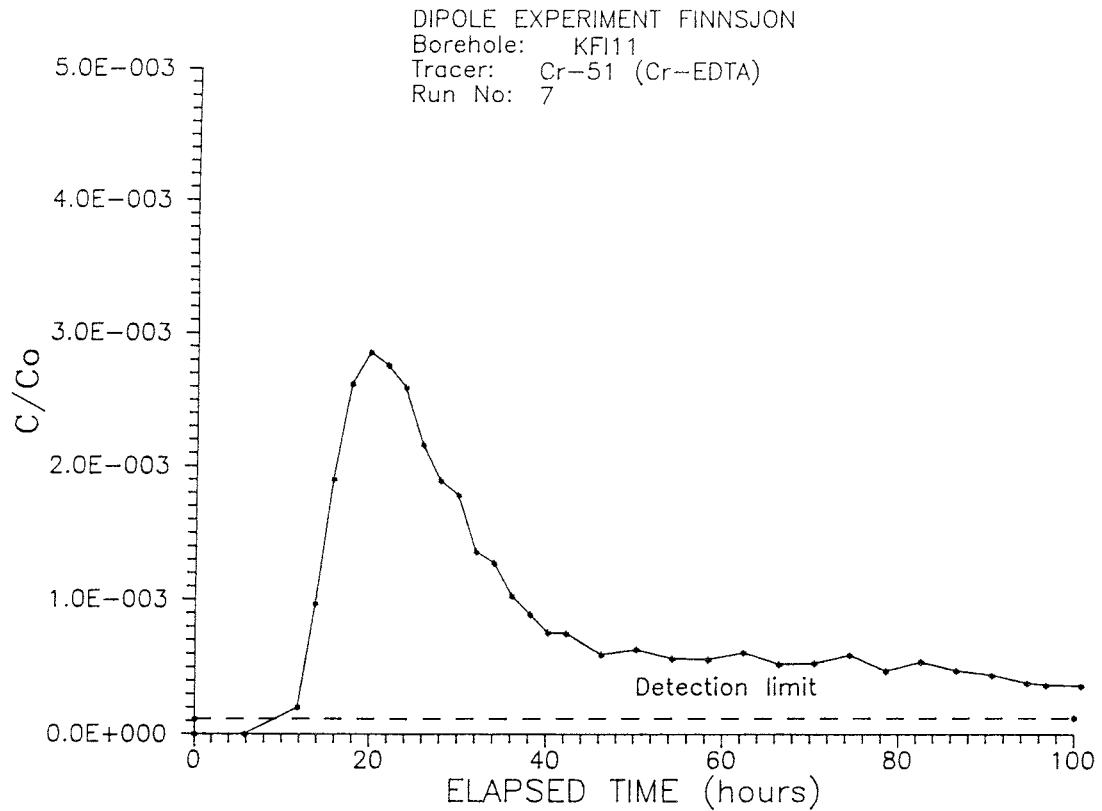
Breakthrough curve for La-140 (Inj. 7) in KFI11, 0-100 h.

B: 9



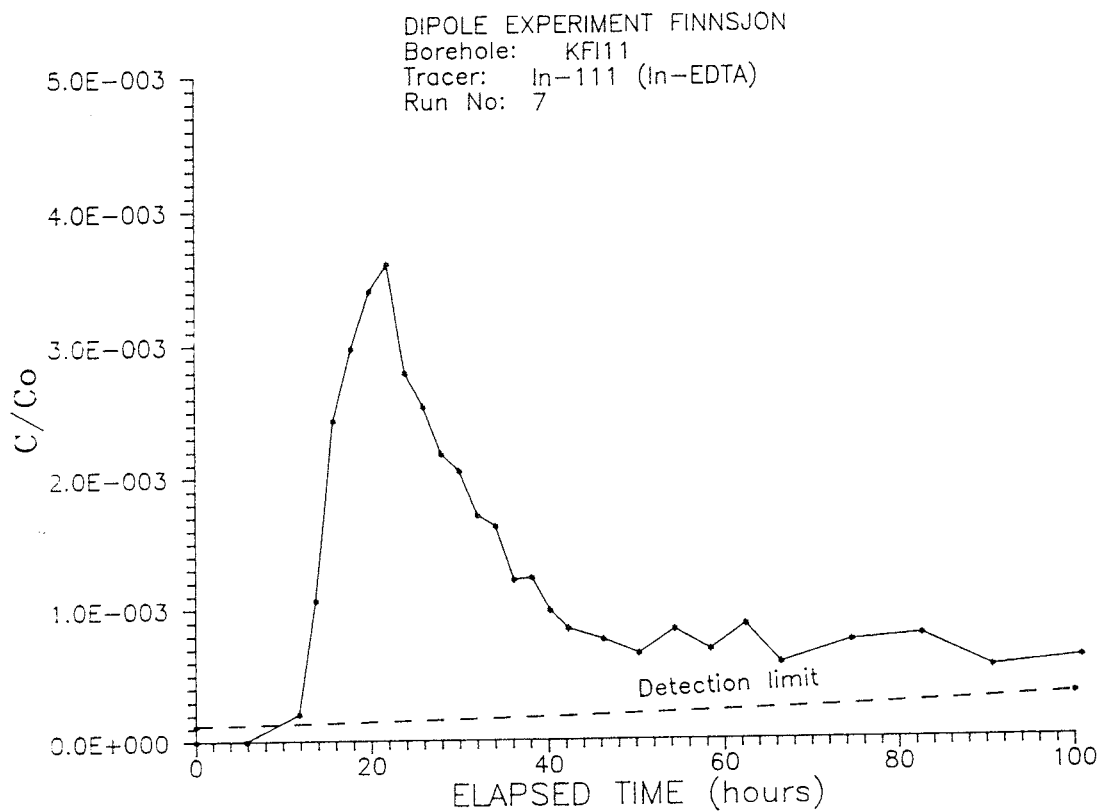
Breakthrough curve for Lu-177 (Inj. 7) in KFI11, 0-100 and 0-300 h.

B: 10



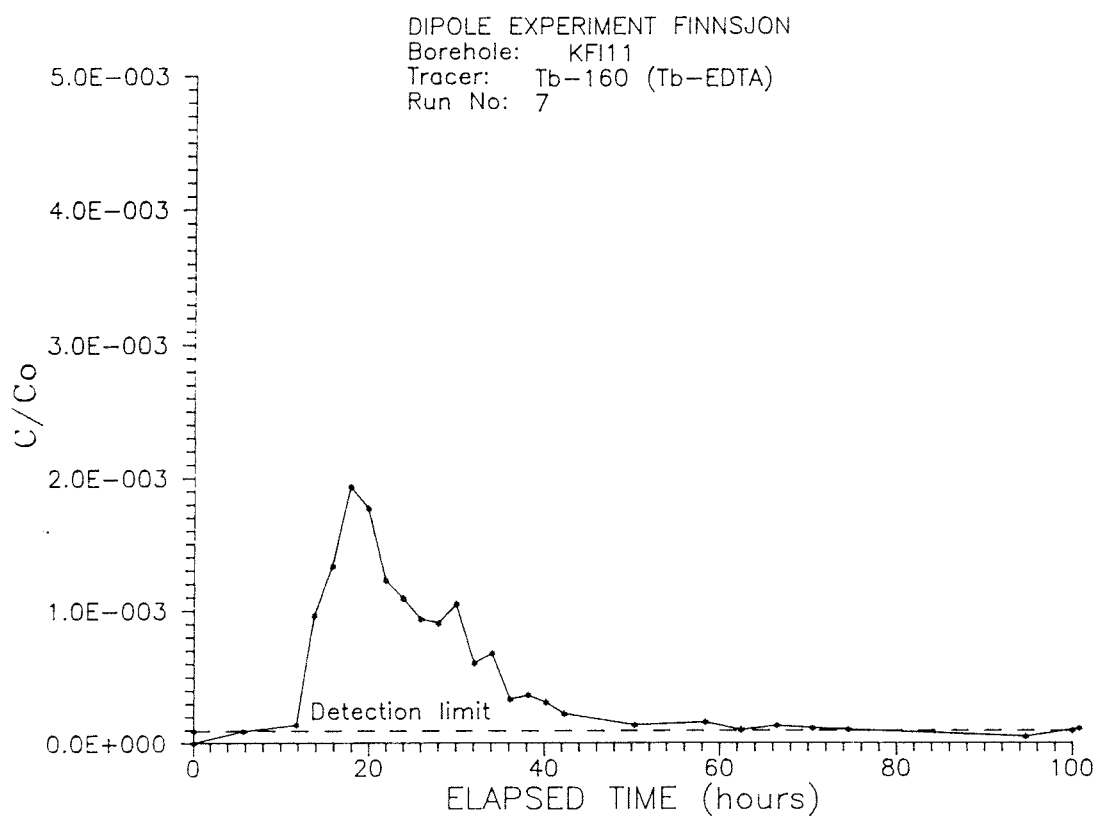
Breakthrough curve for Cr-51 (Inj. 7) in KFI11,  
0-100 and 0-300 h.

B: 11



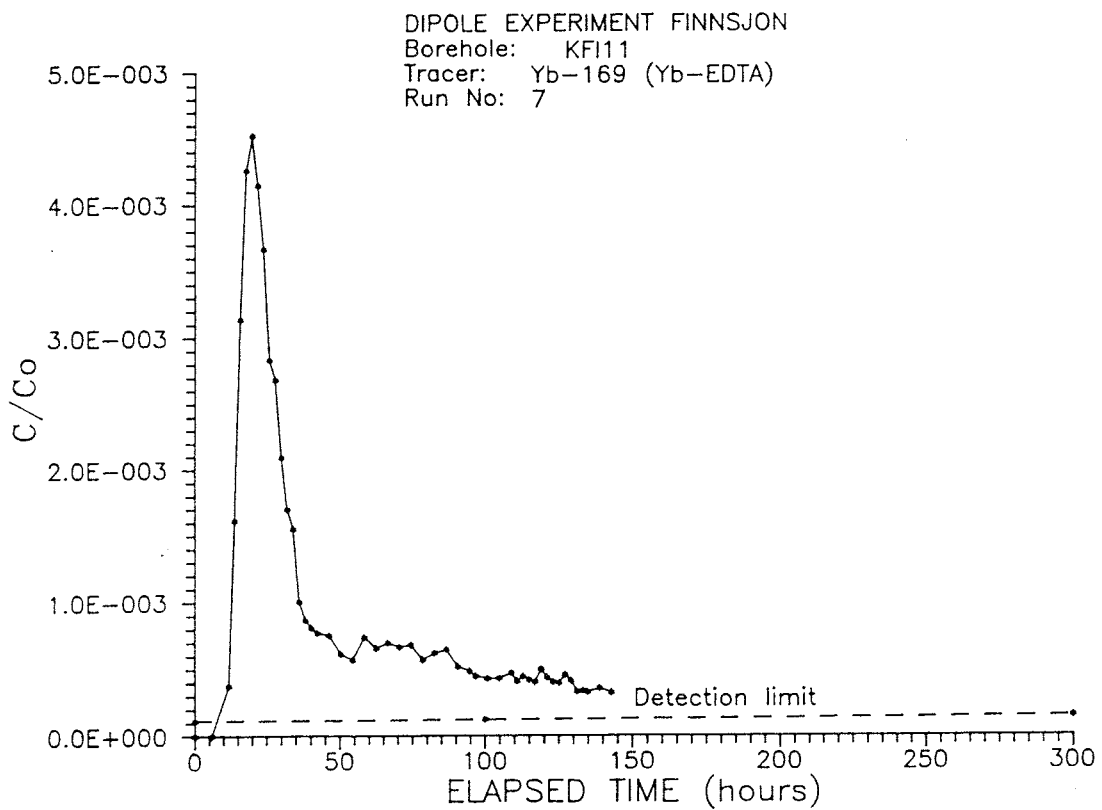
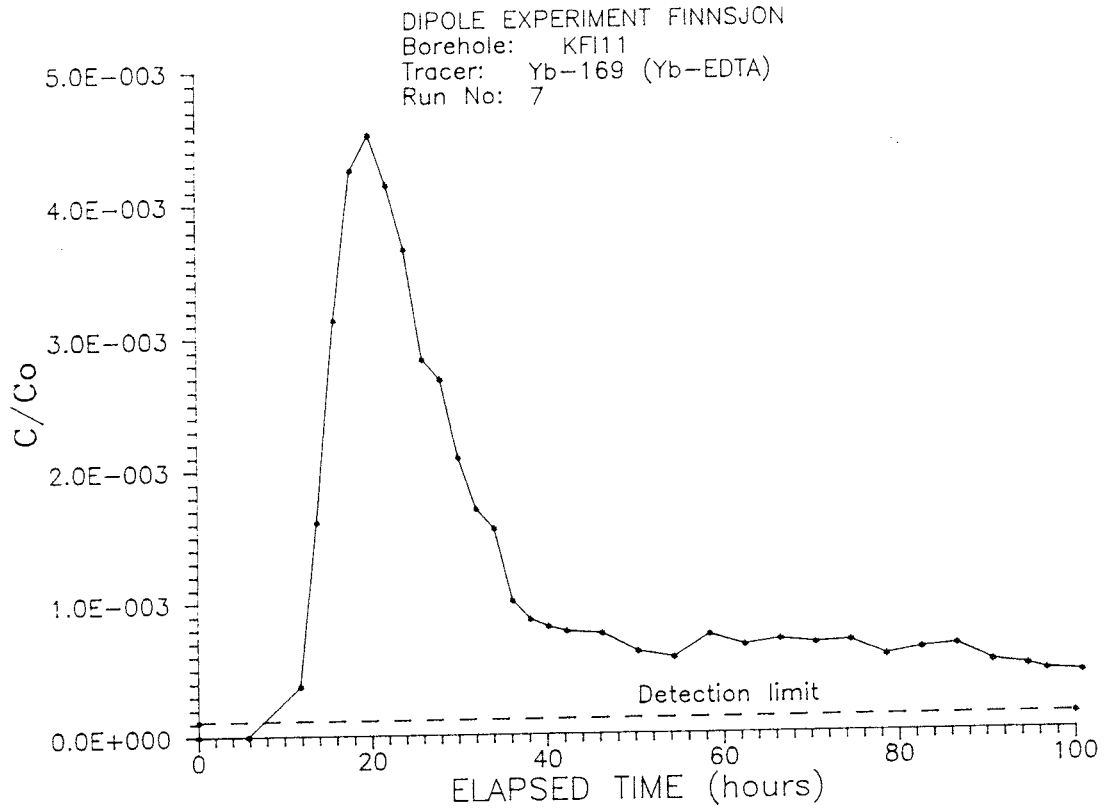
Breakthrough curve for In-111 (Inj. 7) in KFI11, 0-100 h.

B: 12



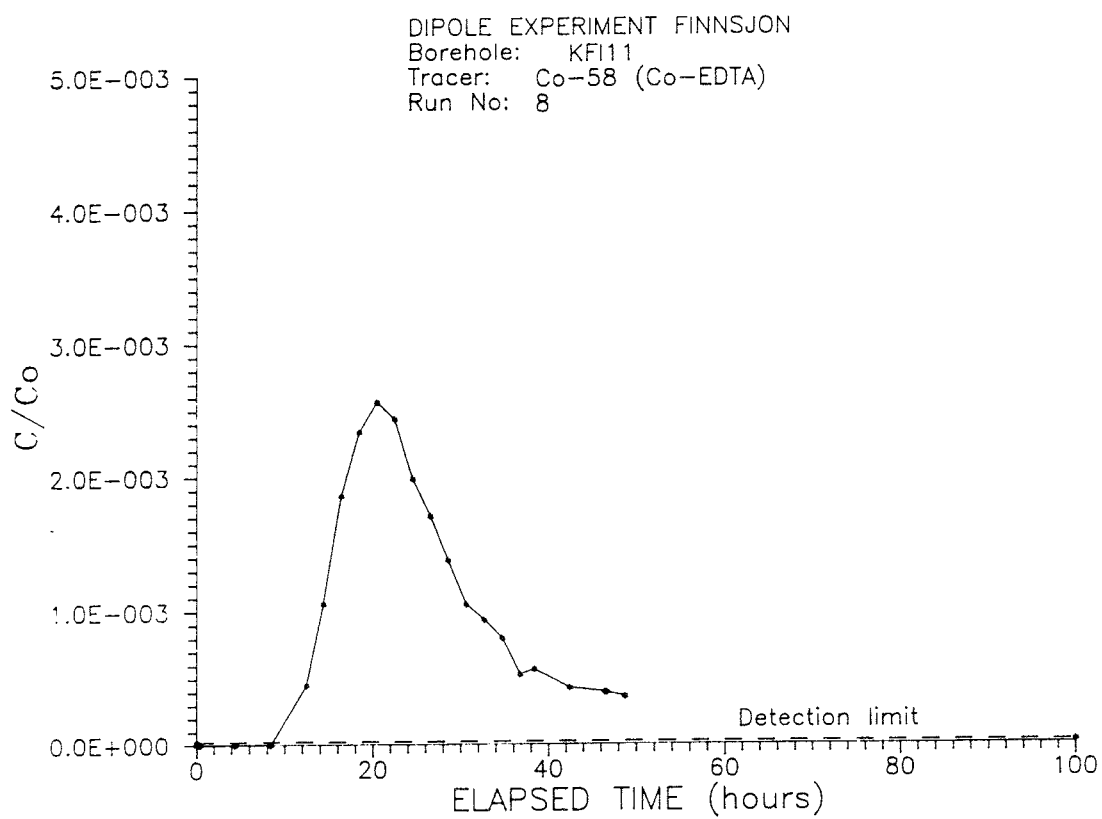
Breakthrough curve for Tb-160 (Inj. 7) in KFI11, 0-100 h.

B: 13



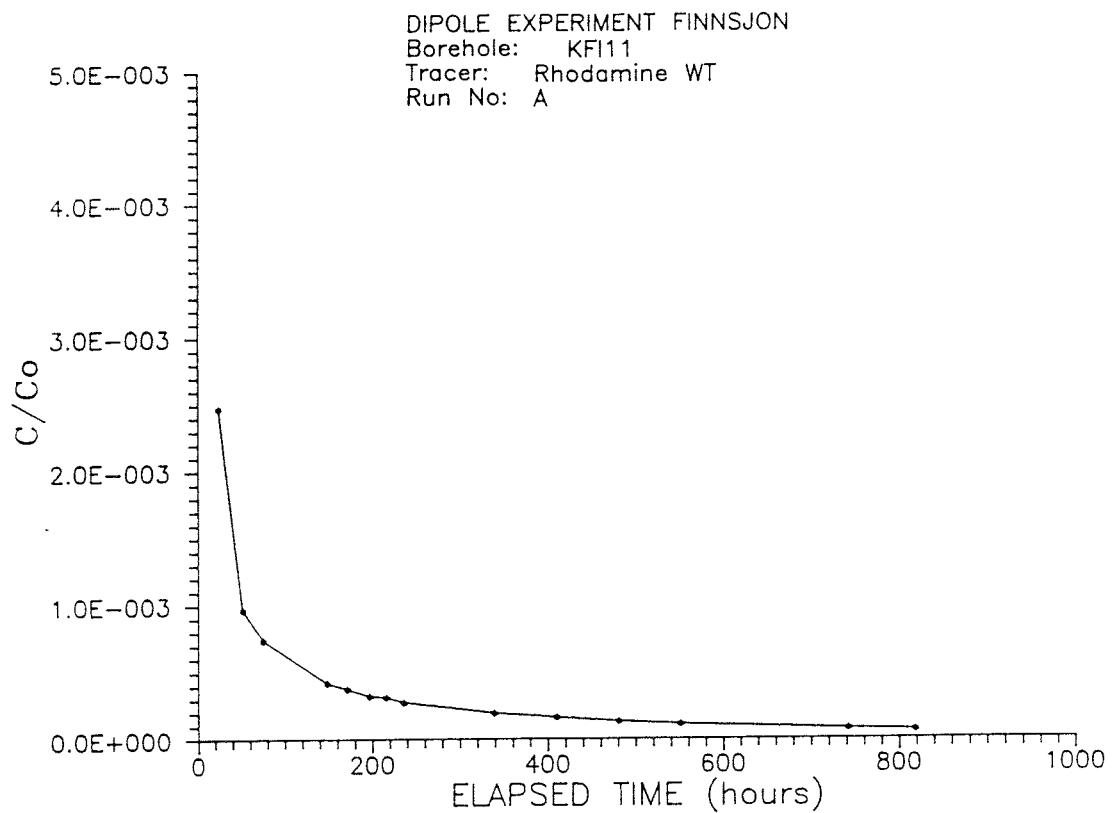
Breakthrough curve for Yb-169 (Inj. 7) in KFI11, 0-100 and 0-300 h.

B: 14



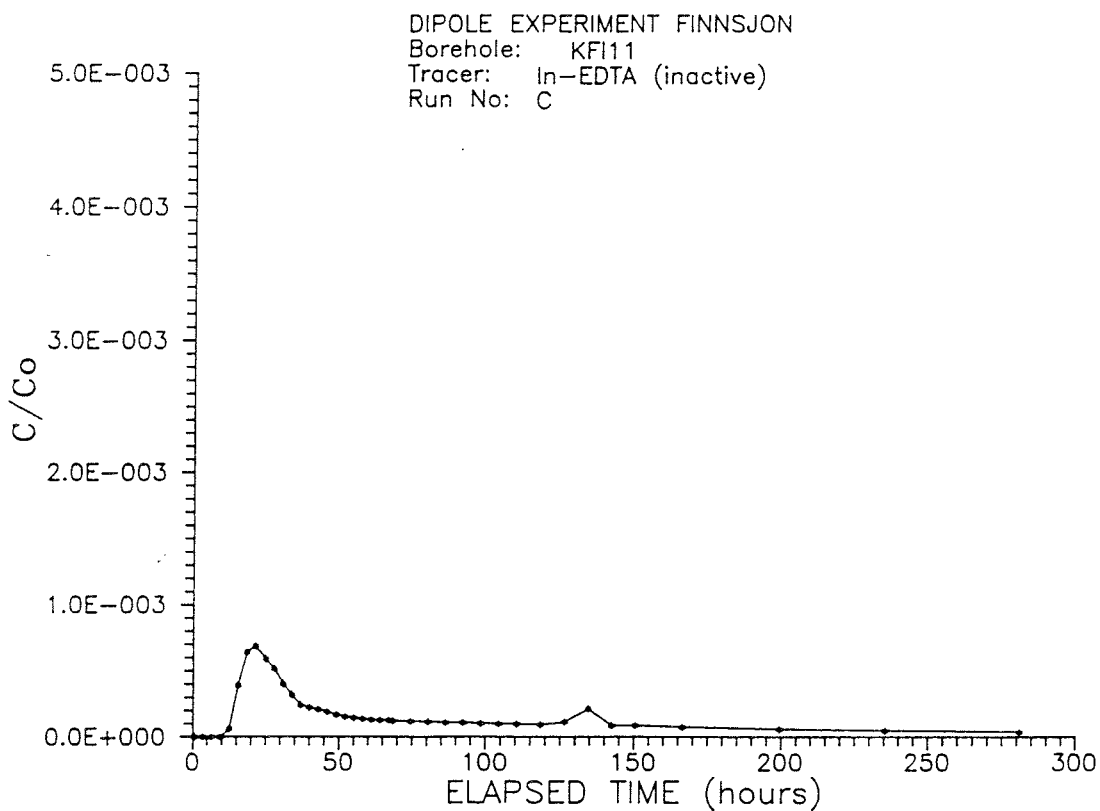
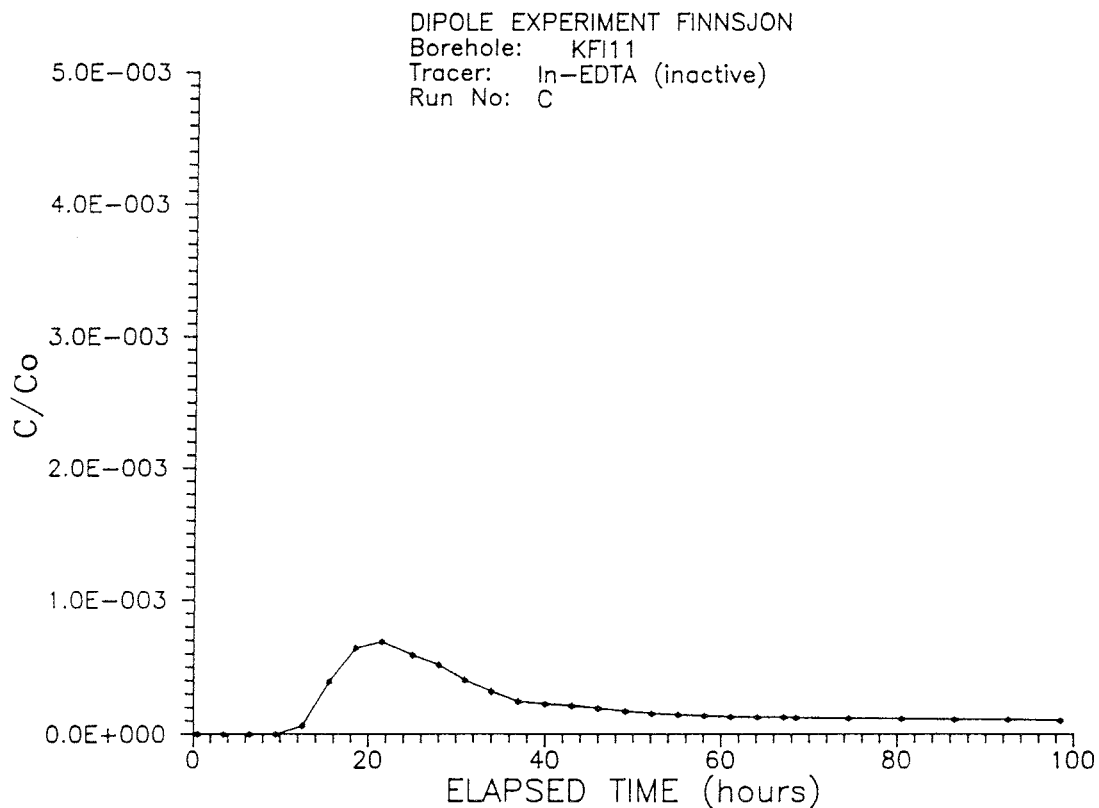
Breakthrough curve for Co-58 (Inj. 8) in KFI11, 0-100 h.

B: 15



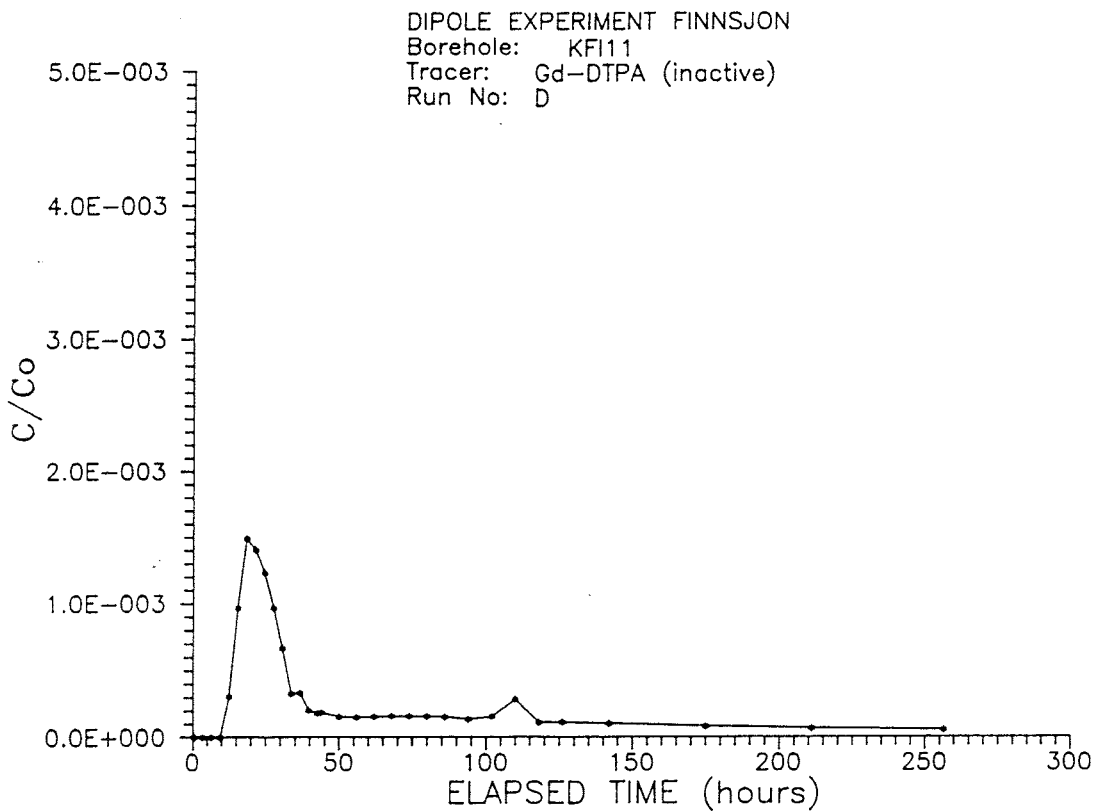
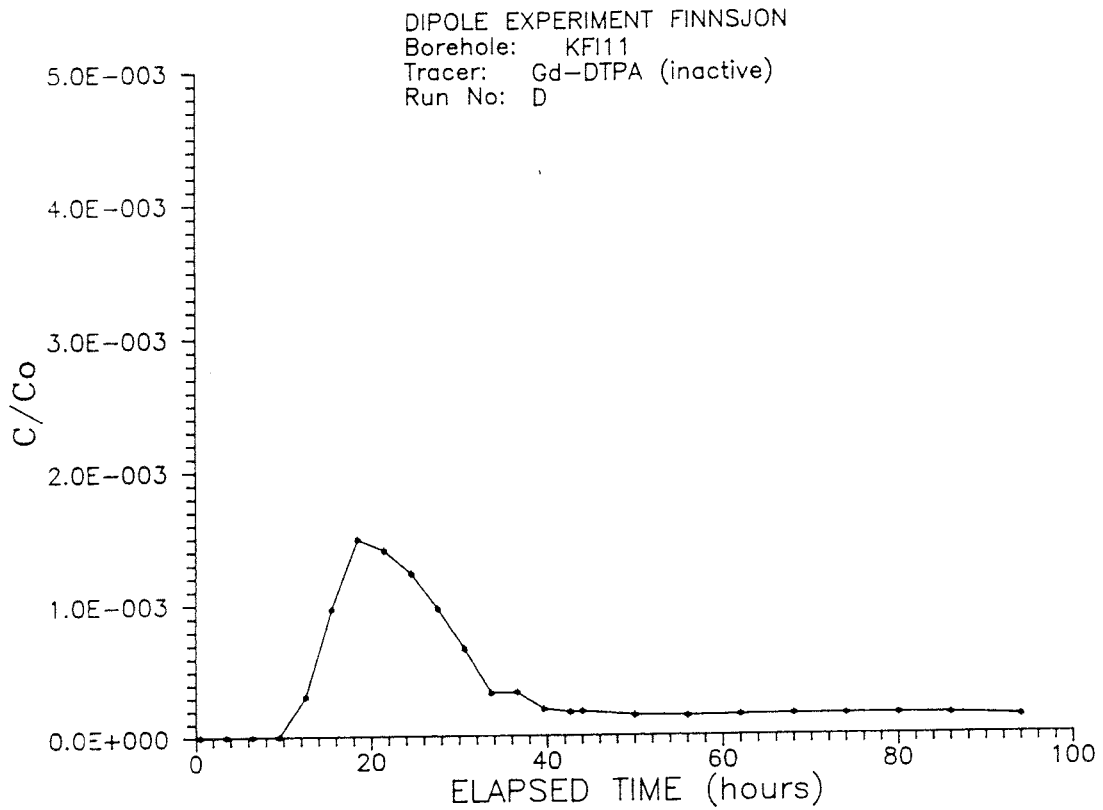
Breakthrough curve for Rhodamine WT (Inj. A) in KFI11,  
0-1000 h.

B: 16



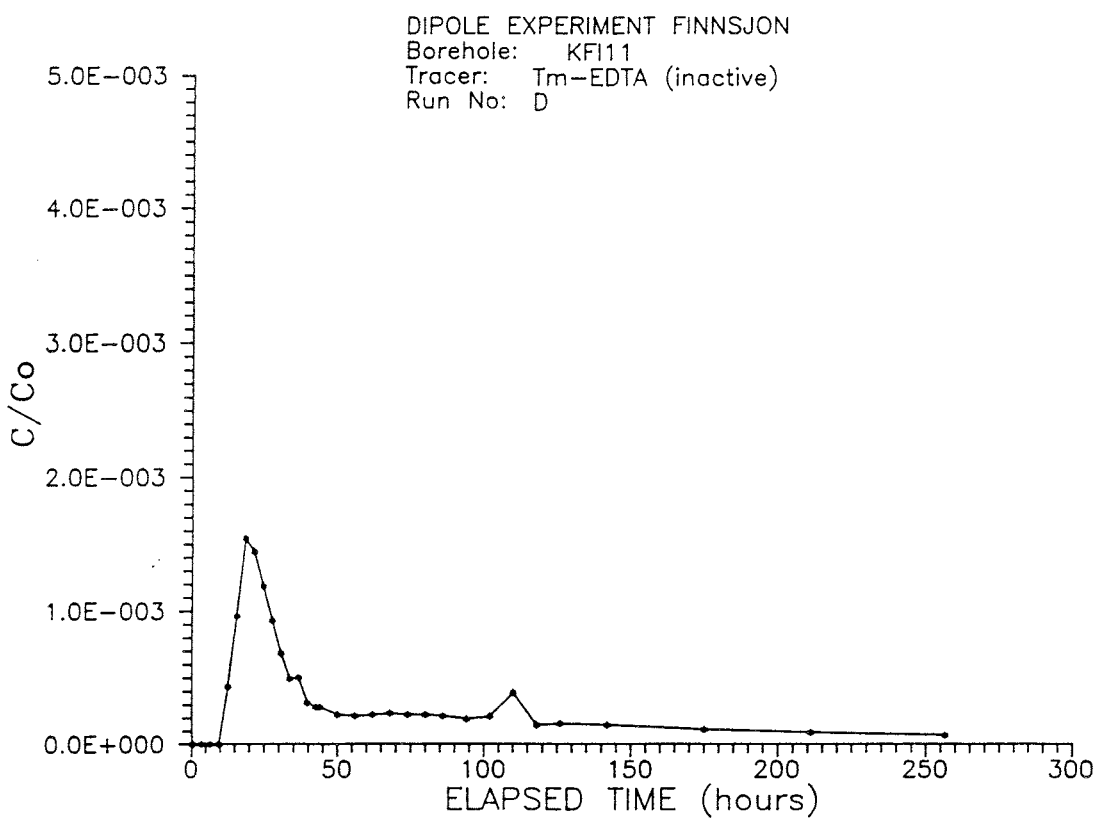
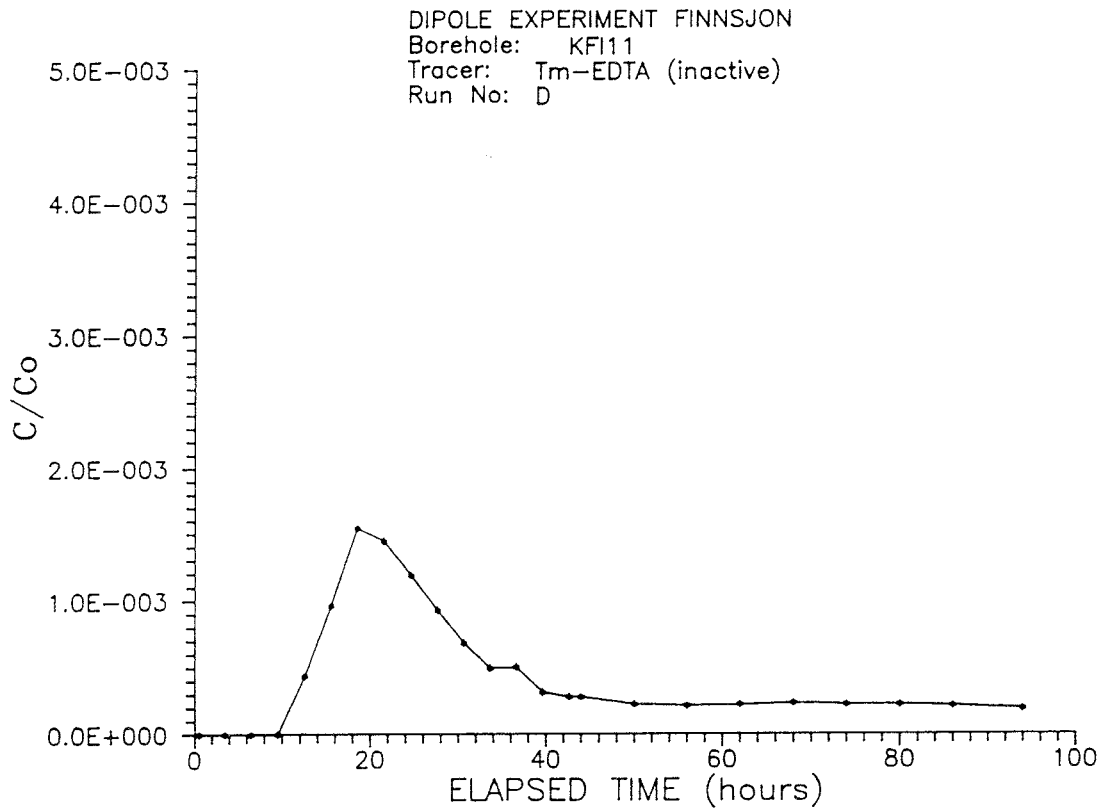
Breakthrough curve for In-EDTA (Inj. C) in KFI11, 0-100 and 0-300 h.

B: 17



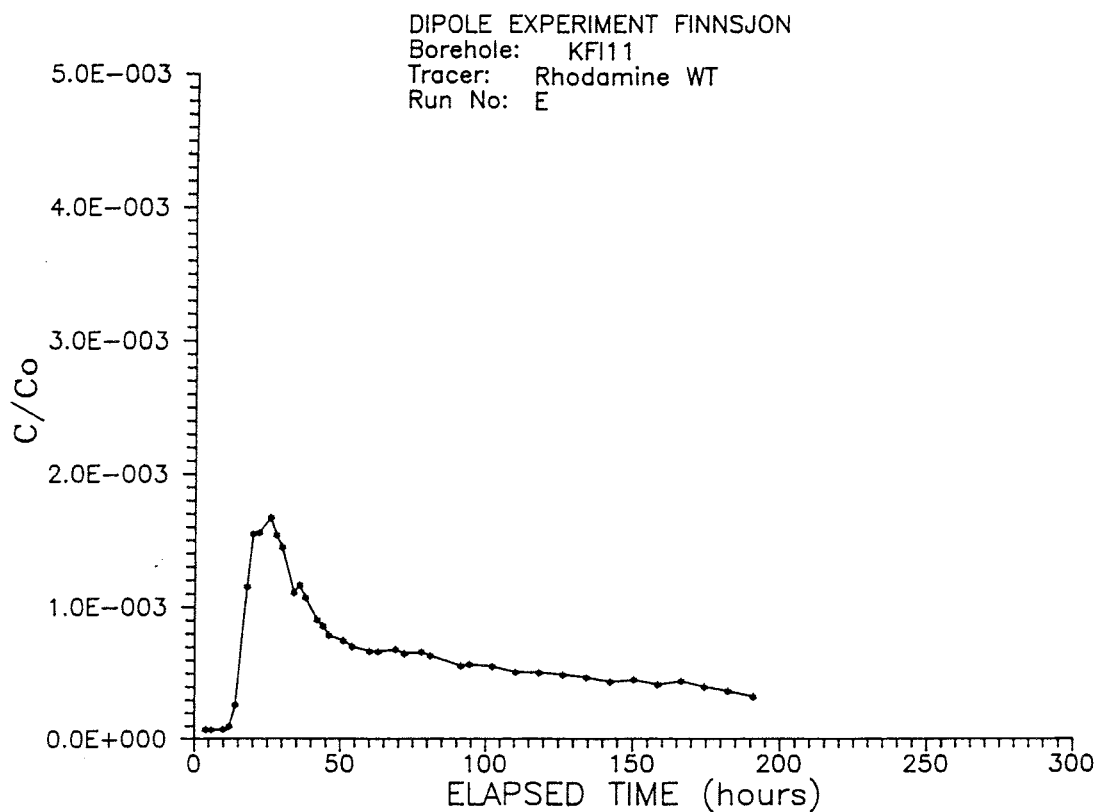
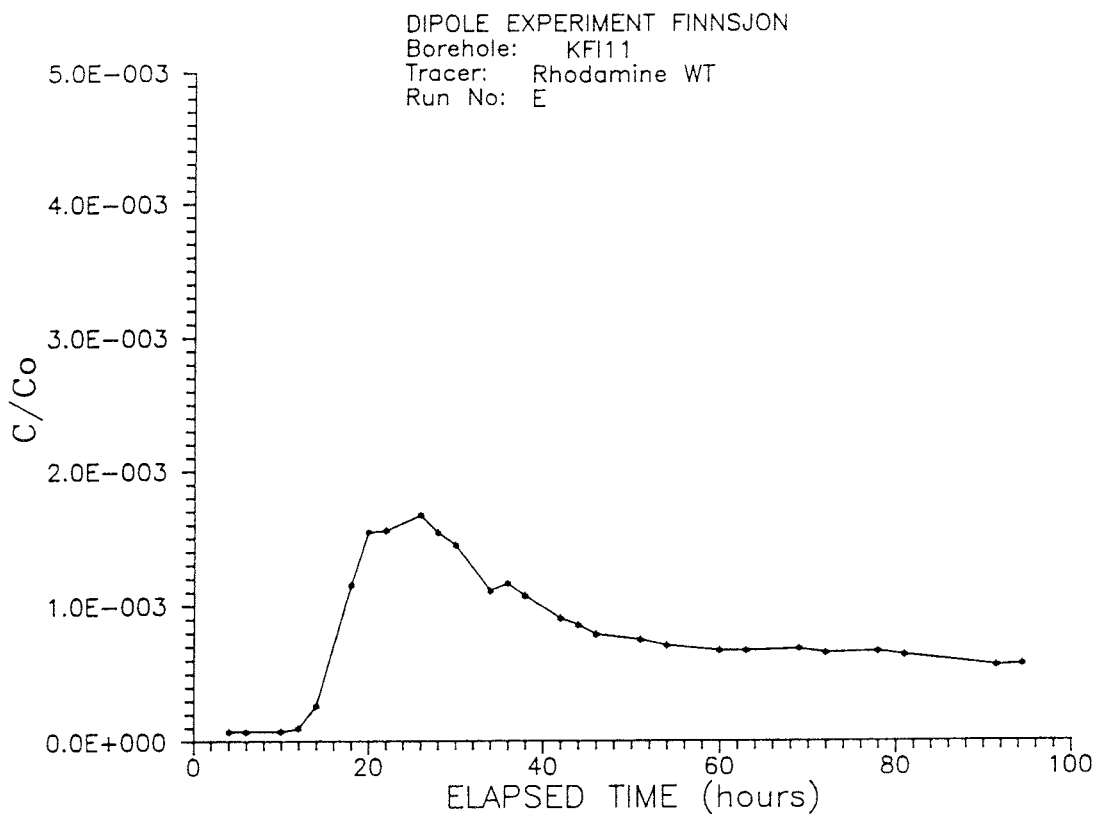
Breakthrough curve for Gd-DTPA (Inj. D) in KFI11,  
0-100 and 0-300 h.

B: 18



Breakthrough curve for Tm-EDTA (Inj. D) in KFI11, 0-100 and 0-300 h.

B: 19



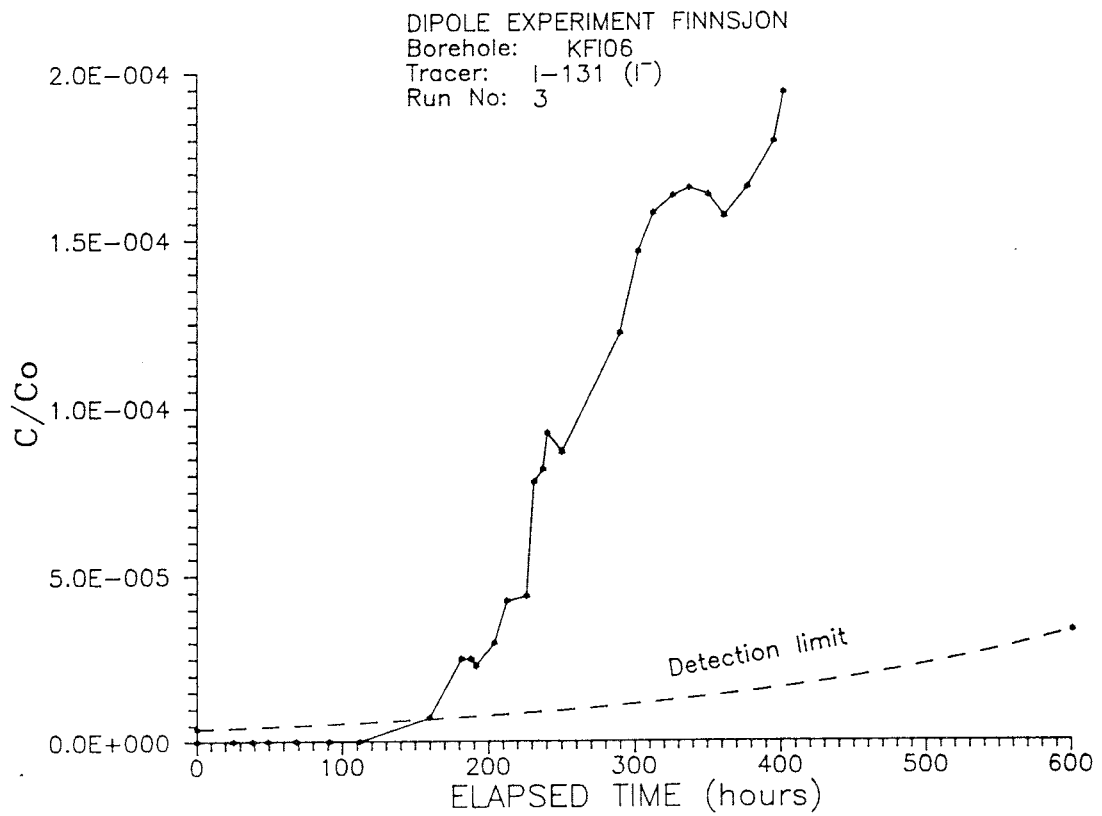
Breakthrough curve for Rhodamine WT (Inj. E) in KFI11, 0-100 and 0-300 h.

## APPENDIX C

## TRACER BREAKTHROUGH IN BOREHOLE KFI06

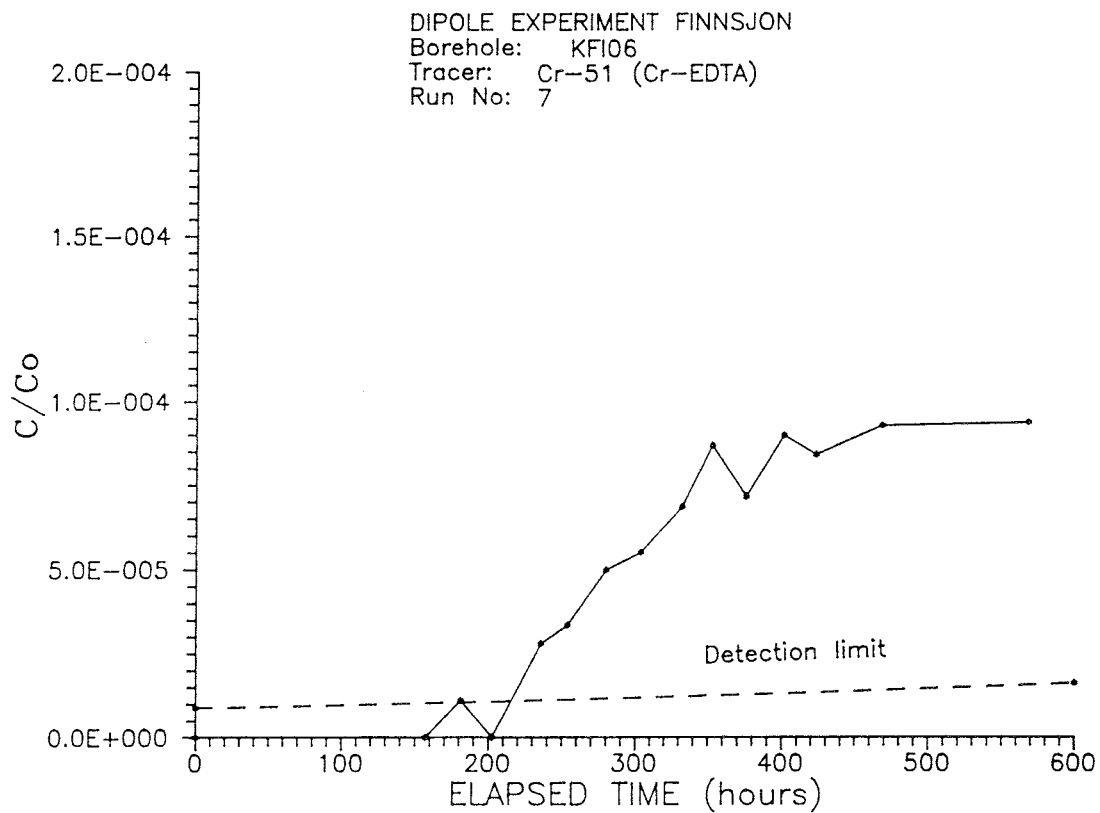
CONTENTS	Page
Breakthrough curve for I-131 (Inj. 3) in KFI06, 0-600 h.	C:1
Breakthrough curve for Cr-51 (Inj. 7) in KFI06, 0-600 h.	C:2
Breakthrough curve for Tb-160 (Inj. 7) in KFI06, 0-600 h.	C:3
Breakthrough curve for Yb-169 (Inj. 7) in KFI06, 0-600 h.	C:4
Breakthrough curve for Co-58 (Inj. 8) in KFI06, 0-600 h.	C:5
Breakthrough curve for Rhodamine WT (Inj. A) in KFI06, 0-600 h.	C:6

C: 1



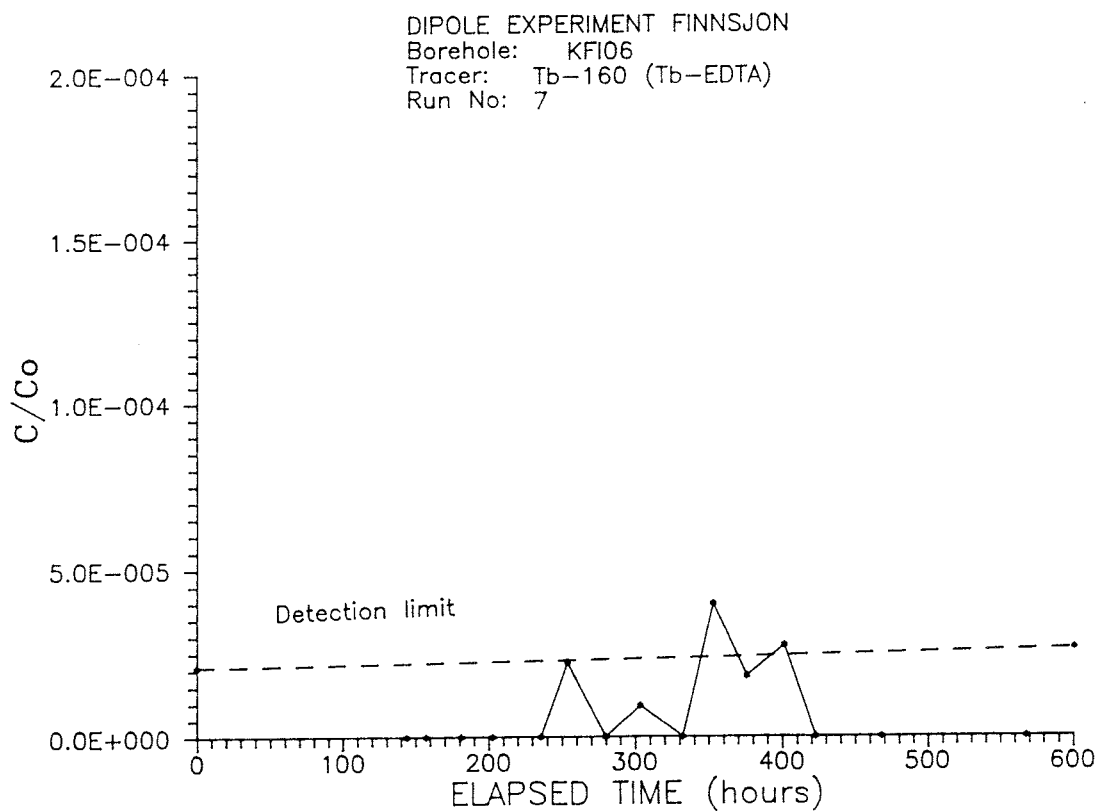
Breakthrough curve for I-131 (Inj. 3) in KFI06, 0-600 h.

C: 2



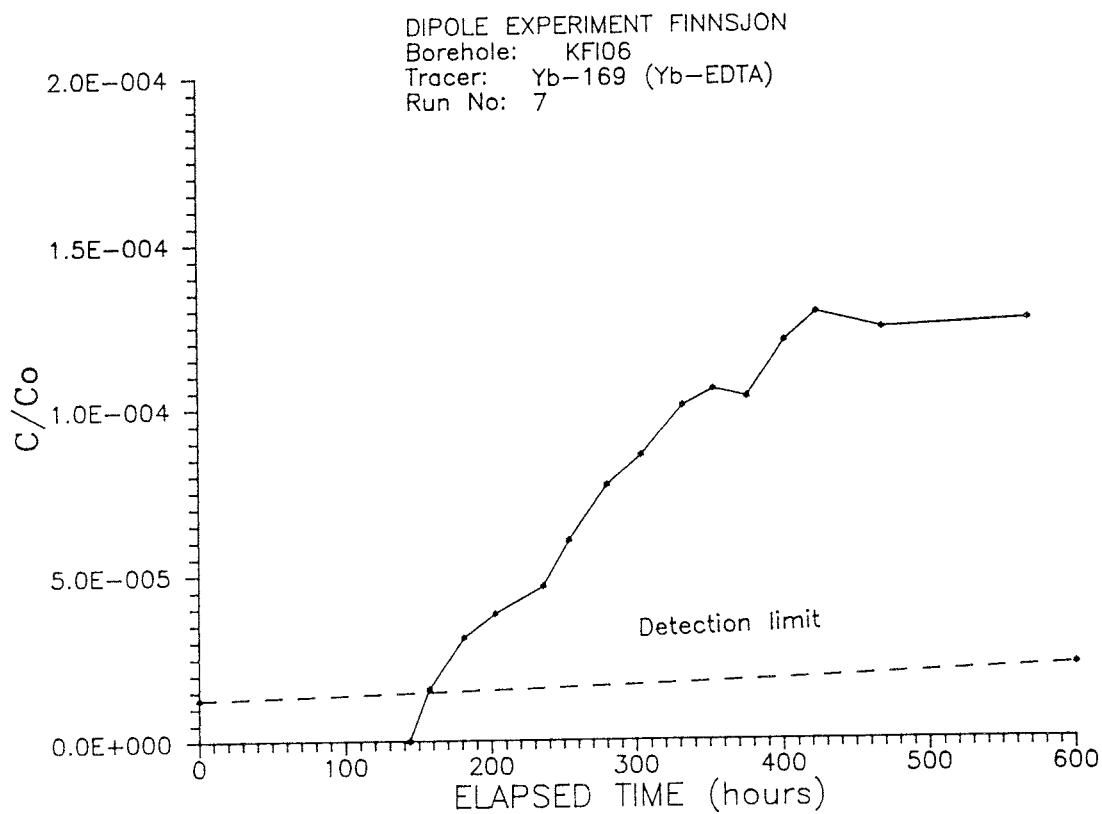
Breakthrough curve for Cr-51 (Inj. 7) in KFI06, 0-600 h.

C: 3



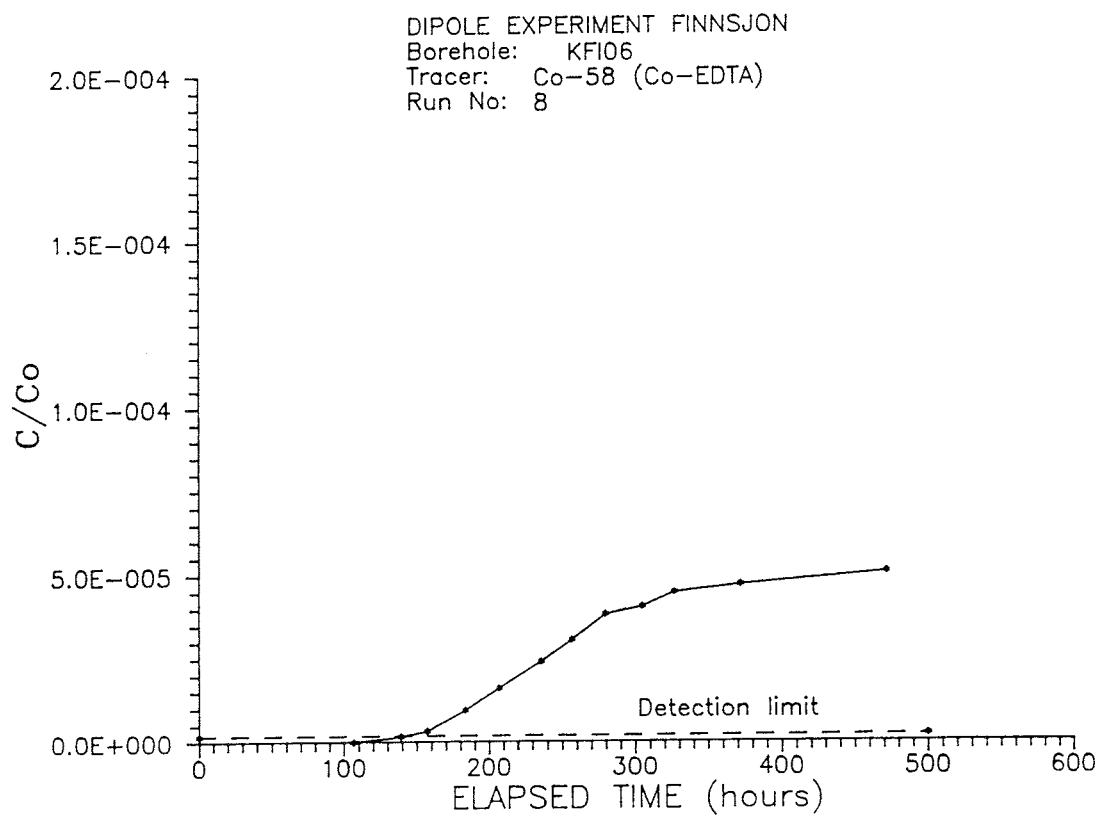
Breakthrough curve for Tb-160 (Inj. 7) in KFI06, 0-600 h.

C: 4



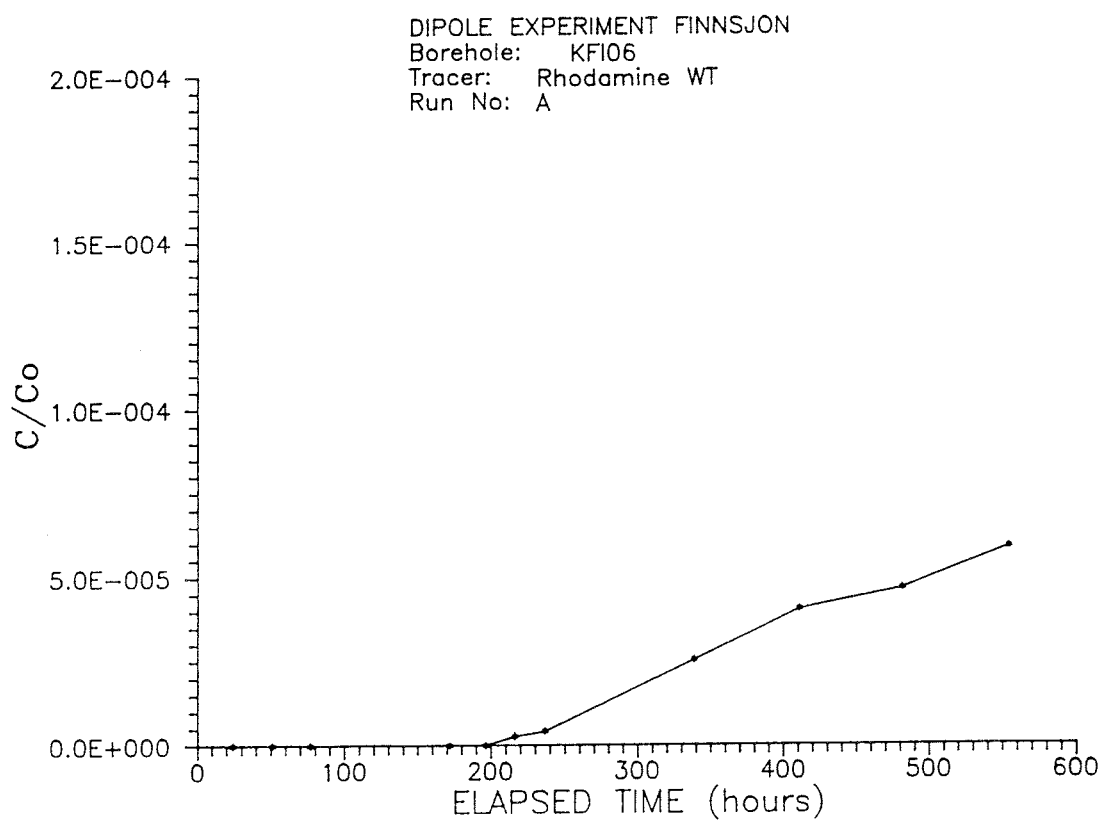
Breakthrough curve for Yb-169 (Inj. 7) in KFI06, 0-600 h.

C: 5



Breakthrough curve for Co-58 (Inj. 8) in KFI06, 0-600 h.

C: 6



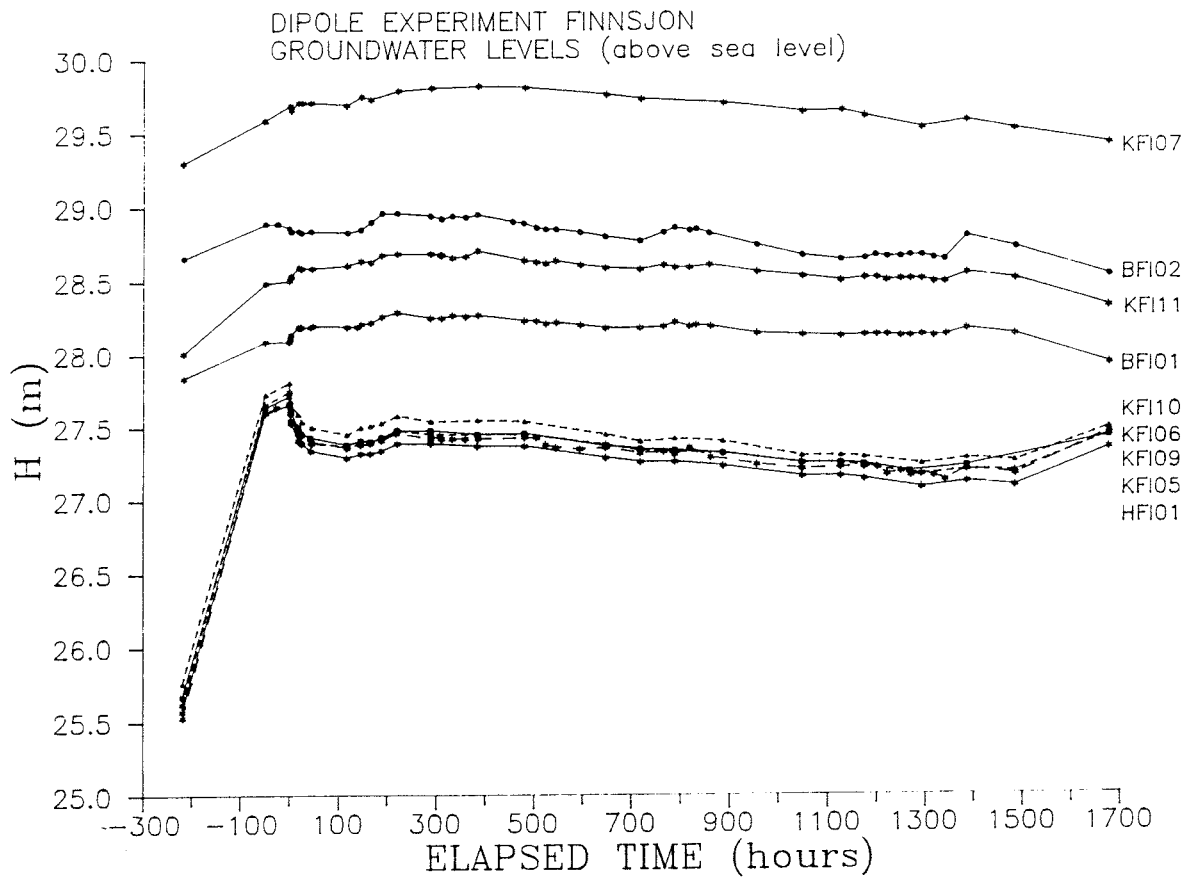
Breakthrough curve for Rhodamine WT (Inj. A) in KFI06, 0-600 h.

## APPENDIX D

## HEAD MEASUREMENTS

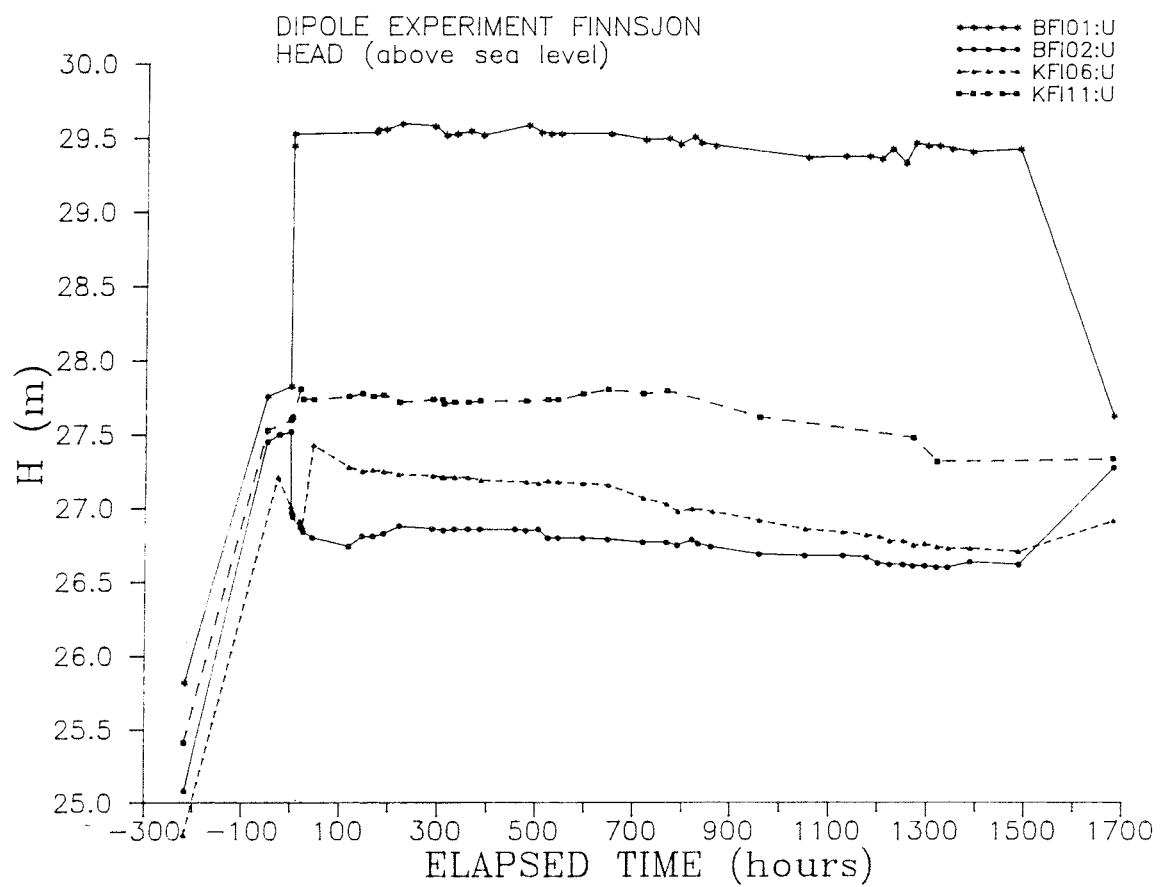
CONTENTS	Page
Groundwater levels during the dipole experiment in 9 boreholes in the Brändan area.	D:1
Hydraulic heads in the sealed off upper intervals of boreholes BFI01, KFI06, and KFI11.	D:2
Hydraulic heads in the sealed off lower and middle intervals of boreholes BFI01, KFI06, and KFI11.	D:3
Head difference relative to the pumped interval in BFI02 for the groundwater levels.	D:4
Head difference relative to the pumped interval in BFI02 for the sealed off upper intervals.	D:5
Head difference relative to the pumped interval in BFI02 for the sealed off middle and lower intervals.	D:6

D: 1



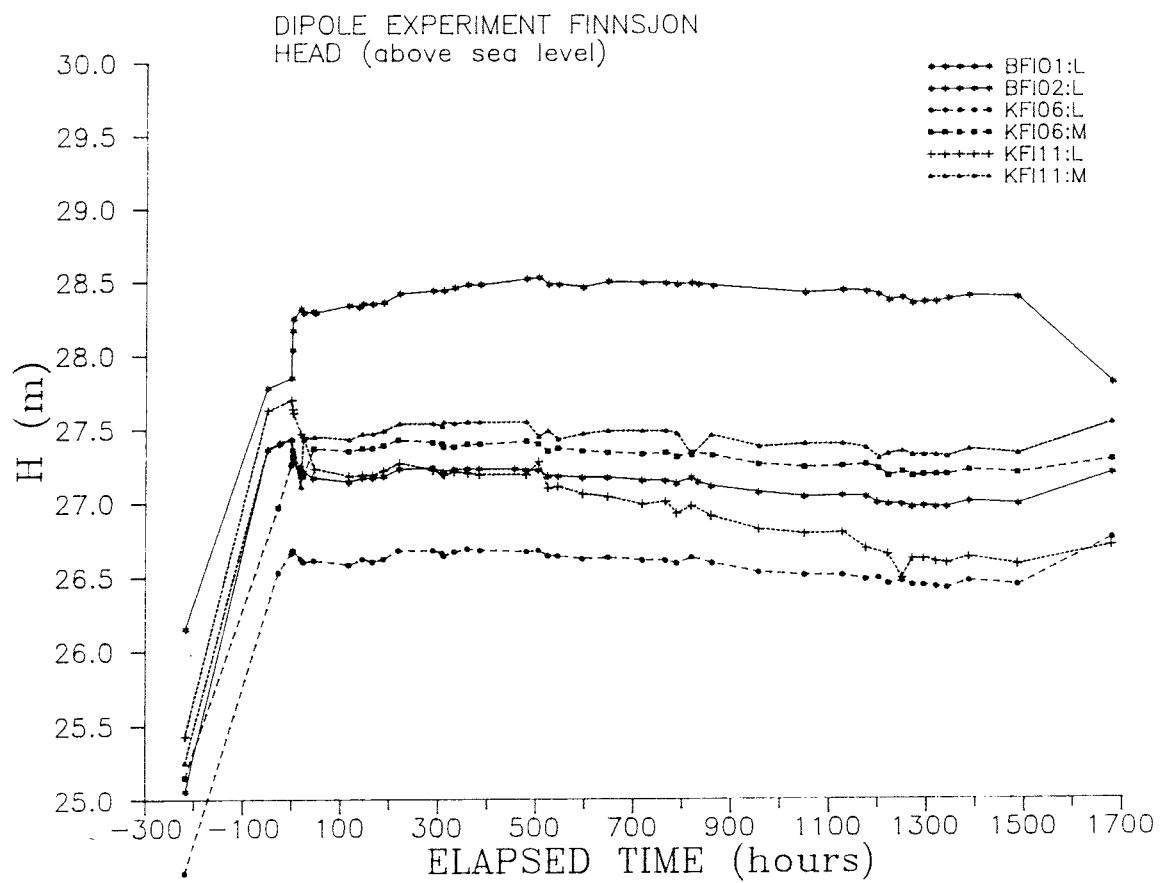
Groundwater levels during the dipole experiment in 9 boreholes in the Brändan area.

D: 2



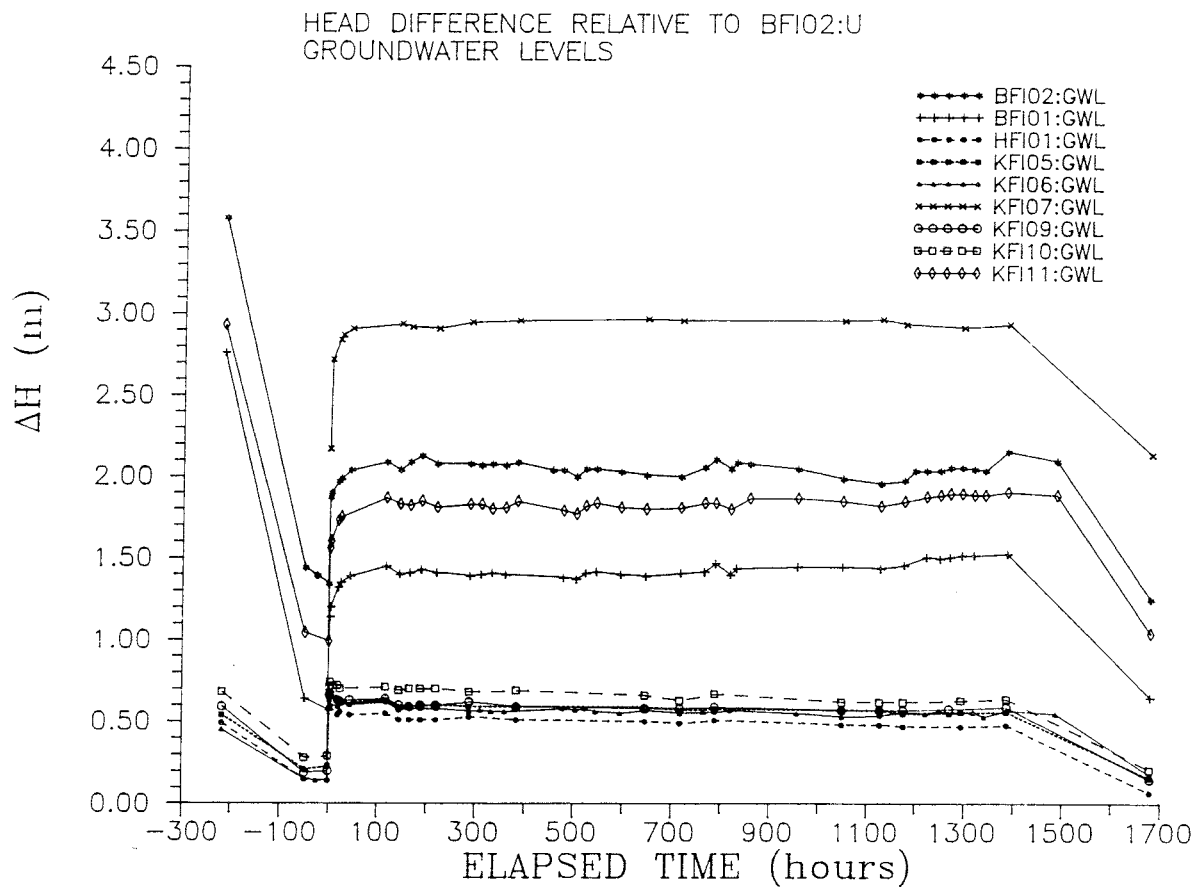
Hydraulic heads in the sealed off upper intervals of boreholes BFI01, KFI06, and KFI11.

D: 3



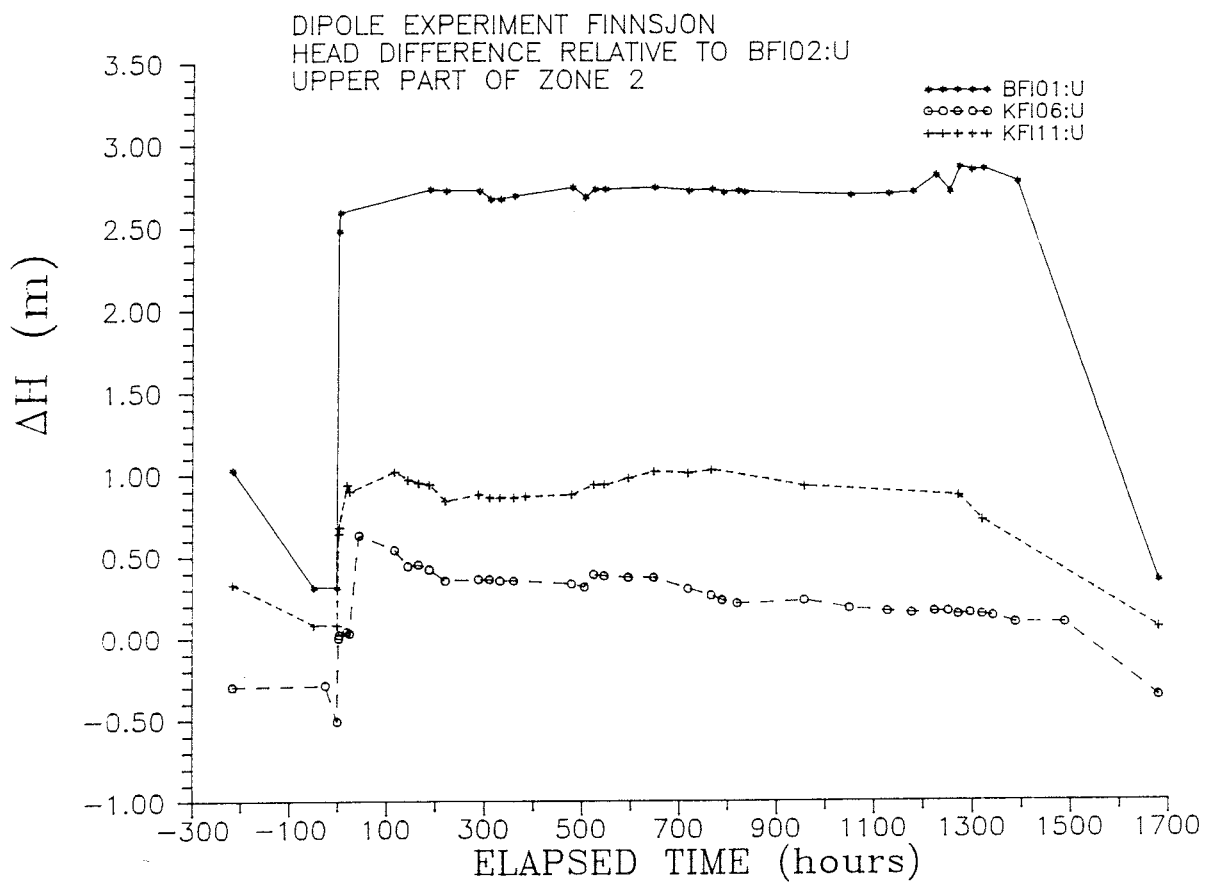
Hydraulic heads in the sealed off lower and middle intervals of boreholes BFI01, KFI06, and KFI11.

D: 4



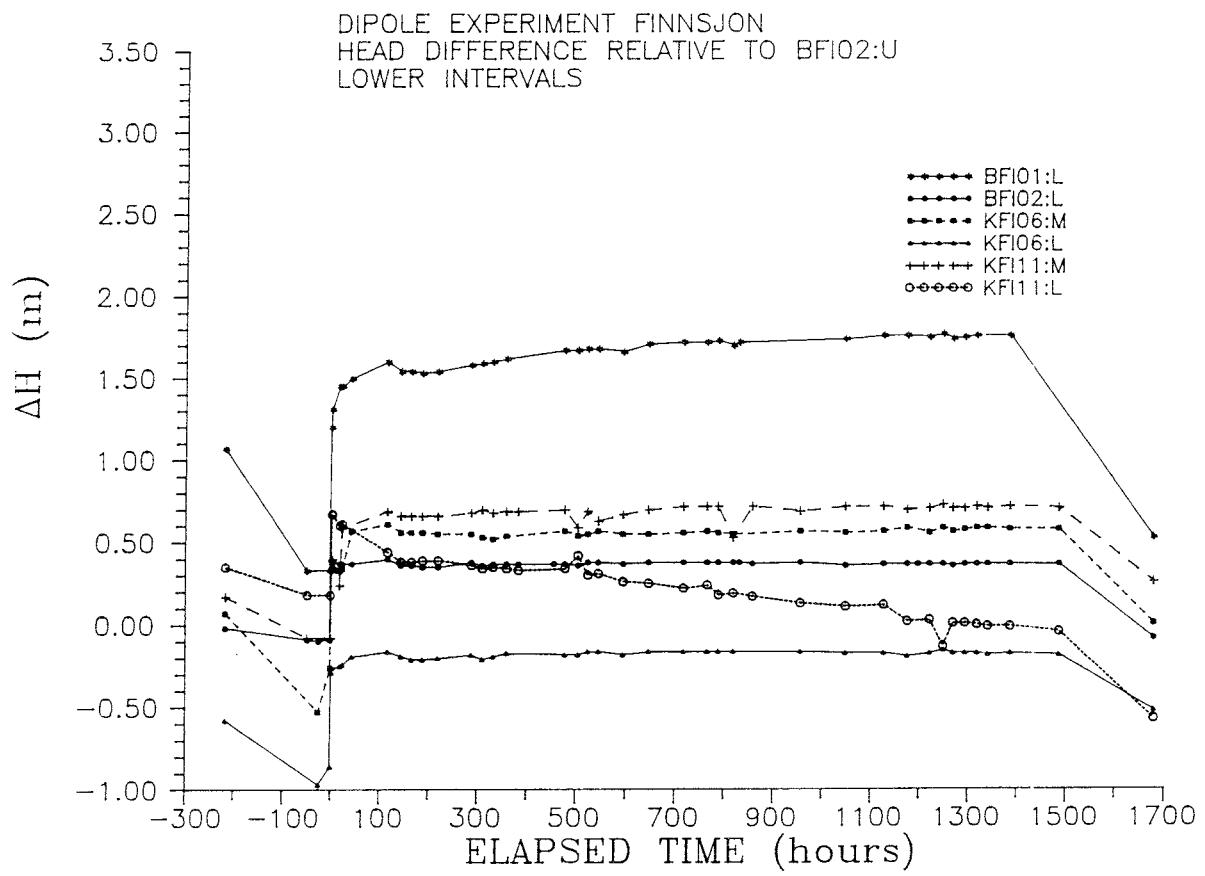
Head difference relative to the pumped interval in BFI02 for the groundwater levels.

D: 5



Head difference relative to the pumped interval in BF102 for the sealed off upper intervals.

D: 6



Head difference relative to the pumped interval in BFI02 for the sealed off middle and lower intervals.

# List of SKB reports

## Annual Reports

1977-78

TR 121

### **KBS Technical Reports 1 – 120**

Summaries

Stockholm, May 1979

1979

TR 79-28

### **The KBS Annual Report 1979**

KBS Technical Reports 79-01 – 79-27

Summaries

Stockholm, March 1980

1980

TR 80-26

### **The KBS Annual Report 1980**

KBS Technical Reports 80-01 – 80-25

Summaries

Stockholm, March 1981

1981

TR 81-17

### **The KBS Annual Report 1981**

KBS Technical Reports 81-01 – 81-16

Summaries

Stockholm, April 1982

1982

TR 82-28

### **The KBS Annual Report 1982**

KBS Technical Reports 82-01 – 82-27

Summaries

Stockholm, July 1983

1983

TR 83-77

### **The KBS Annual Report 1983**

KBS Technical Reports 83-01 – 83-76

Summaries

Stockholm, June 1984

1984

TR 85-01

### **Annual Research and Development Report 1984**

Including Summaries of Technical Reports Issued during 1984. (Technical Reports 84-01 – 84-19)

Stockholm, June 1985

1985

TR 85-20

### **Annual Research and Development Report 1985**

Including Summaries of Technical Reports Issued during 1985. (Technical Reports 85-01 – 85-19)

Stockholm, May 1986

1986

TR 86-31

### **SKB Annual Report 1986**

Including Summaries of Technical Reports Issued during 1986

Stockholm, May 1987

1987

TR 87-33

### **SKB Annual Report 1987**

Including Summaries of Technical Reports Issued during 1987

Stockholm, May 1988

1988

TR 88-32

### **SKB Annual Report 1988**

Including Summaries of Technical Reports Issued during 1988

Stockholm, May 1989

1989

TR 89-40

### **SKB Annual Report 1989**

Including Summaries of Technical Reports Issued during 1989

Stockholm, May 1990

1990

TR 90-46

### **SKB Annual Report 1990**

Including Summaries of Technical Reports Issued during 1990

Stockholm, May 1991

1991

TR 91-64

### **SKB Annual Report 1991**

Including Summaries of Technical Reports Issued during 1991

Stockholm, April 1992

1992

TR 92-46

### **SKB Annual Report 1992**

Including Summaries of Technical Reports Issued during 1992

Stockholm, May 1993

## Technical Reports

### List of SKB Technical Reports 1993

TR 93-01

#### **Stress redistribution and void growth in butt-welded canisters for spent nuclear fuel**

B L Josefson<sup>1</sup>, L Karlsson<sup>2</sup>, H-Å Häggblad<sup>2</sup>

<sup>1</sup> Division of Solid Mechanics, Chalmers University of Technology, Göteborg, Sweden

<sup>2</sup> Division of Computer Aided Design, Luleå University of Technology, Luleå, Sweden

February 1993

TR 93-02

#### **Hydrothermal field test with French candidate clay embedding steel heater in the Stripa mine**

R Pusch<sup>1</sup>, O Karnland<sup>1</sup>, A Lajudie<sup>2</sup>, J Lechelle<sup>2</sup>, A Bouchet<sup>3</sup>

<sup>1</sup> Clay Technology AB, Sweden

<sup>2</sup> CEA, France

<sup>3</sup> Etude Recherche Materiaux (ERM), France  
December 1992

TR 93-03

#### **MX 80 clay exposed to high temperatures and gamma radiation**

R Pusch<sup>1</sup>, O Karnland<sup>1</sup>, A Lajudie<sup>2</sup>, A Decarreau<sup>3</sup>,

<sup>1</sup> Clay Technology AB, Sweden

<sup>2</sup> CEA, France

<sup>3</sup> Univ. de Poitiers, France  
December 1992

TR 93-04

#### **Project on Alternative Systems Study (PASS). Final report**

October 1992

TR 93-05

#### **Studies of natural analogues and geological systems. Their importance to performance assessment**

Fredrik Brandberg<sup>1</sup>, Bertil Grundfelt<sup>1</sup>, Lars Olof Höglund<sup>1</sup>, Fred Karlsson<sup>2</sup>,

Kristina Skagius<sup>1</sup>, John Smellie<sup>3</sup>

<sup>1</sup> KEMAKTA Konsult AB

<sup>2</sup> SKB

<sup>3</sup> Conterra AB

April 1993

TR 93-06

#### **Mineralogy, geochemistry and petrophysics of red coloured granite adjacent to fractures**

Thomas Eliasson

Chalmers University of Technology and University of Göteborg, Department of Geology, Göteborg, Sweden

March 1993

TR 93-07

#### **Modelling the redox front movement in a KBS-3 nuclear waste repository**

L Romero, L Moreno, I Neretnieks

Department of Chemical Engineering,  
Royal Institute of Technology, Stockholm, Sweden  
May 1993

TR 93-08

#### **Äspö Hard Rock Laboratory Annual Report 1992**

SKB

April 1993

TR 93-09

#### **Verification of the geostatistical inference code INFERENS, Version 1.1, and demonstration using data from Finnsjön**

Joel Geier

Golder Geosystem AB, Uppsala

June 1993

TR 93-10

#### **Mechanisms and consequences of creep in the nearfield rock of a KBS-3 repository**

Roland Pusch, Harald Hökmark

Clay Technology AB, Lund, Sweden

December 1992

TR 93-11

#### **Post-glacial faulting in the Lansjärv area, Northern Sweden. Comments from the expert group on a field visit at the Molberget post-glacial fault area, 1991**

Roy Stanfors (ed.)<sup>1</sup>, Lars O Ericsson (ed.)<sup>2</sup>

<sup>1</sup> R S Consulting AB

<sup>2</sup> SKB

May 1993

TR 93-12

#### **Possible strategies for geoscientific classification for high-level waste repository site selection**

Lars Rosén, Gunnar Gustafson

Department of Geology, Chalmers University of Technology and University of Göteborg

June 1993

TR 93-13

#### **A review of the seismotectonics of Sweden**

Robert Muir Wood

EQE International Ltd, Warrington, Cheshire, England

April 1993

TR 93-14

**Simulation of the European ice sheet trough the last glacial cycle and prediction of future glaciation**

G S Boulton, A Payne

Department of Geology and Geophysics,  
Edinburgh University, Grant Institute, Edinburgh,  
United Kingdom

December 1992

TR 93-15

**Analysis of the regional groundwater flow in the Finnsjön area**

Anders Boghammar, Bertil Grundfelt, Hans Widén  
Kemakta Konsult AB

June 1993

TR 93-16

**Kinetic modelling of bentonite - canister interaction. Implications for Cu, Fe, and Pb corrosion in a repository for spent nuclear fuel**

Paul Wersin, Jordi Bruno, Kastriot Spahiu  
MBT Tecnologia Ambiental, Cerdanyola, Spain

June 1993

TR 93-17

**Oxidation of uraninite**

Janusz Janeczek, Rodney C Ewing  
Department of Earth & Planetary Science, University  
of New Mexico, Albuquerque, NM, USA

June 1993

TR 93-18

**Solubility of the redox-sensitive radionuclides <sup>99</sup>Tc and <sup>237</sup>Np under reducing conditions in neutral to alkaline solutions. Effect of carbonate**

Trygve E Eriksen<sup>1</sup>, Pierre Ndalamba<sup>1</sup>, Daqing Cui<sup>1</sup>,  
Jordi Bruno<sup>2</sup>, Marco Caceci<sup>2</sup>, Kastriot Spahiu<sup>2</sup>

<sup>1</sup> Dept. of Nuclear Chemistry, Royal Institute of  
Technology, Stockholm, Sweden

<sup>2</sup> MBT Tecnologia Ambiental, Cerdanyola, Spain

September 1993

TR 93-19

**Mechanical properties of fracture zones**

Bengt Leijon  
Conterra AB

May 1993

TR 93-20

**The Fracture Zone Project - Final report**

Peter Andersson (ed.)

Geosigma AB, Uppsala, Sweden

September 1993

TR 93-21

**Development of "CHEMFRONTS", a coupled transport and geochemical program to handle reaction fronts**

Catharina Bäverman

Department of Chemical Engineering, Royal Institute  
of Technology, Stockholm, Sweden

October 1993

TR 93-22

**Carbon transformations in deep granitic groundwater by attached bacterial populations characterized with 16S-rRNA gene sequencing technique and scanning electron microscopy**

Susanne Ekendahl, Johanna Arlinger, Fredrik Ståhl,  
Karsten Pedersen

Department of General and Marine Microbiology,  
University of Göteborg, Göteborg, Sweden

October 1993

TR 93-23

**Accelerator transmutation of wastes (ATW)**

**- Prospects and safety**

Waclaw Gudowski, Kjell Pettersson,  
Torbjörn Thedéen

Royal Institute of Technology, Stockholm, Sweden  
November 1993

TR 93-24

**Direct fault dating trials at the Äspö Hard Rock Laboratory**

R H Maddock, E A Hailwood, E J Rhodes,  
R Muir Wood

October 1993

TR 93-25

**Radially converging tracer test in a low-angle fracture zone at the Finnsjön site, central Sweden.**

**The Fracture Zone Project - Phase 3**

Erik Gustafsson, Rune Nordqvist  
Geosigma AB, Uppsala, Sweden

October 1993

*ISSN 0284-3757*

CM Gruppen Bromma 1993